

MECHANOTRANSDUCTION AT THE Z-DISC OF SKELETAL MUSCLE

Elliot James Jokl

PhD

University of York

Biology

September 2017

Abstract

The importance of the transglutaminase-like protein kyphoscoliosis peptidase (KY) in skeletal muscle was discovered in a KY-deficient mouse model of hereditary kyphoscoliosis (*ky/ky*). The *ky/ky* pathology primarily affects muscles experiencing high tension, e.g., the soleus, which undergoes regeneration and shows persistent hallmarks of structural damage, including the aberrant localisation of the z-disc crosslinker Filamin C (FLNC) – a known KY interaction partner. However, muscles are globally smaller in size, and fast-twitch muscles (e.g., the *extensor digitorum longus* or EDL) show an inability to undergo hypertrophy in response to elevated tension. A robust function for KY has not been identified. Recently reported human cases of KY-deficient myopathy share hallmarks with the mouse pathology and underscore the value of increasing our understanding of KY and its function.

Chaperone Assisted Selective Autophagy (CASA) is a tension-induced mechanism for FLNC turnover understood to be critical for muscle maintenance. This thesis hypothesises that the absence of KY disrupts CASA, thereby indicating that KY might have a role in CASA. This thesis examines CASA in the *ky/ky* mouse model and describes the generation and analysis of novel cellular (C2C12) and zebrafish models of KY-deficiency. A consistent pattern of CASA marker upregulation is observed, specifically the CASA co-chaperone Bcl2 Associated Athanogene 3 (BAG3), even in tissues with no overt pathology and in the absence of mechanical challenge. This indicates that constitutive upregulation of CASA markers may be a primary hallmark of KY-deficiency. Additionally, an increase in cytoskeleton-associated BAG3 protein in mouse *ky/ky* soleus tissue may indicate inefficient turnover of the CASA complex in tissues experiencing high tension.

It is also shown that *in vivo* overexpression of recombinant KY is not sufficient to drive hypertrophy in normal mice, but may partially rescue fibre size in *ky/ky* mice.

Table of Contents

Abstract	3
List of figures and tables	9
Acknowledgements	11
Author's Declaration	12
CHAPTER ONE: INTRODUCTION	14
1.1 - Overview	14
1.2 - Structure of Skeletal Muscle	16
1.2.1 - Skeletal muscle structure	16
1.2.2 - Zebrafish muscle	20
1.2.3 - The C2C12 myoblast model	21
1.3 - Skeletal Muscle Hypertrophy	21
1.3.1 - Loading induced hypertrophy is independent of the IGF-1/AKT axis	22
1.3.2 - MAPK signalling modules	23
1.3.3 - Myostatin and hypertrophy	24
1.4 - Skeletal Muscle Atrophy	25
1.5 - Protein Turnover Mechanisms	25
1.5.1 - The Ubiquitin-Proteasome System	25
1.5.2 - Autophagy	26
1.5.3 - The relative importance of UPS and autophagy in muscle maintenance	28
1.5.4 - Demand for autophagy varies by muscle type	29
1.6 - Structural Proteins and Muscle Disease	31
1.7 - Protein Turnover and Muscle Disease	32
1.8 - Identification and Characterisation of the <i>ky/ky</i> Mouse	37
1.8.1 The <i>ky/ky</i> mouse	37
1.8.2 The KY protein	38
1.9 - Human Myopathies Associated with KY deficiency	39
1.10 - Additional Insights into KY	40
1.11 - Hypotheses for the Function of KY	41
1.12 CRISPR/Cas9	43
1.13 - Project Aims and Hypotheses	44
CHAPTER TWO: MATERIALS AND METHODS	48
2.1 Buffers and reagents	48
2.2 PCR and qPCR primers and oligos	49
2.3 Antibodies	51

2.4	Cell culture	52
2.4.1	Proliferating cultures	52
2.4.2	Splitting cultures	52
2.4.3	Harvesting cells	53
2.4.4	Differentiation	53
2.4.5	Transfection	53
2.4.6	CRISPR/Cas9 genome editing in cells	53
2.4.7	Cell immunofluorescence and staining	55
2.4.8	- Myoblast stretching	55
2.5	Western Blotting	56
2.6	PCR, RT-PCR and qPCR	57
2.6.1	PCR	57
2.6.2	RT-PCR	58
2.6.3	qPCR	58
2.6.4	Sequencing	59
2.7	Zebrafish	59
2.7.1	Lines	59
2.7.2	Microinjection	59
2.7.3	Fin clipping	60
2.7.4	in situ hybridisation	60
2.7.5	Methylcellulose challenge	62
2.7.6	Birefringence.....	62
2.7.7	Sectioning and histology	62
2.7.8	RNA extraction from tissue	63
2.7.9	Zebrafish gene targeting by CRISPR/Cas9	63
2.8	Mice	64
2.8.1	in vivo electroporation of mouse skeletal muscle	64
2.8.2	Tissue protein fractionation	65
2.9	Genotyping	66
CHAPTER THREE: ANALYSIS OF ENDOGENOUS KY IN THE MOUSE		68
3.1	Introduction	68
3.2	A trend towards higher <i>Ky</i> mRNA expression in fast muscle compared to slow muscle	68
3.3	Conservation of tryptophan residues around the catalytic triad	69
3.4	in silico examination of KY protein structure	70
3.5	Discussion	71
CHAPTER FOUR: CHAPERONE ASSISTED SELECTIVE AUTOPHAGY IN THE <i>ky/ky</i> MOUSE		76

4.1 Introduction	76
4.2 BAG3 turnover in the <i>ky/ky</i> mouse	77
4.3 Increased immunoreactivity for FLNC in the <i>ky/ky</i> soleus	79
4.4 Profiling of other autophagy components.....	79
4.5 Examination of other CASA markers	81
4.6 - Conclusions.....	82
CHAPTER FIVE: GENERATION AND ANALYSIS OF KY-KNOCKOUT MYOBLASTS.....	86
5.1 Introduction	86
5.2 Target identification and CRISPR/Cas9 construct generation.....	86
5.3 Confirmation of mutagenesis	87
5.4 Clonal selection and identification of KY KO clones.....	89
5.5 Morphological analysis of KY-deficient C2C12 myoblasts.....	92
5.6 Differentiation analysis of KY-deficient C2C12 myoblasts.....	95
5.7 CASA in KY-deficient C2C12 proliferating myoblasts	98
5.8 CASA in KY-deficient C2C12 myotubes	98
5.9 Tension induced changes in WT myoblasts.....	101
5.10 Conclusions.....	102
CHAPTER SIX: GENERATION AND ANALYSIS OF Ky-KNOCKOUT ZEBRAFISH	
106	
6.1 – Introduction.....	106
6.2 – Identification and expression analysis of <i>ky</i> orthologue in zebrafish	106
6.3 – CRISPR/Cas9 protocol optimisation – tyrosinase KO	111
6.4 – gRNA designs for <i>ky</i> targeting	113
6.5 – Confirmation of mutagenesis and founder generation.....	113
6.6 – Generation and validation of <i>ky</i> mutant lines	115
6.7 – Morphological and histological analysis of <i>ky^{yo1} / ky^{yo1}</i> zebrafish.....	118
6.8 – qPCR analysis of CASA components in <i>ky^{yo1} / ky^{yo1}</i> zebrafish muscle...	124
6.9 - Methylcellulose challenge of embryos	125
6.10 - Discussion.....	125
CHAPTER SEVEN: IN VIVO OVEREXPRESSION OF KY CONSTRUCTS.....	130
7.1 Introduction	130
7.2 Overexpression of KY in WT mice using in vivo electroporation	130
7.3 Overexpression of KY in <i>ky/ky</i> mice using in vivo electroporation.....	134
7.4 Localisation of mutagenised KY.....	135
7.5 Conclusions.....	139
CHAPTER EIGHT: DISCUSSION AND FUTURE WORK	142
8.1 Overview	142

8.2 Insights from the <i>ky/ky</i> mouse	142
8.3 Insights from KY-deficient C2C12 models	144
8.4 Insights from Ky-deficient zebrafish	144
8.5 Insights from overexpression experiments.....	145
8.6 Overall conclusions	146
8.7 Future experiments	148
8.7.1 Cellular model	148
8.7.2 Zebrafish model	149
8.7.3 Mouse model	150
8.8 Relevance to human KY-deficient myopathies and potential therapies	150
Glossary of abbreviations	153
Appendix 1 – Full murine KY Phyre2 output	155
Appendix 2 – Proteomics analysis and results	162
BIBLIOGRAPHY	173

List of figures and tables

Figure 1.1 - Structure of skeletal muscle.....	17
Figure 1.2 - Diagram of the sarcomere and costamere	19
Figure 1.3 - Hypertrophic and atrophic signalling pathways	23
Figure 1.4 - Simplified diagram of Chaperone Assisted Selective Autophagy	28
Figure 1.5 – Schematic of disrupted autophagy processes relating to skeletal muscle disease	33
Table 1.6 – Genes associated with skeletal muscle pathology with evidence of autophagy	
disruption.....	36
Figure 1.7 - Diagram of CRISPR/CAS9 genome editing	44
Figure 3.1 - A non-significant trend towards elevated ky mRNA in EDL compared to the	
soleus	69
Figure 3.2 - Alignment of human, mouse and zebrafish Ky transglutaminase domains shows	
absence of conserved tryptophan residues.....	70
Figure 3.3 - Phyre2 output of KY protein structural homology.....	71
Figure 4.1 - Quantification of BAG3 protein and transcript in soleus and EDL.....	78
Figure 4.2 - Increased immunoreactivity for cytoskeletal FLNC in ky/ky soleus.....	80
Figure 4.3 - Autophagy markers in the ky/ky mouse	81
Figure 4.4 - No qualitative differences in CHIP expression in ky/ky tissue	82
Figure 5.1 - Generation of specific KY_PX459 targeting vectors.....	87
Figure 5.2 - Confirmation of targeting vector mutagenic capability.....	88
Figure 5.3 - Clonal selection and identification of disruptive clones	90
5.4 - qPCR quantification of Ky transcript in knockout clones.....	91
Table 5.1 - Mutated alleles detected in mutant clones	92
5.5 - Phalloidin staining of myoblasts shows no consistent morphological changes	93
Figure 5.6 - Crystal violet staining of myoblasts indicates morphological changes.....	94
Figure 5.7 - Phalloidin staining of myotubes.....	96
Figure 5.8 - Differentiation capacity of clones measured by myh7 expression.....	97
Figure 5.9 - Expression of CASA components in myoblasts	99
Figure 5.10 - CASA in KY-deficient myotubes.....	100
Figure 5.11 - Proteomic changes in stretched myoblasts	102
Figure 6.1 - in silico identification of the zebrafish Ky ortholog	107
Figure 6.2 - in situ hybridisation does not detect ky expression	108
6.3 - RT-PCR and qPCR identifies ky expression in late embryonic stages and skeletal muscle	
110	
Figure 6.4 – Targeting of tyr using Cas9 protein is more effective than using Cas9 mRNA .	112
Figure 6.5 - sgRNA target sequence identification and targeting methodology	114
Figure 6.6 - Breeding strategy outline.....	116
Figure 6.7 - Generation and identification of mutant alleles.....	117
Figure 6.8 - qPCR confirmation of transcript-level disruption of expression.....	119
Figure 6.9 - Morphological analysis of ky ^{yo1} /ky ^{yo1} zebrafish	120
Figure 6.10 - Birefringence analysis of ky ^{yo1} /ky ^{yo1} embryos show no severe disruption to	
birefringence	121
Figure 6.11 - H&E staining shows no overt differences in muscle health between ky ^{yo1} /	
ky ^{yo1} and WT zebrafish	122
Figure 6.12 – Slow muscle remains laterally localised in ky ^{yo1} /ky ^{yo1} zebrafish.....	123

Figure 6.13 - qPCR analysis of bag3 and flnc in WT and ky^{yo1}/ky^{yo1} zebrafish	124
Figure 6.14 - Methylcellulose challenge induces CASA component upregulation in WT but not ky^{yo1}/ky^{yo1} embryos.....	127
Figure 7.1 - Methodological summary of electroporation experiments	131
Figure 7.2 - KY_V5 expression does not induce hypertrophy after 55 days in WT mice	132
Figure 7.3 - Short term expression of Ky_Tdtomato induces inconsistent changes in WT mice.....	133
Figure 7.4 - Ky_TdTomato induces hypertrophy in ky/ky muscle.....	135
Figure 7.5 - Diagram of mutagenised KY constructs	136
Figure 7.6 - Localisation of Ky_TdTomato constructs in mouse skeletal muscle.....	137
Figure 7.7 – TdTomato-tagged murine KY localises to striations in zebrafish muscle.....	138
Figure 8.1 - Altered CASA activation explains the major phenotypes in KY-deficient models	147

Acknowledgements

Firstly, I would like to thank my two supervisors - Gonz and Betsy - for their support and guidance throughout my PhD project. I would also like to apologise to Gonz for spending all his money, and to Betsy for never (to my recollection) actually potting anything in the Isaacs v. Pownall Christmas pool games. At least I was consistent. Thanks also to the members of my Thesis Advisory Panel, Dr. Paul Pryor and Professor Nia Bryant, for their scrutiny and advice, and to the BBSRC for funding my studentship.

I would also like to thank my colleagues in the Neuromuscular Genetics lab, Dr. Xiang Li and Toby Cracknell for their kind help and putting up with my perpetual untidiness. I am certain they will miss my uncanny ability not to be there when the level of untidiness triggers the ire of Gonz. Thanks also to past and present members of the Frog/Fish lab for their help in keeping everything alive and well, and for being almost as terrible at pool as I am.

Many thanks to the staff of the BSF for their training and support. A special mention to Chris – venting is therapeutic. Thanks also to the staff in infrastructure and stores who quietly keep the important things running.

A huge thanks goes to my family for their support, particularly my parents. Even though “haven’t you cured it yet?” gets a little old, folks.

Last but not least, thanks to Liam: you are the best.

Author's Declaration

I declare that this thesis is a presentation of original work and I am the sole author, with the exception of instances which are explicitly highlighted and acknowledged in the text, for example figures and parts of figures reproduced with permission or under Creative Commons licenses, with attribution in the figure legends.

Additionally, the material in appendix 2, relating to the downstream LC/MS-MS analysis of stretched myoblasts lysates, was generated by Adam Dowle, University of York Technology Facility.

This work has not previously been presented for an award at this, or any other, University. All sources are acknowledged as references.

CHAPTER ONE: INTRODUCTION

CHAPTER ONE: INTRODUCTION

1.1 - Overview

Skeletal muscle is critical for the survival of its organism; it is essential for exploring the environment, obtaining and competing for food and mates, and evading danger. However, skeletal muscle also represents a demanding investment in terms of the energy costs relating to its use and maintenance alongside the sequestering away of amino acids to build the large structural proteins muscle requires. As such, the ability to modulate this investment in proportion to if and how skeletal muscle is being used represents a massive evolutionary advantage by allowing an organism to build muscle mass and strength when necessary to compete and survive in its environment and to release the energy of this investment into metabolism in times of scarcity (Hoppeler and Flück 2002).

This selective pressure has led muscle to become one of the most highly plastic and adaptable tissues in the body. To mediate this plasticity, skeletal muscle must sense and integrate a variety of physiological stimuli and respond via the modulation of growth (hypertrophic) and wasting (atrophic) pathways. Muscle grows in size and strength in response to growth factors and high physical stresses, produces more mitochondria to increase metabolic endurance in response to aerobic exercise, maintains a balance of protein synthesis and degradation under normal physiological conditions and deconstructs itself to release amino acids in response to disuse or starvation (via autophagy and other protein degradation pathways discussed later). The deep interconnectedness of these pathways allows precise and bespoke adaptation of skeletal muscle which can be rapidly redirected or reversed in response to changes in physiological conditions (Reviewed in Flück 2006).

Disruption to, or inappropriate modulation of, these pathways can be both a direct cause of muscle pathology and a common hallmark in other muscle diseases (myopathies). Muscular dystrophies are so named for the dysregulation of muscle mass observed in these diseases. Muscle wastage in other contexts (cachexia) is associated with ageing - termed sarcopenia in this context - and a number of different pathologies including cancer and AIDS. As such, instances of dysregulated and unwanted muscle size adaptation contribute substantially to the morbidity burden of hundreds of millions of people worldwide (von Haehling, Morley, and

Anker 2010; von Haehling, Anker, and Anker 2016; Theadom et al. 2014). An increased understanding of the pathways that regulate muscle size and how they become impaired in ageing and disease will therefore be incredibly beneficial in the development of novel therapies designed to rescue, preserve and enhance muscle function.

Perhaps the most poorly understood aspect of muscle plasticity is how muscle is able to sense levels of physical force (mechanosensation) and translate these into the pathways that regulate muscle size (mechanotranslation). Physical loading of muscle is a highly potent inducer of muscle hypertrophy (Wong and Booth 1988) and it is known that this adaptation is reliant on the activity of molecular Target Of Rapamycin (mTOR) (Bodine, Stitt, et al. 2001), the activation of which promotes net deposition of protein via elevated protein synthesis and the inhibition of protein degradation. However, little is known about the upstream events that modulate mTOR activity in this context (Marcotte, West, and Baar 2015).

The potential importance of the kyphoscoliosis peptidase (KY) protein in this pathway was first observed in the *ky/ky* mouse - a model of recessive, hereditary kyphoscoliosis which arose spontaneously in inbred mice over 40 years ago (Venn and Mason 1986; Dickinson and Meikle 1973; Bridges et al. 1992). As discussed in further detail later, phenotypes from these mice suggest a disruption in the maintenance of postural muscles which experience consistent levels of high tension as well as a failure to induce hypertrophy in response to increased physical stress (G. Blanco et al. 2001). This suggests that the KY protein is necessary for mechanosensation and/or mechanotranslation in these contexts. The recent emergence of human cases of myopathy associated with KY deficiency underscores the importance of its function in muscle maintenance (Hedberg-Oldfors et al. 2016; Straussberg et al. 2016; Yogev et al. 2017). However, no valid function has yet been attributed to KY.

Other phenotypes in the mouse model suggest that impaired maintenance may in part be explained by an inability to efficiently turnover cytoskeletal crosslinkers such as Xin Actin Binding Repeat Containing 1 (XIRP1 - previously XIN) and Filamin C (FLNC) which are critical to the structural integrity of muscle (Beatham et al. 2006). FLNC is also a known interaction partner of the KY protein (Beatham et al. 2004). A mechanism of client-specific protein turnover termed Chaperone Assisted Selective

Autophagy (CASA), mediated in part by the chaperone CEL2 Associated Athanogene 3 (BAG3) has been proposed for the turnover of FLNC irreversibly unfolded by contractile tension (Ulbricht et al. 2013, 2015; Arndt et al. 2010). This pathway is also linked to the elevated synthesis of replacement FLNC protein. This association between KY and FLNC generated the hypothesis that KY may play a role in this maintenance mechanism. This thesis aims to examine CASA in the *ky/ky* mutant mouse and generate additional zebrafish and myoblast (C2C12) models of KY deficiency to provide novel experimental avenues to interrogate the function of the KY protein.

1.2 - Structure of Skeletal Muscle

1.2.1 - Skeletal muscle structure

Skeletal muscle has a highly organised structure that can be broadly thought of as a nested set of bundles, each bound in connective tissue to enhance the overall structural integrity of the muscle (Figure 1.1). The main body of skeletal muscle is composed of a number of parallel fascicles, each of which is composed of a bundle of multinucleated muscle fibres, each of which is composed of bundles of myofibrils. Myofibrils are composed of repeating contractile units running in series along their length, termed sarcomeres. Muscles are connected to each other and to bone by tendons and filaments respectively, which transmit the physical force of contraction to produce movement.

The sarcomere is the fundamental contractile unit of skeletal muscle. The main contractile apparatus consists of the thick myosin filaments and the thin actin filaments which are anchored and supported by a number of large structural proteins and smaller crosslinker proteins. Muscle contraction is mediated by actin and myosin filaments pulling against each other in a cross bridge cycle, shortening the length of the sarcomere thus generating a pulling force (Huxley 1957).

The actin thin filament is comprised of filamentous skeletal muscle alpha actin (ATCN1), isoforms of tropomyosin (TPM1-4) - which covers the myosin binding site of actin between contraction cycles (Parry and Squire 1973) - and troponin (TPNI/C), which displaces tropomyosin in response to increased levels calcium to expose the binding site. Nebulin (NEB) runs along the length of the filament and is thought to regulate the length of the filament during assembly

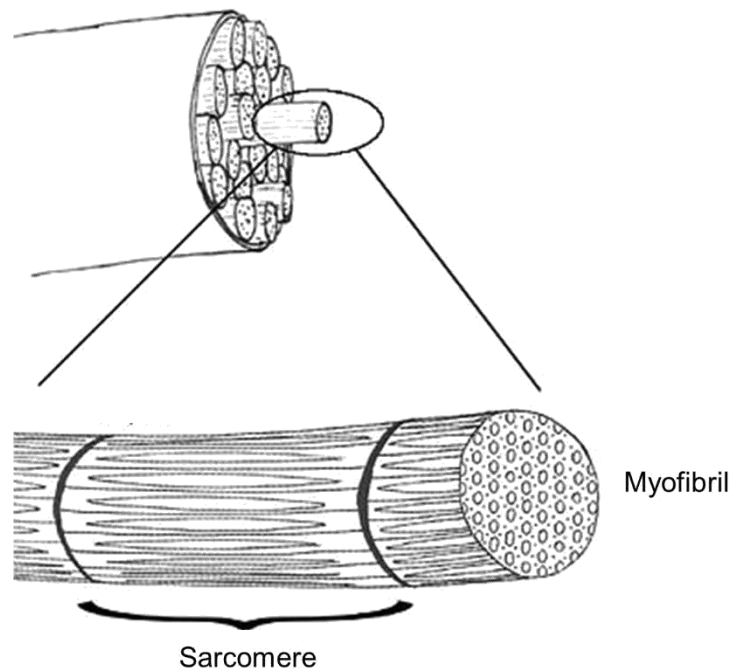
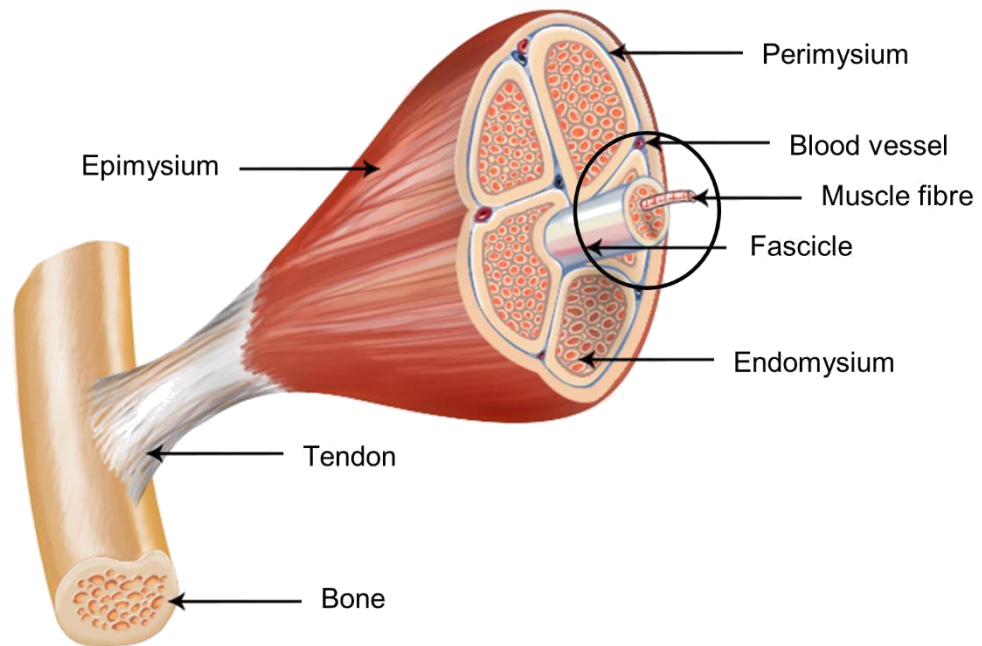


Figure 1.1 - Structure of skeletal muscle

Top - Skeletal muscle attached to a bone via a tendon. The outermost membrane, epimysium, contains a number of parallel fascicles, each of which is bound by perimysium. The fascicles are composed of a number of muscle fibres, each bound by endomysium. Bottom - each muscle fibre is composed of parallel myofibrils, composed of a series of sarcomeres.

Images obtained from https://commons.wikimedia.org/wiki/File:Skeletal_muscle.jpg and reproduced under the GNU Free Documentation License.

(McElhinny et al. 2005). The myosin filament is composed of a myosin heavy chain (MYHC), myosin essential light chain and myosin regulatory light chain (MYL) and myosin binding protein C (MYBC). Different fast and slow isoforms of myosins are expressed in muscle tissue and the relative proportion of each isoform is understood to partially underlie the functional adaptations between fast-twitch and slow muscle types.

The sarcomere itself is subdivided into regions that can be distinguished in electron microscopy images due to the varying distribution of filaments and anchoring/crosslinking proteins (Figure 1.2 - top). The outermost boundary of the sarcomere is the z-disc, which acts as an anchor point for the actin filaments. A-actinin acts as the primary crosslinker for actin filaments, but a number of other crosslinker and structural proteins act to support the structure of the sarcomere during contractions, including FLNC. Though the z-disc was historically considered an inert structure, since the z-disc experiences contractile forces directly it is ideally suited as a site for mechanosensation. Indeed, several signalling proteins are known to reside at the z-disc and are modulated by muscle activity (Frank et al. 2006)

The z-disc is also anchored to the extracellular matrix (ECM) via a set of protein complexes collectively known as the costamere (Figure 1.2 - bottom). Proteins such as dystrophin and desmin link the sarcomere with integrins and ankyrins in the cell membrane which are in turn connected to ECM components such as collagen and proteoglycans (Peter et al. 2011). As discussed later, mutations in costameric components are often highly disruptive to skeletal muscle integrity and underlie a number of myopathies.

Moving inwards from each z-disc the I-bands are regions containing only actin filaments without any overlap from the myosin filaments. The A-band is the central region containing the myosin filaments and is itself composed of denser outer regions where the actin and myosin filaments overlap and a lighter inner region known as the H-band containing only myosin filaments. At the centre of the sarcomere is the M-line, a region containing crosslinking elements such as myomesin.

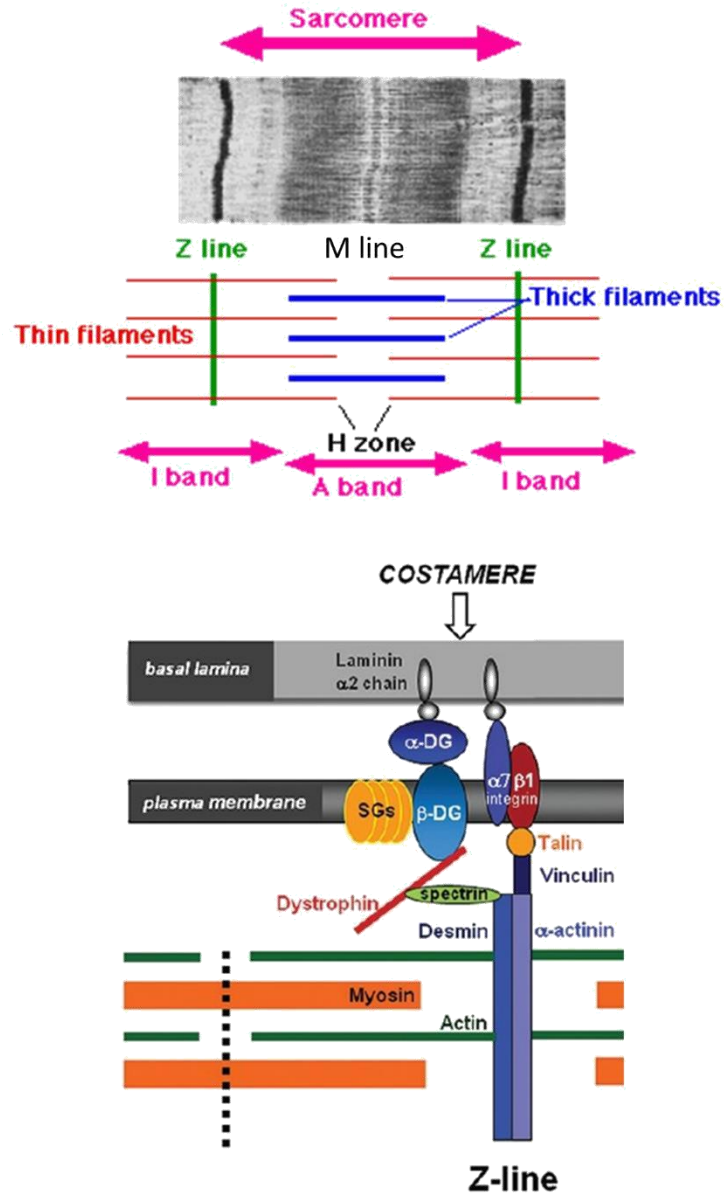


Figure 1.2 - Diagram of the sarcomere and costamere

Top - Diagram of the sarcomere. Image adapted from <https://commons.wikimedia.org/wiki/File:Sarcomere.gif> and reproduced under a creative commons license.

Bottom - Diagram of the costamere. Figure adapted from (Sabatelli et al. 2012) and reproduced under a Creative Commons Attribution-NonCommercial-ShareAlike License (CC BY-NC-SA)

Muscle fibres can be functionally subdivided into types according to the isoforms of MYHC they express, which help to adapt them to the specific physical demands of their muscle. Muscles used for voluntary movement are primarily composed of fast, glycolytic fibres (Johnson et al. 1973). These are best adapted to short bursts of physical activity, are more responsive to hypertrophic (G. Blanco et al. 2001) and autophagic (Mizushima et al. 2004) signalling pathways and are thought to have a higher rate of autophagic flow (Mofarrahi et al. 2013). Muscles used to maintain posture contain slow, oxidative fibres that are best adapted to continuous mechanical strain. These are less sensitive to hypertrophy and atrophy, typically being spared during starvation at the expense of fast muscle (J. B. Li and Goldberg 1976). Additionally, intermediate fibre types occupy the middle ground. The fibre type composition of a muscle can adapt according to the strains placed upon them, e.g. the adaptation towards slow muscle fibre types in the *ky/ky* mutant soleus to compensate for the lower muscle to body weight ratio (G. Blanco et al. 2001).

1.2.2 - Zebrafish muscle

The zebrafish (*Danio rerio*) is an increasingly popular model organism. The rapid and external development of embryos has made it particularly suited to Developmental Biology, particularly since the transparency of the embryo allows live imaging of cells and organs *in vivo* using a variety of imaging techniques, for example the observation of fluorescent reporter expression. This transparency also allows rapid assessment of muscle integrity by birefringence - highly structured muscle is capable of altering the polarisation of light passing through it, whereas disordered regions of muscle cannot (Smith, Beggs, and Gupta 2013). Additionally, proteins and genetic constructs can easily be microinjected into embryos, allowing a variety of overexpression, knockdown and genome-editing experiments. Their short generation time and space-efficiency also lend themselves well to genetic studies.

The molecular and ultrastructural architecture of skeletal muscle in zebrafish is broadly identical to that in mammals. Indeed, orthologues have been identified for many key muscle proteins, including those implicated in human muscle diseases (Steffen et al. 2007). The bulk of zebrafish muscle is organised in discrete myotomes running in series along the vertebral column. In the adult fish, the discrete organisation of fast and slow muscle can be observed in cross section, with slow muscle fibres at the lateral periphery of the muscle tissue and fast muscle fibres forming the main bulk of the tissue.

Though the conservation of CASA in zebrafish has yet to be robustly established, models of filaminopathies (Bührdel et al. 2015; Ruparelia et al. 2012, 2016) and BAG3-related myopathies (Ruparelia et al. 2014) have been produced. These show disruption to sarcomeric integrity and the formation of protein aggregates, suggesting that at least some functions of these proteins may be conserved.

However, most studies of muscle disease in zebrafish examine phenotypes that are overt in the embryonic stages, typically because these models are identified in large scale genetic screening of mutagenised embryos or by knockdown of target genes using transient methods such as antisense morpholinos. As such, models of muscle pathology that emerge post-developmentally are scarce and little is understood about the impact of muscle disease later in the life cycle of the zebrafish. In addition progressive spinal deformities arise naturally in zebrafish populations as they age, which may also confound attempts to examine more subtle muscular phenotypes (Gilbert, Zerulla, and Tierney 2014) .

1.2.3 - The C2C12 myoblast model

The C2C12 cell line is a subclone of a mouse myoblast line originally derived from satellite cells obtained from the muscles of a C3H strain mouse (Yaffe and Saxel 1977). C2C12 myoblasts will undergo differentiation in response to serum withdrawal from culture medium, forming myotubes with sarcomeric structures. The C2C12 line has therefore become a powerful tool for exploring muscle differentiation (Burattini et al. 2009). It is also used widely in studies of muscle physiology, including studies of hypertrophy and atrophy (Sharples, Al-Shanti, and Stewart 2010) and muscle protein turnover (Zhao et al. 2007).

1.3 - Skeletal Muscle Hypertrophy

Skeletal muscle hypertrophy is an increase in muscle mass mediated by the growth in size of muscle fibres due to a net deposition of protein. This process is distinct from an increase in the number of muscle fibres (hyperplasia). Though hyperplasia can contribute to increases in muscle mass, this thesis focuses specifically on the hypertrophic pathway.

1.3.1 - Loading induced hypertrophy is independent of the IGF-1/AKT axis

The primary signalling axis for skeletal muscle hypertrophy has traditionally been thought of as the Insulin-like Growth Factor 1 (IGF-1)/ Protein Kinase B (AKT)/mTOR pathway (Velloso 2008) (Figure 1.3). IGF-1 is a growth hormone synthesised primarily by the liver in response to pro-growth signalling mediated by Growth Hormone (GH) (Mauras 1997). IGF-1 binding to its tyrosine kinase receptor (IGF-1R) leads to the phosphorylation of Insulin Receptor Substrate 1 (IRS-1) which in turn leads to the activation of Phosphatidylinositol 3 Kinase (PI3K) and AKT (Rommel et al. 2001). AKT regulates a number of different substrates and acts as one of the hubs for crosstalk between protein synthesis and degradation pathways. AKT activation of the mTORC1 complex leads to the phosphorylation of proteins involved in protein synthesis, for example ribosomal protein s6 kinase beta-1 (p70s6K) which leads to enhanced mRNA elongation. In addition, the activated mTORC1 complex inhibits autophagy, for example via negative regulation of Unc-51 Like autophagy activating Kinase 1 (ULK1), a positive regulator of autophagosome membrane biogenesis (J. Kim et al. 2011). The result of this is the net deposition of proteins, leading to an increase in muscle fibre hypertrophy.

Many physiological cues positively feed into this signalling axis at various entry points, including high levels of intracellular amino acids, propagation of nervous impulses and physical stresses. Mechanical loading is one of the most potent inducers of hypertrophy. Activation of mTOR has been demonstrated to be necessary for a hypertrophic response to mechanical loading, with rapamycin treatment preventing hypertrophic adaptation (Drummond et al. 2009). However, this activation of mTOR has been demonstrated to occur independently of IGF-1 and AKT activation. This was first shown by the inability of dominant negative IGF-1R expression to prevent hypertrophic responses in this context (Spangenburg et al. 2008). In addition, the activation of mTOR has been shown to occur independently of AKT activation (Hornberger et al. 2004; Spangenburg et al. 2008) and prior to activation of AKT in synergistic muscle ablation experiments (Miyazaki et al. 2011). Thus the immediate mechanosensors and mechanotranslators that feed into mTOR activation have yet to be fully characterised.

- Growth factors
- High amino acid availability
- Physical activity
- Mechanical tension

- Paralysis
- Starvation
- Denervation

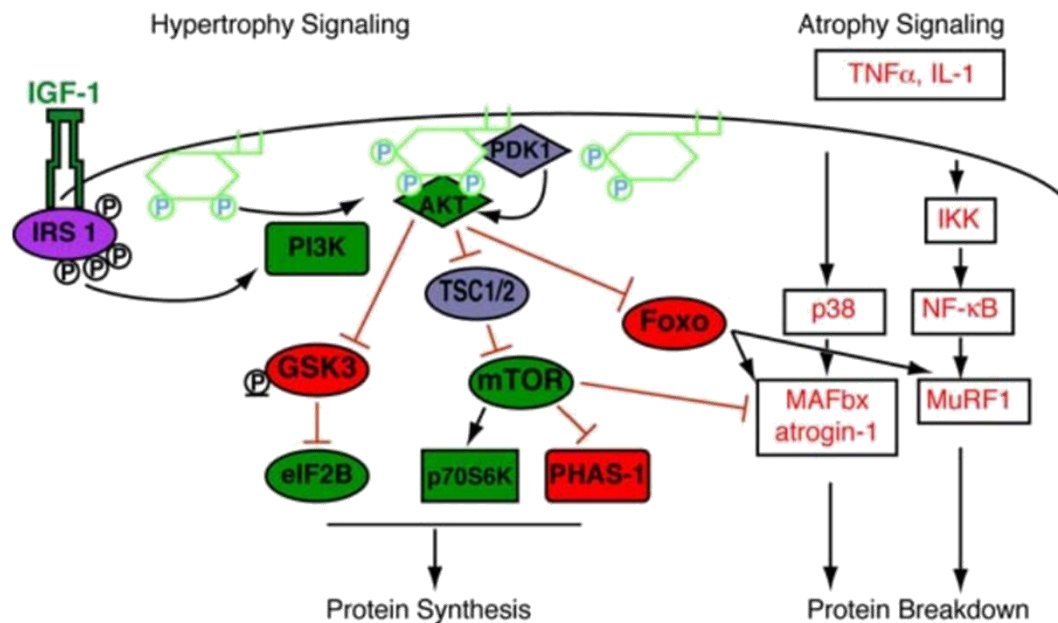


Figure 1.3 - Hypertrophic and atrophic signalling pathways

Schematic of hypertrophic and atrophic signalling pathways, with positive regulators/effectors of hypertrophy in green and positive regulators/effectors of atrophy in red.

Adapted from (Glass 2005) with permission. Copyright © 2005 Elsevier Ltd. All rights reserved.

1.3.2 - MAPK signalling modules

The near-immediate activation of various Mitogen Activated Protein Kinase (MAPK) signalling modules have been shown to correlate to different types and intensities of physical activity (Aronson et al. 1997; Martineau and Gardiner 2001; Kramer and Goodyear 2007). It has therefore been proposed that the relative activation of different MAPK signalling modules downstream of cellular stress, generated non-specifically by the damage and metabolic stresses induced during repeated muscle contraction, might underlie skeletal muscle hypertrophy and other adaptations without the need for a specific mechanosensing factor.

The three primary MAPK signalling modules which respond to physical activity in skeletal muscle are: -

- *Extracellular signal Related Kinase (ERK)*: Elevated phosphorylation of ERK has been shown to occur in response to exercise in a number of studies (Aronson et al. 1997; Nader and Esser 2001) and does so in proportion to the intensity of the exercise (Widegren et al. 2000). ERK is known to synergistically activate mTOR alongside AKT via the inhibition of tuberous sclerosis complex 2 (TSC2) - however this is at least partially in response to activation via IGF-1, thus it is unclear how important this pathway is in the IGF-1-independent hypertrophic process (Mendoza, Er, and Blenis 2011). ERK is known to positively regulate the transcription factor JunB Proto-Oncogene, AP-1 Transcription Factor Subunit (JUNB), the overexpression of which is sufficient to induce hypertrophy in mouse muscle (Raffaello et al. 2010).
- *p38 MAPK*: elevated phosphorylation of p38 has been shown in response to contraction (Aronson et al. 1997; Nader and Esser 2001). Effector pathways are proposed to include regulation of glucose transport and oxidative capacity.
- *c-JUN NH₂-terminal Kinase (JNK)*: JNK appears to be proportionally increased by the magnitude of mechanical force experienced by muscle, potentially indicating a more direct link between mechanical forces and its activation (Martineau and Gardiner 2001). Effector pathways include JUN and FOS, which have roles in the regulation of apoptosis, inflammation and cell proliferation (Aronson et al. 1998; Aronson, Dufresne, and Goodyear 1997).

Though MAPK signalling plays an essential role in skeletal muscle adaptation to exercise, the hypothesis that these pathways represent the main pathway to tension-induced skeletal muscle hypertrophy is not supported by strong evidence. The precise mechanisms by which these signalling modules are activated are not well defined and thus a primary mechanosensing factor cannot be excluded. Additionally, the hypertrophy observed due to overexpression of JUN is not sufficient to demonstrate that the endogenous ERK-JUN pathway is able to induce hypertrophy or is the pathway responsible in loading induced hypertrophy.

1.3.3 - Myostatin and hypertrophy

Myostatin (MSTN) is a negative regulator of muscle growth, acting primarily to limit myoblast proliferation during development (McPherron, Lawler, and Lee 1997).

Inhibition of the MSTN pathway has therefore been adopted as a model of hypertrophy. MSTN prevents hyperplasia and hypertrophy by the transcriptional repression of myogenic factors, including Myoblast Determination protein 1 (MYOD1) and myogenic factor 5 (MYF5), via SMAD2/3 (Trendelenburg et al. 2009; Langley et al. 2002). Animals with MSTN mutations show significant increases in muscle mass due to the release of this repression (McPherron, Lawler, and Lee 1997). Though there is some evidence that the muscles have impaired force generation when the mutations are present from birth (Amthor et al. 2007), experiments targeting MSTN in adult mice show increased muscle mass and strength, indicating that impaired force generation may be the result of developmental perturbations rather than an impact on adult physiology (Whittemore et al. 2003). However, the relevance of this pathway to hypertrophy induced by mechanical stress is unclear.

1.4 - Skeletal Muscle Atrophy

Skeletal muscle atrophy is the decrease in muscle fibre size and mass due to net loss of protein. Atrophy can be triggered in a variety of ways, including denervation, starvation and hindlimb suspension. Additionally, atrophy is a hallmark in the majority of myopathies and is a clinical feature of ageing (Bonaldo and Sandri 2013). Broadly these physiological cues result in the repression of AKT by various means, resulting in the dephosphorylation and nuclear translocation of Histone Deacetylase 1 (HDAC1). This promotes the activity of forkhead box transcription factors (FOXO), which promote the expression of genes regulating atrophic and autophagic processes (Beharry et al. 2014) (Figure 1.3) (discussed in more detail below).

1.5 - Protein Turnover Mechanisms

The two primary protein degradative pathways are the Ubiquitin-Proteasome System (UPS) and the autophagy-lysosomal pathway. Though both processes are upregulated during skeletal muscle atrophy (Mizushima et al. 2004; Medina et al. 1991; Zhao et al. 2007), an efficient baseline of protein degradation is also essential to normal muscle physiology during mass maintenance (Masiero et al. 2009), allowing the turnover and replacement of damaged proteins and organelles.

1.5.1 - The Ubiquitin-Proteasome System

The UPS pathway targets proteins for degradation via the activity of ubiquitin ligases. E1 ubiquitin ligases obtain a ubiquitin molecule, which is transferred to an E2 ubiquitin ligase. E2 ubiquitin ligases form a complex with E3 ubiquitin ligases, which complex with the target protein, allowing the addition of ubiquitin chains that promote the transport of target proteins to the proteasome where they are unfolded and cleaved into short amino acid chains (reviewed in Lecker, Goldberg, and Mitch 2006). The primary E3 ubiquitin ligases in skeletal muscle are muscle specific ring finger protein 1 (MURF1) and Atrogin, which are upregulated in response to atrophic cues such as physical inactivity, starvation and denervation (Bodine, Latres, et al. 2001). Larger sarcomeric proteins are known to first go through an initial cleavage process into smaller fragments, presumably to increase the efficiency of subsequent unfolding and cleavage by the proteasome, e.g. the cleavage of titin by calpain-1 (Lim et al. 2004).

1.5.2 - Autophagy

Autophagy encompasses a number of different processes that involve the capture and degradation of target material in a membrane bound compartment. The three types of autophagy are characterised as macroautophagy, microautophagy and Chaperone Mediated Autophagy (CMA).

In macroautophagy, target material is captured in an autophagosome prior to fusion of this compartment with the degradative lysosome. This process can be non-selective, for example during starvation to release metabolites from unused proteins/organelles or triggered by specific processes for the removal of damaged material, e.g., the targeting of damaged mitochondria during mitophagy (Klionsky 2007).

In microautophagy, cytoplasmic material is non-selectively captured directly by the lysosome via the invagination of the lysosomal membrane (reviewed in Klionsky et al. 2016).

CMA is a process by which a specific type of protein is directed to the lysosome via the activity of the chaperone Heat Shock Cognate 70 (HSC70). HSC70 binds to proteins with an available KFERQ peptide motif which may be exposed under specific circumstances such as the partial unfolding of the protein. The chaperone-protein complex is then directed to the lysosomal surface where the protein is

bound, unfolded and translocated into the lysosome via the Lysosomal Associated membrane protein 2A (LAMP2A) (reviewed in Klionsky et al. 2016).

Chaperone Assisted Selective Autophagy (CASA) is a proposed mechanism for the degradation of specific client proteins via the macroautophagy pathway (Arndt et al. 2010; Ulbricht et al. 2013) (Figure 1.4). This pathway has primarily been characterised using rat smooth muscle cells and in the context of the client protein FLNC, though there is some evidence to suggest this process may operate in other cell types and for other client proteins.(Ulbricht et al. 2013). Limited characterisation has also been undertaken in human muscle biopsies, indicating that the components of CASA are adaptively upregulated in response to repeated resistance training (Ulbricht et al. 2015).

The mechanism is activated when mechanical tension leads to the irreversible unfolding of the FLNC protein. This exposes KFERQ motifs which can be recognised by the chaperone proteins HSC70 and Heat Shock Protein family B member 8 (Hspb8). These in turn recruit the chaperone Bag3, which is upregulated in response to the tension-induced activation of Heat Shock Factor 1 (HSF1). BAG3 is proposed to help solubilise the protein complex from the cytoskeleton to allow translocation to the autophagosome, with the addition of recombinant BAG3 to skeletal muscle extracts being sufficient to increase the proportion of FLNC in the soluble fraction. CHIP, an E3 ubiquitin ligase, is also recruited to the complex, and ubiquitinates the client protein. However, since CHIP deficiency is not sufficient to induce muscle pathology and the authors argue that this process is essential for muscle maintenance, it is argued that there may be some redundancy between E3 ubiquitin ligases. The entirety of the complex is then fed into the autophagosome via the adaptor protein p62 and degraded (Ulbricht et al. 2013; Arndt et al. 2010).

In parallel to the degradation of damaged FLNC, soluble Bag3 inhibits the inhibitors of YAP/TAZ signalling, resulting in elevated *Flnc* transcription. This mechanism therefore promotes the synthesis of new FLNC to replace that which is damaged and degraded. Thus CASA is proposed to maintain the health of skeletal muscle tissue by preventing the formation of insoluble crosslinker aggregates which may result in elevated cell stress, as well as maintaining (and potentially enhancing) the structural stability of the sarcomere by replacing damaged cytoskeletal crosslinkers. The adaptive upregulation seen in resistance-trained humans may therefore allow

this process to occur more efficiently to minimise the burden of mechanical stress on muscle tissue (Ulbricht et al. 2015).

Though there is reasonable evidence to suggest that CASA operates in skeletal muscle, including the upregulation of CASA components in muscles in response to exercise and disease (Ruparelia et al. 2016; Ghaoui et al. 2016; Sarparanta et al. 2012), this process has yet to be robustly examined within an actual skeletal muscle context. As such, the present model have may limitations, for example the inability to identify skeletal muscle specific factors which may have a role in this pathway.

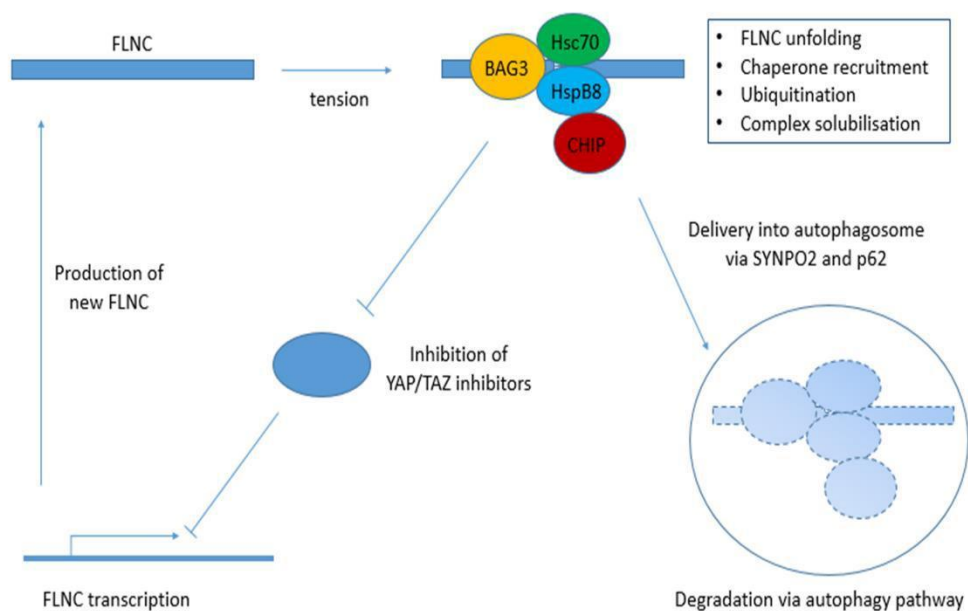


Figure 1.4 - Simplified diagram of Chaperone Assisted Selective Autophagy

Top left to right - FLNC unfolds due to tension, leading to the recruitment of the chaperone complex and resultant ubiquitination and solubilisation of the complex. This is delivered to the autophagosome for degradation via the autophagy pathway (bottom right). Soluble BAG3 inhibits inhibitors of YAP/TAZ, resulting in elevated flnc transcription

1.5.3 - The relative importance of UPS and autophagy in muscle maintenance

An understanding of the relative contribution of the UPS and autophagy to maintaining muscle health will help to determine where therapeutics might be most effectively directed. Studies examining the relative importance of autophagy and UPS regulation in maintaining muscle health have historically considered the UPS

to be more important. In models of atrophy, inhibition of the UPS is able to preserve muscle mass, indicating that the activation of the UPS is the primary driver of protein loss during atrophy (Caron et al. 2011; Beehler et al. 2006). In contrast, inhibition of autophagy is itself sufficient to promote atrophy (Masiero et al. 2009; Masiero and Sandri 2010), indicating autophagy inhibition is a less viable therapeutic candidate for preventing atrophy. However, given the coordinate upregulation of both autophagy and the UPS by FOXO transcription factors in this context (Zhao et al. 2007) it seems probable that autophagy contributes somewhat to enhanced protein degradation in atrophy.

In the context of upregulating protein degradation in response to mechanical tension and enhanced physical activity, the balance of evidence suggests autophagy is more critical. This is intuitive in the case of mitochondrial turnover to replace mitochondria damaged by increased metabolic stresses, which simply cannot be achieved via the UPS. Since degradation of proteins via the proteasome requires protein unfolding, autophagic systems are more suited to deal with insoluble aggregates of damaged proteins. The proposed mechanism behind an adaptive shift towards autophagy is the 'BAG1/BAG3 switch'. Chaperone complexes containing BAG1 tend to direct degradation via the UPS whereas complexes containing BAG3 tend to direct degradation towards autophagy pathways, with elevated BAG3 associated with increased bias towards degradation via autophagy in ageing (Gamerding, Hajieva, and Behl 2009; Minoia et al. 2014). Since BAG3 is upregulated by mechanical tension in response to HSF-1, this increase may mediate a shift towards autophagic degradation when muscle tissue is stimulated by elevated tension.

1.5.4 - Demand for autophagy varies by muscle type

Given that the different muscle types (glycolytic/fast-twitch/phasic; mixed; oxidative/slow/tonic) have different physiological demands placed upon them. It is unsurprising that basal autophagy levels vary between different muscle types. Basal autophagy is required to continuously clear out damaged and unfolded proteins, protein aggregates and worn-out organelles such as mitochondria. Muscles experiencing continuous tension may therefore be expected to have a higher level of basal autophagy as an adaptation to the presumptive increase in protein damage and metabolic strain. This may in part explain differences between muscle groups in terms of the pathological impact of myopathy. It has been shown that the expression

of autophagy and mitophagy proteins is significantly higher in tonic, oxidative muscle when compared to a muscle of mixed fibre types or a phasic, glycolytic muscle (Lira et al. 2013). This study concluded that oxidative muscles have a higher autophagic flux, with increased microtubule associated protein 1 light chain (LC3) LC3-II/LC3-I ratios and lack of p62 (also known as SQSTM1) accumulation, indicating elevated autophagosome turnover. The data underlying this conclusion are supported by the relative levels of LC3-II and p62 protein and mRNA in oxidative and glycolytic muscles of the control group in a different study (Mofarrahi et al. 2013) and the reports agree that highly oxidative muscles have higher levels of mitophagy proteins.

A criticism of (Lira et al. 2013) is that their study pursues an indirect way of estimating autophagic flux, generating interpretations from a snapshot of the relative levels of autophagy markers. It has been argued that flux is better measured directly by examining tissue response to autophagy inhibition, e.g. via colchicine treatment (Mofarrahi et al. 2013) and such approaches are considered more robust in published guidelines for interpreting autophagy assays (Klionsky et al. 2016). The effect of such inhibitors is to prevent the degradation of LC3-II, and measuring the resulting accumulation thus provides a measure of LC3-II synthesis rates. It is argued that the presence of greater amounts of autophagy proteins may not necessarily correlate with high protein turnover. A study using the inhibitor approach concluded that glycolytic muscles have higher autophagic flux (Mofarrahi et al. 2013), contradicting the interpretations in (Lira et al. 2013). However, this approach may not be suitable in the context of examining relative baseline autophagy levels given that blocking autophagy itself is likely to induce aberrant signalling responses in muscle tissues which may vary in intensity and responsiveness between muscle types, particularly with prolonged colchicine treatments. A recent study in macrophages has proposed that colchicine functions to activate AMPK by promoting phosphorylation of liver kinase B1 (LKB1) (Wang et al. 2016). Since fast-twitch muscles are more sensitive to the induction of autophagy, possibly due to higher levels of ULK1 protein allowing rapid activation of LC3-II biosynthesis (Mizushima et al. 2004; Mofarrahi et al. 2013), the use of colchicine is likely to overestimate genuine basal flux in fast-twitch muscles. Shorter treatments with leupeptin are used to provide similar flux measurements. Because of their relative brevity such measurements are likely to be more robust than those obtained using colchicine, but the question of how well tissues with varying sensitivities to autophagy induction can be compared via this method remains unclear. Until this

bias can be controlled for, using snapshots of autophagy markers may represent the more reliable way of estimating comparative basal autophagy between muscle types.

1.6 - Structural Proteins and Muscle Disease

Structural integrity is critical for skeletal muscle to be able to withstand and transmit contractile forces. Mutations in genes encoding key structural components are therefore highly likely to impair muscle function, leading to reduced muscle strength and higher susceptibility to muscle damage. Indeed, examples of such myopathies can be found affecting nearly every structural component of the sarcomere and associated complexes (Hwang and Sykes 2015): -

- **Actin filaments:** at least 177 pathological mutations in actin alpha 1 (ACTA1) have been characterised (Laing et al. 2009) resulting in a range of disorders including nemaline, intranuclear rod and actin filament aggregate myopathies. These are clinically severe, sometimes resulting in fatality. Mutations in isoforms of tropomyosin and troponin are associated with nemaline myopathy (Donner et al. 2002; Lehtokari et al. 2006). Over 60 pathological mutations have been discovered in nebulin (Lehtokari et al. 2006). Mutations in the actin crosslinker FLNC result in a collection of myopathies under the category filaminopathies (Fürst et al. 2013).
- **Myosin filaments:** Myosinopathies are a family of disorders resulting from mutations in MYHC isoforms (Tajsharghi and Oldfors 2013). Severity and onset of muscle pathology depends on the affected isoforms, but many examples share features such as formation of protein aggregates, indicating impaired turnover of unfolded proteins. Mutations in myosin essential light chain and myosin regulatory light chain also result in myopathy (Poetter et al. 1996). Mutations in skeletal MYBC result in arthrogryposis (Markus et al. 2012; Xuefu Li et al. 2015)
- **Costameric proteins:** Disruption to proteins anchoring the sarcomere to the cell membrane and extracellular matrix severely impede muscle function. The most famous example is dystrophin, mutations in which underlie Duchenne's (DMD) and Becker's muscular dystrophies. DMD is an X-linked condition resulting in the absence of dystrophin protein. This affects males with an incidence of approximately 1 in 5000. Onset occurs in early childhood, primarily affecting the upper legs and hips before progressing to

the upper arms. This results in mobility issues by early adolescence. By late adolescence, respiratory muscle impairment results in the need for respiration assistance (Nowak and Davies 2004). Dystrophin is thought to be critical for the maintenance of the muscle fibre cell membrane. Recent research also suggests that dystrophin is critical for the correct polarisation of satellite cells during muscle repair, leading to an impaired ability to regenerate damaged muscle (Dumont et al. 2015). Becker's is a less severe form resulting from truncations and in frame deletions in dystrophin, allowing some retention of function.

1.7 - Protein Turnover and Muscle Disease

The importance of efficient protein turnover is illustrated by the effects of impaired protein turnover on skeletal muscle. The list of genes associated with neuromuscular disorders is significantly enriched in those annotated to have some functional relationship with autophagy (Jokl and Blanco 2016). Mutations which disrupt basal and induced autophagy have an impact on skeletal muscle homeostasis, with skeletal and cardiac muscle often being the most affected tissues in systemic autophagic defects (Figure 1.5 and Table 1.6). The same enrichment was not found for genes associated with the UPS.

Induction of autophagy occurs rapidly after exercise (He et al. 2012) and is achieved via the dissociation of Beclin-1 and B-Cell Lymphoma 2 (BCL2) due to BCL2 inactivation via phosphorylation in the endoplasmic reticulum (Pattingre et al. 2005) at three key residues (Thr69, Ser70, Ser84) (Wei et al. 2008). The dissociated Beclin-1 then interacts with vacuolar protein sorting-associated protein 34 (VPS34), which functions to nucleate autophagosome membrane synthesis (Kihara et al. 2001). Mice with a knock in mutation of the phosphorylation residues prevents the dissociation of Beclin-1 and BCL2, thereby preventing the induction of elevated autophagy, though basal levels of autophagy remain (He et al. 2012). This was shown to result in impaired exercise endurance, reduced maximal running distance and impaired glucose metabolism following chronic exercise and a high fat diet. These results indicate that the ability to rapidly induce autophagy plays a key role in maintaining muscle performance. However, other studies with more precise methodologies have failed to confirm these results, including Beclin-1 heterozygous mice (Lira et al. 2013) and constitutive (K. H. Kim et al. 2013) and inducible muscle-specific deletion of Atg7 (Lo Verso et al. 2014). Autophagy related 7 (ATG7) is an

E1-like enzyme responsible for the activation of the E3-like ubiquitin ligase autophagy related 5 (ATG5) to form a complex with autophagy related 12 (ATG12). This is required for the conjugation of phosphatidylethanolamine to LC3-I to form LC3-II (Tanida et al. 2001). These studies found no evidence of changes to acute exercise performance or glucose homeostasis, undermining the argument that inducible autophagy is critical for muscle health. However, accumulation of damaged mitochondria was observed, alongside a failure to improve endurance in measurements of maximal treadmill running distance (Lira et al. 2013). In addition, neuromuscular junction degeneration is observed in muscle-specific ATG7 knockout mice (Carnio et al. 2014), indicating that impaired basal autophagy leads to early signs of ageing.

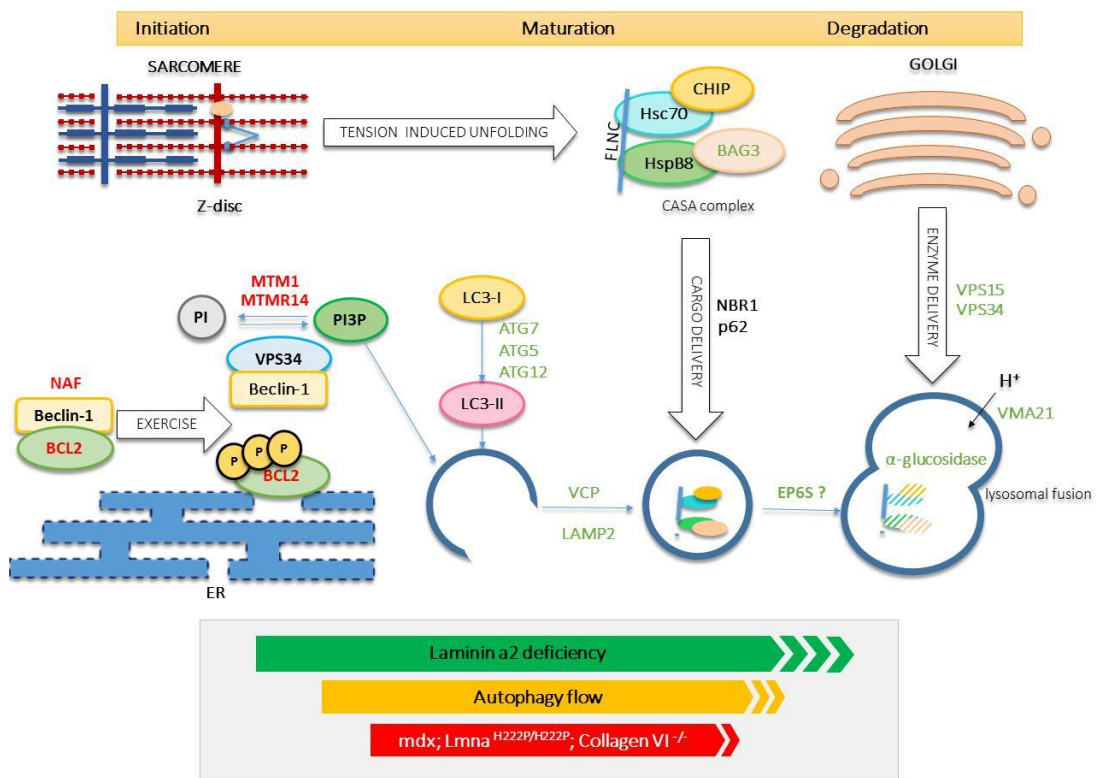


Figure 1.5 – Schematic of disrupted autophagy processes relating to skeletal muscle disease

Disruption of many genes with roles in autophagy result in muscle disease, indicating the importance of functional autophagy in skeletal muscle health. These genes are distributed in virtually all stages of autophagy, including exercise-induction via phosphorylation of BCL2, response to sarcomeric protein unfolding via the CASA pathway as well as autophagosome biosynthesis and maturation. Genes with green text indicate promoters and components of the autophagy pathway, and red text indicates negative regulators of autophagy, whose disruption is known to result in muscle pathology. In addition, upregulation of autophagy (e.g. laminin a2 deficiency) and downregulation of autophagy (e.g. collagen VI $-/-$) have been shown to play a role in the pathogenic mechanism of certain muscle diseases.

Reproduced from (Jokl and Blanco 2016) with author's permission

Defects in later stages of autophagy are also known to result in muscle pathology. X-linked myopathy with excessive autophagy (XMEA) is caused by haploinsufficiency in vacuolar ATPase assembly factor (VMA21), a transmembrane subunit of the V-ATPase lysosomal protein channel. This leads to an elevated pH in the lysosome, impairing degradation. The disruption to protein degradation leads to a reduction in free amino acids, inhibiting mTOR activation and resulting in excessive autophagy activation, resulting in the net loss of muscle mass (Ramachandran et al. 2009). Danon disease is caused by mutations in LAMP2, a major component of the lysosomal membrane which is essential for the fusion of the autophagosome and lysosome, though the proteolytic capacity of the lysosome is unaffected (Eskelinen et al. 2004, 2002) . This results in the accumulation of unfused autophagic vacuoles with sarcolemmal features (Nishino et al. 2000), especially in skeletal and cardiac muscle (Sugie et al. 2002).

Pompe disease is an accumulation of glycogen due to mutations in acid maltase that prevent lysosomal degradation. This leads to buildup of autophagosomes and muscle atrophy. In human cases, this manifests as an accumulation of p62 puncta and atrophy. It has been proposed that the early elevation of autophagy activation is a cell protective mechanism which backfires when autophagosome and glycogen accumulation becomes chronic. Again, skeletal and cardiac muscle are among the most affected tissues (Nascimbeni et al. 2012).

VICI syndrome is caused by mutations in ectopic p-granules autophagy protein homolog (EPG5). The molecular function of EPG5 is unknown, but its absence leads to the accumulation of autophagosomes, evidenced by buildup of p62 and LC3-II in patient-derived fibroblasts, indicating a failure in either autophagosome-lysosome fusion or degradation (Cullup et al. 2013; Tian et al. 2010).

Mice lacking BAG3 show a severe and fatal myopathy with some parallels to the *ky/ky* pathology. These mice have smaller, weaker muscles with the postural muscles being most affected. Muscle tissue appears healthy in embryonic stages, with postnatal onset of muscle damage suggesting that the onset of mechanical activity and gravity-induced tension causes damage that cannot be effectively repaired (Homma et al. 2006). The emergence of this mouse model predated the emergence of the CASA hypothesis, thus FLNC turnover was not examined in these mice. Given the central role proposed for BAG3 in the CASA mechanism, it is possible that disruption to CASA prevents efficient muscle maintenance under

tension, leading to myopathy. However, a structural role for BAG3 has also been proposed in the stabilisation of myofibers under tension along with Hsc70 and capping actin protein of muscle z-line (CAPZ). It is proposed that the absence of BAG3 leads to the improper localisation of CAPZ, which is degraded via the proteasome (indicating this is not another client of the CASA pathway) (Hishiya, Kitazawa, and Takayama 2010). This means that the pathological changes observed due to BAG3 deficiency may reflect structural instability resulting from CAPZ mislocalisation as opposed to impaired protein turnover.

Mutations in myotubularins, responsible for the inhibition of lysosomal membrane biosynthesis, result in impaired autophagy inhibition and myopathy (Fetalvero et al. 2013), with mutations in myotubularin 1 (MTM1) and myotubularin related protein 14 (MTMR14) causing X-linked myotubular myopathy (Laporte et al. 1997) and congenital disease centronuclear myopathy (Tosch et al. 2006) respectively. Mutations in valosin containing protein (VCP), required for autophagosome maturation, result in inclusion body myopathy (Custer et al. 2010; Tresse et al. 2010).

As well as mutations in autophagy components contributing to myopathies, altered protein turnover is a common hallmark in muscle diseases, often exacerbating the underlying mechanism of disease. In mdx mice and patients with Duchenne's Muscular Dystrophy, autophagic flow is impaired (De Palma et al. 2012; Eghtesad et al. 2011; Pauly et al. 2012). Mutations in Lamin A (LMNA) result in Emery-Dreifuss muscular dystrophy, where enhanced mTORC1 signalling results in reduced autophagy (Ramos et al. 2012; Choi et al. 2012). Collagen VI (COL6A) mutations in mice lead to impaired autophagy activation and flow.(Grumati et al. 2010). In these cases, enhancing autophagy by inhibiting mTOR ameliorates the disorder. In the other direction, mouse models of Laminin- α 2 deficiency leads to upregulation of autophagy components, and the inhibition of autophagy ameliorates the dystrophy in this instance (Carmignac et al. 2011).

These examples illustrate the critical nature of effective and well-balanced protein degradation in maintaining healthy muscle as well as a tight correlation between muscle disease and perturbations in protein turnover mechanisms. Thus the modulation of protein degradation pathways has become a focus for therapeutics, albeit in contradictory directions depending on the specific hallmarks of pathology.

Inhibition of the UPS helps to improve the dystrophic phenotype in the mdx mouse model (Assereto et al. 2006; Gazzero et al. 2010; Bonuccelli et al. 2007), as does activation of autophagy (De Palma et al. 2012; Pauly et al. 2012). This likely reflects the distinct roles of each pathway. If the UPS is the primary effector of atrophy, blocking this process prevents the deconstruction of the muscle architecture. If atrophic signalling is in part induced by high cellular stress, elimination of damaged organelles and protein aggregates via enhanced autophagy will serve to alleviate these stresses. Increasing autophagy helps to clear protein aggregates and damaged organelles in other animal models (Rodríguez-Navarro et al. 2010; Schaeffer et al. 2012; Ruparelia et al. 2014). The target, direction and efficacy of this modulation will depend on the specific state of protein turnover in each pathology.

Table 1.6 – Genes associated with skeletal muscle pathology with evidence of autophagy disruption

Reproduced from (Jokl and Blanco 2016) with author's permission

Gene	Disease/model	Evidence of autophagy disruption
VMA21	X-Linked Myopathy with Excessive Autophagy (XMEA)	Reduced lysosomal proton influx
LAMP2	Danon disease	Autophagosome accumulation
GAA	Pompe disease	Impaired autophagosome-lysosome fusion
EPG5	VICI syndrome	Autolysosome clearance defect
MDX	Duchenne muscular dystrophy	Impaired autophagy signalling
LMNA	Emery-Dreifuss muscular dystrophy	Enhanced mTORC1 signalling resulting in inhibited autophagy
MTM1	X-linked tubular myopathy	Defects in autophagy inhibition
MTMR14	Congenital disease centronuclear myopathy	Defects in autophagy inhibition
VCP	Inclusion body myopathy	Altered autophagosome maturation
LAMA2	Mouse model	Constitutive upregulation of autophagy genes
COL6A	Mouse model	Impaired autophagy induction and flux
GNE	Hereditary inclusion myopathy	Ultrastructural evidence of autophagy and uncleared inclusions
KY	Hereditary kyphoscoliosis	Ultrastructural evidence of autophagy
SIL1	Marinesco-Sjogren syndrome	Impaired autophagic clearance
SOD1	Mouse model	Elevated oxidative stress resulting in constitutively elevated autophagy
DNAJB6	Limb girdle muscular dystrophy	Loss of autophagy co-chaperone
BAG3	Mouse model of fulminant myopathy	Central chaperone to Chaperone Assisted Selective Autophagy

ATG7	Inducible deletion/ muscle specific deletion	Accumulation of dysfunctional mitochondria
BCL2	Mouse knock in	Prevention of exercise induced autophagy
BECN1	Haploinsufficient mouse model	Impaired upregulation of autophagy
CISD2 (NAF-1)	Mouse model of Wolfram Syndrome 2	Enhanced basal autophagy
VPS15	Autophagic vacuolar myopathy	Defects in late endosomal/lysosomal functions

1.8 - Identification and Characterisation of the *ky/ky* Mouse

1.8.1 The *ky/ky* mouse

The *ky/ky* mouse is a model of recessive, hereditary kyphoscoliosis which arose spontaneously in the BDL mouse strain (Dickinson and Meikle 1973). This was demonstrated to be the result of a GC deletion in the *Ky* gene at codon 24, which results in a premature stop codon at position 105 and the absence of *KY* protein in homozygous mutant mice (*ky/ky*) (G. Blanco et al. 2001). Such mice develop an abnormal spinal curvature which is clearly evident by x-ray at 100 days of age. The decline in strength in the paraspinal muscles can be distinguished shortly after weaning (around 21 days old) by a failure to reach out and grasp a nearby ledge when suspended by the tail – a test known as a placing response (G. Blanco et al. 2001).

To date there has been no phenotype associated with embryonic development and it is not possible to distinguish *ky/ky* mice from their WT or heterozygous littermates by overt appearance at birth. During the phase of postnatal muscle growth, postural muscles experience a cycle of fibre death and regeneration, likely reflecting an inability to cope with the physical stresses associated with maintaining posture under the influence of gravitational forces, exacerbated by having a higher body weight to muscle mass ratio due to impaired muscle growth. After this, regenerating fibres can persistently be seen in postural muscles (Bridges et al. 1992; Venn and Mason 1986). These muscles also undergo an adaptive shift towards type-I fibres, likely to increase the resilience of these muscles to consistent high tension (G. Blanco et al. 2001). Electron microscopy of *ky/ky* muscles showed the accumulation of autophagic vesicles in the soleus in mice as young as 6 days old, which also emerge in other muscles experiencing consistent tension such as the gracilis and

diaphragm. Indicators of sarcomeric damage can be seen in the soleus muscle, including z-disc thickening and a-band streaming (Bridges et al. 1992).

Molecular phenotyping of the *ky/ky* mouse has demonstrated an upregulation of stretch response and energy-transducing mitochondrial proteins in the dystrophic soleus muscle (G. Blanco et al. 2004) as well as the upregulation of titin-associated signalling molecules and the cytoskeletal crosslinker XIRP1 (Beatham et al. 2006). The cytoskeletal protein FLNC also appears to accumulate and become mislocalised as the *ky/ky* mouse ages (Beatham et al. 2004). This response profile is comparable to muscles undergoing eccentric contraction (i.e. muscle lengthening under tension) and therefore may represent the increased mechanical load in proportion to the reduced size of muscle, particularly in the dystrophic soleus. It is apparent that the absence of KY leads to an impaired ability to maintain and repair muscle under consistent high tension.

Another phenotype of the *ky/ky* mouse is the inability to undergo loading induced hypertrophy in response to compensatory overload. Excision of the *tibialis anterior* (TA) leads to hypertrophy of muscle fibres in the EDL muscle in WT mice, but not *ky/ky* mice (G. Blanco et al. 2001). Given the EDL is a fast-twitch muscle which is relatively spared by the *ky/ky* pathology, this suggests a fundamental inability to translate mechanical tension into hypertrophic pathways which is not secondary to the atrophy and necrosis seen in postural muscle.

1.8.2 The KY protein

KY encodes a 72kDa protein which contains a transglutaminase-like domain between residues 171 and 282. This domain is the only characterised feature. The catalytic triad remains intact, though this may be misaligned, preventing protease function and meaning this domain may have instead been co-opted for protein-protein interactions (Anantharaman, Koonin, and Aravind 2001). However, extensive biochemical assays have yet to establish protease function (Baker et al. 2010). The protein sequence is highly conserved among mammals and has orthologues across vertebrates, suggesting it plays an important role in muscle physiology (Beatham et al. 2004).

KY interacts with immunoglobulin rich proteins at the z-disc, including fragments of titin and myosin binding protein (Baker et al. 2010). It is also known to interact with

the crosslinker FLNC and the novel protein immunoglobulin-like and fibronectin type III domain containing 1 (IGFN1) at the z-disc. The functional significance of this complex is unclear (Baker et al. 2010). IGFN1 is known to be upregulated in response to atrophic signalling (Chen et al. 2014), and repressed during hypertrophy (Rahimov et al. 2011). The IGFN1_v1 isoform has been shown to be needed for myoblast differentiation and fusion (Xiang Li et al. 2017). IGFN1 is also known to interact with mitogen-activated protein kinase 20 (MLTK), members of the MAPKKK family, with MLTK β being the primary isoform in skeletal muscle (Xiang Li 2017). MLTK overexpression has been shown to result in cardiac hypertrophy (Huang et al. 2004) via p38/JNK signalling (Hsieh et al. 2015), and *in vivo* overexpression of MLTKB in skeletal muscle also induces hypertrophy (Unpublished, personal communication).

1.9 - Human Myopathies Associated with KY deficiency

Three reports of human muscle pathology associated with homozygous disruption to KY have been published.

The first report examined a 7.5 year old girl with a homozygous deletion in the *KY* gene, resulting in a frame-shift. The clinical features of her pathology include walking difficulties, generalised muscle weakness, lordosis and contractures. MRI scans revealed atrophy and fatty infiltration in the gastrocnemius and soleus muscles. The vastus lateralis showed abnormal distribution of FLNC and XIRP1, which broadly co-localised in sarcomeric lesions. This muscle also showed variability in fibre sizes, with small fibres expressing foetal myosin isoforms. Electron microscopy revealed rod structures and thickened z-discs (Hedberg-Oldfors et al. 2016).

The second report examined two brothers, describing a progressive congenital myopathy resulting from a C>A base change, resulting in an early stop codon at the start of exon 6. The elder sibling was more mildly affected, showing foot deformities, mild atrophy and weakness of the lower limbs. He also developed tongue atrophy, elbow contractures and kyphosis. The pathology was more severe in the younger sibling, including bicep and tricep atrophy, learning difficulties, muscle cramps and elevated creatine phosphokinase. Electron microscopy detected streaming of the Z-disc and unstructured core targetoid defects. FLNC was shown to be accumulated in the core targetoid defects (Straussberg et al. 2016).

The third report details 12 Bedouin Israeli individuals homozygous for a disruptive single base insertion in the first exon of KY. The authors describe the condition as a congenital spastic paraparesis. Onset of pathology was apparent from 0-24 months, with spasticity of the lower limbs. Older patients showed kyphosis with variable scoliosis. Some patients had intellectual impairment. The authors report that KY is expressed in normal CNS tissue, albeit at lower levels than in skeletal muscle. They thus argue that the absence of KY may result in CNS impairment, accounting for the neurological aspects they observe in the pathology (Yogev et al. 2017). However, this contradicts the conclusions of (Hedberg-Oldfors et al. 2016) that expression was predominantly in skeletal muscle, which is also the case in the mouse, alongside some detection of transcript in the heart (G. Blanco et al. 2001). Muscle biopsies were not examined for the accumulation of FLNC.

These reports share marked similarities both to each other and to the mouse model, in particular the consistent involvement of FLNC when examined and involvement of primarily postural muscles. This indicates that the function of KY is highly conserved, demonstrates the importance of KY in human muscle physiology and shows the relevance of data generated from animal models of this pathology. The variability of the human pathology is likely to be at least partially accounted for by confounding accumulation of other mutations in highly inbred populations. Given that none of these reports indicates disruption to transcript levels by nonsense mediated decay, it may also be that the certain mutations are more likely to produce a truncated protein which may generate a gain of function effect.

1.10 - Additional Insights into KY

Ky expression in the mouse has been shown to have high periodicity at the mRNA level, with expression increasing during resting hours, peaking before the onset of active hours and declining consistently until resting resumes. Additionally, expression was shown to be much higher in the fast-twitch TA than the postural soleus, where expression remained consistently low. Denervation of muscle led to a reduction of *ky* expression loss of periodicity (Dyar et al. 2015). A rat model of post-synaptic paralysis also showed significant downregulation of *Ky* post-paralysis, increasing with the length of paralysis (Llano-Diez et al. 2011). A model of hypertrophy induction via myostatin inhibition showed a significant upregulation of *Ky* expression (Miao et al. 2015). Thus, *Ky* expression correlates positively with

hypertrophy, negatively with models of atrophy and yet appears to inversely correlate with physical activity in ordinary physiological conditions.

1.11 - Hypotheses for the Function of KY

A specific function for KY has yet to be established, and the present experimental evidence supports a number of different hypotheses.

KY as a protease: Though there is a distinct lack of positive evidence for a protease function, as well as putative misalignment of the active site, the question of whether KY might function as a protease has yet to be definitively answered. Co-expression of KY and FLNC constructs in vitro led to an apparent decrease in FLNC levels, indicating the possibility that KY might mediate or positively regulate the degradation of FLNC (Beatham et al. 2004). Large cytoskeletal proteins are sometimes cleaved into fragments to facilitate degradation, and KY might fulfil this role for cytoskeletal crosslinkers such as FLNC and XIRP1. However, this model seems unlikely as several efforts to specifically test this biochemically have failed to produce positive evidence.

KY as a solubilisation factor: A related hypothesis suggests that KY may function to help solubilise the protein complexes formed during the initial stages of protein degradation, e.g. the CASA complex to allow efficient degradation. The aberrant localisation of FLNC in the *ky/ky* mouse and human pathology suggest that there is at least some disruption to efficient FLNC turnover. The fact that KY and FLNC are interaction partners supports this hypothesis, and this hypothesis may be able to account for the decreased FLNC levels observed in the in vitro KY/FLNC co-expression study if KY indirectly promotes degradation by facilitating solubilisation.

KY as a structural protein: Given that the *ky/ky* pathology primarily affects postural muscles which experience consistent tension, resulting in damage to sarcomeric structures, it is possible that KY directly facilitates the structural integrity of skeletal muscle. However, the structure of KY is atypical for a structural protein. Such proteins are typically larger, and are rich in immunoglobulin domains. RNA expression analysis has also suggested that KY is more highly expressed in fast muscles than slow muscles, which seems counterintuitive if KY plays a solely structural function in maintaining muscles under tension.

KY as a hypertrophic/mechanosensing factor: The *ky/ky* mouse appears to be unable to undergo loading-induced hypertrophy in response to surgical overloading. This was characterised in EDL muscle, which is relatively non-pathological. This suggests that the inability to undergo hypertrophy might be a primary effect of KY deficiency, rather than a secondary effect of dystrophy. Given that KY resides at the z-disc, which is the anchor point of the sarcomere and experiences strain during muscle contraction, it would seem ideally placed to sense mechanical forces. Though KY expression appears to positively correlate with hypertrophy and negatively correlate with atrophy, the inverse correlation between physical activity and onset of elevated expression suggests that alteration of KY expression is not a direct consequence of physical activity. This makes it less likely that KY acts immediately downstream of mechanical activity, though does not exclude the possibility that it operates to promote hypertrophy under certain conditions.

KY in neuromuscular junction maintenance: The progressive disruption to neuromuscular junction structure in the *ky/ky* mouse indicates that KY may help in its preservation. However, the relevance of this phenotype to the pathology is unclear, particularly given that nerve conduction studies performed in human cases was normal (Hedberg-Oldfors et al. 2016; Straussberg et al. 2016).

KY as a signalling scaffold: A tenuous link between KY and MAPK-mediated hypertrophic signalling can be drawn via direct interaction between IGFN1 and indirect interaction with MLTK. Given that IGFN1 is negatively correlated with hypertrophy, any functional interaction with MLTK is likely to be inhibitory. Elevated expression of KY in hypertrophic conditions could competitively inhibit IGFN1-MLTK interactions to allow activation of the MAPK pathway. In the absence of KY, this interaction continues undisrupted, preventing hypertrophic signalling. This hypothesis seems unlikely given the lack of established link between MAPK pathways and IGF1-independent mTOR activation described previously.

Some aspects of these proposed functions may be inter-related. Degeneration of the neuromuscular junction similar to that observed in the *ky/ky* mouse model has been observed as a result of muscle-specific autophagy inhibition. If KY aids efficient autophagy, or the absence of KY indirectly results in impaired autophagy, this may account for the inability to properly maintain sarcomeric structures (i.e., via CASA), the disruption to hypertrophic signalling due to the associated cellular stresses, and the neuromuscular junction phenotype.

1.12 CRISPR/Cas9

Clustered Regularly Interspaced Short Palindromic Repeats (CRISPR)/Cas9 endonuclease genome editing technology arose from the adaptation of a defence mechanism against viral DNA insertion in bacterial and archaeal genomes. Integration of viral DNA into a region rich in palindromic clusters results in the production of single guide RNA strands (sgRNAs). These consist of a region complementary to the inserted sequence and a generic sequence with a secondary structure that mediates interactions with the nuclease, Cas9. sgRNAs thereby recruit the Cas9 enzyme to the inserted sequence, where the Cas9 induces a double strand break (DSB) which is then repaired in an error prone fashion using Non-Homologous End Joining (NHEJ) (Figure 1.8). The mutations induced by this defence mechanism prevent expression of integrated viral genes (Barrangou et al. 2007; Horvath and Barrangou 2010) and can be used to knock out gene function.

The relative ease of generating sgRNAs alongside their low toxicity have made them a preferable option to older technologies such as Transcriptional Activator-Like Effector Nucleases (TALENs) and Zinc-Finger Nucleases (ZFNs). TALENs and ZFNs relied on generating a series of protein domain modules complementary to the target sequence. Although modular assembly of these nucleases became relatively straightforward, the interactions between the protein modules and nucleotides was often less specific and their design imposed a number of target sequence constraints. This meant that some genes might either not contain a suitable target sequence at all, or else only have a suitable target region in later exons, reducing the disruptive effect of gene targeting (Doudna and Charpentier 2014).

In contrast, CRISPR/Cas9 technology demonstrates remarkable specificity, in part because it depends on highly specific Watson-Crick base pairing. with the ability to target multiple alleles simultaneously by expressing multiple specific gRNAs. This approach has been used successfully in a wide variety of organisms, with the successful and specific targeting of upwards of 14 distinct genomic loci simultaneously in *Arabidopsis* (Peterson et al. 2016) demonstrating the remarkable power and flexibility of this approach.

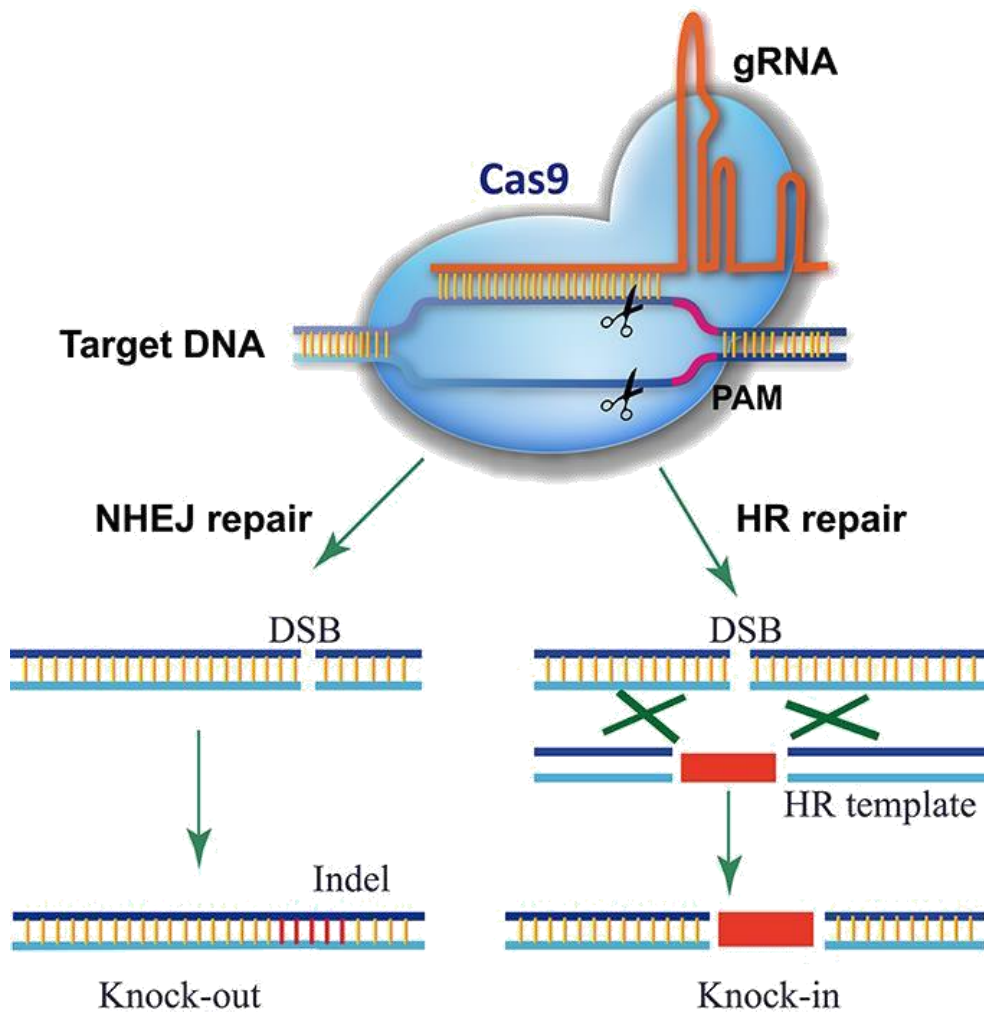


Figure 1.7 - Diagram of CRISPR/CAS9 genome editing

CRISPR/Cas9 genome editing tools are comprised of the Cas9 endonuclease which is guided to a specific genomic target by a guide RNA containing complementary sequence. Cas9 cleavage of DNA requires a proximal PAM site. Cas9 generates a double strand break which is repaired either by error-prone Non-Homologous End Joining (NHEJ) or by Homologous Recombination (HR) if a HR template is provided. NHEJ produces random indels which have a chance of producing a frame shift which disrupts protein expression.

Reproduced from (Ding et al. 2016) under a Creative Commons Attribution License (CC BY)

1.13 - Project Aims and Hypotheses

The central aim of this thesis is to explore the hypothesis that KY is involved in the turnover of cytoskeletal crosslinkers via the CASA mechanism. The objectives contained within this thesis are: -

- **Exploration of the state of CASA in the *ky/ky* mouse:** primarily determining the expression levels and localisation of CASA components to uncover any evidence of impairment to the CASA pathway
- **Generation of a KY-deficient C2C12 line:** providing a more dynamic model to explore the state of tension-induced signalling in the absence of KY
- **Generation and characterization of a KY knockout zebrafish line:** exploring whether the role of KY is conserved in non-mammalian vertebrates
- ***In vivo* overexpression of KY:** establishing whether ectopic expression of KY is sufficient to induce a hypertrophic response, both in WT and *ky/ky* mice.
- **Characterisation of mutagenised KY constructs:** To answer whether the catalytic triad and transglutaminase domains of KY are required for correct localisation and function

CHAPTER TWO:
MATERIALS
AND METHODS

CHAPTER TWO: MATERIALS AND METHODS

2.1 Buffers and reagents

Solution	Composition	Source
10x Tris-Glycine running buffer	25 mM Tris, 192 mM Glycine, 0.1% w/w SDS in ddH ₂ O	Generated in-lab
10x Western Transfer buffer	25 mM Tris, 192 mM Glycine in ddH ₂ O NB: dilution to 1x buffer in the ratio 1:2:7 concentrated buffer:methanol:ddH ₂ O	Generated in-lab
Phosphate-buffered saline (PBS)	1 tablet in 100mls ddH ₂ O (Final concentrations: 10 mM PO ₄ ³⁻ , 137 mM NaCl, and 2.7 mM KCl)	PBS tablets, Thermo Scientific (BR0014)
Tris-buffered saline (TBS)	20 mM Tris and 150 mM NaCl, pH 7.6	Generated in-lab
10x TAE Buffer	400 mM Tris-acetate, 10mM EDTA in ddH ₂ O	Generated in-lab
10x TBE buffer	890 mM Tris-borate, 890 mM boric acid, 20 mM EDTA in ddH ₂ O	Generated in-lab
LB broth	1% w/w vegetable tryptone, 0.5% w/w yeast extract, 1% w/w NaCl in ddH ₂ O	Generated in-lab
LB agar	1% w/w vegetable tryptone, 0.5% w/w yeast extract, 1% w/w NaCl, 2% w/w agar in ddH ₂ O	Generated in-lab
DMEM	DMEM + 4.5g/L D-Glucose, +L-Glutamine +Pyruvate	Gibco by Life Technologies (41966-029)
Cell culture growth media	10% Fetal Bovine Serum (FBS), 100U/ml Penicillin and Streptomycin, 0.5 µg/mL Fungizone in DMEM	Generated in-lab
Cell culture differentiation media	2% Fetal Bovine Serum (FBS), 100U/ml Penicillin and Streptomycin, 0.5 µg/mL Fungizone in DMEM	Generated in-lab
RIPA buffer	150 mM NaCl, 1.0% v/v IGEPAL® CA-630, 0.5% w/w sodium deoxycholate, 0.1% w/w SDS, 50 mM Tris, pH 8.0	Sigma (R0278)
E3 media	5mM NaCl, 0.17mM KCl, 0.33mM CaCl ₂ , 0.33mM MgSO ₄ in ddH ₂ O	Generated in-lab
Western blocking buffer	5% w/w dried skimmed milk in PBS (or TBS) + 0.1% v/v TWEEN 20	Generated in-lab
Western washing buffer (PBST)	PBS (OR TBS) + 0.2% v/v TWEEN 20	Generated in-lab
Immunofluorescence blocking buffer	3% w/w Bovine Serum Albumin in PBST + 0.05% Triton x100	Generated in-lab
Fin clip lysis buffer	10% Chelex 100 resin w/v, 250 µg/mL Proteinase K, 50mM Tris pH7, 50mM NaCl, 0.5% w/v SDS	Generated in lab
Hybridisation buffer	50% v/v formamide, 25% v/v 20 x	Generated in lab

	SSC buffer, 0.1mg/ml heparin, 2% v/v 50 x Denhart's solution (Invitrogen 750018), 0.1% v/v Tween 20, 0.1% CHAPS, 10 mM EDTA, 1mg/ml yeast RNA in ddH ₂ O	
MAB buffer	0.1 M malic acid, 150 mM NaCl in ddH ₂ O. MABT includes 0.2% v/v TWEEN 20	Generated in lab

2.2 PCR and qPCR primers and oligos

Primer name	Sequence	Reference	Experiment
HPRT FWD	GTT GGA TAC AGG CCA GAC TTT GTT	(Cassel et al. 2008)	Mouse tissue and cell C2C12 RTPCR/qPCR
HPRT REV	GAT TCA ACT TGC GCT CAT CTT AGG		
FLNC FWD	CCT TAC TCG CCC TTC CGC ATC CAT	(Chevessier et al. 2015)	
FLNC REV	CTC GGG AGC TGT GTA GTA GAT GTC		
BAG3 FWD	ATG GAC CTG AGC GAT CTC A	(Rusmini et al. 2015)	
BAG3 REV	CAC GGG GAT GGG GAT GTA		
MYH7 FWD	ACC CTC AGG TGG CTC CGA GA	(Anderson, Russell, and Foletta 2015)	
MYH7 REV	TGC AGC CCC AAA TGC AGC CA		
P62 FWD	GCA CCT GTC TGA GGG CTT CT	(Kishta et al. 2017)	
P62 REV	GCT CCA GTT TCC TGG TGG AC		
LC3 FWD	GAC GGC TTC CTG TAC ATG GTT T	(Sakuma et al. 2016)	
LC3 REV	TGG AGT CTT ACA CAG CCA TTG C		
MYH3 FWD	ACC TTG CCA AGA AGA AGG ACT CCA	(Kokkonen 2013)	
MYH3 REV	TGG ATG CGG ATG AAC TTG CCA AAG		
Myogenin FWD	CAC TGG AGT TCG GTC CCA A	(Song, Choi, and Lee 2015)	
Myogenin REV	TGT GGG CGT CTG TAG GGT C		
CHIP FWD	CGC AAG GAC ATT GAG GAG CA	Self-designed	
CHIP REV	TAG TCC TCT ACC CAG CCG TT	Self-designed	
HSPB8 FWD	GCA ATG AAA TCA TCA GCT GGC	Self-designed	
HSPB REV	GGG TTG CAG ACT TTC TCC AGT	Self-designed	
KY FWD	ACA GCA TGT ACC ACA AGA GTG AA	Self-designed	
KY REV	TCT CGA TGG TGA TTG TGG CTT T	Self-designed	

MYOD FWD	CCC CGG CGG CAG AAT GGC TAC G	(Al Madhoun et al. 2011)	
MYOD REV	GGT CTG GGT TCC CTG TTC TGT GT		
KY GENO FWD	GGG GCC ATT TGC AGC CTA	Self-designed	mouse/C2C12 genotyping
KY GENO REV	CGG AGA GGT TCG GAT TAG CC	Self-designed	
KY GENO FWD	AGC CAC CAA TCA GAA GAA GCA	Self-designed	Zebrafish genotyping
KY GENO REV	GTG TTA GCA CAG AGT GCA CAA	Self-designed	
AGPAT3 FWD	TGG ACC ATG ATT CAA CTG CCC	Self-designed	
AGPAT3 REV	: AGC TAC ACT GTT CTG CTC CG	Self-designed	
Ky exon 2 FWD	CAG AAG AAG CAG GCT CAA ACA ATG	Self-designed	Template generation for DIG probe synthesis for <i>in situ</i> hybridisation
Ky exon 2 REV	GAT AAG GTC TCC CGC TCT GC	Self-designed	
Ky exon 7 FWD	CTC TGC GGT GGG TTT GTT CTC TTG	Self-designed	
Ky exon 7 REV	CGG CCT TGG GGT GCA TTT ACT AT	Self-designed	
Ky nickase 1 FWD	TAA TAC GAC TCA CTA TAG GGA GGG GTT TCA CAA TCT CCT CTG TTT TAG AGC TAG AAA TAG CAA	Designs modified from (Nakayama et al. 2013)	Zebrafish sgRNA template
Ky nickase 2 FWD	TAA TAC GAC TCA CTA TAG GGC CAG CCC TGG CAT GCA GAG GTT TTA GAG CTA GAA ATA GCA AG		
Tyr FWD	TAA TAC GAC TCA CTA TAG ATG CAT TAT TAC GTG TCC CGT TTT AGA GCT AGA AAT AGC AAG		
Generic reverse	AAA AGC ACC GAC TCG GTG CCA CTT TTT CAA GTT GAT AAC GGA CTA GCC TTA TTT TAA CTT GCT ATT TCT AGC TCT AAA AC		
EIF1α FWD	CTG GAG GCC AGC TCA AAC AT	(Tang et al. 2007)	Zebrafish qPCR/RTPCR primers
EIF1α FWD	ATC AAG AAG AGT AGT ACC GCT AGC AT		
BAG3 FWD	TGC CCA TTC AGA TTC AAC AG	Self-designed	
BAG3 REV	GGC TGC TGT GTA GGT TGT TG	Self-designed	
LC3B FWD	AAT GTG ACG ATT GGA CAC GAG T	(Ganesan et al. 2014)	
LC3B REV	AGT ACA ACA GCT CAC GGT TAT GC		
FLNCA FWD	CCT TCG TGG GTC AGA AGA AC	(Solchenberger et al. 2015)	
FLNCA REV	GGA GTT CTA GGA CCG TGG AC		

FLNCB FWD	GGC CCT ACA AAG TGG ACA TC		
FLNCB REV	CTT CAA ACC AGG CCC ATA AG		
KY 1_2 FWD	CCA CCA CGA ACA CCC CTA AA	Self-designed	
KY 1_2 REV	CGC TCC ACT GAC TGT GAA CT	Self-designed	
KY 2_3 FWD	AGT TCA CAG TCA GTG GAG CG	Self-designed	
KY 2_3 REV	TCC GTG ACT GCA TGA GCA	Self-designed	
QKY FWD 1	TGA CCC TCA TAC ATC CCA AGC	Self-designed	
QKY REV 1	GAG CTC CTG TCT GGG GAT CA	Self-designed	
QKY FWD 2	ACC CTT GAG GAC ATC AGC ATT	Self-designed	
QKY REV 2	TAG AGC TCC TGT CTG GGG AT	Self-designed	
Ky site 1 a	CAC CGC ACT CCG AGA AGC GGC GCG	Self-designed	oligo pairs for cloning into px459 for CRISPR/Cas9 mutagenesis of C2C12
Ky site 1 b	AAA CCG CGC CGC TTC TCG GAG TGC		
Ky site 2 a	CAC CTC ATC GTG CAC TCC GAG AAG		
Ky site 2 b	AAA CCT TCT CCG AGT GCA CGA TGA		
Ky site 3 a	CAC CGA AGA AGG ACA GCA ACG CTG		
Ky site 3 b	AAA CCA GCG TTG CTG TCC TTC TTC		

2.3 Antibodies

Primary antibodies

Target	Antibody code	Supplier	WB concentration	IF concentration
BAG3	10599	Proteintech	1:2000	1:200
LC3A/B	D3U4C	Cell Signalling Technology	1:500	1:100
GAPDH (HRP)	G9295	Sigma	1:50,000	n/a
FLNC	RR90	Peter van Der Venn	1:1000	1:100
P62	sc-10117	Santa Cruz Biotechnology	1:500	1:50
CHIP	PC711	Calbiochem	1:500	n/a
V5	V8137	Sigma	n/a	1:1000
α -tubulin	T6199	Sigma	1:2000	n/a
Fast muscle	12/101	DSHB	n/a	1:20
Slow muscle	f59	DSHB	n/a	1:20

Slow muscle	s58	DSHB	n/a	1:20
-------------	-----	------	-----	------

Secondary Antibodies

Target	Code	Supplier	WB concentration	IF concentration
Mouse IgG HRP	sc-2134	Santa Cruz Biotechnology	1:10,000	n/a
Mouse IgA HRP	sc-3791	Santa Cruz Biotechnology	1:10,000	n/a
Goat IgG HRP	sc-2350	Santa Cruz Biotechnology	1:10,000	n/a
Rabbit IgG HRP	sc-2030	Santa Cruz Biotechnology	1:10,000	n/a
Rabbit IgG FITC/TRITC	ab6717/ ab6718	Abcam	n/a	1:70
Mouse IgG FITC/TRITC	ab6785/ab6786	Abcam	n/a	1:70
Mouse IgA FITC	ab97234	Abcam	n/a	1:70

2.4 Cell culture

2.4.1 Proliferating cultures

Reagents used in cell culture were pre-heated to 37°C in a water bath prior to use unless otherwise stated. Cell cultures were grown in a 37°C incubator with 5% CO₂.

Aliquots of frozen C2C12 cells were thawed prior to plating in a T25 or T75 tissue culture flask with the appropriate amount of growth media. Media was replenished once cells were attached to remove residual DMSO from the culture. Growth media was replaced every other day. Once cells achieved approximately 80-90% confluency, cells were either harvested for analysis of proliferative cells, differentiated or split to expand the culture.

2.4.2 Splitting cultures

To split cultures, growth media was completely removed prior to 2-3 gentle washes with PBS to ensure removal of residual media. Sufficient 0.05% trypsin solution (diluted in sterile PBS from Gibco 10x Trypsin-EDTA solution; 15400054) was added to cover the bottom of the culture flask. Flasks were returned to the incubator for optimal trypsin activity. Detachment of cells was monitored periodically with a light microscope. Gentle swirling and tapping of the culture flask was used to facilitate cell detachment. Once the majority of the cells were detached, cells were either split equally between new culture flasks preloaded with growth media (when number of seeding cells did not need to be controlled) or aliquoted according to number of cells after estimation of cell density using a haemocytometer.

2.4.3 Harvesting cells

To harvest cellular material for downstream analyses, media was removed prior to three washes with cold PBS. The appropriate amounts of RIPA buffer (for protein extraction), Trizol (for RNA extraction - Invitrogen; 15596026) or cell lysis buffer (for downstream PCR) were added directly to the washed cells. A cell scraper was used to harvest the cellular material.

2.4.4 Differentiation

For differentiation, cells were allowed to grow to confluency in growth medium. Once confluency was achieved, cells were switched to differentiation media, with the differentiation response triggered by the reduction of serum from 10% to 2%. Differentiation media was changed every other day until harvesting. Progression through the differentiation process through alignment, fusion and myotube formation was assessed visually under light microscopy.

2.4.5 Transfection

Transfection of plasmid DNA was performed in suspension using GenJet In Vitro DNA Transfection Reagent for C2C12 cells (SignaGen; SL100489-C2C12) on proliferating myoblasts at ~90% confluency according to manufacturer's instructions (available at <http://signagen.com/DataSheet/SL100489-C2C12.pdf>)

2.4.6 CRISPR/Cas9 genome editing in cells

An available plasmid encoding the Cas9 enzyme and generic portion of sgRNA was obtained (px459, Addgene) described in (Ran et al. 2013). To produce a plasmid

with target specificity, 5'-Phosphorylated oligo pairs were designed containing the target sequence for *Ky* that when annealed were flanked with overhangs complementary to those flanking the insertion site in the main px459 plasmid following *Bbsl* digestion (NEB; R0539). Annealed oligos and the digested plasmid were ligated using T4 DNA ligase (NEB; M0202), with the products being transformed into competent *E. coli* (SoloPack Gold; Agilent; 230325) using a standard method (e.g. <https://www.addgene.org/protocols/bacterial-transformation/>) before overnight growth at 37°C on LB-agar plates enriched with ampicillin. Picked colonies were expanded overnight in 5mls of LB media at 37°C. DNA minipreps were performed using a Plasmid Miniprep Kit with the standard manufacturer's protocol (Qiagen; 27104). This process eliminated the *Bbsl* digestion site, so failure to undergo *Bbsl* digestion was used as a screen for successful insertion. Successful insertion of correct product was confirmed by sequencing.

Confirmation of the mutagenic capacity of these plasmids, C2C12 cells were transfected with each plasmid as described above. 24h after transfection cells were subject to puromycin selection by enrichment of media at 5µg/ml. Surviving cells were left to grow to confluency before being harvested in cell lysis buffer. The target region was amplified by PCR. PCR products were subjected to a T7 Endonuclease I (T7el) assay to test for the presence of mutated PCR products using an assay kit (Genecopoeia; IC005). Successful mutagenesis produces heteroduplex "bubbles" in mismatched PCR products at the site of mutation that are detected and cleaved by T7el, producing digestion products of a predictable size. The plasmid demonstrating successful mutagenesis with the most upstream target sequence was carried forward as the targeting vector.

Following a fresh transfection of C2C12 cells with the targeting vector, a number of puromycin resistant colonies were selected and expanded (25 colonies, named A to Y). To detect successful mutagenesis in individual colonies, the target site was amplified by PCR and amplicons from each clone were mixed and annealed with amplicons from WT C2C12s. In the presence of mutated alleles, this process produces heteroduplexes which can be detected via slower mobility in high percentage acrylamide gel electrophoresis (see Section 2.9). For clones showing evidence of mutagenesis, t-cloning (using Promega pGEM-T Easy Vector System with standard protocols; A1360) and sequencing of PCR products was used to determine the sequence of individual alleles and screen for clones carrying

disruptive mutations in both alleles. Disruption to *ky* expression was evaluated by qPCR (See 2.6.3).

2.4.7 Cell immunofluorescence and staining

For immunofluorescence studies cells were typically plated and grown on glass coverslips in 6 or 24 well plates. Media was removed from cells followed by at least 2 washes in cold PBS. Dependent on antibody compatibility, cells were either fixed in a 50/50 mix of ice cold methanol/acetone or in PFA at RT for 5-10 minutes. Fixation solutions were washed off with 2-3 PBS rinses. Cells were blocked and permeabilised in immunofluorescence buffer (see 2.1) for 30 minutes prior to replacement with immunofluorescence buffer enriched with primary antibody (See 2.3 for antibody concentrations). Primary antibody incubation was typically for 2h at RT or overnight at 4.C. After incubation cells were washed in washing buffer (same formulation as the western washing buffer) for 3 x 10 minute washes. Secondary antibody incubation was performed for 1h at RT in the dark, followed by 3 x 10 minute washing buffer washes. Coverslips were mounted onto glass slides with mowiol mounting media, typically enriched with DAPI. Cells were imaged using a Microphot FXA fluorescent microscope (NIKON) mounted with a DFC450C camera (Leica). For actin staining, fluorophore-conjugated phalloidin (Alexa Fluor 488 Phalloidin; Invitrogen; A12379) was added to immunofluorescence buffer for the secondary incubation stage.

Crystal Violet staining was performed using the methanol fixation protocol followed by a 10 minute incubation with 0.5% Crystal Violet (ALFA; B21932) (w/v) in 20% methanol. Excess stain was washed off in dH₂O until the water ran clear. Coverslips were mounted in DPX mounting media.

Cell size analysis was performed using ImageJ software using the 'measure particles' tool.

2.4.8 - Myoblast stretching

Undifferentiated C2C12 myoblasts from a near-confluent T75 flask were split via trypsinisation into a 6-well Bioflex Collagen-I plate (FlexCell) with 1×10^6 cells per well in standard growth medium. After 24hrs the plate was loaded onto the Flexcell 4000T baseplate. Stoppers were applied to 2 wells to prevent stretching for the

control, unstretched sample. The remaining wells were subjected to a dynamic stretching program of 20% elongation for 3hrs at 0.18Hz (Ulbricht et al. 2013).

Immediately after stretching, media was removed and cells were rinsed twice with ice-cold PBS. Cells were harvested via scraping in fresh PBS and pairs of wells were pooled to produce 'unstretched', 'stretched 1' and 'stretched 2' samples. Cells were pelleted via centrifugation (1000g, 3mins, 4°C) followed by washing in ice cold PBS and repelleting. Cell pellets were resuspended in 50µl ice-cold RIPA buffer (Sigma) enriched with protease inhibitors (Roche) and incubated on ice for 15mins. Samples were vortexed for 30secs followed by a further 5min incubation on ice and 30sec vortexing. Samples were centrifuged (13,000g, 20mins, 4°C) and the supernatant retained. Protein concentration was determined by Bradford assay against a BSA standard and concentrations adjusted to 1µg/µl.

Proteomic analysis was performed by Adam Dowle at the University of York Technology Facility. Protein was isolated from the samples by Polyacrylamide gel electrophoresis and in-gel digestion. Digested samples were loaded onto a nanoAcuity UPLC system (Waters) which was interfaced with a maXis HD LC-MS/MS system (Bruker Daltronics). Spectra were obtained using AutoMSMS mode and searched against mouse and rat UniProt database subsets and filtered using Mascot software (Matrix Science Ltd.). Relative quantification was performed using Progenesis QI (Waters) to compare MS1 precursor area. Full details of the methodology can be found in appendix 2.

2.5 Western Blotting

Concentration of protein samples was determined by Bradford assay using BradfordUltra (Expedeon; BFU) and an MRX microplate reader with Revelation software (Dynex Technologies). A 10-fold dilution of sample in ddH₂O was used to prevent interference from detergents in the lysis buffer. Protein concentration was determined against a standard curve generated using dilutions of BSA in 10% RIPA buffer.

Samples were prepared for SDS-PAGE typically using 20µg, but up to 50µg, of protein combined with 4x NuPAGE LDS buffer (Invitrogen; NP0008) and 10x NuPAGE sample reducing agent (Invitrogen; NP004). Samples were heated to 70°C for 10 minutes to promote denaturation prior to loading onto a Tris-Glycine gel.

Gels were run for approximately 1 hour at 180V using a Mini-PROTEAN Tetra Cell system (Biorad), until the dye front reached the bottom of the gel.

Transfer was performed either using the iBlot gel transfer system (Invitrogen) and nitrocellulose stacks (Invitrogen; IB301002), or using a wet transfer method (Mini Trans-blot cell; Biorad) onto nitrocellulose or PVDF membranes.

Ponceau S staining was used to check for adequate transfer of proteins to the membrane. Excess staining reagent was removed using ddH₂O prior to blocking for 1hr at RT in blocking buffer with shaking. Membranes were then incubated with primary antibody diluted in blocking buffer (see table 2.3 for concentrations) overnight at 4°C with shaking. Three ten minute washes in washing buffer were performed to remove unbound primary antibody before the addition of HRP-conjugated secondary antibody (see table 2.3 for concentrations). Secondary antibody incubation was at RT for 1hr with shaking. Three further washes were performed to remove unbound secondary antibody.

The membrane was incubated in Lumisensor HRP substrate (Genscript; L00221V60) for 1 minute prior to visualisation. Earlier experiments used exposure to X-ray film to detect the HRP reaction, which was then developed using an Xograph film developer. Later experiments used a CHEMIsensor (Syngene; GeneGenius) to directly detect the HRP reaction. Levels of protein were determined by band intensity relative to the loading control as calculated by densitometry using ImageJ software.

2.6 PCR, RT-PCR and qPCR

2.6.1 PCR

PCR reactions were typically prepared as follows: -

- 15µl 2x PCR Master Mix (Thermo Scientific)
- 1µl 10µM forward primer
- 1µl 10µM reverse primer
- 1-2µl DNA
- to 30µl with PCR water (Thermo Scientific)

PCR reactions were performed using a Geneamp 9700 Thermocycler (Applied Biosciences) with the following program:

1 x	Initial Denaturing	95°C	3 minutes
30-40 x	Melting	95°C	30 seconds
	Annealing	Primer dependent	30 seconds
	Extension	72°C	Product dependent
1 x	Final extension	72°C	5 minutes
1 x	Holding	4°C	Hold

Products were mixed with 6x DNA loading dye (NEB) prior to loading on a 1.5% agarose/TBE electrophoresis gel containing a 1:10,000 v/v dilution of SYBR Safe Dye, with alterations to the agarose percentage to maximise resolution of the product if needed. Electrophoresis was performed using a BioRad power pack, running at 50-100v until sufficient migration of the dye front was achieved. Upon completion of electrophoresis, products were visualised using an EZ Gel Doc imager (BioRad).

2.6.2 RT-PCR

Conversion of isolated RNA samples to cDNA was performed using ReadyScript cDNA synthesis mix (Sigma; RDRT). 1µg of RNA was loaded per 20µl reaction. Since the reverse transcriptase enzyme is included in the mix, “no RT” controls refer to the loading of an equivalent amount of isolated RNA samples into the subsequent RT/qPCR reaction rather than the absence of reverse transcriptase in the reaction mix. This provides an equivalent check for amplification from genomic DNA contamination.

The cDNA synthesis reaction was performed in a thermocycler (5 minutes at 25°C; 30 minutes at 42°C; 5 minutes at 85°C; 4°C hold). RT-PCR experiments were then performed as per the PCR protocol in 2.6.1.

2.6.3 qPCR

qPCR reactions were prepared as follows (per well) :-

- 5µl 2x SYBR Green Fast qPCR Mix (Applied Biosciences)
- 1µl 5µM forward primer
- 1µl 5µM reverse primer
- 1µl cDNA (or water/No RT controls)

- 2µl PCR water

Reactions were performed in triplicate to give three technical replicates per biological sample. qPCR was performed on a QuantStudio 3 Real-Time PCR System (Applied Biosciences) using the standard fast protocol, including melt curve analysis.

Data was analysed according to the DDCt method, measuring target gene expression relative to a control (typically *Hprt* in mouse/cell experiments or *ef1a* for zebrafish unless otherwise stated).

2.6.4 Sequencing

All sequencing of PCR products or DNA plasmids was performed using GATC Biotech Light Run sequencing service, with samples and primers prepared to their recommended concentrations.

2.7 Zebrafish

All experiments with zebrafish were performed in accordance to The Animals (Scientific Procedures) Act, under the appropriate project and personal licenses. All experimental protocols were approved by an ethics committee.

Zebrafish were sacrificed according to the approved Schedule 1 methods of killing, namely the administration of anaesthetic overdose by gradual delivery of MS222 into tank water. Death was confirmed by observation of cardiac arrest prior to removal from anaesthetic and downstream processing.

2.7.1 Lines

The London Wildtype (LWT) zebrafish strain was the primary strain used in the characterisation of zebrafish ky and the generation of the ky knockout line. The Ky knockout line was also crossed with a Myl2::GFP reporter line and a Mnx::GFP reporter line.

2.7.2 Microinjection

Fine glass needles were pulled and fitted onto a gas microinjector and filled with water to ensure there were no blockages. Injection volume was determined by the

diameter of the bubble produced with a single injection into mineral oil, as measured on a reticule. Injection settings were adjusted to produce an injection volume of 1nl. The needle was then cleared before loading injection material, typically including phenol red dye to allow visualisation of successful injections.

Embryos were aligned using an agarose trench and injected between the 1- and 8-cell stages in the yolk sac, proximal to the cells to allow efficient transfer of the material from the yolk to the cells via the cytoplasmic bridge. Multiple injections were performed up to 3nl to deliver higher doses of material. Embryos were returned to E3 media for recovery in a 28^oC incubator.

2.7.3 Fin clipping

Tail fin clips were collected to provide genomic DNA to examine for the presence of mutations, or to genotype lines. Typically this was performed on fish at 3 months post-fertilisation to provide an ample tissue sample. Fish were anaesthetised using 0.4% MS222 in 0.01M Tris pH7 in an approximate 1:4 dilution with tank water (final concentration of MS222 ~0.01%). Once fish ceased being responsive to touch stimuli they were transferred onto a tissue culture plate coated with 1% agarose in H₂O. 2-3mm of tail fin was clipped and immediately placed in fin clip lysis buffer (see table 2.1). Fish were then transferred into a fresh tank and observed for recovery.

Samples in fin clip lysis buffer were heated to 55.C for 1 hour, followed by 15 minutes at 95.C to deactivate the proteinase K. Samples were typically diluted 1/10 in ddH₂O before using 1µl of diluted lysate in a 30µl PCR reaction as in 2.6.1 followed by genotyping analysis as in 2.9.

2.7.4 *in situ* hybridisation

PCR amplicons were generated from a 400bp sequence within exon 2 and a 500bp sequence within exon 7 of the zebrafish ky from WT genomic DNA. Amplicons were ligated into pGEM T-easy vectors using the standard manufacturer's protocol and transformed into competent bacteria. Colony PCR was performed to determine successful insertion, and plasmid DNA was miniprepped from positive clones. Orientation of the insert was determined by sequencing to determine which plasmids would produce suitable template for the synthesis of the antisense probe. Suitable plasmids were linearised with *Nco*I for 2hrs at 37 degrees. Linearised

template was purified by phenol/choloroform extraction. DIG probe synthesis reactions were prepared as follows: -

- 1µg linerarised DNA
- 4µl 5 x T7 Transcription buffer
- 2µl NTP-DIG-RNA
- 1µl RNase inhibitor
- 1µl T7 RNA polymerase
- up to 20µl molecular grade water

and incubated for 2hrs at 37°C. Following synthesis, DNA template was eliminated by the addition of 2µl RNase free DNase and incubation at 37.C for 15 minutes. The RNA probe was isolated via LiCl precipitation by the addition of 1:1 volume of 4M LiCl to the sample before incubation at -20°C for 1hr. The sample was then centrifuged at 13,000 x g at 4°C for 15 minutes. The supernatant was removed and the pellet air dried before resuspension in molecular biology grade water. 2µl was run on an agarose gel to determine successful probe synthesis. DIG probes were stored at -80°C until use.

Embryos were collected at various stages, dechorionated manually using sharp forceps and fixed overnight at 4.C overnight on rollers. Fixed embryos were gradually dehydrated by a series of 5 minute incubations in increasing concentrations of methanol. Dehydrated embryos were stored at -20.C until used.

At the beginning of the protocol, embryos were rehydrated gradually into PBST with 5 minute incubations in 75, 50, 25 and 0% methanol in PBST. Embryos were treated in 10µg/ml proteinase K with incubation times varying according to stage: -

- Gastruala/blastula - 30 seconds
- Early somitogenesis - 1 minute
- Late somitogenesis - 5 minutes
- 24hpf - 15 minutes
- 36+hpf - 30 minutes

Embryos were refixed for 20 minutes in 4% PFA/PBS before 5 x 5 minute washes in PBST and a 5 minute incubation in a 50/50 mix of hybridisation buffer and PBST. Embryos were prehybridised in hybridisation buffer for 3-4 hours at 70°C with rocking. From this point all solutions were prewarmed to ensure consistent temperature. 5ul of *in situ* probe was heated to 80°C for 3 minutes before adding to fresh hybridisation buffer. The prehybridisation buffer was replaced with the

hybridisation buffer containing the probe and incubated with rocking overnight at 70°C.

The following day the embryos were washed with 2 x 10 minute incubations in hybridisation buffer, 3 x 20 minute washes in 2 x SSC + 0.1% Tween 20, 3 x 30 minute washes in 0.2 x SSC + 0.1% v/v Tween 20 (all at 70°C) and 2 x 15 minute washes in MABT at RT.

Embryos were blocked in 20% heat treated lamb serum and 2% BMB (Roche: 1096176) in MABT for 2 hours at RT with rocking. Blocking buffer was replaced with a fresh blocking solution containing a 1/2000 dilution of anti-DIG antibody and incubated overnight with rocking at 4°C.

The next day embryos were washed for 3 x 5 minute and 3 x 1hr incubations in MABT with rocking at RT. Visualisation of hybridisation was done via incubation with BM purple. Once sufficient signal was visualised, the reaction was stopped with 2 x 15 minute washes in PBST followed by refixing overnight in 10% formalin at RT.

2.7.5 Methylcellulose challenge

Embryos were raised to 3dpf in normal E3 media, dechorionated and split between unchallenged groups (remaining in normal media) and challenged groups (transferred to media enriched with 1% w/w methylcellulose). Embryos were left for 48 hours before harvesting for downstream analyses.

2.7.6 Birefringence

Evaluation of muscle integrity *via* birefringence was performed by placing anaesthetised embryos on a polarising filter cap on an underlit dissection scope. A second filter cap was placed on top and aligned such that only light polarised by muscle was visible. Representative images were captured on a light microscope.

2.7.7 Sectioning and histology

Muscle tissue was dissected from sacrificed fish and snap-frozen in LN₂-cooled isopentane. Sections were generated using a cryostat. Immunofluorescence protocols were similar to those in 2.4.7

For Hematoxylin and Eosin (H&E) staining of tissue sections, the following protocol was observed:

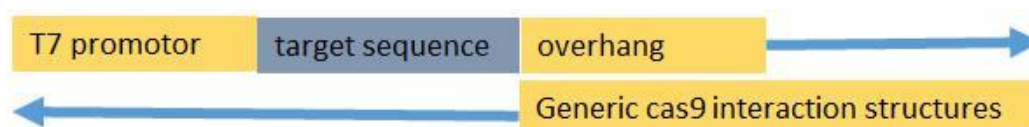
- Fixation in acetone for 5 seconds
- Air dry
- 1 minute incubation in Gill's Hematoxylin
- Washing with running water on the back of the slide until clear
- One dip in eosin (no more than 10 seconds)
- Twenty dips in 100% Alcohol (6 alcohol changes)
- 5 dips in Histoclear
- 30 second incubation in clean Histoclear
- Mount under glass coverslips with TPX

2.7.8 RNA extraction from tissue

Dissected tissue or pooled embryos were ground in a pestle and mortar under LN₂. Ground tissue was collected in an 1.5ml microcentrifuge tube prior to the addition of 1ml TRIZOL reagent and mixing by vortexing. 200µl of chloroform was added to each sample prior to vortexing and centrifugation at 12,000g for 15 minutes at 4°C. The resulting aqueous phase was pipetted into a fresh tube, with care taken not to disrupt the interphase or organic phase. 500µl of isopropanol was added to each new tube with mixing by tube inversion. Precipitated RNA was pelleted by centrifugation at 13,000g for 30 minutes at 4°C. The pellet was subjected to two cycles of 70% ethanol washes and centrifugation steps. The cleaned pellet was then air dried before being resuspended in 20-50µl of molecular biology grade H₂O. Concentration and quality was determined using a Nanodrop spectrophotometer and software (Thermo Scientific).

2.7.9 Zebrafish gene targeting by CRISPR/Cas9

Gene targeting of zebrafish was performed using a method described in (Nakayama et al. 2013). Briefly, a template for *in vitro* transcription of sgRNA was produced by annealing and extending a pair of oligos, one containing a T7 transcription promoter and the target sequence and the other containing generic sgRNA sequence:



This was then used as a template for sgRNA synthesis using a MEGAscript T7 transcription kit (Thermo Scientific; AM1334) following the manufacturer's instructions

(https://assets.thermofisher.com/TFS-Assets/LSG/manuals/1330M_G.pdf).

Cas9 protein was provided by Dr. Olga Moroz, York Structural Biology Laboratory.

Cas9 protein and sgRNA were coinjected into embryos as per 2.9.2, with a dosage of 400pg sgRNA and 2ng Cas9 protein in each embryo. Embryos were screened for successful mutagenesis using the lysis and PCR method described for fin clips in 2.7.3.

Putatively mutagenised embryos were raised and screened for the presence of mutations via fin clipping. Successfully mutagenised fish were collected as the founders (F0). Founder fish were outcrossed to WT LWT fish to produce F1 embryos heterozygous for a single mutant allele. The mutation was characterised by sequencing of PCR from genomic DNA extracted from a proportion of embryos in the clutch. This produced double peak readings in the sequencing output. The mutant allele could be deduced by elimination of the WT sequence. Clutches containing desired mutations (a disruptive 5bp deletion and a non-disruptive 3bp deletion) were raised to allow individual screening of fish via gel genotyping, correlated with sequencing (as in 2.9). Fish heterozygous for the same mutation were pooled together and incrossed to produce homozygous mutant fish.

2.8 Mice

All experiments using mice were done in accordance to The Animals (Scientific Procedures) Act, under the appropriate project and personal licenses. All experimental protocols were approved by an ethics committee. Mice were sacrificed according to the approved Schedule 1 methods of killing, typically exposure to a rising concentration of CO₂ followed by confirmation of death via cervical dislocation.

The strains used in this thesis were the C3H/HeH line and homozygous ky mutant line (*ky/ky*) in the C3H/HeH background. Mice were kept with free access to food and water.

2.8.1 *In vivo* electroporation of mouse skeletal muscle

2 hours prior to the electroporation procedure, the TA muscles of each mouse were injected with 50µl of 0.4U/µl hyaluronidase in saline to disrupt the extracellular matrix and increase efficiency of DNA transfer.

Immediately prior to the procedure, mice were anaesthetised using isoflurane. Sufficient depth of anaesthesia was assessed by the absence of the pedal withdrawal reflex and maintained with continuous delivery of isoflurane. Mice were transferred to a heated mat to maintain body temperature throughout the procedure.

Electrodes of a NEPA21 electroporator (Nepagene) were inserted into the TA muscle through the skin, with an impedance check to ensure insertion into muscle tissue. Plasmid DNA was then injected into the muscle between the two electrodes. Poration pulses (3 x 50msec; 50V, 1Hz) and transfer pulses (3 x 50msec, 20V, 1Hz) were delivered to the muscle to promote DNA uptake into muscle fibres. This procedure was then repeated for the other hindlimb. Mice were returned to their cages and observed for recovery. Mice were left for around 6 weeks to allow construct expression and recovery of muscle tissue prior to being sacrificed.

The TA muscle was dissected out and observed under a fluorescent microscope to confirm construct expression. Muscles were then briefly fixed in 4% paraformaldehyde in PBS for ten minutes prior to snap-freezing in liquid nitrogen-cooled isopentane. 10µm thick sections were prepared on a cryostat to allow observation of fibre morphology.

Fibre size analysis was performed using ImageJ software, manually measuring the area and colour intensity of each fibre. Fibres were then sorted according to colour intensity, and a cut off threshold was decided based on the background intensity. Fibres above this threshold were counted as successfully electroporated and those below the threshold were counted as untransfected.

2.8.2 Tissue protein fractionation

Protein fractions were isolated from freshly dissected muscle tissue using a Subcellular Protein Fractionation Kit For Tissues (Thermo Scientific; 87790) following the manufacturer's protocol (https://assets.thermofisher.com/TFS-Assets/LSG/manuals/MAN0011756_Subcell_Protein_Fraction_Tissue_UG.pdf).

Fractions were stored at -80.C until used.

2.9 Genotyping

For mouse genotyping, ear notches were prepared by the animal facility. Tissue lysis was performed using a HotSHOT protocol. Notches were incubated for 30 minutes at 95°C in 70µl 0.05M NaOH followed by the addition of 10µl 0.08M Tris-HCl and 0.2mM EDTA and vortexing for 30secs. 1µl of lysate was used in a 30µl PCR reaction.

Determination of genotype was performed using a system adapted from (Zhu et al. 2014). Heterozygotes or samples carrying non-homozygous mutations were determined by the formation of heteroduplexes during PCR amplification of a target region. PCR products were loaded onto a TBE gel containing 15% Acrylamide and run in TBE buffer for 90-120 minutes at 150-180V, or at 65V overnight. Gels were stained with either SYBR safe or ethidium bromide solution (1:10,000 in dH₂O) for 15 minutes prior to visualisation on a BioRad EZ GelDoc system. The presence of additional bands above the expected PCR product indicates heteroduplex formation and therefore the existence of multiple alleles in the sample.

To differentiate between WT and homozygous mutant samples, neither of which produces heteroduplexes in this assay, PCR products were mixed with known WT products. The mixture was subjected to a melt-anneal programme in a PCR thermocycler (5 mins at 95°C; cooling at 0.1°C/second to 40°C; 4°C hold) to generate mixed pairing before running on the gels. Heteroduplex formation in this test combined with no heteroduplex formation when the sample is run on its own indicates that the sample sequence is homozygous mutant.

The accuracy of this method was verified by correlation with sequencing results for each specific application.

CHAPTER THREE:
ANALYSIS OF
ENDOGENOUS KY IN
THE MOUSE

CHAPTER THREE: ANALYSIS OF ENDOGENOUS KY IN THE MOUSE

3.1 Introduction

Exploration of the structure and expression of endogenous KY will provide some indirect insights into the function of this protein. For example, the *ky/ky* mouse pathology is known to primarily affect slow, postural muscles that consistently experience high levels of tension whilst sparing fast-twitch muscles. There are two main hypotheses for how this disparity might arise. The first hypothesis is that KY might have a direct role in preventing or repairing structural damage, thus the postural muscles are most impacted by its absence. In this scenario, we might expect higher levels of KY expression in the postural muscles of WT mice, representing an adaptation to minimise structural damage. An alternative hypothesis is that KY is necessary for hypertrophic adaptation to mechanical tension. A failure to undergo hypertrophy in the absence of KY leads to a decreased muscle to body mass ratio. This leads to a critical overload of postural muscles which are consistently bearing tension from body weight. In this instance we might expect a higher level of KY expression in these muscles since it is known that fast-twitch muscles are more responsive to hypertrophic stimuli in this context (G. Blanco et al. 2001).

3.2 A trend towards higher *Ky* mRNA expression in fast muscle compared to slow muscle

It has already been reported that *Ky* expression is elevated in the fast-twitch TA relative to the slow soleus. However, the significance of this difference was not explored. In addition, the analysis was generated from microarray data without an attempt to specifically validate these differences (Dyar et al. 2015). To determine whether there is a significant difference in *Ky* expression between fast and slow muscle, soleus and EDL muscles were dissected from WT C3H/HeH mice. RNA was extracted and converted into cDNA from which *Ky* expression was examined by qPCR. In a first experimental cohort of 4 sibling, 6 week old males, the EDL showed an average 5.75 fold increase in expression over the soleus. However, due to a high degree of variability between mice, this trend did not reach significance (paired Student's t-test, $p=0.088$, $n=4$). A further three age and sex matched mice were added to the analysis, which reduced the mean fold change to 2.9 and increased

the p-value to 0.099. Thus, no overall significance was detected for this trend (Figure 3.1).

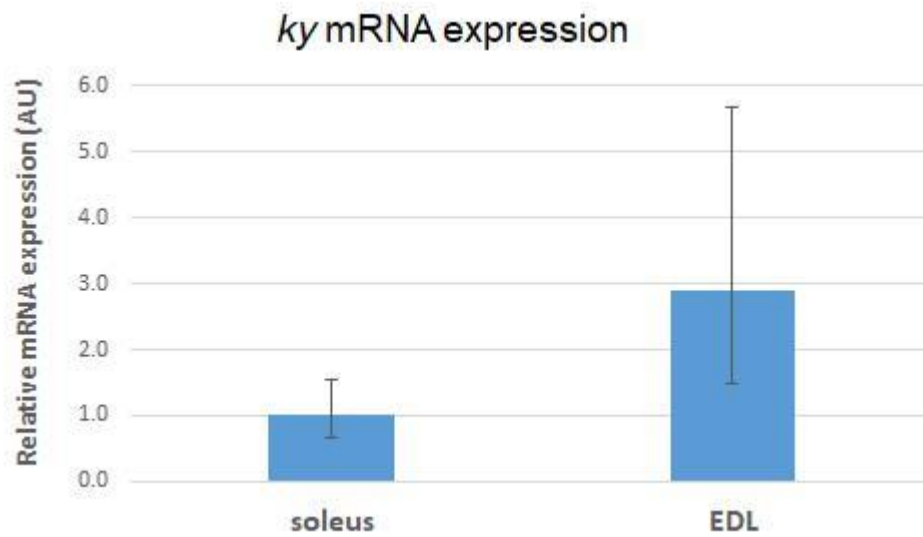


Figure 3.1 - A non-significant trend towards elevated ky mRNA in EDL compared to the soleus

The EDL has an average 2.9 fold increase in ky mRNA compared to the soleus, though this is not significant at the $p=0.05$ level (Paired Student's t-test; $p=0.099$; $n=7$). Error bars indicate standard deviation

3.3 Conservation of tryptophan residues around the catalytic triad

Structural insights into the KY protein may provide additional clues to its function. The question of whether KY protein has a protease function remains unresolved, although the balance of experimental evidence suggests not. The presence of several key tryptophan residues has been shown to be necessary for transglutaminase function and binding efficiency and are highly conserved in human transglutaminases. (Murthy et al. 2002). Examination of the sequence surrounding the catalytic triad suggests that some, but not all, of these residues are conserved. A residue essential for catalytic activity is conserved in mouse, human and zebrafish Ky, though one shown to assist in substrate binding efficiency is lost (Figure 3.2).

```

KY_HUMAN      LLQEHTDLERVRAI W I W I C H H I E Y D I A A A Q E K D R Q A F K P T D I L R T Q K T N D G Y A G L F E R 234
KY_MOUSE      LLQEHSDDLERVRAI W I W I C H H I E Y D V E A A Q E K D R Q A F K P T D I L R T Q K T N D G Y A G L F E R 234
F1QDV7_DANRE VTEVARNEVEKLRAT W I W L C H N I E Y D I E G Y L G L S Q K I C S L D E V I R N G K G V S G Y S N L C V E 113
CONSERVED W                                     W                                     W

KY_HUMAN      M C R L A G V Q C M T V P G Y S K G F G Y Q I G Q S F S G E - F D A N A V Y L E G R W H L V D S T W G S G L V I T I 293
KY_MOUSE      M C R V A G V Q C V T V P G Y S K G F G Y Q I G Q S F S G E - F D A N A V Y L E G R W H L V D S T W G S G L V I T I 293
F1QDV7_DANRE M C R E V G I E C V E V S G Y S K G I G Y Q A R H S L A E C S D E N A V F I D G Q W W L L D A C W G A G I V M K 173
CONSERVED W                                     W                                     W

```

Figure 3.2 - Alignment of human, mouse and zebrafish Ky transglutaminase domains shows absence of conserved tryptophan residues

Alignment of human, mouse and zebrafish transglutaminase domains shows the conserved catalytic C, H and D residues (red). Conserved W shows predicted position of tryptophan residues deemed critical for efficient enzymatic function in human transglutaminase II. Conserved residues are highlighted in green, absent residues are highlighted yellow. The most upstream tryptophan, deemed critical for catalytic activity, is conserved but other residues are lost.

3.4 *in silico* examination of KY protein structure

As yet, the only annotated feature of the KY protein is the transglutaminase-like domain. To explore whether KY may contain additional identifiable features, the protein sequence of mouse KY was examined *in silico* using the Phyre2 structural analysis tool to detect structural homology to other proteins (Kelley et al. 2015). The full output of identified homologous domains can be found in Appendix 1.

As expected, the strongest homology was detected in the transglutaminase domain, with several transglutaminase core models scoring over 95% confidence of homology. Alignment shows the presence of deletions in the region containing the putative catalytic triad, supporting the conclusion that the triad is misaligned (Figure 3.3).

Additional homology was observed in the C-terminal domain, with >90% confidence of homology to transferases. Intriguingly, human FLNC Ig-like domains 4 and 5 returned as a result with >85% confidence of homology, with lesser confidence of homology to Ig-like domains 16-17 (75%) and 18-19 (59.6%) of FLNA.

#	Template	Alignment Coverage	3D Model	Confidence	% I.d.	Template Information
1	c4xz7A			100.0	20	PDB header: transferase Chain: A; PDB Molecule: putative uncharacterized protein; PDBTitle: crystal structure of a tgase
2	c3lsrB			99.9	16	PDB header: hydrolase Chain: B; PDB Molecule: transglutaminase-like enzymes, putative cysteine protease; PDBTitle: the crystal structure of a putative cysteine protease from cytophaga2 hutchinsonii to 1.9a
3	c3kd4A			99.5	12	PDB header: hydrolase Chain: A; PDB Molecule: putative protease; PDBTitle: crystal structure of a putative protease (bdl_1141) from2 parabacteroides distasonis atcc 8503 at 2.00 a resolution
38	c3v8oB			85.4	8	PDB header: structural protein Chain: B; PDB Molecule: filamin-c; PDBTitle: human filamin c ig - like domains 4 and 5
46	c2k7pA			75.0	12	PDB header: structural protein Chain: A; PDB Molecule: filamin-a; PDBTitle: filamin a ig-like domains 16-17

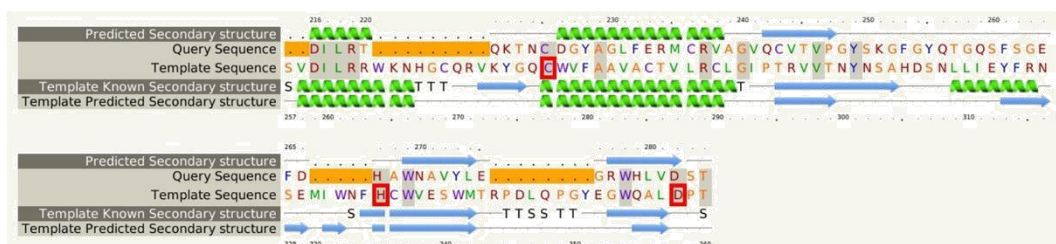


Figure 3.3 - Phyre2 output of KY protein structural homology

Top - Selected examples of homologous domains within mouse KY identified by PHYRE2 structural homology analysis (Kelley et al. 2015). The strongest homology was for transglutaminase-like proteins. Some C-terminal sequence also had homology to Filamin domains.

Bottom - Sequence alignment of KY (query) against the transglutaminase sequence. Orange highlighted areas indicate deletions in the KY sequence relative to the transglutaminase, suggestive of active site misalignment. Note that this includes sequence between the catalytic triad, indicated by the residues in the red box.

3.5 Discussion

The trend towards increased *Ky* expression in fast muscle is consistent with a previous report (Dyar et al. 2015) and thus appears likely to represent a genuine difference in expression. In addition, the report showed that levels of *Ky* expression in the soleus are consistently low whereas the level in the TA is circadian, decreasing rapidly during active hours and increasing progressively during inactive hours. Though care was taken to sacrifice both cohorts at approximately the same time of day, this may account for the variance seen in fold change differences in *Ky*

expression between the two cohorts. This expression pattern suggests that the role of KY is more physiologically relevant to fast twitch muscle, favouring the hypothesis that the pathology may arise as a result in a failure to undergo hypertrophy in response to tension as previously demonstrated in compensatory hypertrophy experiments in the EDL of *ky/ky* mice (Blanco et al. 2001). This hypertrophic blunting may have a disproportionately damaging effect on postural muscles as reduced muscle mass relative to body mass is combined with consistent levels of high tension in these muscles. Whether the hypertrophic blunting is a primary effect of the absence of KY or a secondary effect of disruption to some other mechanism that keeps muscle in a state in which it is capable of responding properly to hypertrophic stimuli is difficult to uncouple. If evidence of impaired muscle maintenance (for example, impaired FLNC turnover as determined by western blot and qPCR analyses) can be seen in juvenile mice that have yet to exhibit overt muscle pathology or show reduced muscle mass relative to body mass, this may indicate that impaired maintenance is the primary event of the pathology. Conversely, if inhibited hypertrophy (as measured by activation of the mTOR pathway and its downstream effectors) is seen in juvenile mice with no other indications of impaired muscle maintenance, this indicates the inability to undergo hypertrophy is the primary event.

However, this analysis was only performed at the mRNA level. If turnover of KY protein is lower in the soleus than the EDL, it is possible that there is no correlating trend at the protein level. Western blot analysis may help to further define the relative physiological levels of KY between muscle types. However, previous attempts to define this have been frustrated by poor antibody specificity (unpublished, personal communication).

The cross-species conservation of a tryptophan residue shown to be essential for catalytic activity, but not other residues that are conserved in other transglutaminases, indicates a selective pressure to retain activity and provides weak support to the argument that KY has an enzymatic function. However, analysis of structural homology supports the previous conclusion that the catalytic triad is misaligned. It is therefore possible that the conserved tryptophan residues are simply important in protein-protein interactions, as has been argued for the catalytic triad. Resolving the structure of KY and analysing the 3D structure of the catalytic pocket would perhaps be the most efficient way of determining whether or not catalytic activity is possible.

The presence of regions with homology to filamin ig-like domains indicates a possibility that KY might bind to FLNC-interacting proteins. FLNC domain 4 has been shown to have ligand binding properties (Sethi et al. 2014). It has been shown that FLNA domains 16-17 have a novel domain packing mode that allows unmasking of the adhesion receptor binding site of domain 17, which has been proposed as a potential mechanosensing mechanism (Heikkinen et al. 2009). Nonetheless, the small number of such potential domains would still be atypical for a structural protein and similar structural examination of the homologous regions in the KY protein would be required to determine whether these potential domains function in a similar way.

CHAPTER FOUR:
CHAPERONE
ASSISTED SELECTIVE
AUTOPHAGY IN THE
ky/ky MOUSE

CHAPTER FOUR: CHAPERONE ASSISTED SELECTIVE AUTOPHAGY IN THE *ky/ky* MOUSE

4.1 Introduction

Many of the phenotypes observed in the *ky/ky* mouse could be attributed to impaired or misregulated protein turnover, including accumulation/mislocalisation of the cytoskeletal crosslinkers FLNC and XIRP1 (Beatham et al. 2004), degeneration of the neuromuscular junction (G. Blanco et al. 2001) and the presence of autophagic vacuoles in electron microscopy of pathological muscle (Bridges et al. 1992). Impaired protein turnover may also account for an inability to undergo loading-induced hypertrophy, with the resultant cellular stress and sequestering of amino acids in aggregates inhibiting mTOR activation.

To date, no molecular examination of autophagy has been performed in the *ky/ky* mouse. Of particular interest is the novel CASA pathway, proposed to be a client-specific turnover mechanism for FLNC - a known KY interaction partner. The experiments in this chapter examine the expression levels and localisation of various factors involved in CASA and autophagy, aiming to provide insights into the state of these pathways in the *ky/ky* pathology.

CASA can be broadly broken down into the following stages: -

- Unfolding of FLNC due to tension
- Recognition of unfolded FLNC by chaperones and formation of the CASA complex
- Solubilisation of the CASA complex
- Degradation via autophagy
- Upregulation of *Fln*c transcription by soluble BAG3 (indirectly)

Evidence of impairment in any of these stages would be suggestive of a role for KY in this process, either as an active factor or as a component necessary to maintain muscle in a competent state to efficiently activate and execute this pathway. These experiments primarily examined two specific hindlimb muscles: the soleus and the EDL. The soleus is a slow, postural muscle which experiences consistent tension. The EDL is a fast-twitch muscle which is only mechanically engaged during voluntary movement. In the *ky/ky* mouse, the soleus is atrophic and shows hallmarks of structural damage and regeneration. The EDL, though smaller than its

WT counterpart, shows no overt pathology. Thus, data about the soleus can provide insights into the extent and impact of the atrophic pathology whereas data about the EDL may provide insight into the primary effects of the absence of KY without the confounding secondary effects of atrophy and regeneration.

4.2 BAG3 turnover in the *ky/ky* mouse

Given that BAG3 is a central co-chaperone in CASA, and an indicator of cell stress, levels of BAG3 protein were examined in mutant muscle tissue. Initial experiments were unable to detect a difference in BAG3 protein levels between WT and *ky/ky* muscle lysates extracted using RIPA buffer (data not shown). This extraction was only capable of extracting soluble proteins, and thus did not allow the detection of elevated amounts of insoluble or cytoskeleton-associated proteins. Since impairments to CASA are likely to result in elevated levels of these latter proteins, a fractionation kit was used to obtain soluble and cytoskeletal protein fractions, including intermediary fractions (see methods 2.8.2 for details). In this analysis, elevated levels of cytoskeleton-associated BAG3 were observed in the soleus muscle of *ky/ky* mice compared to WT (Figure 4.1 A and B). Consistent with the previous experiments, there was no significant increase in the amount of soluble BAG3 in the soleus. This suggests that an increased proportion of BAG3 protein is associated with the cytoskeleton in the *ky/ky* soleus compared to WT. The non-atrophic EDL showed no indication of elevated soluble or cytoskeletal BAG3 protein.

Examination of *Bag3* mRNA levels shows a significant increase in the EDL, but not in the soleus (Figure 4.1 C). This indicates that the elevated amount of cytoskeletal BAG3 protein in the soleus may not be accounted for by elevated mRNA levels, but is instead indicative of reduced turnover. Given that the only increase occurred in the cytoskeletal fraction, this may indicate a failure to solubilise BAG3 or its interaction partners. In contrast, the comparable BAG3 protein levels between *ky/ky* and WT EDL combined with elevated mRNA indicates that BAG3 turnover is elevated in the mutant EDL tissue.

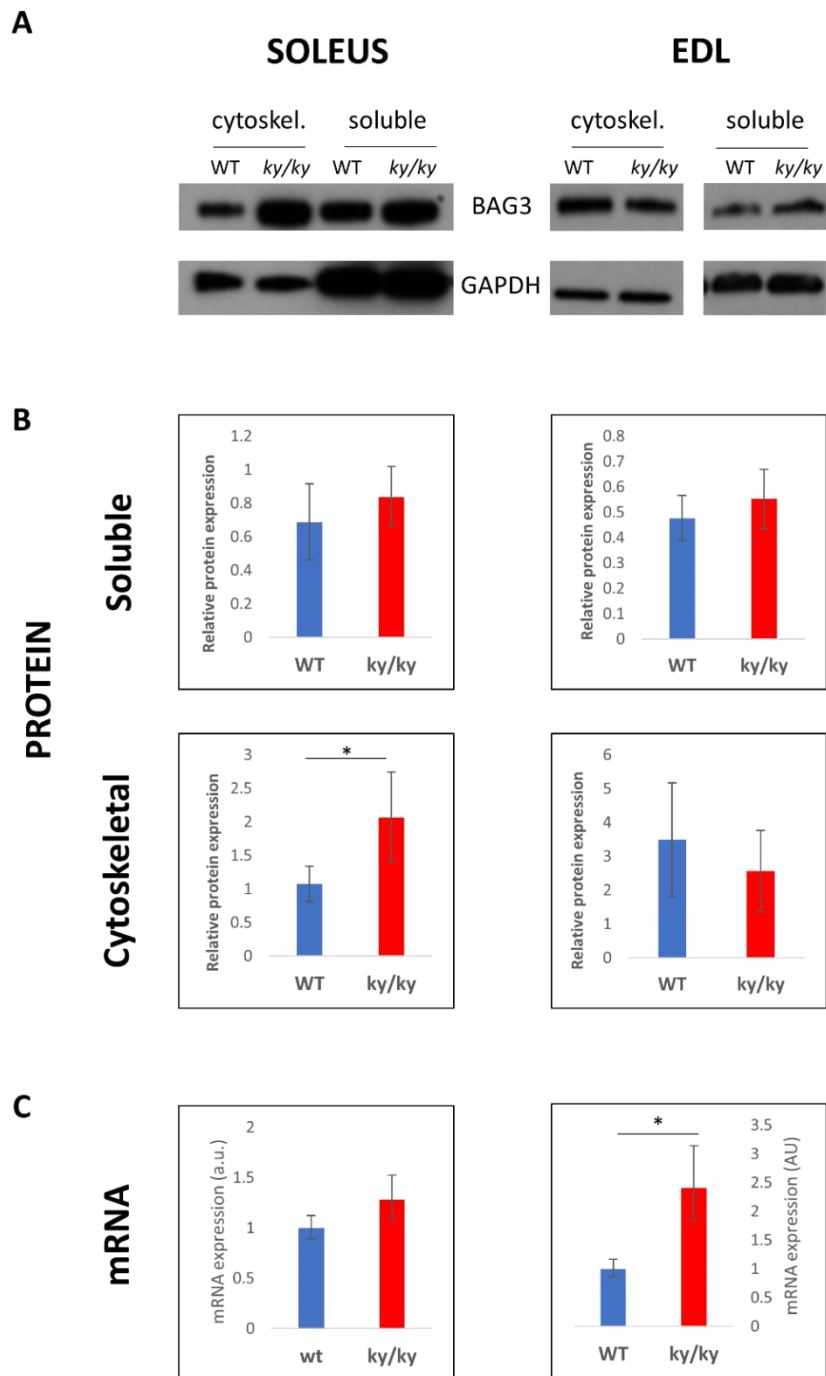


Figure 4.1 - Quantification of BAG3 protein and transcript in soleus and EDL

A) Representative WB of cytoskeletal and soluble BAG3 and GAPDH expression in the WT and ky/ky soleus and EDL. B) Quantification of BAG3 protein levels by densitometry normalised to GAPDH. The cytoskeletal proportion of BAG3 protein is significantly enhanced in the ky/ky soleus (Student's t-test, $p < 0.05$, $n = 8$) though no other significant changes in protein level were detected. C) mRNA quantification of Bag3 transcript relative to the housekeeping gene hprt. The EDL shows a significant increase in Bag3 expression (Student's t-test, $p < 0.05$, $n = 3$). Error bars indicate standard deviation.

4.3 Increased immunoreactivity for FLNC in the *ky/ky* soleus

Immunofluorescence experiments were performed to visualise the levels and localisation of BAG3 and FLNC in *ky/ky* and WT soleus sections (Figure 4.2 A). Both BAG3 and FLNC were elevated in a subset of fibers in the *ky/ky* mutant. Those fibres showing particularly high levels of BAG3 also showed similarly elevated FLNC. The proteins remained primarily co-localised in a striated pattern, presumably the z-disc. This is consistent with an increased proportion of cytoskeletal-associated BAG3 (Figure 4.2 A overlay). qPCR was performed to explore whether this increased immunoreactivity represented an increase in *Fln*c transcription (Figure 4.2 B). No significant increase in *Fln*c transcript was detected between WT and *ky/ky* tissues. Similarly to BAG3, this may indicate lower turnover of FLNC protein in the *ky/ky* soleus. Given that BAG3 and FLNC primarily seem to co-localise, this reduces the likelihood that KY is essential for interactions between BAG3 and FLNC, or the recognition of unfolded proteins given that the BAG3-FLNC interaction is mediated by co-chaperones binding to exposed KFERQ motifs. The elevated reactivity for cytoskeletal protein may represent a failure to solubilise the CASA complex.

4.4 Profiling of other autophagy components

To examine for evidence that autophagy might be activated differently in *ky/ky* muscles, qPCR of *Beclin*, *p62* and *Lc3* was undertaken. No significant differences were detected at the mRNA level, suggesting activation of autophagy is similar between WT and *ky/ky* tissue (Figure 4.3). However, in the absence of protein-level characterisation, only limited conclusions can be drawn concerning autophagy flow.

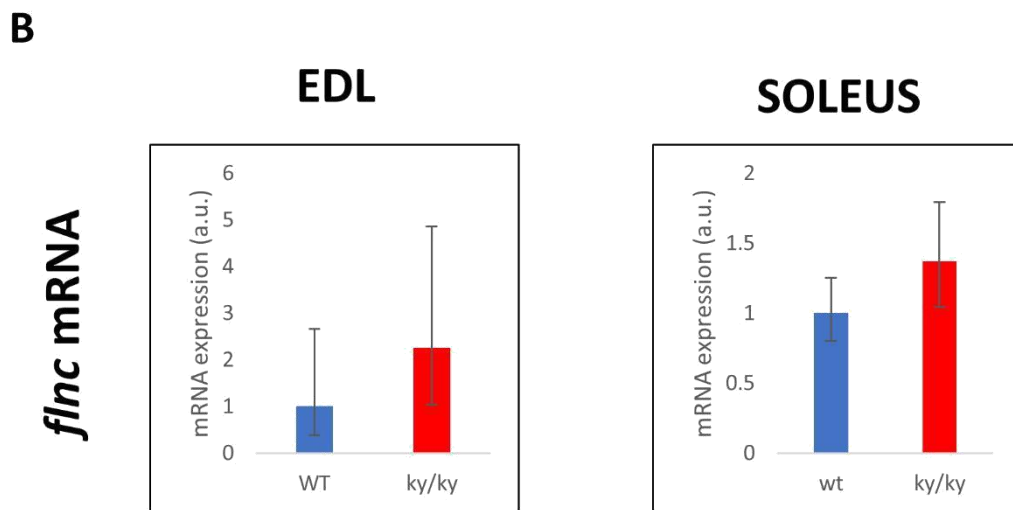
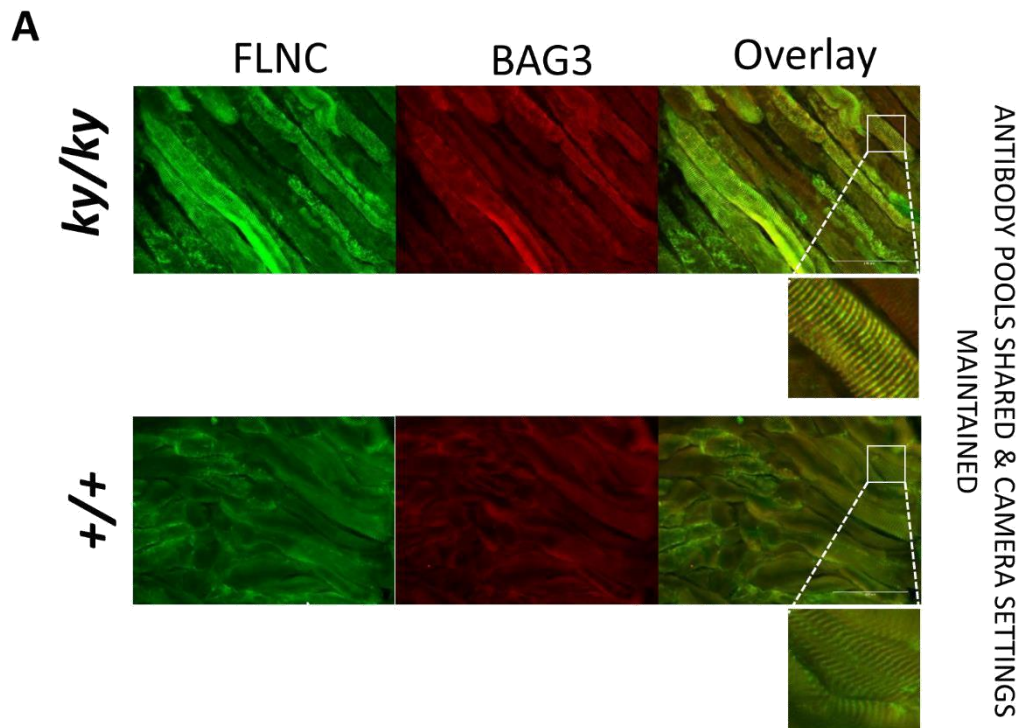


Figure 4.2 - Increased immunoreactivity for cytoskeletal FLNC in *ky/ky* soleus

A) Representative longitudinal sections of soleus muscle from 8-week old mice showing endogenous FLNC (FITC) and BAG3 (TRITC). The *ky/ky* mouse showed higher immunoreactivity to both FLNC and BAG3 in a subset of fibres, which is primarily co-localised to the cytoskeleton - presumably the z-disc (Inset). However, some fibres in the WT section do not appear to have been cut fully longitudinally B) qPCR of *Flnc* in the EDL and soleus of WT and *ky/ky* mice shows no significant differences in expression between WT and mutant (Student's *t*-test, $P > 0.05$, $n = 3$). Error bars indicate standard deviation.

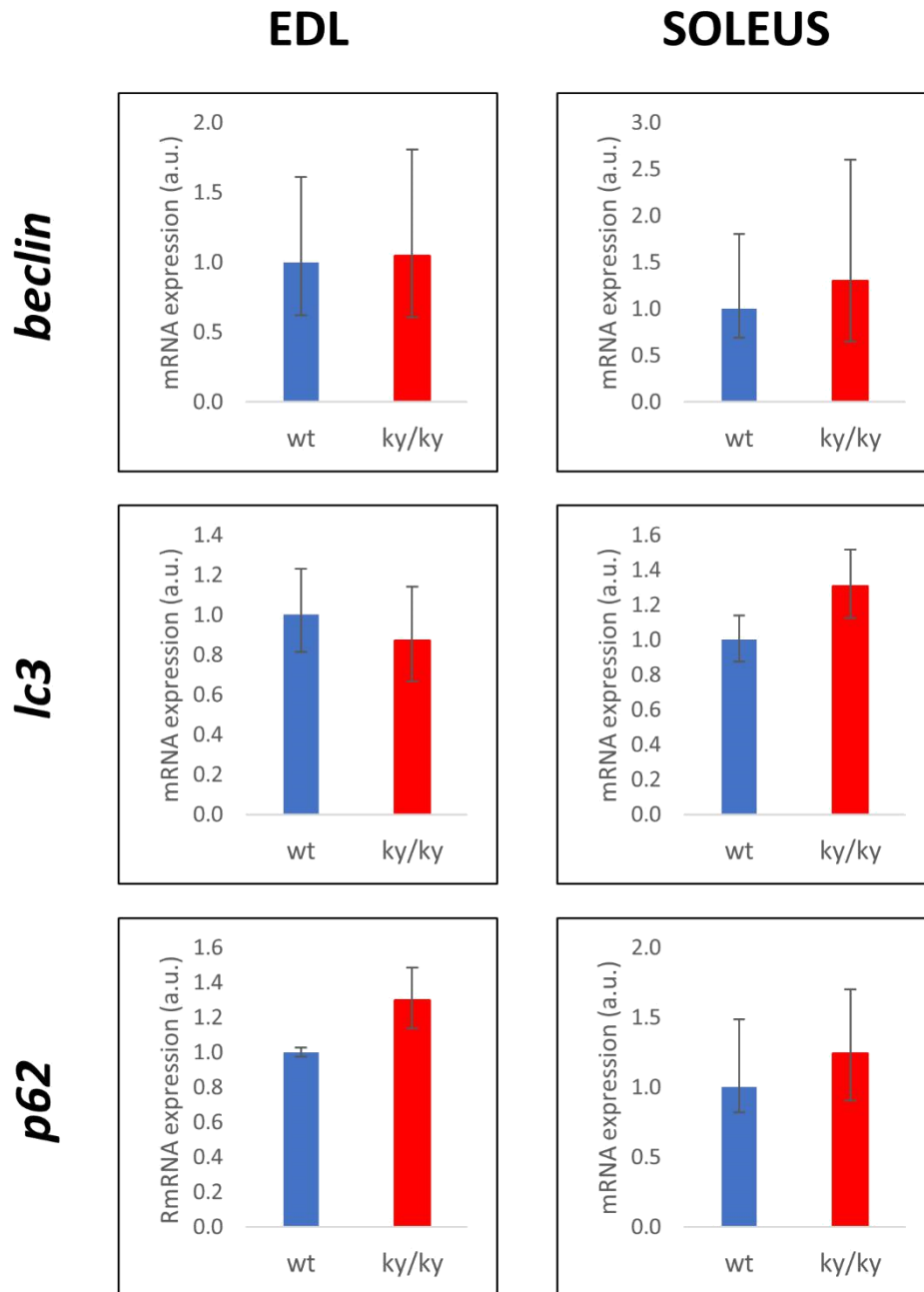


Figure 4.3 - Autophagy markers in the ky/ky mouse

qPCR profiling of Beclin, Lc3 and p62 show no significant differences between WT and mutant tissues (Student's t-test, $p > 0.05$) Error bars indicate standard deviation

4.5 Examination of other CASA markers

Western blot analysis of CHIP was made particularly difficult by the presence of multiple bands (figure 4.4). Qualitative assessment showed no consistent differences between band intensities between WT and *ky/ky* tissue in either soluble

or cytoskeletal fractions, indicating no evidence of CHIP also failing to solubilise in the *ky/ky* mutant. However, this could be accounted for by redundancies between E3 ubiquitin ligases diluting this effect.

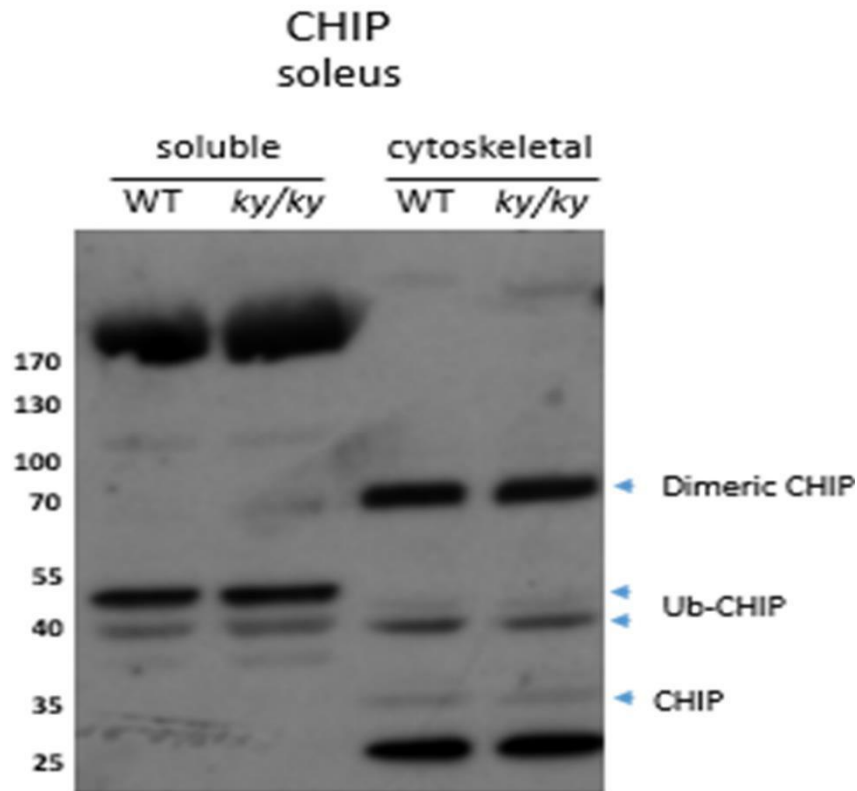


Figure 4.4 - No qualitative differences in CHIP expression in *ky/ky* tissue

The CHIP antibody reacts to a number of different CHIP species and non-specific bands, including CHIP, mono- and di-ubiquitinated CHIP and dimeric CHIP, approximately labelled by the blue arrows. The difficulty in precisely identifying each species impeded quantitative analysis, but qualitative assessment indicates no differences between WT and *ky/ky* tissue

4.6 - Conclusions

The enhanced reactivity for cytoskeletal BAG3 and FLNC in the *ky/ky* soleus, in the absence of transcriptional upregulation, indicates that turnover of these proteins may be impacted in tissue that experiences high tension. The cytoskeletal colocalisation is consistent with the notion that the CASA complex may be failing to solubilise. Further IF analysis using additional CASA markers, such as HSPB8 and CHIP might provide additional evidence that the increased reactivity represents higher levels of unfolded protein if these markers also show increased colocalization to the cytoskeleton with FLNC and BAG3. However, the level of resolution provided

by IF is not sufficient to properly determine protein-protein interactions. Other imaging techniques such as Förster Resonance Energy Transfer (FRET) between fluorescently tagged BAG3 and FLNC proteins may provide data about BAG3-FLNC interactions at a more meaningful resolution. Additionally, increased signal in IF may represent better epitope availability of the FLNC and BAG3 proteins in the absence of KY, rather than demonstrating higher protein levels in isolation. As such, fractionated western blot data for FLNC would be critical for determining whether there is genuinely a greater level of cytoskeletal FLNC.

qPCR of autophagy components provides no evidence of altered activation of autophagy gene transcription. However, relative autophagy levels can only be robustly determined with protein-level characterisation which is lacking in this analysis due to difficulty in consistently detecting LC3 and p62 by western blot. Evidence in the literature indicates an accumulation of autophagic vacuoles in the affected *ky/ky* muscles (Bridges et al. 1992). If there is no transcriptional upregulation of autophagy, this may indicate that this accumulation represents a bottleneck in autophagosome turnover.

In contrast the *ky/ky* EDL shows apparent enhanced BAG3 turnover, potentially indicating enhanced activation of the CASA pathway even in the absence of overt muscle pathology. This indicates that KY is not required for the sensing of mechanical forces in the context of CASA and that CASA upregulation may be an early hallmark of the *ky/ky* pathology. However, whether dysregulation of CASA is a causal factor in the *ky/ky* pathology or the result of (for example) underlying structural instability in the absence of KY cannot be resolved with this data.

CHAPTER FIVE:
GENERATION
AND ANALYSIS OF
KY-KNOCKOUT
MYOBLASTS

CHAPTER FIVE: GENERATION AND ANALYSIS OF KY-KNOCKOUT MYOBLASTS

5.1 Introduction

The aim of this chapter was to develop and analyse a C2C12 myoblast cell line deficient in KY using CRISPR/Cas9 technology. This would serve to provide a more tractable experimental model to explore the hypothesis generated from mouse experiments that KY may act to help solubilise the CASA complex. The mouse model was able to provide 'snapshots' of the state of CASA and autophagy in the *ky/ky* mouse but lacked the ability to easily provide mechanistic insights. It was hoped that a cellular model would provide a means to more directly explore the effects of mechanical stimulation and autophagy modulation on cells and how these processes may be impacted by KY deficiency. In addition, this would work towards the 3 R's guiding animal experimentation: reducing, refining and replacing the use of mice.

5.2 Target identification and CRISPR/Cas9 construct generation

The E-CRISP online tool (Heigwer, Kerr, and Boutros 2014) was used to select several potential target sequences in the *ky* gene (<http://www.e-crisp.org/E-CRISP/>). Figure 5.1B shows the identified target sequences and their location in the *Ky* gene.

This project utilised the existing PX459 vector from Addgene, which contains sequence encoding the Cas9 enzyme, the generic portion of the guide RNA as well as antibiotic resistance genes, including puromycin. The construct is made specific by cloning the target sequence into a specific site on the plasmid, completing the gRNA coding sequence (Figure 5.1 A). For the cloning, pairs of oligonucleotides were ordered that, upon annealing, contain the target sequence (Figure 5.1 B) as well as overhangs complementary to the sticky ends generated in the plasmid by digestion with *Bbsl*. Ligation of the annealed oligonucleotides and vector backbone was undertaken with T4 DNA ligase, with ligation products transformed into competent *E. coli*. Minipreps of the resulting colonies produced copies of the plasmids which could be screened for insertion by digestion with *Bbsl*, as this site should be eliminated in successful cloning (Figure 5.1 C). Correct insertion of the target sequence was confirmed via sequencing (Figure 5.1 D).

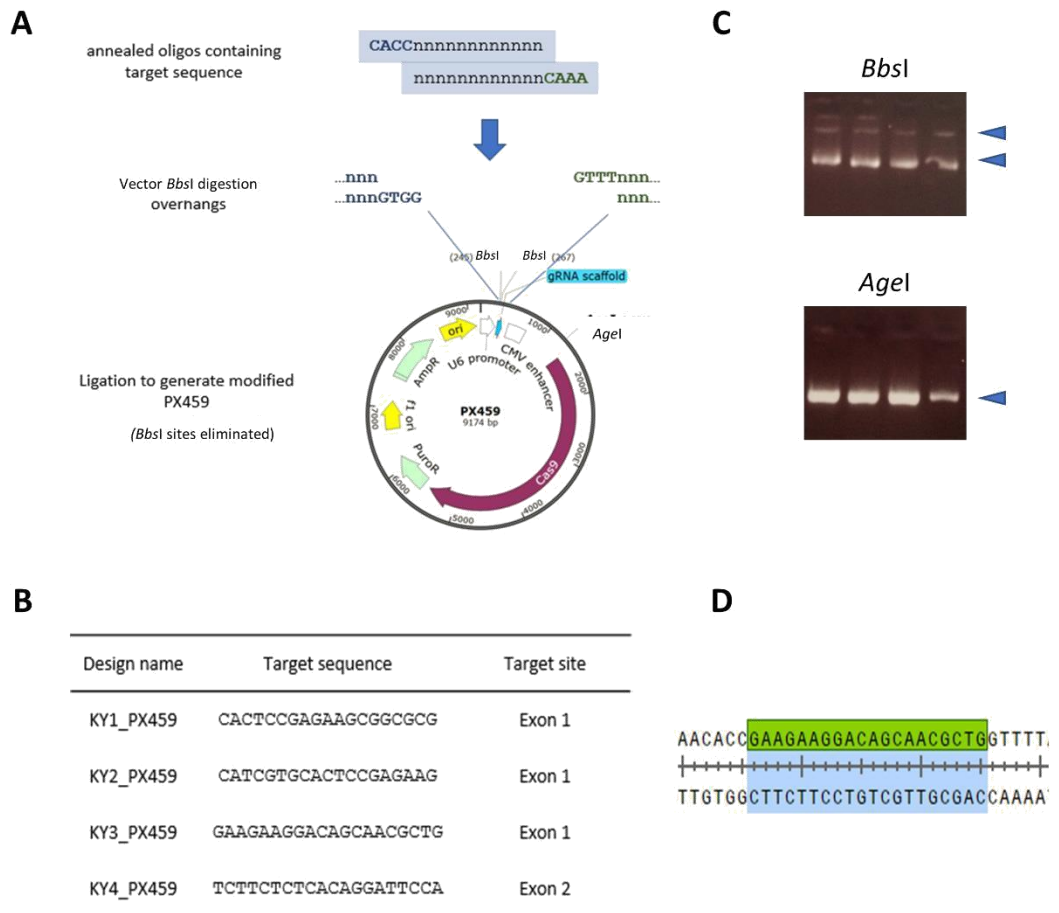


Figure 5.1 - Generation of specific KY_PX459 targeting vectors

A) Method of targeting vector assembly. Annealed oligo pairs containing target sequence (B) and complementary overhangs to those left by *BbsI* digestion of PX459. Ligation of annealed oligos and digested PX459 produces the Ky targeting vectors and eliminates the *BbsI* digestion site. C) Screening for successful insertion was performed by digestion tests using *AgeI* (positive control, shows linearised plasmid only) and *BbsI* (negative control, shows supercoiled plasmid band) and D) sequencing..

5.3 Confirmation of mutagenesis

C2C12 cells in 6-well plates were transfected with the KY-PX459 plasmids (as named in Figure 5.1 B) and left to express the construct for 48h prior to selection using puromycin-enriched media. The surviving cells were grown to confluency, remaining under puromycin selection.

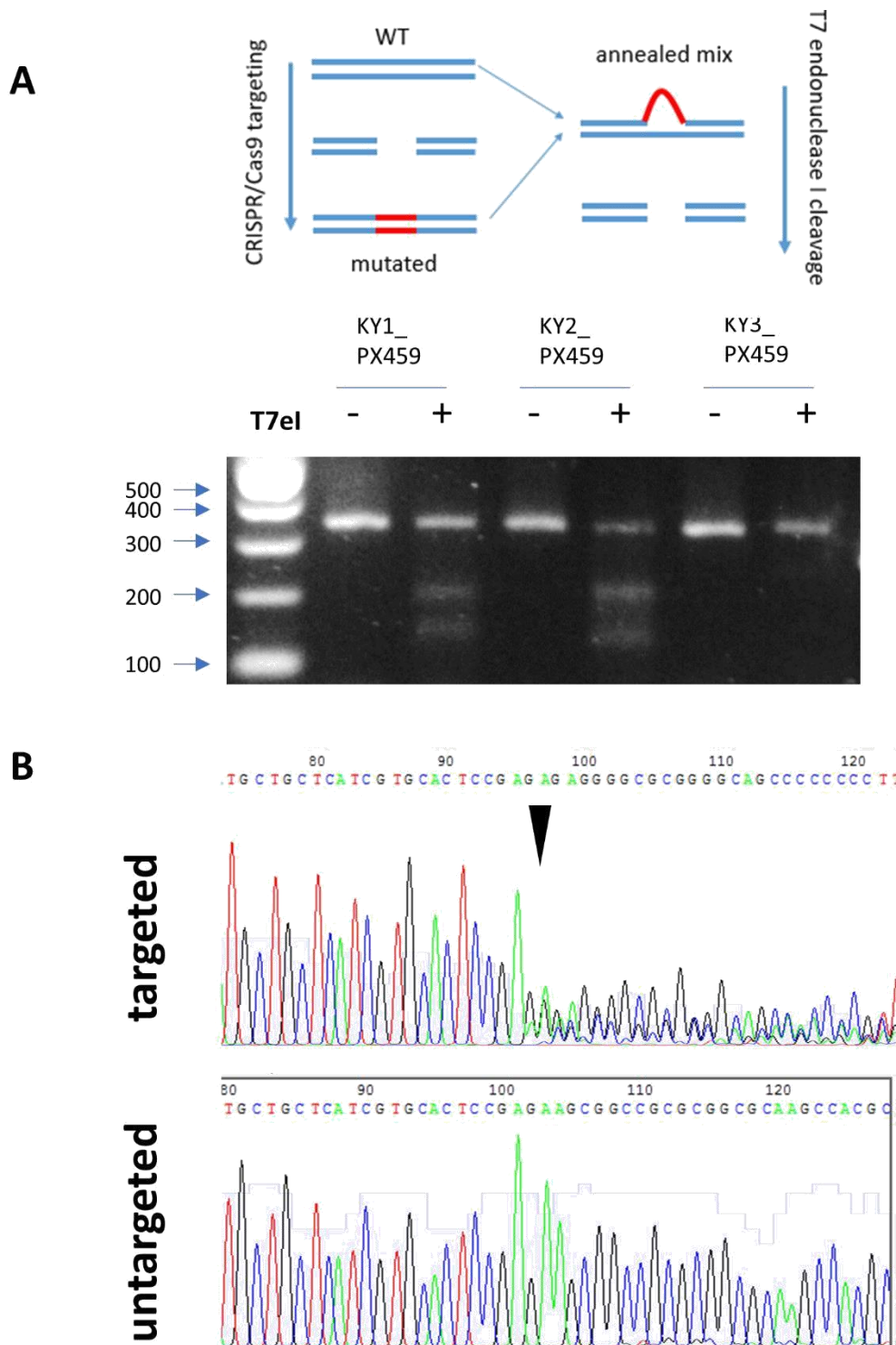


Figure 5.2 - Confirmation of targeting vector mutagenic capability

A) Schematic of the *T7el* assay and results using PCR products obtained from cells transfected with targeting vector. The production of digestion products indicates the generation of mutations. B) Sequencing data from the same PCR products shows a sharp transition to multiple basecalls at the predicted cleavage site (black arrow), indicating mutagenesis has generated multiple alleles.

Cells were harvested and pelleted before lysis and PCR. PCR products were treated with T7 endonuclease I (T7el) to test for the presence of mismatches between annealed PCR products – i.e. heteroduplexes - arising as a result of mutagenesis (See Figure 5.2 A). T7el is expected to cleave heteroduplexes at the site of the mismatch, resulting in digestion products of specific sizes. Detection of digestion products of expected sizes were produced from C2C12s transfected with KY1-PX459 and KY2-PX459. Sequencing of PCR products from targeted cells shows a sharp transition to ambiguous basecalls near to the predicted Cas9 cleavage site, indicating the presence of mutant alleles (Figure 5.2 B). Given KY1-PX459 was the most upstream target sequence, this was selected to cause maximum disruption to the *Ky* gene.

5.4 Clonal selection and identification of KY KO clones

An outline of the clonal selection methodology is shown in Figure 5.3. Transfection of C2C12 cells with KY1-PX459 was repeated in 6-wells of a 6-well plate. Similarly, puromycin selection was undertaken 48h post-transfection. To maximise the efficacy of puromycin selection - which works best on proliferating cells - cells were split across two 6-well plates prior to the addition of puromycin-enriched media to ensure that the cells were not confluent. Across the plates, approximately 30 surviving colonies were observed. Whether they arose from single cells or multiple cells in close proximity was often unclear. To ensure that colonies arose from a single cell, cells across the plates were mixed and individual cells were isolated by dilution across a 96 well plate to ensure the generation of individual clones. 25 clones were generated, named A through Y. Mutagenesis of the mixed population was confirmed by lysis and PCR, and the detection of heteroduplexes in high percentage acrylamide gels in order to ensure that the transfection was successful before analysis of the individual clones.

Individual clones were allowed to proliferate without the addition of puromycin to the media, as continued enrichment of the media with puromycin appeared to have an inhibitory effect on growth even in apparently resistant cells (data not shown). Once sufficiently grown, cells were split, with one fraction frozen and the other lysed for PCR. To test for mutation of *Ky* in these clones, PCR products from colonies were first mixed and annealed with WT PCR product and run on high percentage acrylamide gels to detect the presence of heteroduplexes. From the original 25, seven clones were thus identified: B, D, F, G, I, K and U.

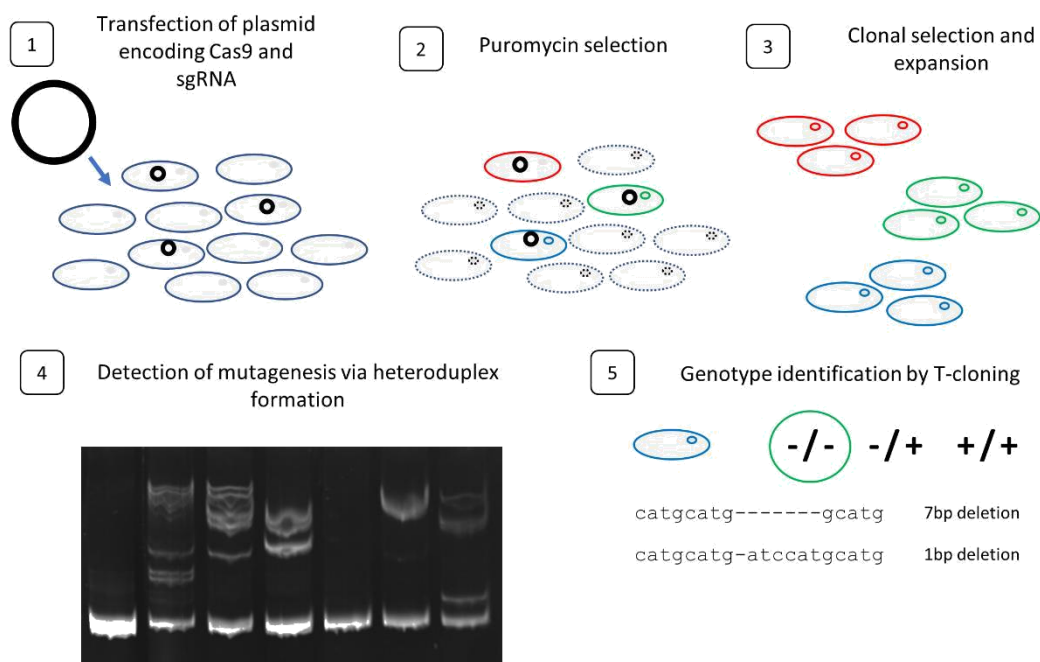
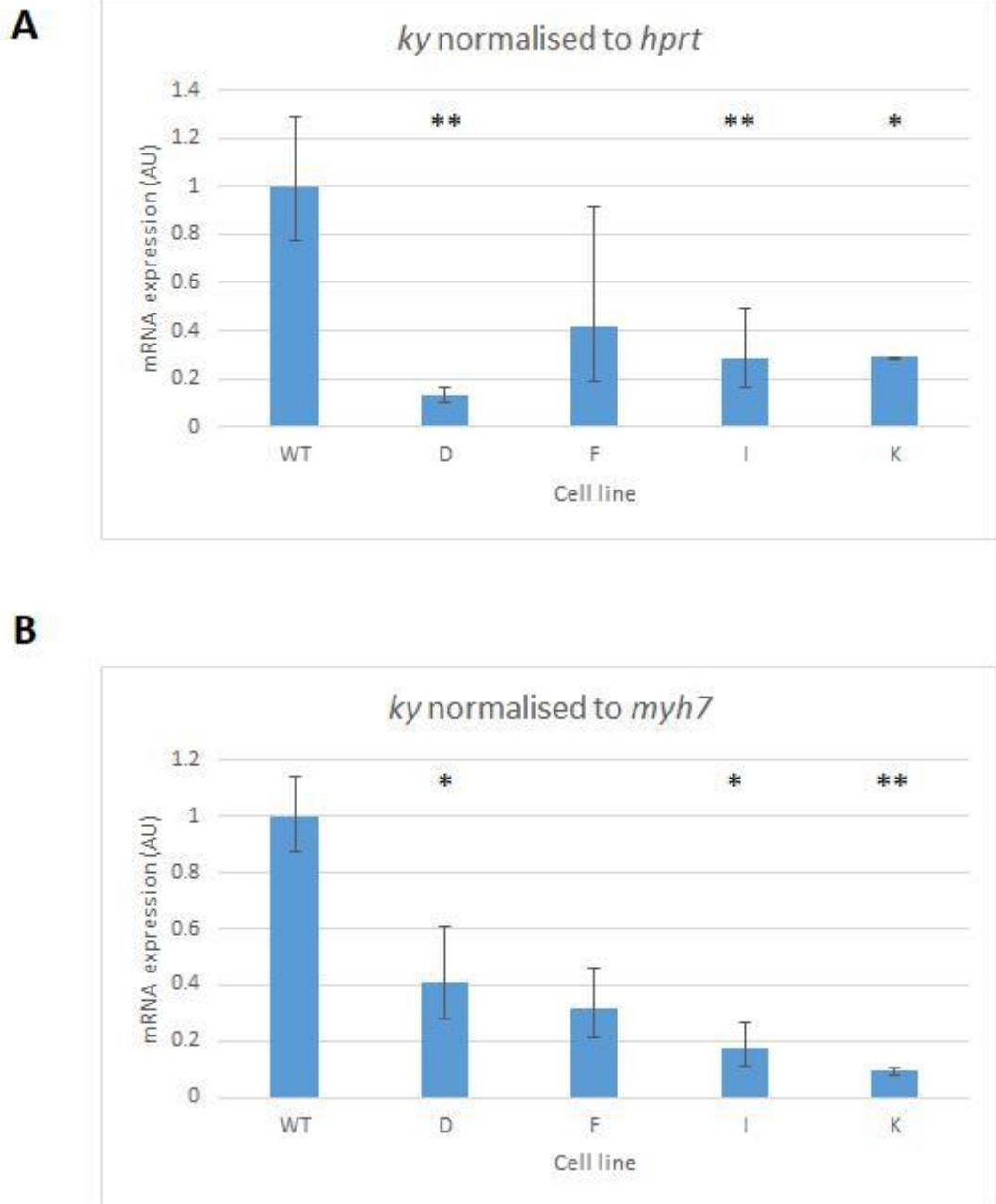


Figure 5.3 - Clonal selection and identification of disruptive clones

Top) Process of clonal selection and screening: 1) Cells were transfected with the KY_PX459 construct and 2) selected for puromycin resistance. 3) Clones were expanded from the surviving cells. 4) High percentage acrylamide electrophoresis of PCR products from successfully mutagenised cells produces heteroduplex banding (representative gel shown). 5) T-cloning of mutagenised cells identifies mutant alleles.

T-cloning of PCR products from these clones was performed to isolate individual alleles. Table 5.1 shows the alleles identified in each clone. From this, it was predicted that clones D, F, I and K contain two disruptive alleles, and thus were likely to be deficient in KY. The genotype of I and F appears to be identical. However, both have been carried forward independently as differences between the two may act as a measure of the stochastic effects of clonal selection. Only a WT allele could be isolated from clone U due to a lack of efficiency in the T-cloning protocol, but this was sufficient to eliminate it as a full knockout clone. qPCR analysis of *Ky* expression indicates significant reduction of transcript in clones D, I and K when normalised to *Hprt* (Student's T-test, $p < 0.05$, $n \geq 2$) (Figure 5.4 A). To eliminate the potential confounding factor of different states of differentiation, normalisation to *Myh7* was used. D, I and K remained significantly lower, though all

clones still showed reduction in transcript levels (Student's T-test, $p < 0.05$, $n \geq 2$) (Figure 5.4 B).



5.4 - qPCR quantification of *Ky* transcript in knockout clones

A) *Ky* expression normalised to the housekeeping gene *hprt* in differentiated myotubes. B) *Ky* expression normalised to *myh7*. * indicates significant reduction of transcript at the $p < 0.05$ and ** $p < 0.01$ level compared to WT expression. (Student's t-test, $n \geq 2$). Error bars indicate standard deviation.

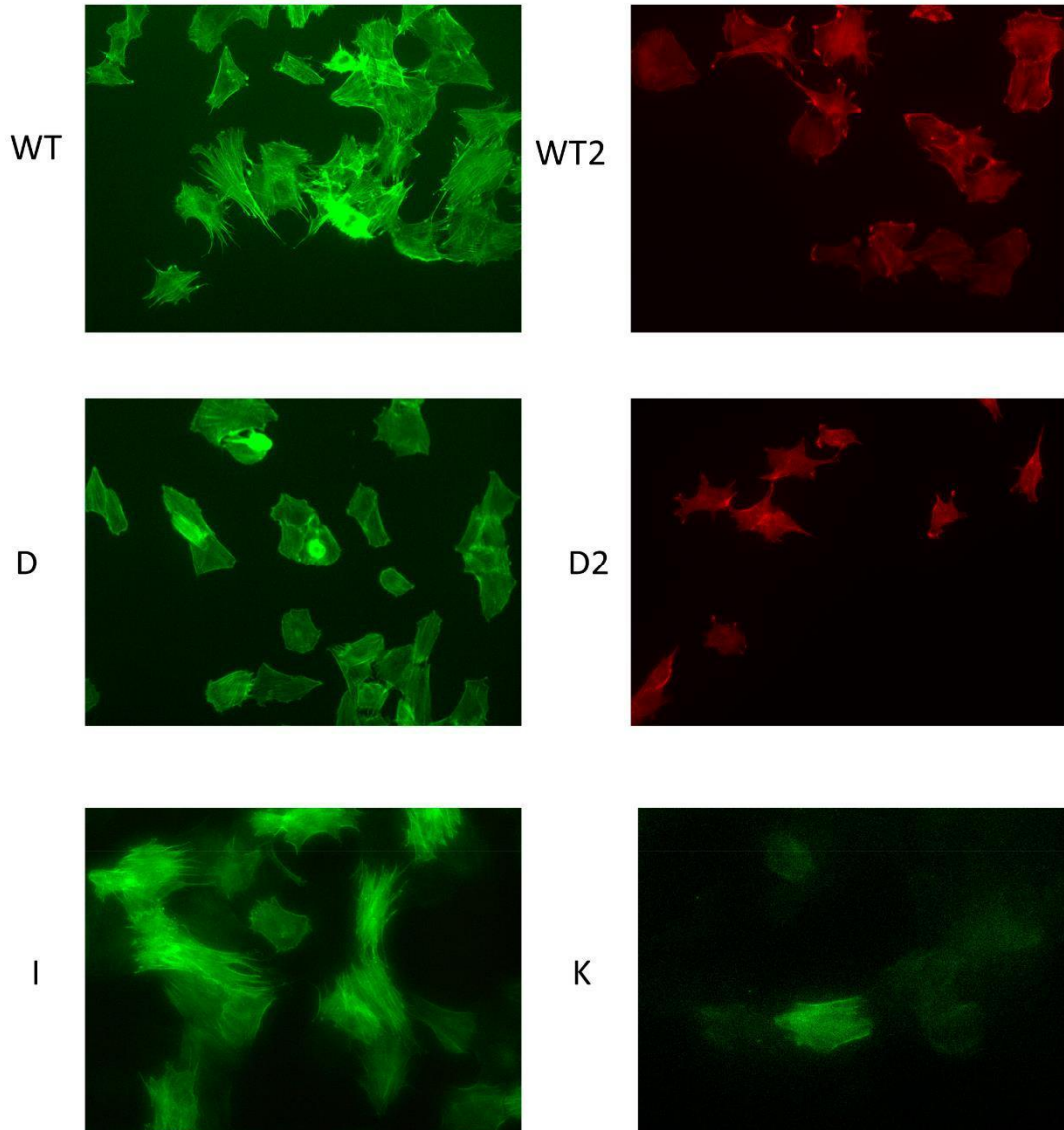
Table 5.1 - Mutated alleles detected in mutant clones

Clone	Allele sequences	Mutation	Disruptive?
B	CGTGCACTCCGAGAAGCGGCGCGGG	None	No
	CGTGCACTCCGAGAA-CGGCGCGCGG	1 bp deletion	Yes
D	CGT-----CGCGCGG	16 bp deletion	Yes
	CGTGCACTCCG-----CGCGG	10 bp deletion	Yes
F	CGTGCACTCCGAGAAGCGGC C GCGCGG	1 bp insertion	Yes
	CGTGCACTCCGAGAAGCGGC G GCGCGG	1 bp insertion	Yes
G	CGTGCACTCCGAGAAGCGGC G GCGCGG	1 bp insertion	Yes
	CGTGCACTCCGAGAA---GCGCGCGG	3 bp deletion	No
I	CGTGCACTCCGAGAAGCGGC C GCGCGG	1 bp insertion	Yes
	CGTGCACTCCGAGAAGCGGC G GCGCGG	1 bp insertion	Yes
K	CGTGCACTCCGAGAAGCGGC C GCGCGG	1 bp insertion	Yes
	CGTGCACTCCGAG-----GCGCGG	7 bp deletion	Yes
U	CGTGCACTCCGAGAAGCGGCGCGGG (no second allele recovered)	None ?	No ?
WT	CGTGCACTCCGAGAAGCGGCGCGGG	None	No

5.5 Morphological analysis of KY-deficient C2C12 myoblasts

The disruptive clones showed no overt morphological changes under brightfield microscopy alone. Phalloidin staining was performed in order to examine whether the difference in size might be due to differences in the actin cytoskeleton organisation. Though there were some differences in morphology observed (examples shown in figure 5.5) they were not observed consistently meaning it is unlikely to be a genuine effect of Ky-deficiency. Crystal violet staining shows that the cells have similar morphology, but quantification of cell area indicated that myoblasts from clones D, I and K were significantly smaller on average than WT controls (Student's t-test, $p < 0.01$, n shown in figure 5.6). Attempts to rescue this phenotype by transfection with KY constructs did not reach sufficient efficiency to

allow quantification (data not shown). However, the consistency of this trend across multiple mutant clones indicates that this may present a genuine phenotype..



5.5 - Phalloidin staining of myoblasts shows no consistent morphological changes

Some differences in morphology were initially observed between WT and D, with D showing fewer projections and more rounded cells. I and K showed a more similar phenotype to WT. However, on repeating, the contrast between WT2 and D2 is much less marked, indicating the initial differences observed were stochastic and not a genuine phenotype.

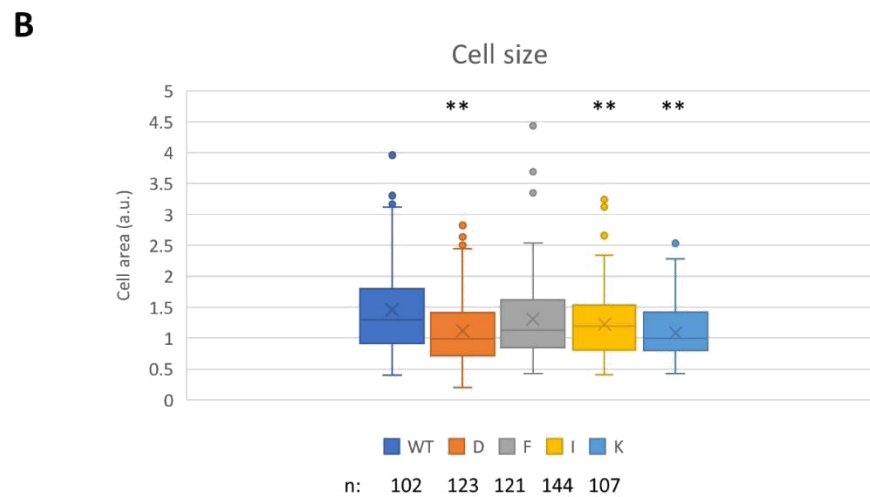
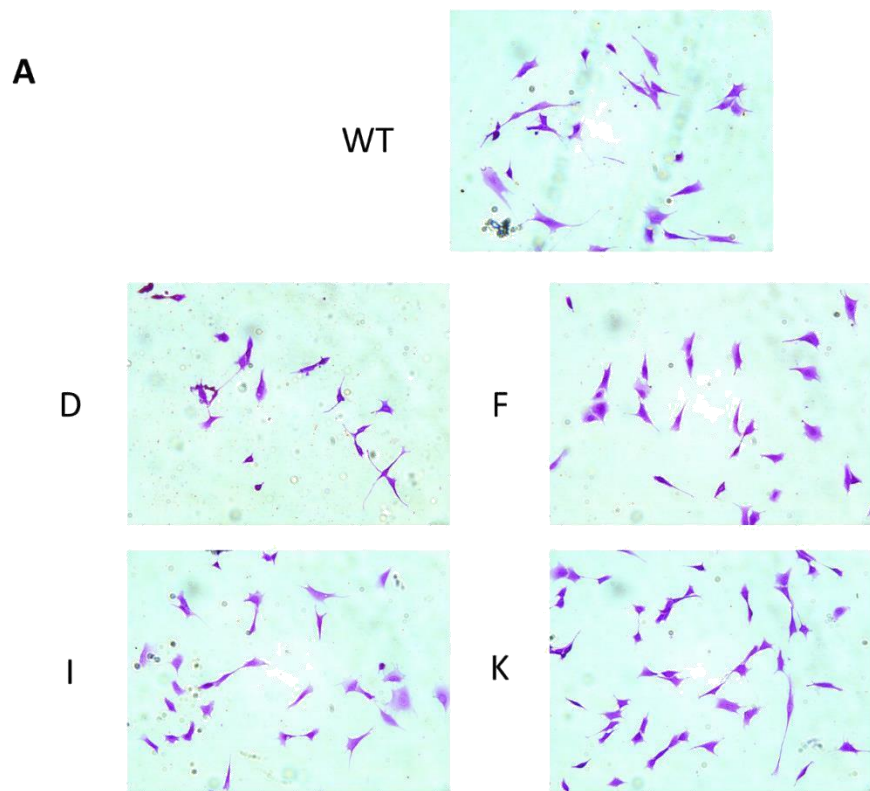


Figure 5.6 - Crystal violet staining of myoblasts indicates morphological changes

A) Representative images of myoblasts stained with crystal violet solution. B) Box-and-whisker plot of quantification of cell area. Analysis shows clones D, I and K are significantly smaller on average compared to WT (Student's t-test, $p < 0.01$, number of cells shown on graph). The box represents the upper and lower quartiles, with the central horizontal line indicating the median. The x indicates the mean value. The limits of the whiskers indicate the maximum and minimum values, excluding the outliers represented as circles.

5.6 Differentiation analysis of KY-deficient C2C12 myoblasts

All disruptive clones were able to undergo differentiation. Phalloidin and DAPI staining of myotubes shows that all clones were able to form multinucleated tubes, further evidencing the capacity for differentiation (Figure 5.7). *Myh7* increases in the late stages of C2C12 differentiation and can therefore be used as a measure of differentiation capacity (Figure 5.8 A(i)). Expression levels of *Myh7* were examined by qPCR between WT and mutant myotubes after 10 days in differentiation medium. Though there was some variance, including a significant 2-3 fold higher level of expression in clone K compared to WT, this falls far short of the ~250-fold induction of *Myh7* reported during C2C12 differentiation (Wright et al. 2014), indicating that *Myh7* expression was robust in all clones (Figure 5.8 B). These differences are therefore likely to represent stochastic differences in differentiation, for example the proportion of myotubes in advanced stages of differentiation, rather than indicating an impaired or enhanced capacity to differentiate.

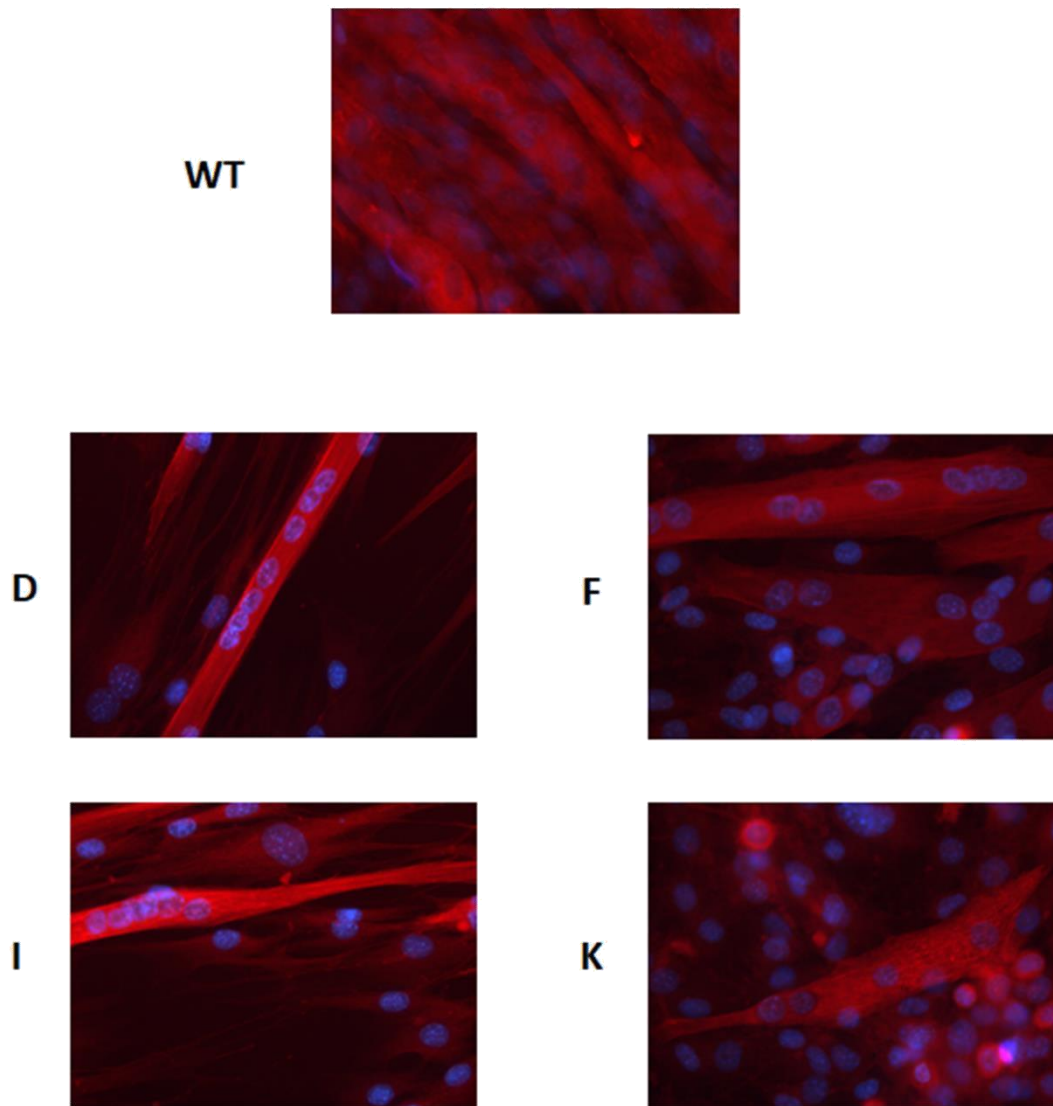


Figure 5.7 - Phalloidin staining of myotubes

Phalloidin staining of myotubes shows that all clones were capable of forming multinucleated tubes, indicating the capacity for cell fusion and myotube formation.

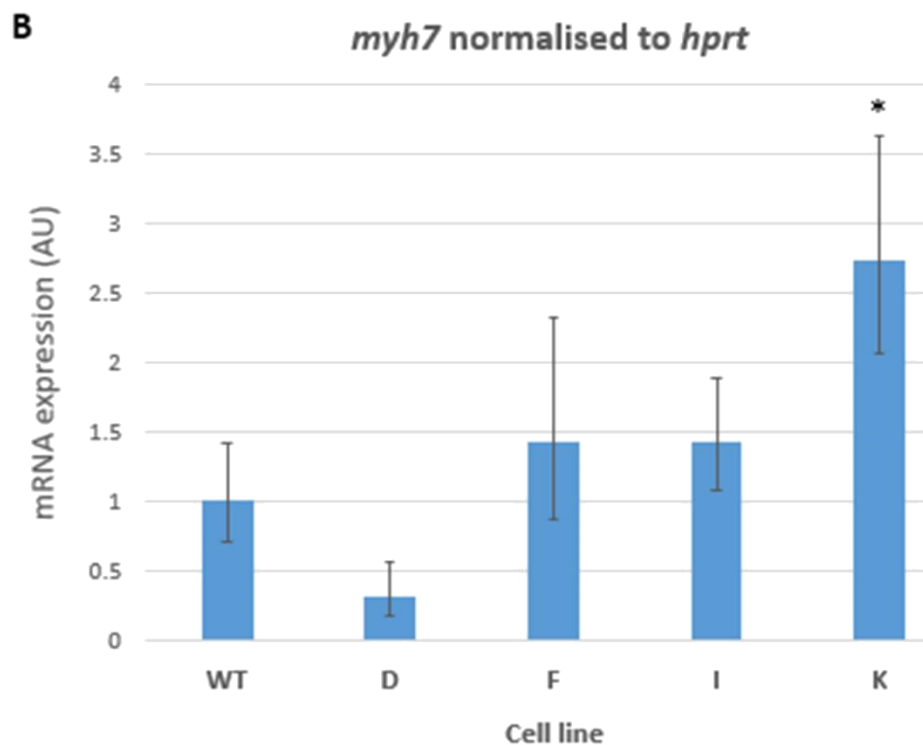
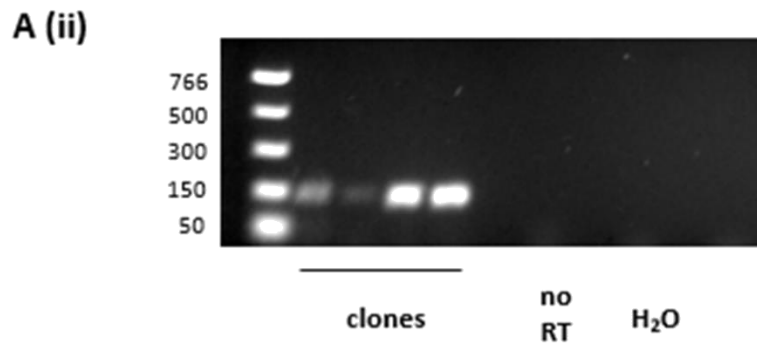
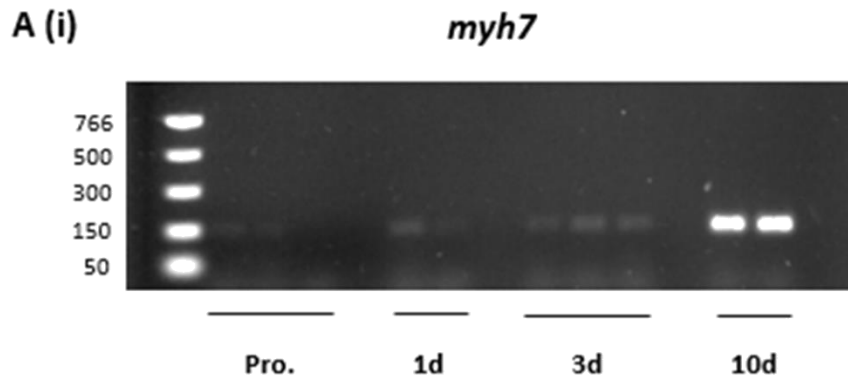


Figure 5.8 - Differentiation capacity of clones measured by *myh7* expression

Ai) RT-PCR from proliferating myoblasts and differentiating cells after 1, 3 and 10 days in differentiation media shows a progressive increase in *myh7* expression, demonstrating its suitability as a late-stage differentiation marker. Aii) RT-PCR from miscellaneous clones shows *myh7* expression. B) qPCR of *myh7* for clones shows some variance, but only clone K is significantly different with a 2.7-fold increase (Student's *t*-test, $p < 0.05$, $n = 3$). Error bars represent the standard deviation.

5.7 CASA in KY-deficient C2C12 proliferating myoblasts

Given that *Ky* is expressed in proliferating myoblasts (Fig 5.9 A), and the CASA mechanism was characterised in smooth muscle cells, it was hypothesised that FLNC turnover might still be impacted by the absence of KY in myoblasts even though the expression of the FLNC client is much lower in myoblasts than in myotubes. However, qPCR analysis of *Bag3* and *Fln*c transcription was incredibly noisy and no useful interpretations could be made of the data (Fig 5.9 B). This suggests that the C2C12 proliferative myoblast model may not be suitable for examining the CASA pathway.

5.8 CASA in KY-deficient C2C12 myotubes

Since differentiation generates sarcomeric structures, a myotube model better represents the physiology of skeletal muscle. Additionally, FLNC expression is more robust in myotubes, making it a more suitable model for examining the proposed mechanism of its turnover. *Ky* has also been shown previously to be robustly expressed in differentiated myotubes (Baker et al. 2010). Comparisons between WT and *ky*-deficient myotubes therefore represent the best model for examining a role for KY in CASA *in vitro*.

qPCR analysis shows a consistent, but non-significant, upward trend in *Bag3* transcription across the mutant lines (Figure 5.10 A).. For *Fln*c transcription, when normalised to the housekeeping gene *Hprt* clones D and F showed significant increases in transcript, with I and K showing non-significant increases. When normalised to *Myh7* to account for potential differences in differentiation state between samples, D, F and I show significant increases, with K showing a non-significant increase (Student's t-test, $p < 0.05$, $n = 3$) (Figure 5.10 A). *Chip* and *Hspb8* also show trends to increased transcription across the mutant clones, which reaches significance in clones D and K for *Chip* and clones I and K for *Hspb8*. WB examination of BAG3 protein levels showed no significant differences between WT and mutant levels of BAG3, and no consistent trend was apparent (Figure 5.10 B)

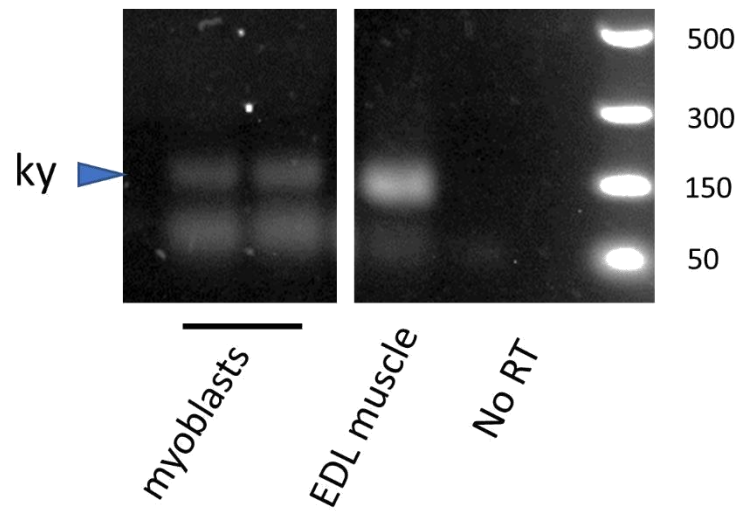
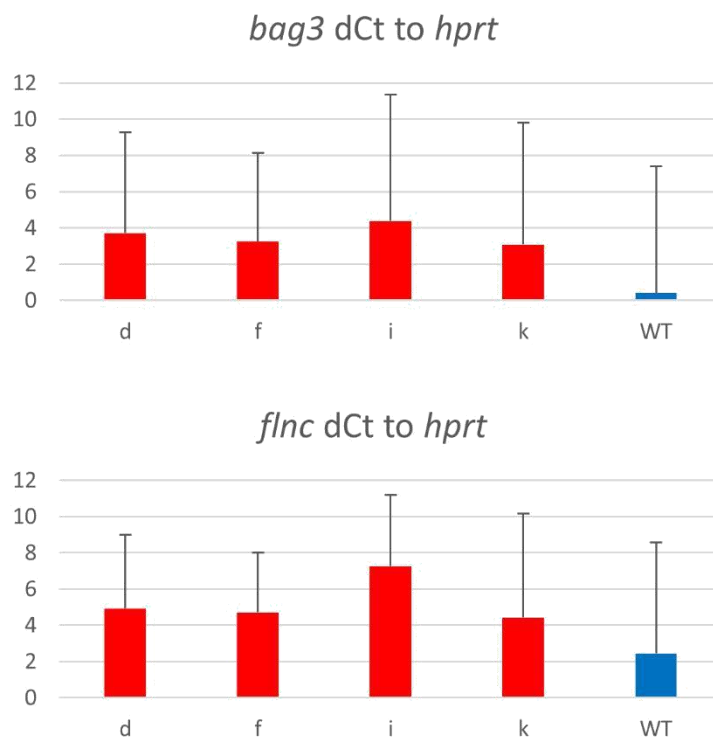
A**B**

Figure 5.9 - Expression of CASA components in myoblasts

A) RT-PCR shows myoblasts express *Ky* transcript, possibly at lower levels than skeletal muscle. B) qPCR of *Bag3* and *Flnc* showed high levels of variation. Shown are the average dCt values of each gene relative to the housekeeping gene *Hprt*. Though both *Flnc* and *Bag3* could be detected, the variance in expression was too high to observe any changes between WT and mutant lines. Error bars indicate standard deviation. N=3.

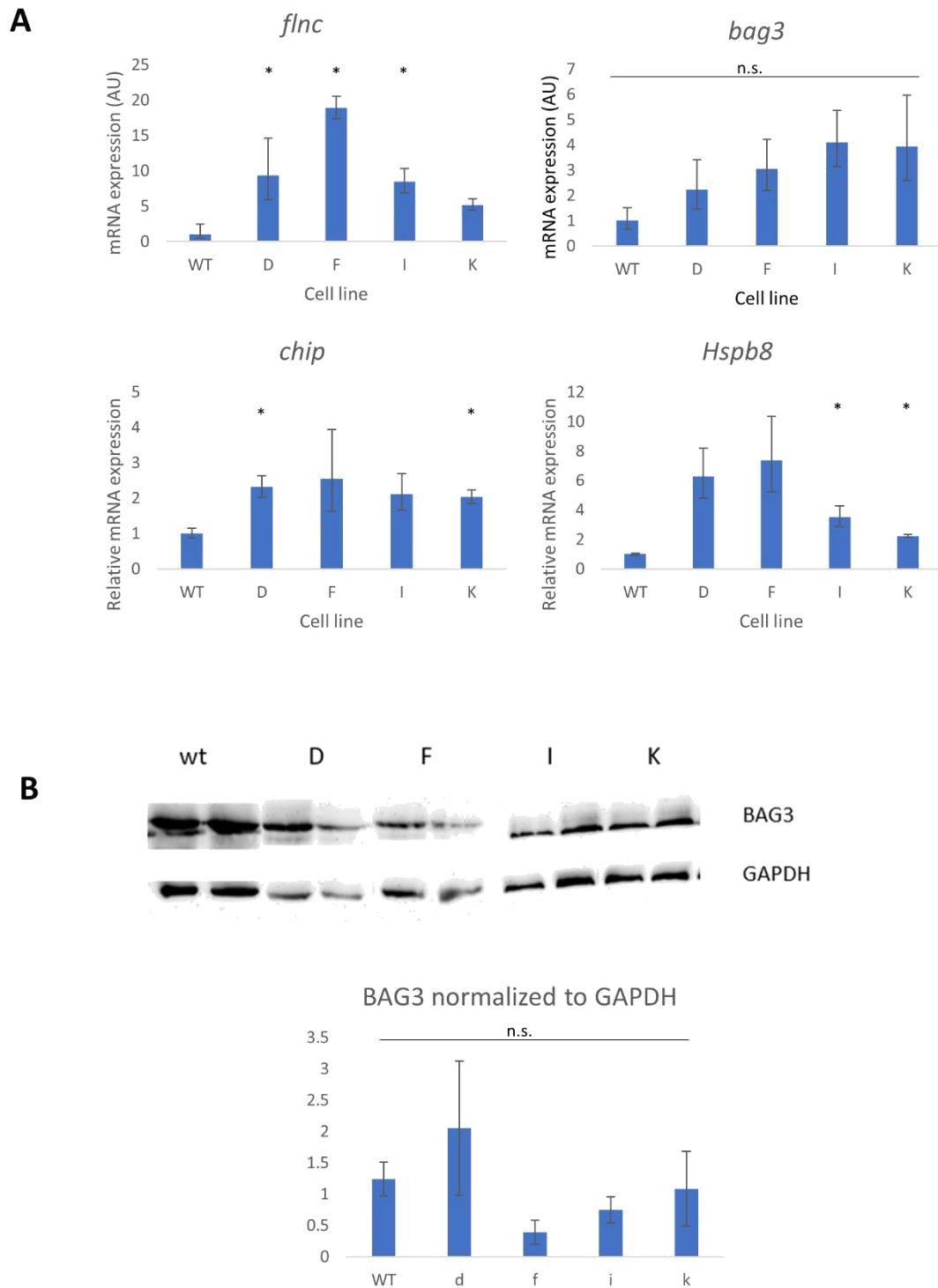


Figure 5.10 - CASA in KY-deficient myotubes

A) qPCR of *Bag3* shows no significant differences between WT and mutant lines, though there is a consistent upward trend. Consistent upregulation is seen in other CASA components which reaches significance in some instances. *Flnc* is significantly upregulated in clones D, F and I. *Chip* is significantly upregulated in D and K and *Hspb8* is significantly upregulated in clones I and K (Student's t-test, $p < 0.05$, $n \geq 2$). B) WB analysis of BAG3 shows no significant difference in protein levels or consistent trend across mutant lines. Error bars represent standard deviation.

5.9 Tension induced changes in WT myoblasts

To determine whether the cell stretching protocol outlined in (Ulbricht et al. 2013) would similarly induce expression of BAG3 and FLNC, WB analysis of lysates generated from stretched and unstretched myoblasts was performed (Figure 5.11 A). Though the use of myotubes might provide more relevant physiological insights, the use of myoblasts provided a less technically challenging approach for initial experiments by not having to account for potential differences in differentiation between samples. A clear qualitative increase in BAG3 expression in stretched myoblasts is observed, particularly in the second biological replicate (S2 in figure 5.11). No consistent trend for FLNC could be determined. However, it was clear that the stretching protocol was capable of inducing a response in WT myoblasts.

To further examine the protein-level changes between stretched and unstretched myoblasts, LC-MS/MS analysis was performed on these samples **by Adam Dowle (University of York Technology Facility)**. Extended results and analysis can be found in Appendix 2. Of particular interest was an apparent decrease in levels of several cytoskeletal proteins (Figure 5.11 B). This may indicate that the cell stretching protocol led to enhanced degradation of these proteins due to irreversible unfolding. Given that the protocol only took 3 hours, this may have been insufficient time for an adaptive upregulation of cytoskeletal protein levels to replace degraded protein. However, it should be noted that the changes observed in the S2 replicate were not always common to S1, though the upregulation of ribosomal proteins and downregulation of proteasome proteins was common. S2 was selected as it had the greatest impact on BAG3 expression in western blot and thus was seen as more likely to represent a robust stretch response.

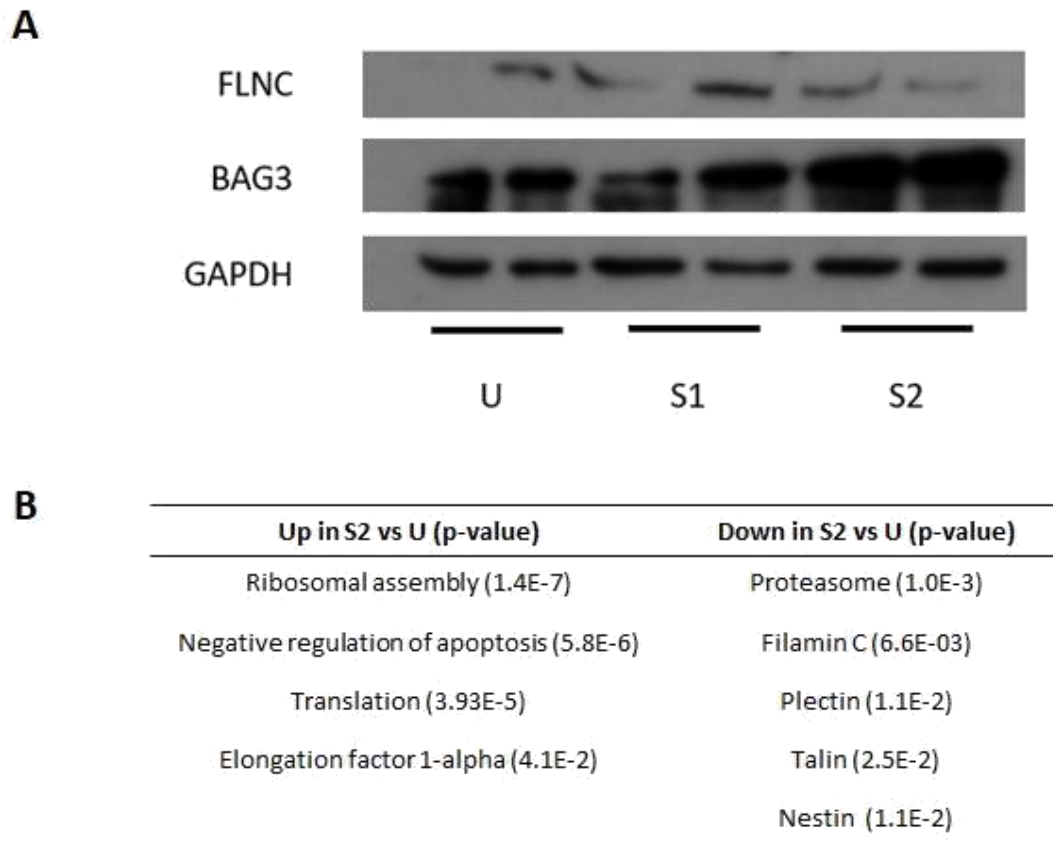


Figure 5.11 - Proteomic changes in stretched myoblasts

A) Western Blot analysis of FLNC and BAG3 expression in unstretched (U) and two stretched (S1 and S2) myoblast samples. Upregulation of BAG3 can be qualitatively observed in the stretched samples, particularly S2. B) Selected outputs from proteomic analysis **performed by Adam Dowle (University of York Technology Facility)** indicate elevated ribosomal activity and translation. Reduction of several cytoskeletal proteins was also observed, possibly indicating enhanced degradation. Extended proteomic analysis can be found in Appendix 2.

5.10 Conclusions

This chapter has outlined the successful generation of myoblast lines shown to have disruptive mutations in both alleles of *Ky* and significant reduction in *Ky* transcript. This provides a useful additional resource to interrogate the function of *KY* and potentially explore the efficacy of future pharmacological treatments of the human myopathy. Ideally, the validation in this chapter could be complemented with evidence of disruption at the protein level. However, inconsistent antibody performance and the presence of unspecific bands prevented this during this project (data not shown).

The size reduction of KY-deficient myoblasts suggests that KY might play a role in regulating cell size or responsiveness to growth pathways. Though this effect is consistently observed across mutant clones, rescue experiments should be performed to determine whether this phenotype is a genuine effect of KY-deficiency. However, given the lack of apparent developmental phenotype in the *ky/ky* mouse and human pathology, and the relative health of non-postural muscles, it appears unlikely that any altered myoblast morphology impacts fundamentally on muscle development and physiology. However, since the *ky/ky* pathology impacts on the maintenance of postural muscles, it could be speculated that altered myoblast function could exacerbate damage if it impacts the efficiency of muscle repair. Since the myoblasts seem capable of robust differentiation, this model seems unlikely. This could be further explored, for example, by inducing damage in non-postural muscles and comparing the speed of recovery between *ky/ky* and WT mice.

The normal differentiation capacity of KY-deficient myoblasts also suggests that its function is distinct from IGFN1_v1, which has been shown to be required for fusion and differentiation (Xiang Li et al. 2017). However, the analysis in this chapter is more qualitative than the fusion index used in the IGFN1_v1 analysis, and a similar approach may yet detect more subtle differences in differentiation.

Examination of CASA in resting, proliferative myoblasts was not successful, at least in part because robust expression of FLNC, the client protein, is induced in differentiating myotubes and in response to tension. When the myotube model was examined, consistent trends were observed indicating elevated transcription of *FlnC*, *Chip*, *Hspb8* and *Bag3*, though this only reached significance for some genes in some of the mutant clones. If genuine, this may represent elevated activation of the CASA pathway in the absence of external mechanical stimulus. This would suggest that the normal endogenous tension experienced by cells in culture was sufficient to induce a stress response. This increased sensitivity implies either structural instability leading to enhanced levels of cell damage and stress, or impaired regulation of these pathways. Given that the actin cytoskeleton of WT and *ky*-deficient myoblasts appeared comparable, it seems unlikely that there is such an inherent lack of structural stability and thus more likely that the absence of KY leads to the dysregulation of cell stress pathways. Similarly to the morphology experiments, rescue of this cell stress phenotype upon transfection with *Ky*

constructs would be the most robust way to demonstrate that this phenotype is a genuine result of *ky*-deficiency

It appears that the stretching of C2C12 myoblasts is sufficient to induce increased degradation of cytoskeletal proteins, including FLNC, and enhanced expression of BAG3, mirroring at least in part the CASA pathway as described in the literature (Arndt et al. 2010; Ulbricht et al. 2013). However, the changes observed in stretched cells were not always common to both replicates (S1 and S2) suggesting that further repeats are necessary to robustly determine the genuine stretch response. Repeating these experiments with KY-deficient myoblasts may demonstrate whether the absence of KY impacts on the induction of these pathways. Ideally, experiments involving differentiated myotubes would more closely recapitulate the physiology of skeletal muscle. On the basis of the pathology and data from experiments in this chapter, it would seem likely that the absence of KY would lead to an enhanced cell stress response to tension. It may also be possible to observe increased levels of cytoskeletal FLNC accumulating in longer term stretching experiments if FLNC turnover is impacted absent KY. Unfortunately, these experiments could not be pursued in the scope of this project due to financial constraints.

CHAPTER SIX:
GENERATION
AND ANALYSIS OF
KY-KNOCKOUT
ZEBRAFISH

CHAPTER SIX: GENERATION AND ANALYSIS OF KY-KNOCKOUT ZEBRAFISH

6.1 – Introduction

The overall aim of the experiments in this chapter was to explore the functional conservation of Ky in non-mammalian vertebrates by generating a Ky-deficient zebrafish model. Any phenotypes observed might provide additional insights into the function of the Ky protein, and cross-species functional conservation would underscore the importance of this protein in skeletal muscle physiology. As discussed in chapter one, zebrafish are an excellent model for skeletal muscle disorders. An additional advantage is the relative ease of genetic manipulation via CRISPR/Cas9 and other genome-editing technologies via embryonic injection. The relatively short generation time also makes the timescales of the subsequent outcrosses and incrosses required to produce homozygous mutant fish manageable, as well as outcrossing into other reporter lines.

6.2 – Identification and expression analysis of *ky* orthologue in zebrafish

In order to identify the Ky orthologue in zebrafish, mouse KY protein sequence was used as a query in a protein-BLAST search specific to zebrafish protein databases. The search identified a 477aa protein fragment based on an incomplete cDNA sequence (ENSDART00000131255.1) annotated as Ky. The alignment from this fragment had 32% identity and 51% positives, primarily concentrated in the transglutaminase-like domain (Figure 6.1 B). HM-HMM modelling with the European Bioinformatics Institute's 'PHMMER' tool using the zebrafish Ky fragment as a query returned the mouse KY protein as the top-scoring hit within the mouse protein databases with an E-value of $4.2e^{-33}$. No synteny was detected when comparing the surrounding genes to those in other organisms, but the previous evidence was sufficient to identify this gene as the putative zebrafish Ky. A query in the NCBI gene database identified a predicted complete mRNA model and resulting 841aa protein sequence (XM_001335276.4 and XP_001335312.3 respectively). This extended model included an additional upstream exon, a 5' extension of the (now) second exon and a 3' extended final exon (Figure 6.1 A, C).



Figure 6.1 - in silico identification of the zebrafish Ky ortholog

A – Exon structure with sequence identified from cDNA library (black) extended with the NCBI mRNA model (blue). B – NCBI BLAST output for partial alignment of mouse (MM) and zebrafish (DR) Ky protein sequences. Orange highlights indicate the conserved catalytic triad. C – Full protein sequence containing the sequence predicted from the cDNA fragment (black) and the additional sequence from the mRNA model (blue). Highlighted in grey is the sequence encoding the transglutaminase-like domain. Bold, underlined and red are the catalytic triad.

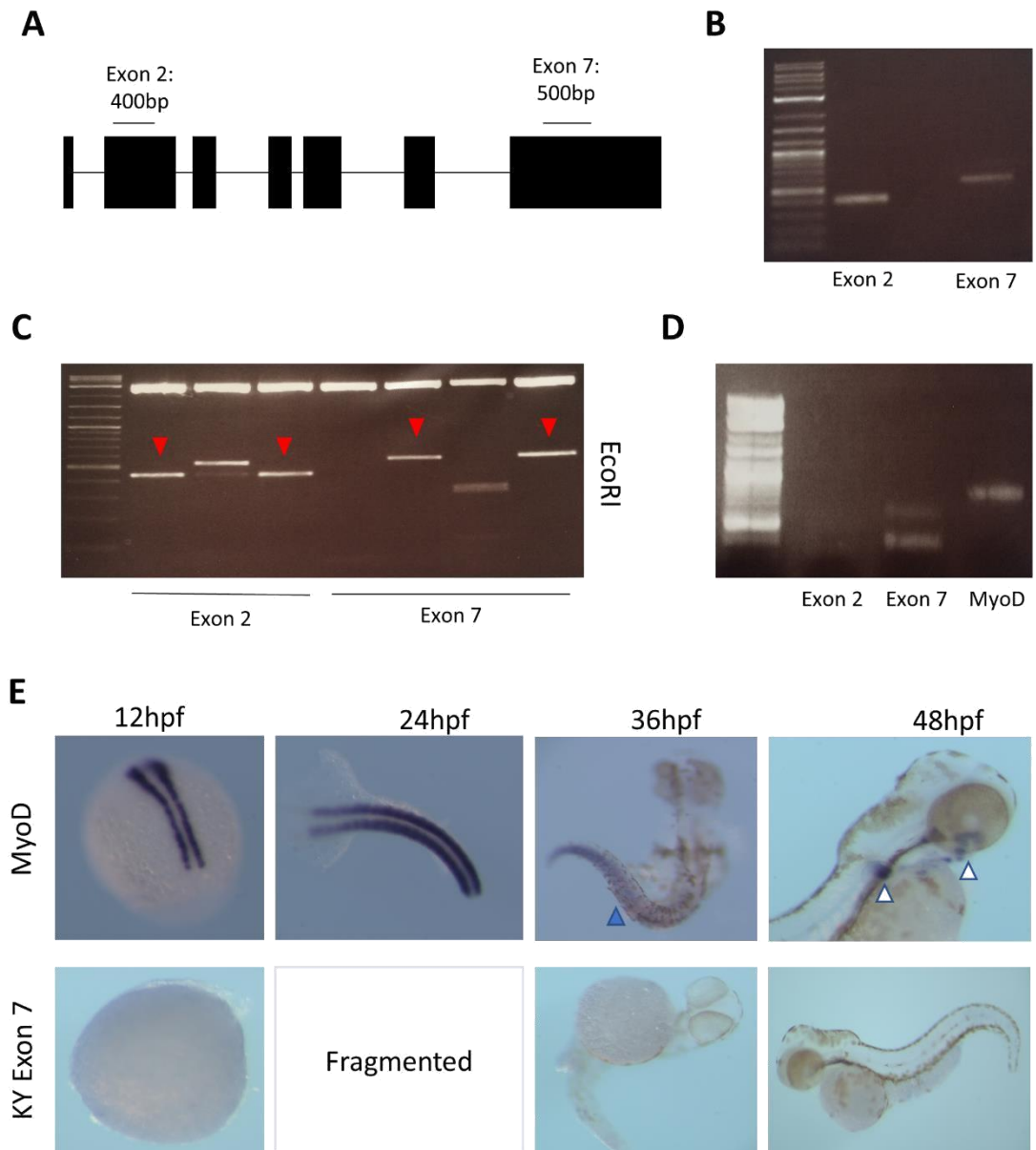


Figure 6.2 - *in situ* hybridisation does not detect *ky* expression

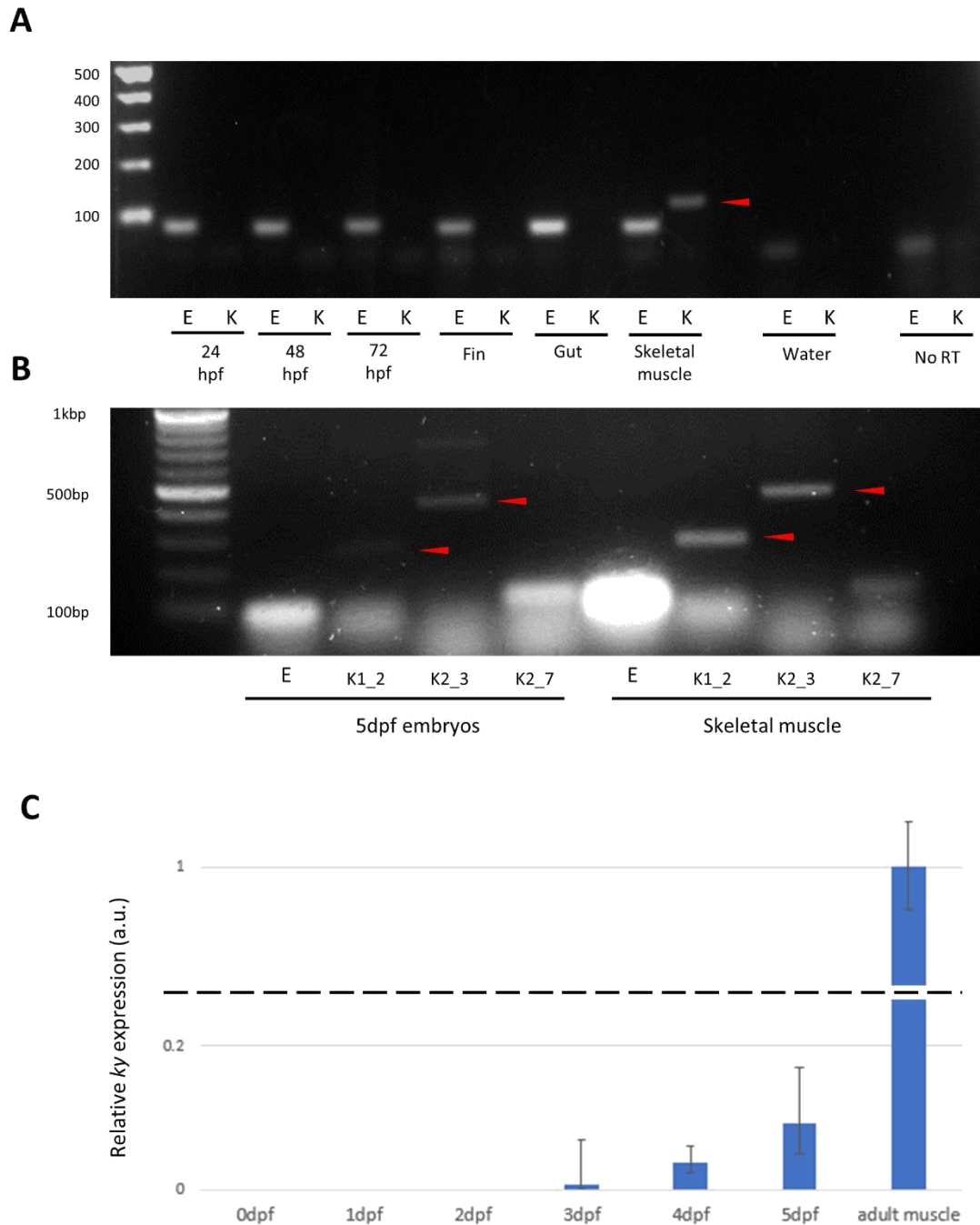
A) *ky* exon model showing approximate site and size of target regions for PCR amplification. B) PCR amplification of exon sequence for cloning into template vectors. C) *EcoRI* digest of template vectors to determine correct insertion. Red arrows indicate expected digestion products. D) Antisense DIG probes generated by SP6 transcription. Some probe against exon 2 is visible. ***myoD* probe was generated from a template provided by Dr Betsy Pownall.** E) *in situ* hybridisation shows successful detection of *myoD* expression in the developing somites at 12 and 24hpf, the developing posterior muscle at 36hpf (blue arrow) and the developing limb bud and jaw muscles in later stages (white arrows). No signal was observed at any stage using the probe against exon 7 (shown) or exon 2 (not shown).

Two approaches were taken to determine if and where the *ky* orthologue is expressed in zebrafish: *in situ* hybridisation and Reverse Transcriptase PCR (RT-PCR).

For *in situ* hybridisation, DIG probes were generated using sequence from exons 2 and 7 of the *ky* orthologue (Figure 6.2 A-D). *myoD* template was provided by Dr. Betsy Pownall to generate a positive control probe. Embryos were collected at approximately 12, 24, 36 and 48hpf. No *ky* expression was detected, indicating a lack of early embryonic expression (Figure 6.2 E).

RT-PCR was performed using various primer sets, spanning exons 1-2, 2-3, 2-7 and 6-7. cDNA was generated from 1, 2, 3 and 5 dpf embryos as well as adult tissues, including skeletal muscle, gut and fin tissue (Figure 6.3 A-B). Detection of the expected product from primers spanning exons 1 and 2 (K1_2) validates the upstream extension of the predicted RNA model. The earliest stage at which *ky* expression was detected was in 5 dpf embryos, consistent with the lack of expression detected via *in situ* hybridisation of younger embryos. Detection was also seen in adult skeletal muscle, and not gut or fin tissue, implying at least some degree of tissue specificity, which is consistent with mouse expression of *Ky* which is restricted to skeletal muscle and heart tissues.

To determine the onset of *ky* expression, qPCR was performed (Figure 6.3 C). No transcript was detected in newly fertilised eggs (0dpf) or 1dpf or 2dpf embryos. Expression becomes detectable at 3dpf and appears to rise through 4 and 5dpf. The level is lower than that seen in adult skeletal muscle, but this difference can at least partly be accounted for the fact that cDNA was prepared from whole embryos. Thus if expression is primarily restricted to skeletal muscle, this will have diluted the relative expression of *ky* compared to isolated muscle tissue.



6.3 - RT-PCR and qPCR identifies *ky* expression in late embryonic stages and skeletal muscle

A) RT-PCR of *ef1α* (E, +ve control) and *ky* (K) shows no expression in the early embryonic stages or fin or gut tissue, but red arrow indicates expression in skeletal muscle (*ky* product spans exons 6 & 7) B) RT-PCR shows expression in 5dpf embryos and skeletal muscle using primers spanning exons 1-2 and 2-3 but not 2-7. C) qPCR of *ky* shows onset of *ky* expression at 3dpf, appearing to increase through day 4 and 5. Error bar indicates standard deviation from three technical replicates.

6.3 – CRISPR/Cas9 protocol optimisation – tyrosinase KO

In order to optimise the efficacy of the genome editing protocol and demonstrate competency in the microinjection technique, the *tyr* gene was targeted in zebrafish embryos (Figure 6.4). This gene encodes tyrosinase, an enzyme critical for zebrafish pigmentation. Disrupting its expression therefore provides an overt measure of the success of the protocol. Zebrafish have a cytoplasmic bridge between the yolk and dividing cells up to around the 16-cell stage which allows the passage of large molecules into the cells. Injection into the yolk of the embryo in the proximity of this cytoplasmic bridge is an effective means to transfer proteins and genetic material.

Two approaches were undertaken, one using Cas9 mRNA generated from a template vector via *in vitro* transcription and the other using Cas9 protein. In each case, sgRNA targeting *tyr* was generated via *in vitro* transcription from a template generated from annealing and extending two oligonucleotides; the first containing the target sequence and the second containing the generic Cas9 interaction structures (See Figure 6.5 B for a schematic). Given the translation of Cas9 protein from mRNA will result in a delay before genome targeting is active, this was presumed to increase the chances of highly chimeric fish since an increased number of cell divisions will have occurred in this time, i.e. there are more copies of the genome to target. Direct injection of the protein ought to result in earlier targeting and disruption and a less chimeric phenotype. In the context of generating a mutant line, this makes it more likely to transmit these mutations to the germ line.

Indeed, the approach using injected Cas9 protein was much more successful (Figure 6.4 B), showing reduction in pigmentation in almost 70% of embryos compared with less than 10% using Cas9 mRNA. In addition, the resulting reduction in pigmentation was more severe in protein-injected embryos, with some showing complete absence of pigmentation, indicating total disruption to the *tyr* gene. This was the approach carried forward for ky mutagenesis.

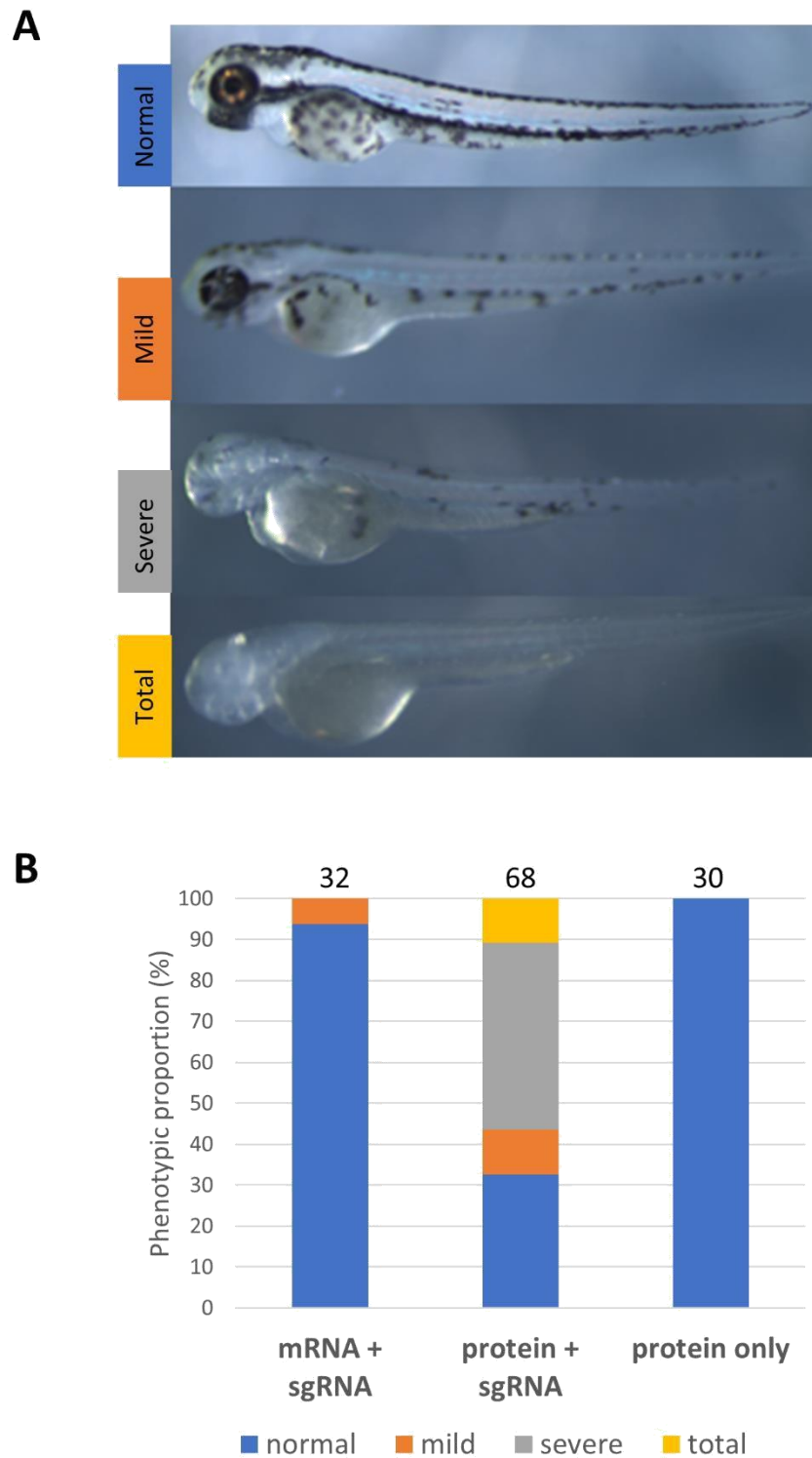


Figure 6.4 – Targeting of *tyr* using Cas9 protein is more effective than using Cas9 mRNA

A) phenotype scoring system ranging from normal embryos through to mild, severe and total disruption to pigmentation development. B) quantification of the scoring proportions from experiments using Cas9 mRNA and sgRNA, Cas9 protein and sgRNA, and Cas9 protein only. Total number of embryos displayed above each bar.

6.4 – gRNA designs for *ky* targeting

The identification of potential *ky* target sites was undertaken before the Cas9 protein became available, provided as a gift from Dr. Olga Moroz (York Structural Biology Laboratory). It was initially intended to generate a pair of gRNAs to use alongside RNA encoding the nickase Cas9 variant, with the paired approach increasing the specificity of targeting. The e-CRISP online tool was used to identify potential target site pairs. The most 5' design was selected, as this has the greatest chance of disruptive effects. The target sites identified were in exon 2 (See Figure 6.5). Both target sites are upstream of the transglutaminase-like domain, which is the only distinguishable feature of the protein, and thus frame-shift mutations generated at the target sites would be highly disruptive.

gRNA template was generated by annealing-extension of oligonucleotides, as per the *tyr* experiments. Nickase Cas9 mRNA was generated via *in vitro* transcription. Injections of both gRNAs and nickase Cas9 mRNA were attempted, but no evidence of mutagenesis was generated in these early attempts (data not shown). Once the Cas9 protein was generated, sgRNA from the most upstream target site was used exclusively, coinjected with the Cas9 protein.

6.5 – Confirmation of mutagenesis and founder generation

The efficacy of the *ky*-targeting sgRNA was determined via sequencing of PCR products amplified from genomic DNA extracted from Cas9 and sgRNA injected embryos. The disruption of sequence reads commencing immediately downstream of the predicted cleavage site indicated the presence of multiple alleles induced by successful CRISPR/Cas9 mutagenesis. Targeted embryos were then raised to approximately three months old to enable genotyping via fin-clip. Again, disruption of sequencing reads identified fish carrying mutations in the *ky* gene. Examples of comparable data can be seen in figure 6.7.

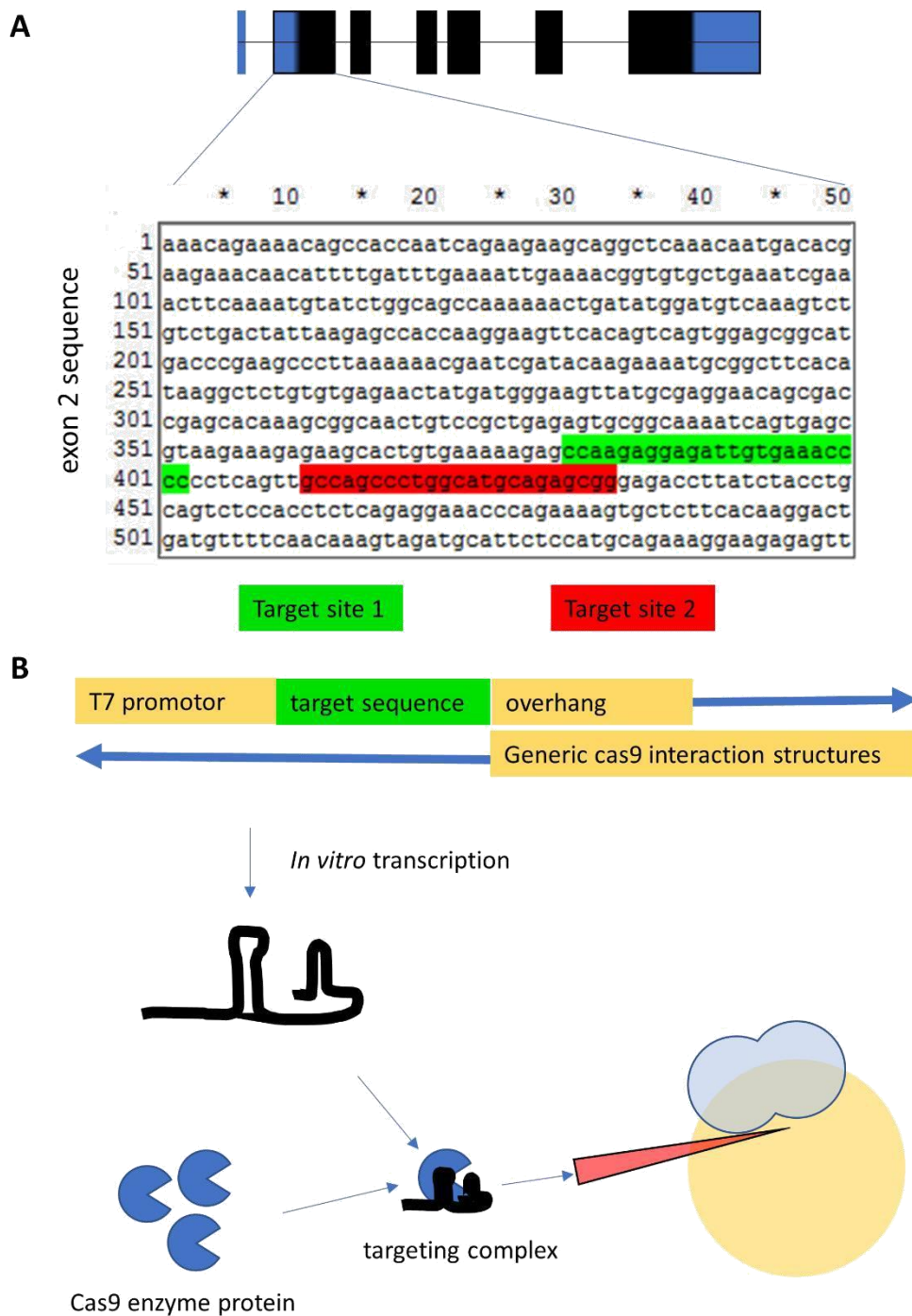


Figure 6.5 - sgRNA target sequence identification and targeting methodology

A) Location of identified target sites in the *ky* gene. B) Targeting methodology: *in vitro* transcription of sgRNA from an annealed-extended oligo template containing target sequence followed by complexing with Cas9 protein to form targeting complexes that are microinjected into zebrafish embryos in the yolk proximal to the cell body, allowing transport through the cytoplasmic bridge

6.6 – Generation and validation of *ky* mutant lines

The founder fish that were generated were likely to be genetically chimeric. In order to generate a *Ky*-deficient zebrafish line, it was necessary to outcross these fish to generate heterozygotes, which could then be screened and characterised. From these outcrosses, those carrying disruptive mutations could be collected and incrossed to produce homozygous mutant fish. A schematic of the breeding and screening strategy can be seen in Figure 6.6.

Each founder fish was mated with a WT zebrafish of the same background strain (LWT). Embryos were collected at 24hpf, lysed and PCR performed to amplify the region around the target site. In addition, the region around the most likely off-target site was also amplified, identified as *agpat3* using the *ky* target site as a BLAST query. As well as giving a measure of the specificity of targeting, this stage provided the best opportunity to segregate away such off-target effects given *ky* and *agpat3* reside on different chromosomes. The presence of mutant alleles was detected via altered heteroduplex migration in high percentage acrylamide gels (Figure 6.7 A). No instances of heteroduplex formation were seen for *agpat3* in any of the outcrosses, indicating the targeting was specific. Sequencing of *agpat3* amplicons also showed no indication of mutation (Figure 6.7 B). All outcrosses showed heteroduplex bands, indicating that every founder fish had some degree of germline mutagenesis. In some instances, different banding patterns were observed between embryos from the same mating pair. Given that the exact banding pattern is consistent for a given mutation, this indicates that some founder fish had chimeric germlines.

Selected PCR products from samples showing heteroduplex banding were submitted for sequencing, along with some samples that did not show heteroduplex banding to validate the efficacy of the approach. The samples that did not show heteroduplex banding returned WT sequence. The sequencing data from samples generating heteroduplex bands returned double peaks in the basecalls from the cleavage site, indicating the difference in sequence between the mutant and WT alleles. By subtracting the known WT sequence, the remaining sequence indicates that of the mutant allele (Figure 6.7 C).

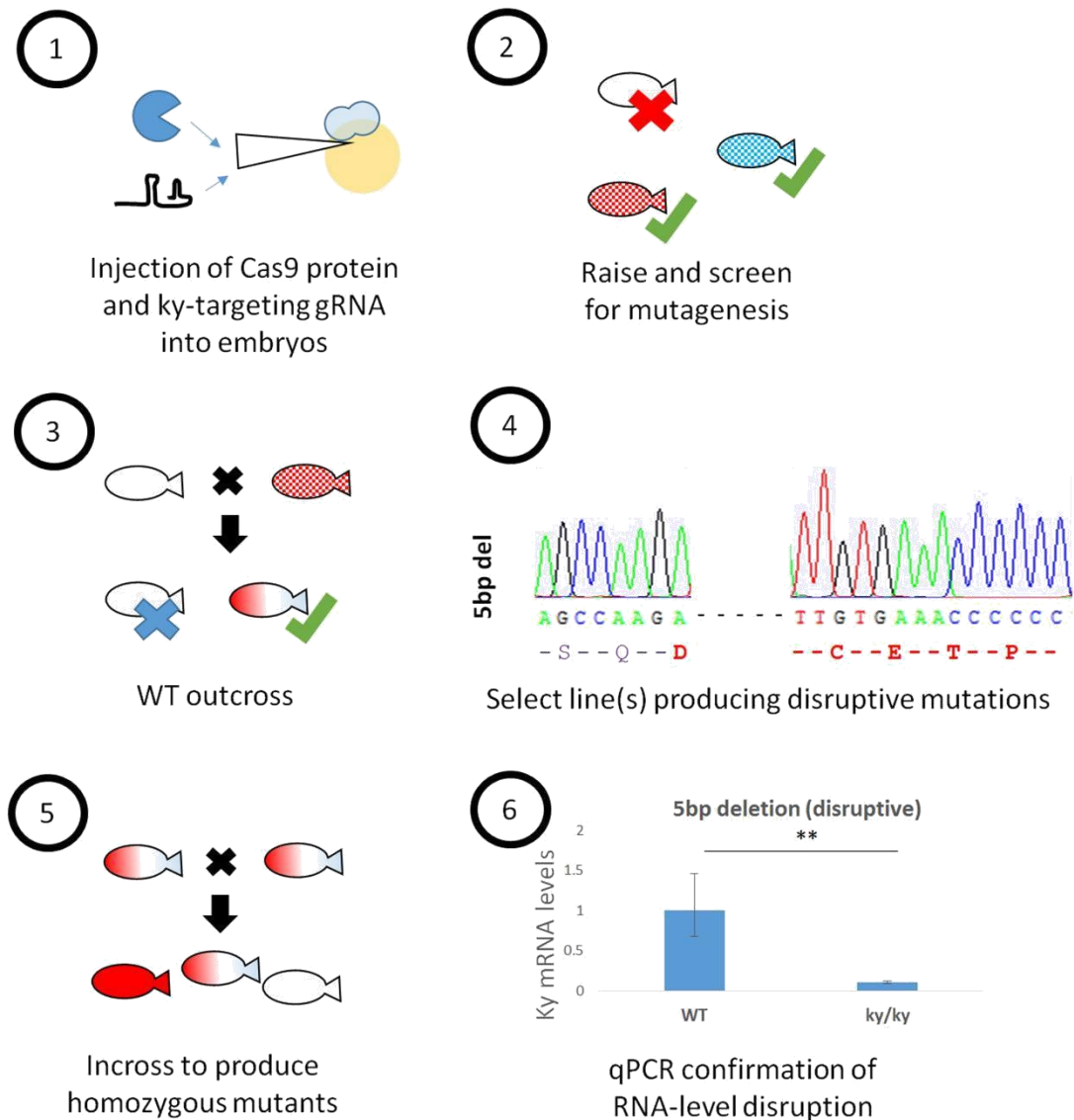


Figure 6.6 - Breeding strategy outline

1) targeting of *ky* via embryonic microinjection of Cas9 protein and *ky*-targeting sgRNA. 2) Screening of targeted fish for mutations in the *ky* gene via fin-clipping. 3) Outcrossing of successfully mutagenised fish to WT fish to isolate individual mutated alleles. 4) Identification and characterisation of mutant alleles and the selection of disruptive mutations. 5) Incross of fish heterozygous for the same disruptive mutation to produce homozygous mutant fish. 6) Confirmation of disruption to gene expression by transcript quantification by qPCR.

The effects of these mutations were modelled. A 5bp deletion was modelled as disruptive, resulting in a frame shift before an early stop codon at 612bp and this outcross was raised. A 3bp-deletion outcross (resulting in a E deletion, but no frame shift or early stop codon) was also raised to act as a negative control. In each instance, fish were raised to two months old before identification of heterozygotes via fin clipping, PCR,

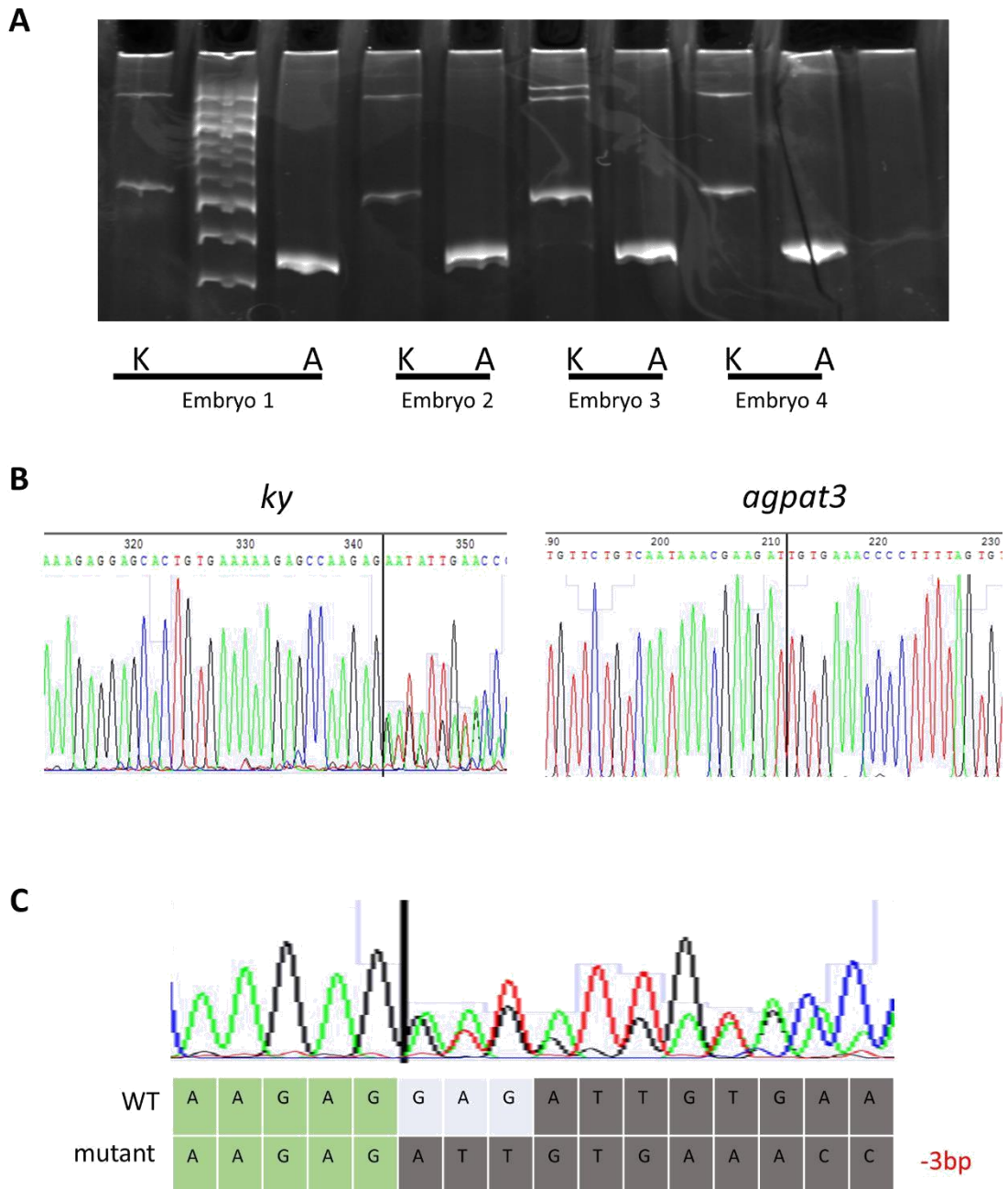


Figure 6.7 - Generation and identification of mutant alleles

A) Representative 15% PAGE of PCR products from targeted embryos. The presence of heteroduplex bands in products from *ky* (K) but not *agpat3* (A) indicates the specificity of targeting. B) Representative sequencing reads from *ky* and *agpat3* PCR products from targeted embryos/fish. *Ky* shows multiple basecalls after the expected cleavage site (vertical black line) but *agpat3* does not, supporting the conclusions from the gel assay. C) Identification of mutant alleles from sequencing assay double peaks. The segregation of expected basecalls from the WT sequence leaves the mutant sequence, in this instance a 3bp deletion.

heteroduplex detection and sequencing. Heterozygous fish were kept and raised to maturity before incrossing to produce homozygous mutant fish.

Disruption to *ky* expression was evaluated at the mRNA level by qPCR (figure 6.8). Two primer sets were generated, both spanning the junction between exons 6 and 7. Each primer set showed a significant reduction in *ky* mRNA expression between fish homozygous for the 5bp deletion and WT fish (7.7 and 9.5 fold reduction, $p=0.01$ and 0.007 respectively, t-test, $n=2$). The 3bp deletion fish showed no significant reduction in mRNA levels, consistent with the predicted effect of the mutation not inducing a frame shift or early stop codon. The 5bp deletion mutant allele has been given the zfin classification ky^{yo1} and the fish homozygous for this mutation are hereafter referred to as ky^{yo1}/ky^{yo1} .

6.7 – Morphological and histological analysis of ky^{yo1}/ky^{yo1} zebrafish

To examine whether disruption to *ky* expression resulted in impaired growth, fish were measured with three metrics: length from protruding jaw to the border of the caudal fin, height at the anterior of the anal fin (HAA) and area of the tail between the border of the caudal fin and the line measured for the HAA (Figure 6.9). No significant differences were observed between WT and ky^{yo1}/ky^{yo1} siblings, indicating that the absence of *ky* does not impact on growth in the early adult stages. During the scope of this initial analysis, care was taken to ensure the WT and ky^{yo1}/ky^{yo1} fish were fed equally and kept in equal numbers within tanks to prevent these being confounding factors on growth.

Similarly, no elevated hallmarks of muscle pathology were observed in H&E staining of muscle sections, with both WT and ky^{yo1}/ky^{yo1} siblings showing a small number of pathological fibres at 3 months (Figure 6.10). Slow muscle tissue remained well defined, with no indication of the fibre type adaptation observed in the mouse (Figure 6.11).

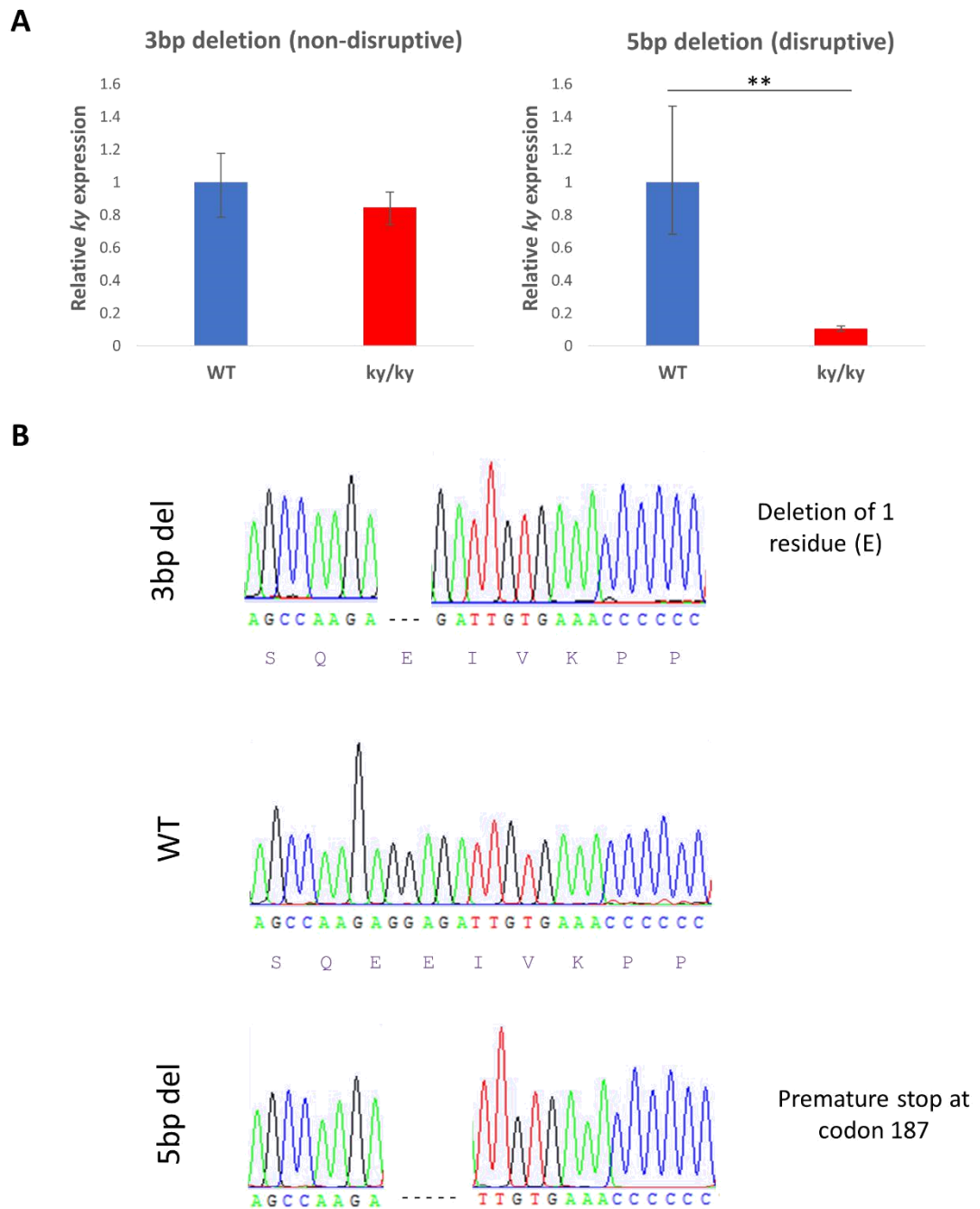


Figure 6.8 - qPCR confirmation of transcript-level disruption of expression

A) qPCR quantification of *ky* transcript levels in skeletal muscle of 3 month old fish. Fish homozygous for a 3bp deletion, modelled to not cause a frame shift or early stop codon, show no difference in transcript levels compared to WT siblings. Fish homozygous for a 5bp deletion show significant 9.5-fold reduction in transcript (Student's paired t-test, $p < 0.01$, $n=2$). B) sequencing data from homozygous fish confirms the sequence of the mutant alleles, the effects of which have been modelled as an E residue deletion from the 3bp deletion and frame-shift and premature stop codon from the 5bp deletion.

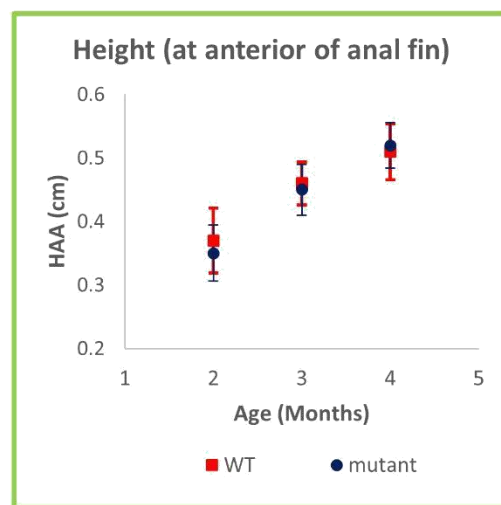
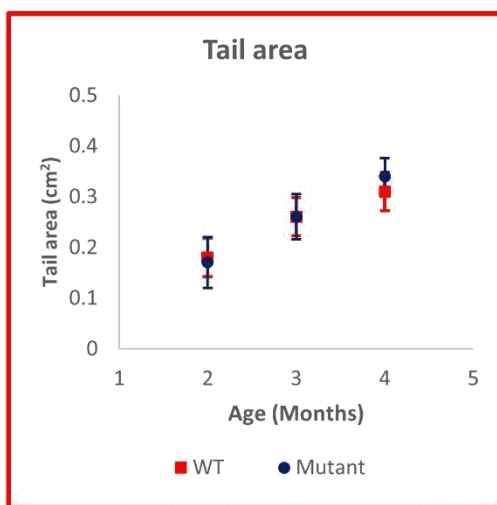
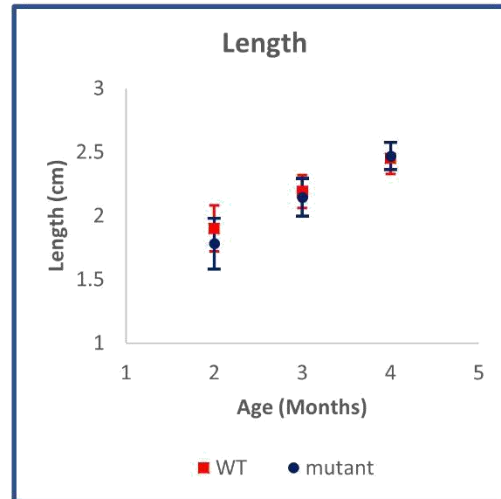
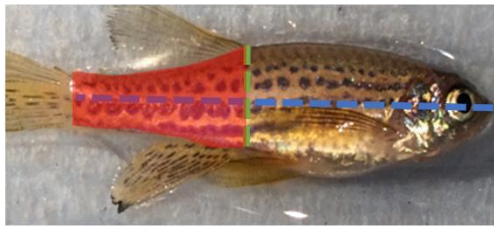


Figure 6.9 - Morphological analysis of ky^{yo1}/ky^{yo1} zebrafish

Measurements were taken of the length, height at the anterior of the anal fin and the tail area to examine for any overt changes in fish morphology. No differences were observed, indicating that the absence of ky does not recapitulate the smaller organism size seen in mice.

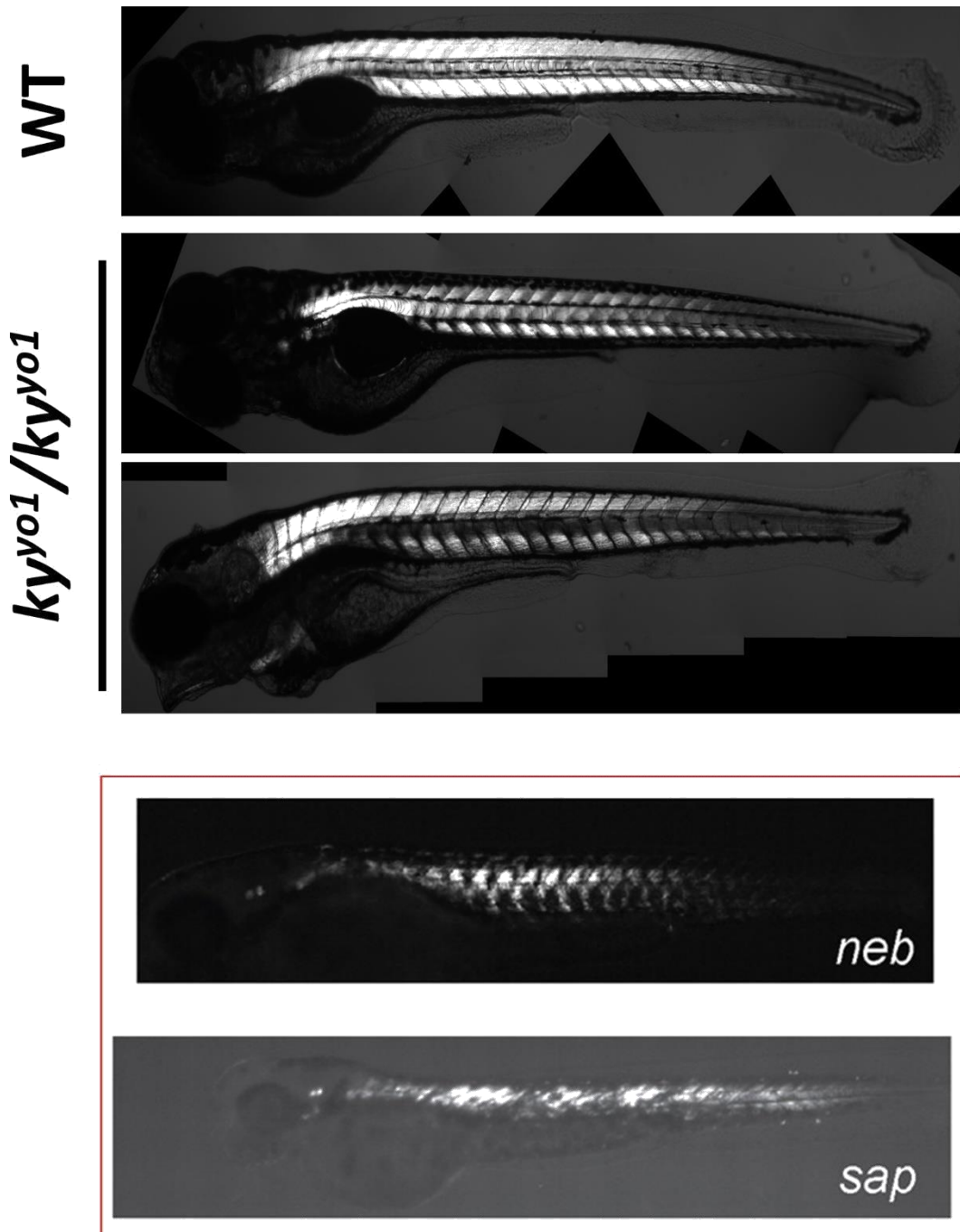


Figure 6.10 - Birefringence analysis of ky^{yo1}/ky^{yo1} embryos show no severe disruption to birefringence

Representative examples of birefringence images of 5dpf WT and ky^{yo1}/ky^{yo1} embryos are shown. Though there appears to be some loss of birefringence in the mutant zebrafish, any differences are very modest when compared to **examples in the literature as shown in the red box, taken from Telfer et al. 2012 under a Creative Commons License**. It thus appears that the absence of Ky has little to no impact on the overall structural integrity of embryonic muscle.

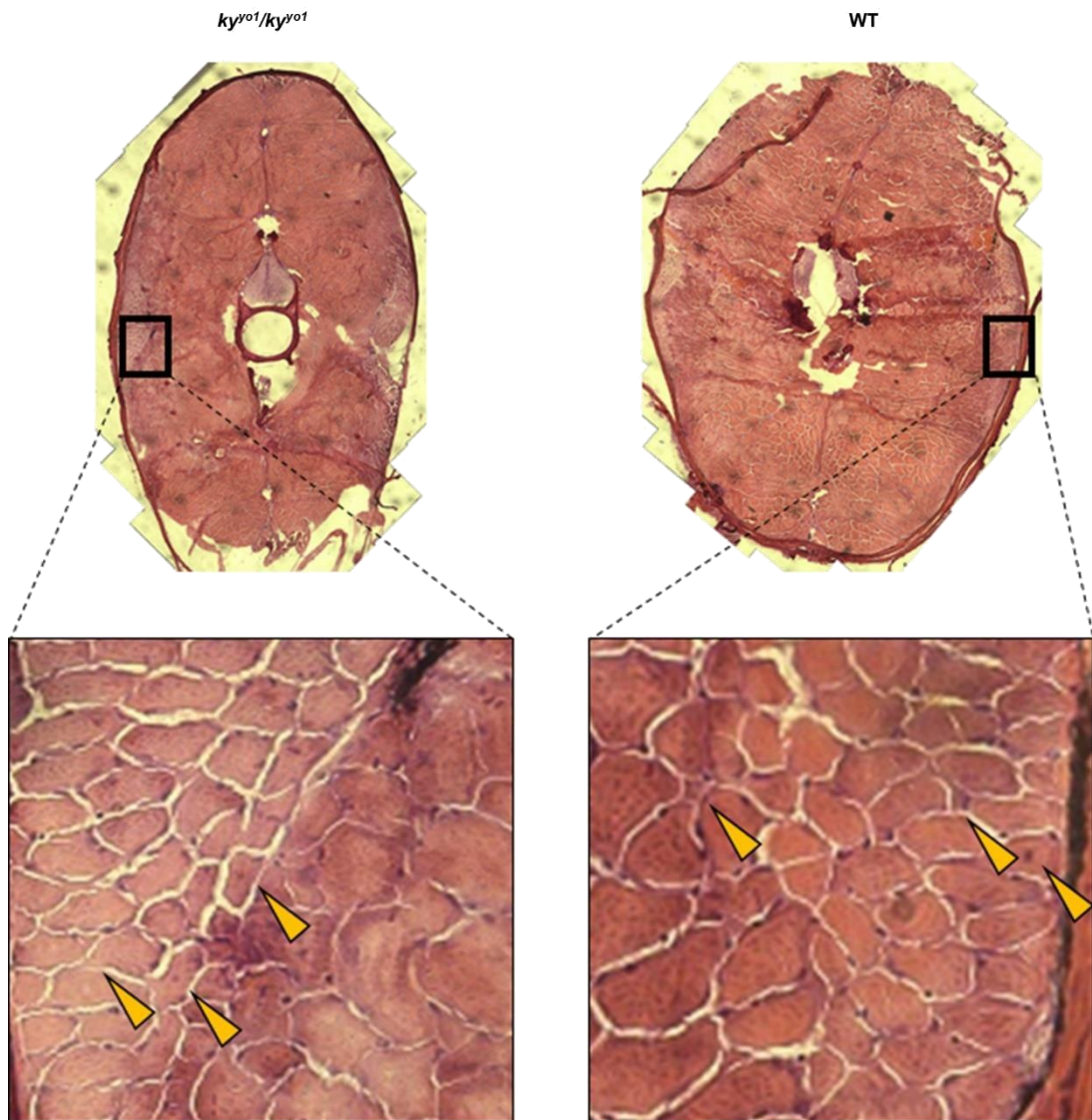


Figure 6.11 - H&E staining shows no overt differences in muscle health between ky^{yo1}/ky^{yo1} and WT zebrafish

Transverse sections through 3-month-old zebrafish muscle reveals muscle fibres in cross section. Both the WT and ky^{yo1}/ky^{yo1} fish show a small number of fibres with centralised nuclei or small fibre size (yellow arrows).

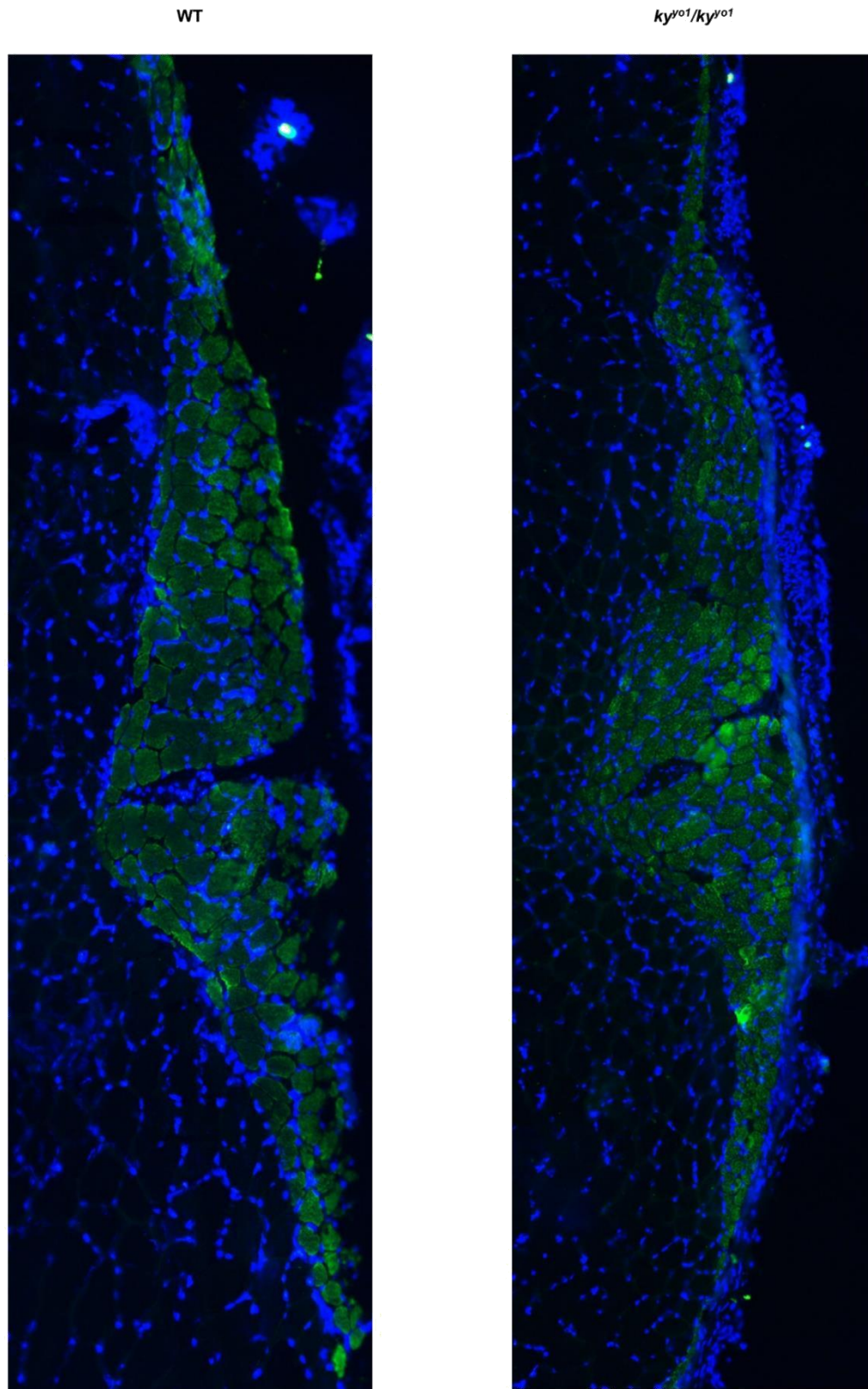


Figure 6.12 – Slow muscle remains laterally localised in ky^{y01}/ky^{y01} zebrafish

Representative images of Immunofluorescence staining against slow muscle (s58) of transverse sections of 3-month-old zebrafish shows no changes in slow muscle organisation between WT and ky^{y01}/ky^{y01} . Note that the sections come from different levels of the anterior-posterior axis, so fibre sizes are not comparable.

6.8 – qPCR analysis of CASA components in ky^{yo1}/ky^{yo1} zebrafish muscle

Examination of the expression of CASA components *bag3* and *flnc* (*flnc*a and *flnc*b) was performed at 7 days, 3 months and 7 months (Fig 6.13). *bag3* showed a consistent upward trend in mutant muscle, though this only reached significance at the 3 month stage.

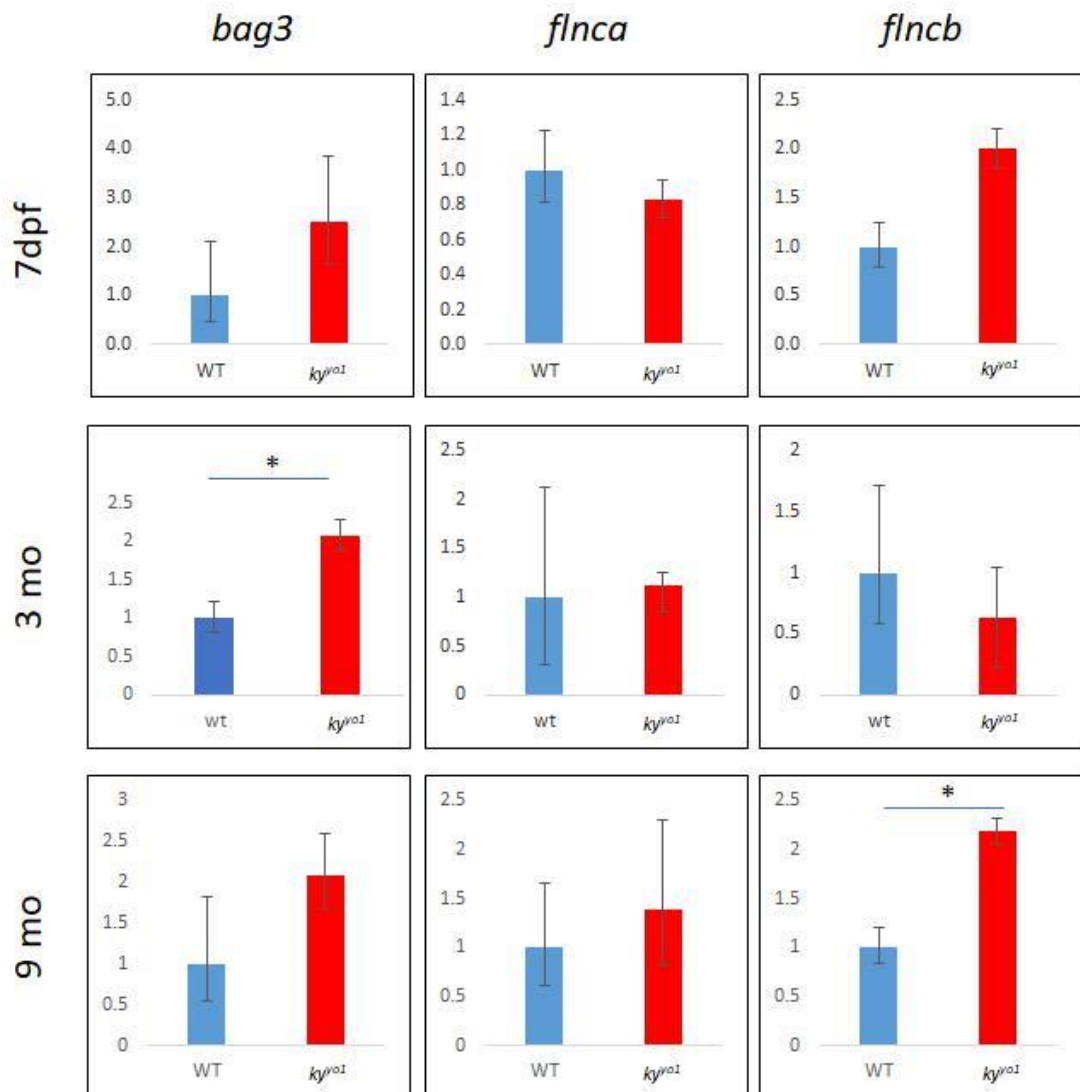


Figure 6.13 - qPCR analysis of *bag3* and *flnc* in WT and ky^{yo1}/ky^{yo1} zebrafish

Analysis was performed for *bag3*, *flnc*a and *flnc*b at 7dpf, 3 months (3 mo) and 9 months (9 mo). *bag3* shows a consistent upward trend in ky^{yo1}/ky^{yo1} embryos, though this is only significant at the 3 month stage (Student's *t*-test, $p < 0.01$, $n = 3$). *flnc*a shows no differences. *flnc*b shows a non-significant increase at 7dpf, no difference at 3 months and a significant upregulation at 9 months (Student's *t*-test, $p < 0.05$, $n = 3$). Error bars represent the standard deviation.

6.9 - Methylcellulose challenge of embryos

Given that upregulation of *bag3* and *flncb* was observed in mutant larvae, it was hypothesised that even embryonic muscle may be more susceptible to stress. To test this, 3dpf WT and *ky^{yo1}/ky^{yo1}* embryos were incubated in viscous media enriched with 1% methylcellulose for 48hrs to provide resistance to swimming and thus induce muscle damage. No overt signs of muscle pathology were observed under brightfield microscopy or by analysis of birefringence (data not shown). As expected, WT embryos show significant upregulation *bag3* and *flnca*, as well as a trend towards increased *flncb* when incubated in methylcellulose enriched media (Figure 6.14). However, it can be seen that untreated *ky^{yo1}/ky^{yo1}* embryos have significantly higher *flnca*, *flncb* and *bag3* compared to WT controls. This indicates that *ky^{yo1}/ky^{yo1}* embryos experience similar levels of cellular stress in normal media as WT embryos do in methylcellulose. Additionally, the methylcellulose treatment induced no further increase in transcript levels in the mutant embryos. This indicates that the *ky^{yo1}/ky^{yo1}* embryos are unable to adapt to increased physical resistance to movement.

6.10 - Discussion

The conservation of a muscle-specific Ky ortholog in zebrafish, particularly the preserved catalytic triad of the transglutaminase-like domain, indicates that this protein still fulfils an important role in muscle tissue. The absence of an organism or tissue level phenotype in the absence of Ky may likely be explained by the absence of the same consistent gravitational stresses experienced by mice and humans. Given overt pathology is restricted to muscles experiencing consistent tension in mammals, it is possible that there is no equivalent tissue in zebrafish where the absence of Ky becomes catastrophic.

Examination of the pathology in this project has primarily been at the organism, tissue and molecular level. Closer analysis of muscle, for example at the scale of electron microscopy, may reveal subtle structural phenotypes than can be observed by H&E and immunofluorescence, such as z-disc thickening. Additionally, examination of the cytoskeleton of muscle fibres may show more minor signs of damage, for example broken myofibrils.

However, the trend towards upregulation of *bag3* and *flncb* may indicate that mutant muscles are experiencing elevated levels of cell stress even in the absence of overt hallmarks of pathology. This may indicate that upregulation of these components is

one of the primary effects of the absence of the Ky protein. This is further supported by the methylcellulose challenge experiment, which demonstrated elevated expression of *bag3*, *flnca* and *flncb* in untreated 5dpf *ky^{yo1}/ky^{yo1}* embryos equivalent to that seen in WT embryos in methylcellulose. Since this represents only a short period of time without *ky* expression, this indicates that the elevated expression of these markers is an immediate hallmark of Ky deficiency. The inability to upregulate these markers further in response to methylcellulose challenge suggests that Ky may be important to respond to tension.

The elevated transcription of CASA components should also be set in the wider context of autophagy to determine whether it is CASA specifically that shows signs of elevated activation, or whether this is part of a wider signalling cascade.

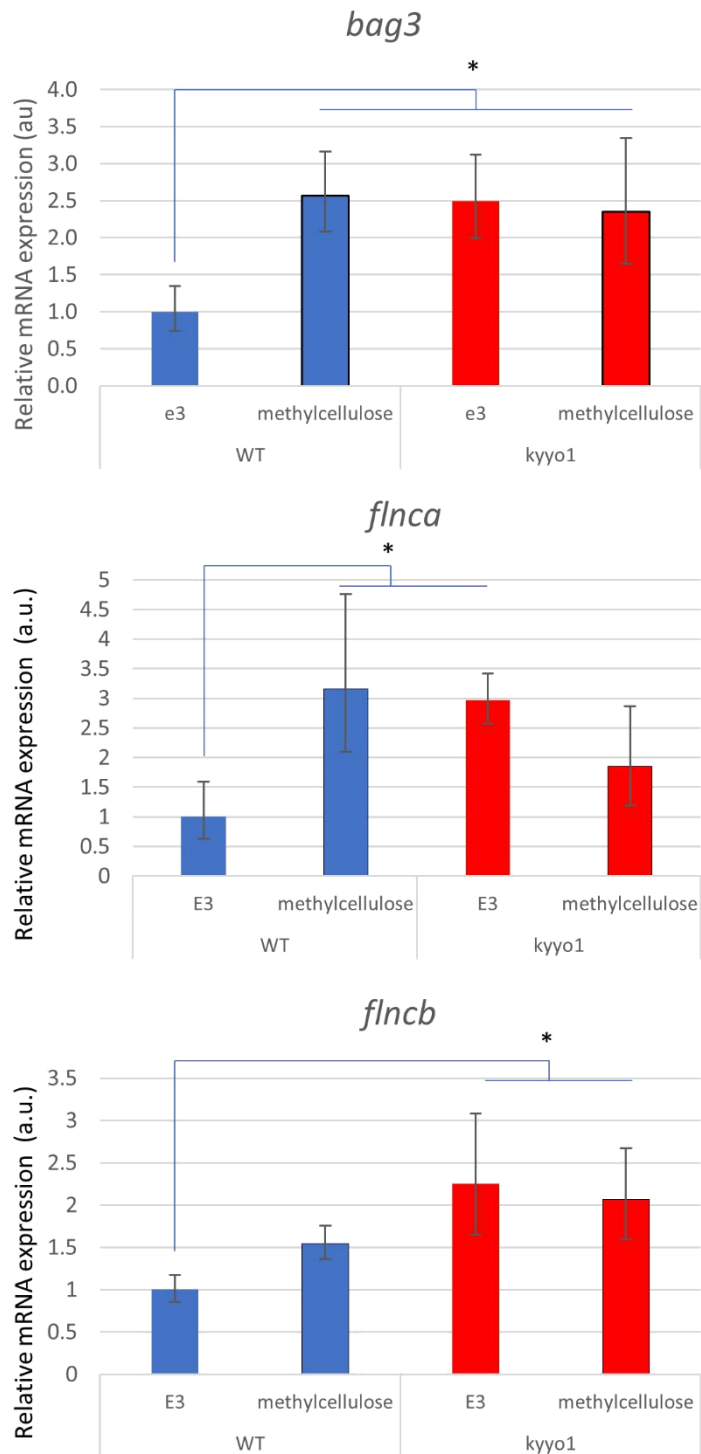


Figure 6.14 - Methylcellulose challenge induces CASA component upregulation in WT but not ky^{y01}/ky^{y01} embryos

qPCR of *bag3*, *flnca* and *flncb* in wt and ky^{y01}/ky^{y01} embryos incubated in normal media (E3) or 1% methylcellulose enriched media. WT embryos incubated in methylcellulose show significantly increased *bag3* and *flnca* (Student's *t*-test, $p < 0.05$, $n = 3$) alongside a trend to increased *flncb*. ky^{y01}/ky^{y01} in E3 show significantly higher levels of all three transcripts relative to WT (Student's *t*-test, $p < 0.05$, $n = 3$) with no additional upregulation when incubated in methylcellulose.

CHAPTER SEVEN: *IN*
VIVO
OVEREXPRESSION OF
KY CONSTRUCTS

CHAPTER SEVEN: *IN VIVO* OVEREXPRESSION OF KY CONSTRUCTS

7.1 Introduction

The experiments in this chapter examine the effects of *in vivo* overexpression of recombinant KY protein in muscle tissue.

Previous experiments established that KY is necessary to generate a hypertrophic response to the surgical overloading of muscle in mice. It has yet to be established whether overexpression of KY is itself sufficient to induce a hypertrophic response. If KY is necessary but not sufficient to induce hypertrophy, this increases the likelihood that the inability to induce hypertrophy in the *ky/ky* mouse is a secondary effect of the pathology, for example an increased sensitivity to sarcomeric damage due to overloading which inhibits hypertrophic pathways. If KY is both necessary and sufficient to induce hypertrophy, this increases the likelihood that KY acts directly in a hypertrophic signalling pathway. This in turn increases the likelihood that this may be the causative mechanism in the *ky/ky* pathology, with enhanced damage in postural muscles due to the decreased muscle mass to body mass ratio.

Additionally, this method can be used to induce KY expression in *ky/ky* muscle tissue to see whether this is sufficient to rescue muscle fibre size in this context.

Another question that remains unanswered is the importance of the catalytic triad in KY's transglutaminase domain. This triad is conserved among vertebrates, though studies have indicated that the catalytic pocket is misaligned, preventing enzymatic function. It has therefore been postulated that this domain has been co-opted for protein-protein interactions. Thus, overexpression of KY with the catalytic triad mutagenised will provide information on the importance of this triad in localisation to the z-disc and any functional impact of KY overexpression.

7.2 Overexpression of KY in WT mice using *in vivo* electroporation

A schematic of the experimental methodology is shown in figure 7.1. To explore whether KY is sufficient to induce muscle hypertrophy, two DNA plasmids were transferred into mouse *tibialis anterior* (TA) muscle using *in vivo* electroporation. One encoded a V5-tagged KY construct (KY_V5) and the other a bright GFP construct to allow easy visualisation of successful electroporation of fibres, (pMAX_GFP). After 10 weeks of expression, animals were sacrificed, the TA was dissected, fixed, snap-frozen and sectioned to allow observation of the cross

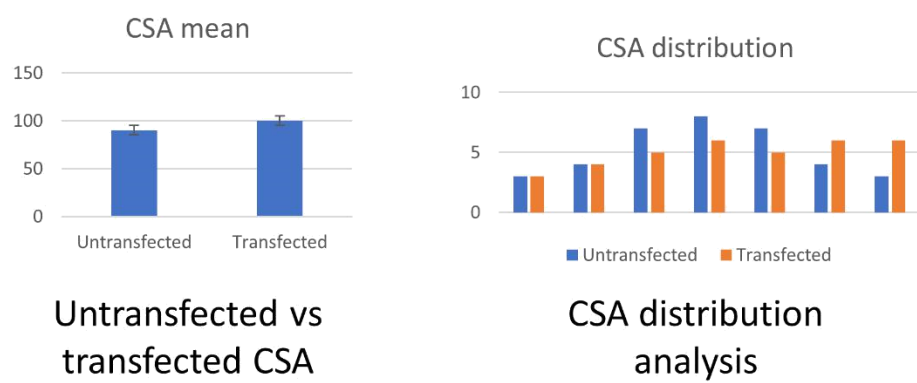
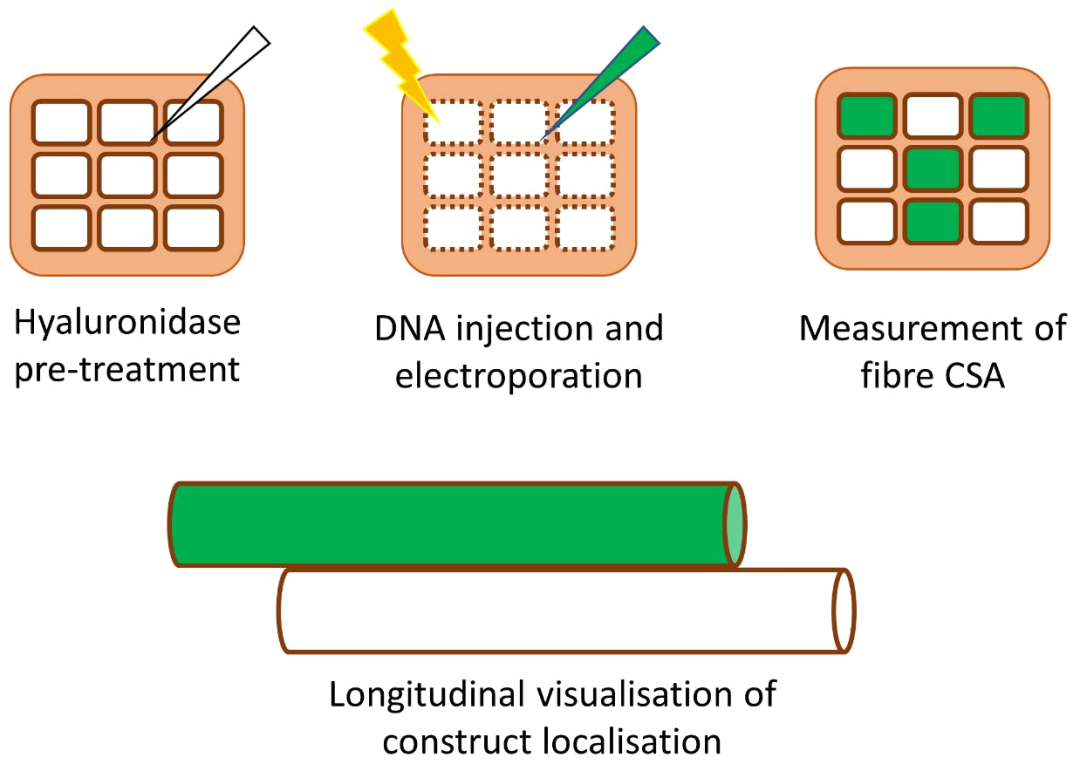


Figure 7.1 - Methodological summary of electroporation experiments

Pre-treatment by intramuscular injection of 0.4U/ul hyaluronidase was used to disrupt the ECM and increase electroporation efficiency. After 2 hours, DNA was injected into the EDL/TA immediately followed by DNA transfer into muscle by electroporation. Mice were allowed to recover and express the DNA construct for various lengths of time, after which the localisation of the encoded KY protein and the impact of overexpression on muscle fibre cross-sectional area (CSA) was assessed.

sectional area of transfected and untransfected fibres. No significant differences in CSA mean were observed between untransfected and transfected fibres either for fibres expressing KY_V5 and pMAX_GFP (Figure 7.2 B), or pMAX_GFP alone. There was also no apparent size distribution shift between untransfected and KY_V5/pMAX_GFP transfected fibres when individual fibre CSAs were plotted on a

histogram (Figure 7.2 C). This suggests that overexpression of KY_V5 was not sufficient to induce a hypertrophic response in WT mice.

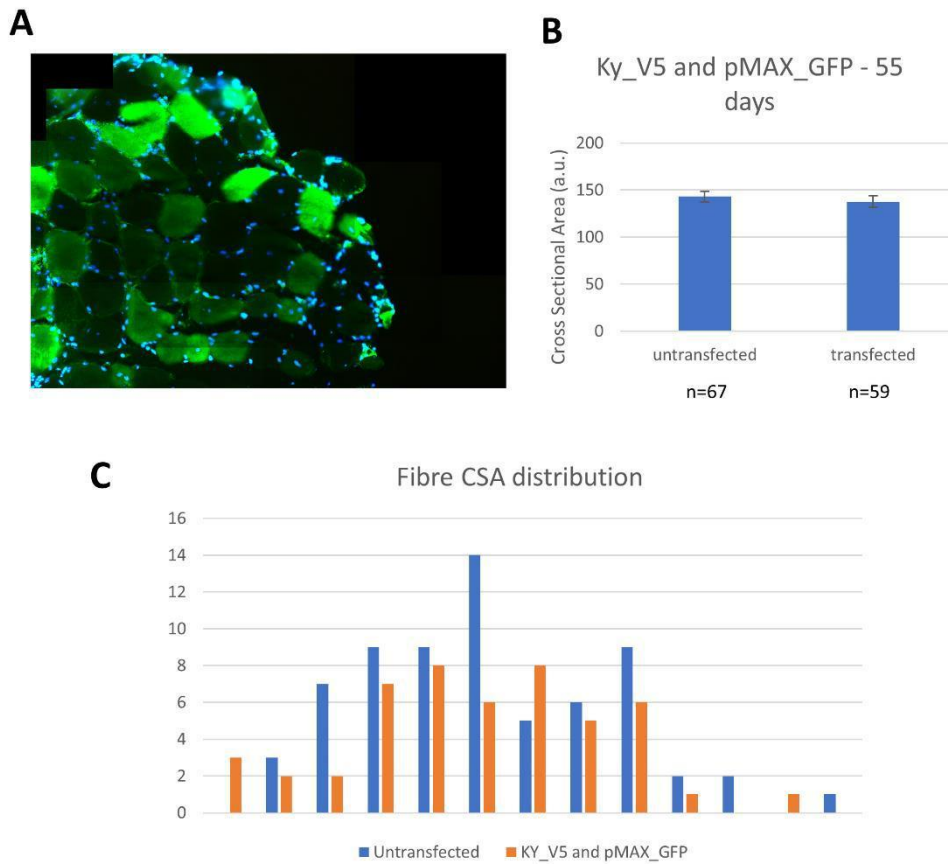
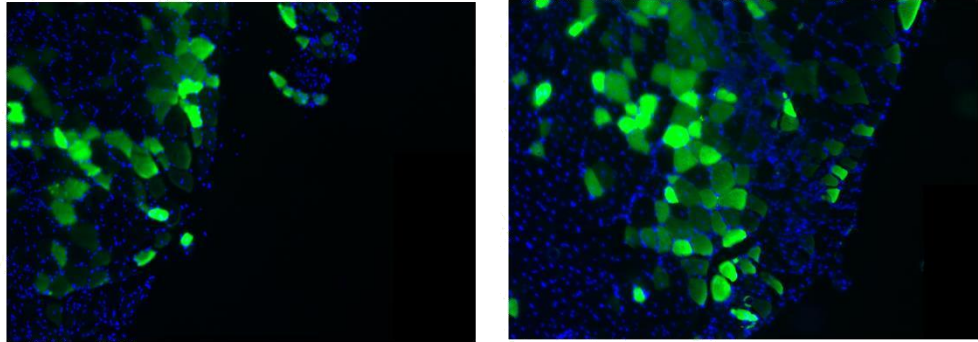


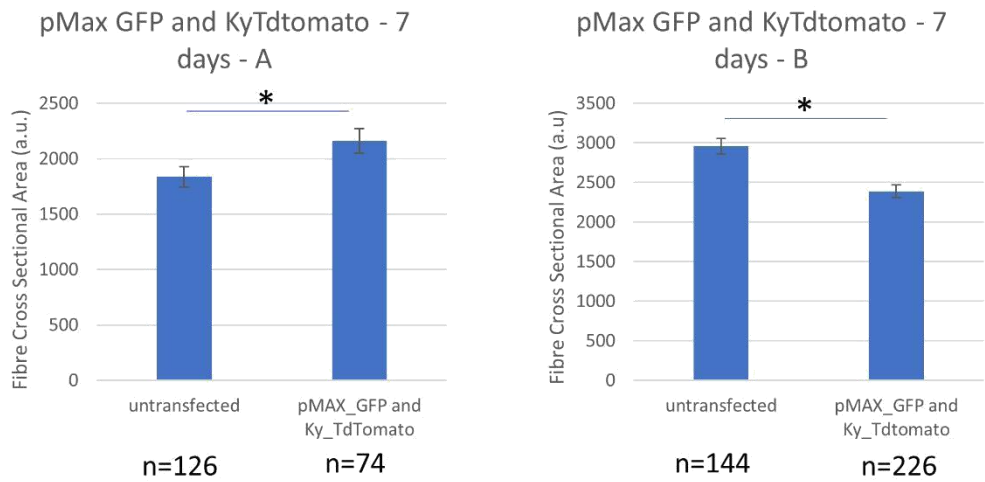
Figure 7.2 - KY_V5 expression does not induce hypertrophy after 55 days in WT mice

A) Representative field of view showing successfully transfected mouse muscle in cross section. B) CSA quantification shows no difference in mean CSA between transfected and untransfected fibres. Error bars indicate standard error of the mean, n indicated under series legend C) Fibre size distribution shows no apparent shift in CSA.

A



B



C

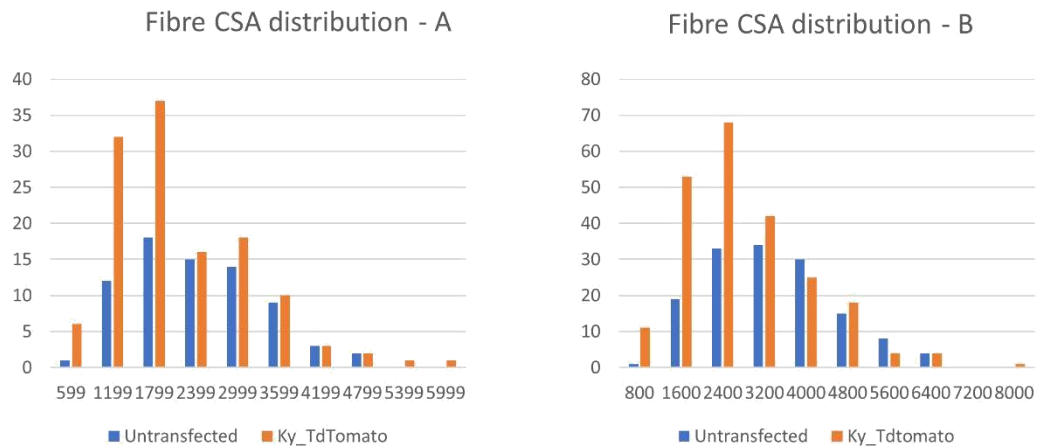


Figure 7.3 - Short term expression of *Ky_Tdtomato* induces inconsistent changes in WT mice

A) Representative fields of view of successfully transfected fibres. B) Quantification of mean CSA indicates significant upregulation in mouse A and significant downregulation in mouse B (T-test, $p < 0.05$, n shown under axis legend). C) Fibre size distribution shows a distribution shift towards smaller fibres, potentially as a result of regeneration. A small number of larger, transfected fibres can also be seen.

The length of time in which mice were left to recover was designed to allow full tissue recovery, therefore removing the impact of muscle damage and fibre regeneration as confounding factors in CSA analysis. However, given that long term overexpression of protein has the potential to activate negative feedback loops which may inhibit the impact of protein overexpression, it was decided that shorter expression times might also be informative in determining the impact of KY overexpression. In these experiments, Ky_TdTomato and pMAX_GFP were used, with a shorter expression time of one week. The results of this analysis were unclear, with data suggestive of a modest increase in fibre CSA with expression of Ky_TdTomato in one case and decreases in fibre CSA in another (Figure 7.3 B). When individual fibre CSAs were plotted on a histogram, it is clear that a larger variability in fibre sizes may account for the noise, with a greater number of small fibres, presumably due to damage and regeneration (Figure 7.3 C). This would disproportionately affect transfected fibres as these tend to be more proximal to the electroporation site – however, small fibres expressing the construct are not likely to have undergone regeneration, as this would require highly efficient transfection of satellite cells. Given there are a small number of very large transfected fibres, it is possible that the residual damage and regeneration induced by the protocol masks a shift towards increased CSA. Overall, however, these experiments produced no consistent evidence that KY_TdTomato could induce skeletal muscle hypertrophy.

7.3 Overexpression of KY in *ky/ky* mice using *in vivo* electroporation

To explore whether delivery of functional Ky would be sufficient to rescue the *ky/ky* phenotype, KY_V5 was transfected alongside pMAX_GFP into the TA muscle of *ky/ky* mice. Though the soleus has the most severe phenotype and would be the ideal candidate for rescue, the muscle could not be consistently or specifically targeted with this protocol due to its very small size and the fact that such precise electrode placement could not be achieved in our minimally-invasive protocol. In this experiment, a significant increase in fibre CSA was observed (Figure 7.4 A). This indicates that restoring KY expression in mouse muscle rescues the reduction in muscle mass observed in *ky/ky* mice.

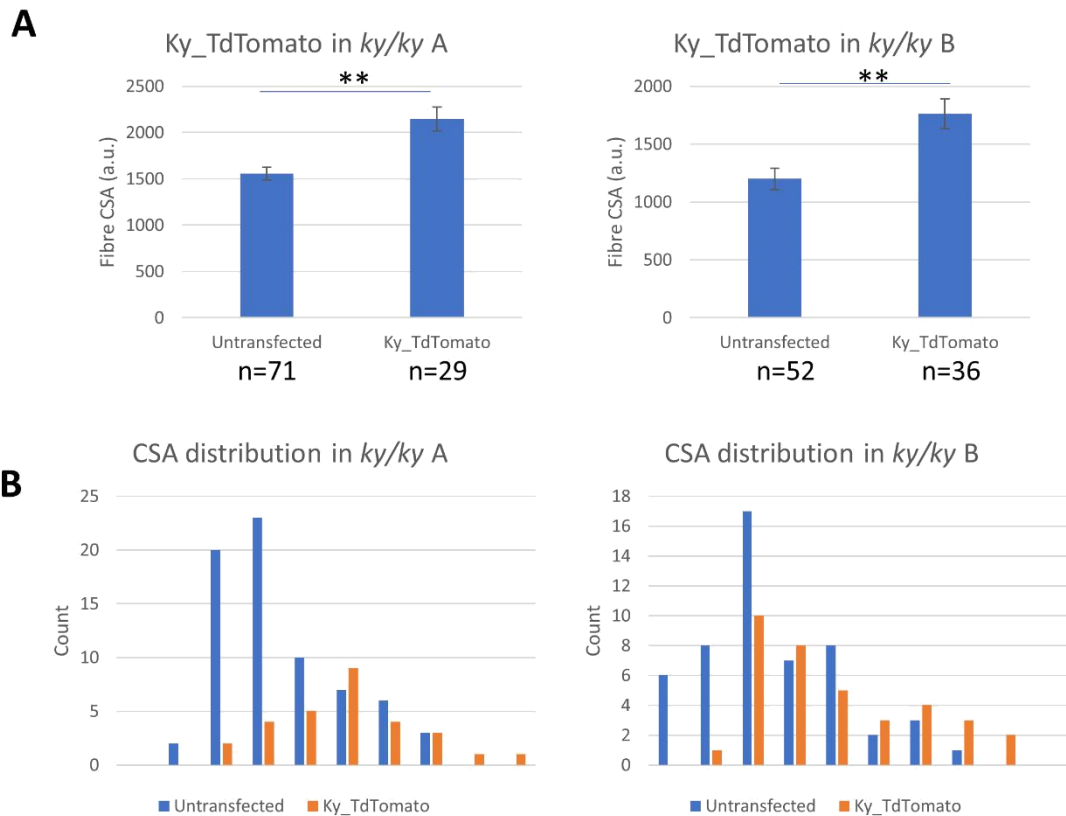


Figure 7.4 - Ky_TdTomato induces hypertrophy in ky/ky muscle

A) Mean fibre CSA is higher in Ky_TdTomato transfected fibres in ky/ky mouse muscle (Student's T-test, $p < 0.01$, n displayed under chart legend). Error bars indicate SEM. B) CSA distribution shows a shift towards larger fibres.

7.4 Localisation of mutagenised Ky

Note: Constructs encoding a mutagenised Ky_Tdtomato with a C->A substitution in the catalytic triad (KY_Td-SM) were generated by George Atkinson in his Master's project. Constructs encoding a mutagenised Ky_Tdtomato with substitution of the three catalytic residues (KY_Td-TM) and deletion of the sequence containing the catalytic triad (KY_Td-DEL) were generated by Merve

To determine the importance of the catalytic triad in the localisation and function of Ky, mutagenised constructs were generated as described above and in Figure 7.5 and electroporated into mouse muscle (Figure 7.6 A). All constructs appeared to show some level of perinuclear localisation and transverse striations, presumed to be the z-disc based on previous data. Qualitatively, Ky_Td-TM appeared to show strong striation patterning, indicating that the specific catalytic residues are not required for z-disc localisation. However, Ky_Td-DEL showed much weaker striation

patterning, indistinguishable from an apparent optical artefact observed across fluorescent channels when the confocal exposure was increased (Figure 7.6 D). It therefore appears that the absence of the catalytic domain impairs the z-disc localisation of KY, possibly fully.

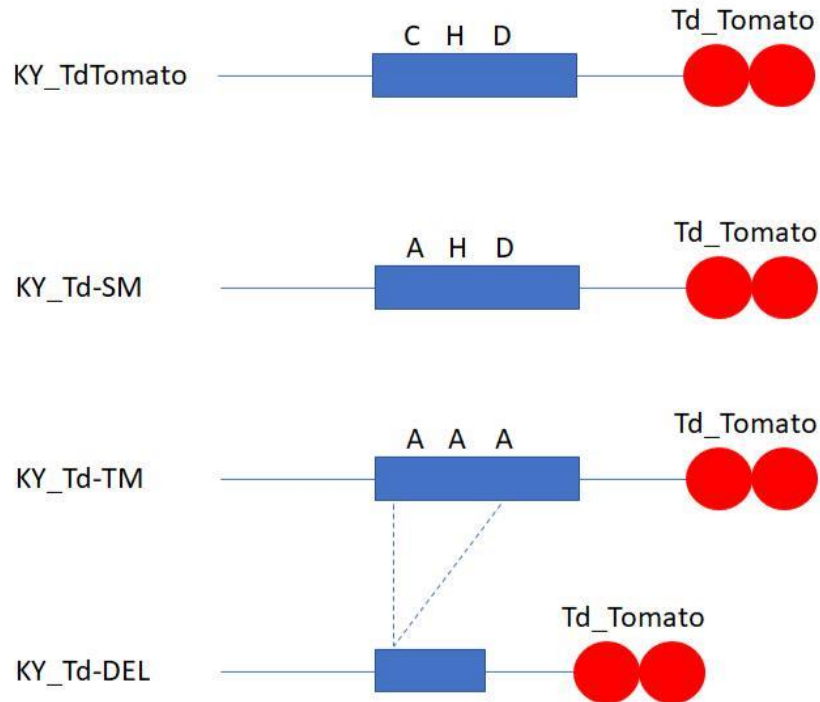


Figure 7.5 - Diagram of mutagenised KY constructs

KY_TdTomato encodes the WT KY protein, including the transglutaminase domain (blue box) with the C,H and D catalytic residues, with a TdTomato fluorescent tag. *Ky_TD-SM* contains a single mutation substituting the catalytic cysteine residue (C) for alanine (A). *KY_Td-TM* contains a triple mutation, substituting the catalytic triad with A. *KY_Td-DEL* deletes the region containing the catalytic triad from the site of the original C residue to the D residue inclusively.

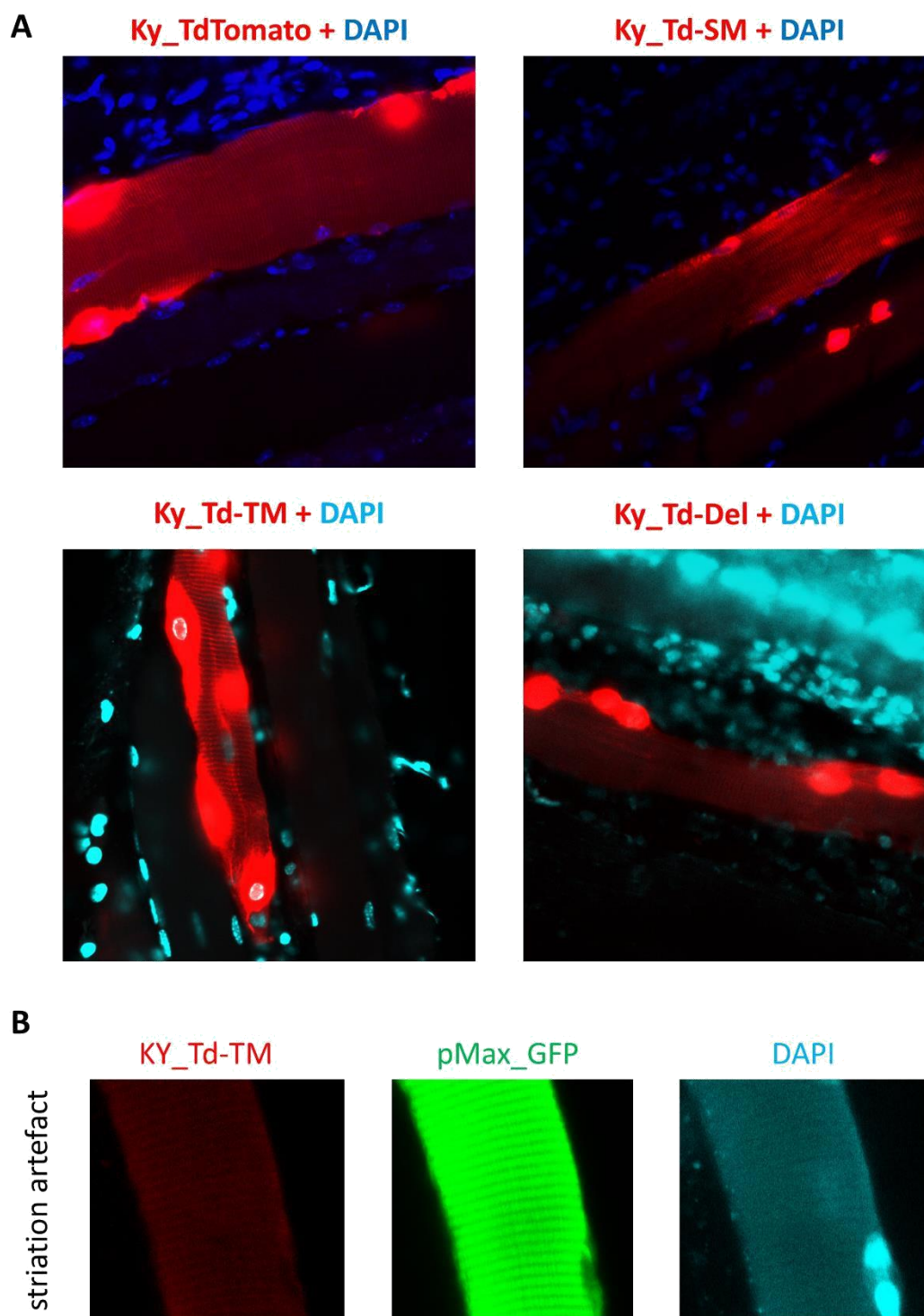


Figure 7.6 - Localisation of Ky_TdTomato constructs in mouse skeletal muscle

A) Constructs show variability in striation patterning, though localisation to striations appears qualitatively strong in KyTd_TM, indicating the catalytic residues are not critical for z-disc localisation. Though some striation appears in KyTd_Del, it can be seen that similar patterning can be observed across channels (B), indicating this patterning occurs as an optical artefact in certain conditions. It therefore appears that the catalytic domain may be required for efficient z-disc localisation

7.5 Overexpression of murine KY_Tdtomato in zebrafish

Given the transparency of zebrafish muscle and the relative ease of inducing the expression of genetic constructs by microinjection, KY overexpression in zebrafish was also attempted. The murine KY_Tdtomato was cloned into pCS2+ plasmid. Attempts to induce expression were made both by injection of the DNA plasmid and injection of RNA obtained by *in vitro* transcription using the plasmid template. Both methods proved highly inefficient, with a high degree of embryonic lethality. However, expression could be observed in a small number of fibres (Figure 7.7). This appeared to primarily exist as aggregates, likely a consequence of protein misfolding at the cooler body temperature of the zebrafish (28 degrees). However, some degree of localisation to striations could be observed. Though colocalization with z disc markers would be required to confirm these striations are at the z-disc, this appears to be evidence that at least some of the protein is localising correctly, suggesting the 'niche' for murine KY is conserved in the zebrafish. However, given the low efficiency and low proportion of correctly localised protein, this method was not pursued further.

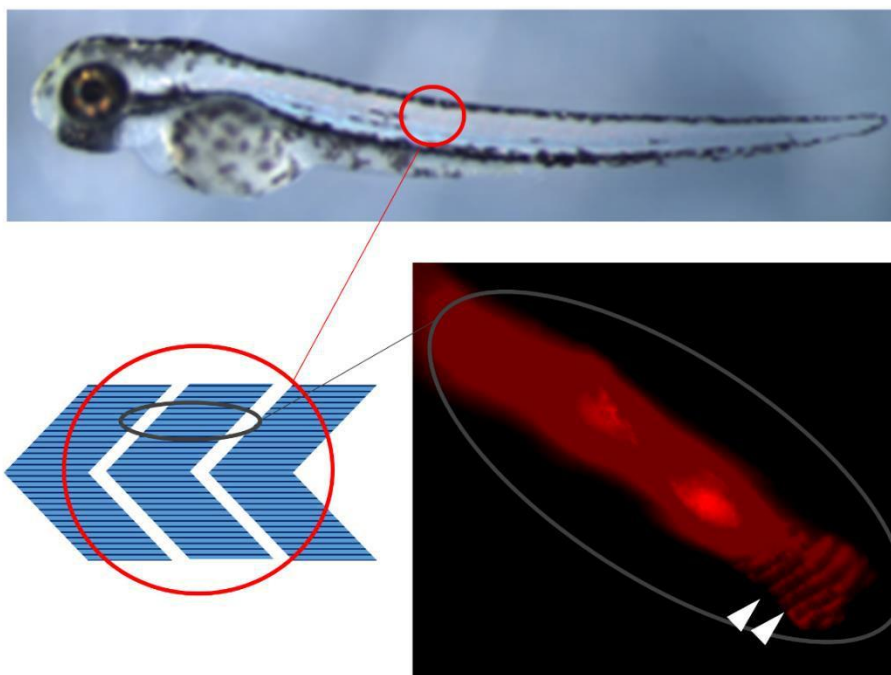


Figure 7.7 – TdTomato-tagged murine KY localises to striations in zebrafish muscle

Top) Image of a zebrafish embryo with a skeletal muscle somite encircled in red. Bottom left) diagram of the somite which is constructed of parallel muscle fibres. Bottom right) Image of a zebrafish muscle fibre expressing murine Ky_Tdtomato after embryonic injection of mRNA. Though much of the protein appears to aggregate, localisation to distinct striations can also be observed.

7.6 Conclusions

Overexpression of KY appears unable to consistently induce a hypertrophic response, indicating KY is not sufficient for hypertrophy. This is not conclusive evidence that KY does not operate in a hypertrophic pathway, but is consistent with the conclusion that the absence of hypertrophic responses observed in the *ky/ky* mouse model may be due to misregulation of the CASA pathway. The ability of KY overexpression to rescue muscle fibre CSA in the *ky/ky* mutant may represent the restoration of CASA efficiency and regulation, reducing the cell stress burden in muscle and therefore releasing inhibition of growth pathways. However, this hypothesis needs to be further explored by direct examination of CASA in rescued tissue - though this represents a technical challenge in consistently and efficiently targeting pathological tissue to have the greatest chance of observing an effect.

Molecular profiling of electroporated muscle may also have provided insights into the signalling cascades activated by KY overexpression. For example increased levels of phosphorylated p70s6k in response to electroporation with KY constructs, but not controls, would indicate mTOR activation and hypertrophic responses. However, this would be technically challenging to produce a clear picture within the context of muscle damage and regeneration that occurs due to the electroporation procedure.

The expression of mutagenised KY constructs has given some indication that the catalytic domain may be important for protein-protein interactions, though the specific residues do not seem to be necessary for the normal localisation of the protein. Additionally, the deletion of the catalytic domain may have unintended effects on the structure of the resulting protein which impair interactions related to other regions of the protein. The strongest candidate based on *in silico* analysis in chapter 3 is the region with some degree of homology to Filamin domains which may allow interaction with FLNC interaction partners. Expression of a construct containing only the transglutaminase domain would clarify which of the two is critical for z-disc localisation.

Ultimately, the mutagenised constructs require a phenotypic test to determine whether the catalytic residues and the catalytic domain are important for KY function. If mutagenised constructs can recapitulate the apparent rescue of *ky/ky* tissue by WT KY overexpression, this undermines the argument that KY acts via

catalytic activity. In that instance, it would seem likely the function of KY is to facilitate protein-protein interactions.

CHAPTER EIGHT:
DISCUSSION AND
FUTURE WORK

CHAPTER EIGHT: DISCUSSION AND FUTURE WORK

8.1 Overview

The primary aim of this thesis was to gain functional insights into the KY protein by exploring the existing *ky/ky* mouse model as well as by the development of novel zebrafish and C2C12 models of KY deficiency.

The hypothesis driving this project has been a potential role for KY in CASA. CASA is proposed as the primary recycling mechanism for FLNC, a known KY interaction partner which is aberrantly localised in tension-bearing muscles of *ky/ky* mice. Inefficiencies in CASA would account for this aberrant localisation and the susceptibility of tension-bearing muscles to structural damage and atrophy. The resulting cellular stress may also account for the failure of muscle to undergo compensatory hypertrophy by inhibition of mTOR activation.

If KY operates in the CASA mechanism, it could feasibly have a number of different functions: -

- Structurally supporting FLNC to limit the amount of irreversible unfolding
- Promoting the tension-induced expression/activation of chaperones, e.g. BAG3
- Promoting the recognition of unfolded FLNC by chaperones and/or the assembly of the CASA complex
- Facilitating the solubilisation of the CASA complex from the cytoskeleton into the cytoplasm
- Facilitating the degradation of the CASA complex via the autophagolysosomal pathway
- Facilitating the expression of replacement FLNC or its correct localisation to the sarcomere

8.2 Insights from the *ky/ky* mouse

Elevation of CASA markers is evident in both the atrophic, postural soleus and the relatively non-pathological, fast-twitch EDL in *ky/ky* mice.

In the *ky/ky* EDL, increased transcription of *Bag3* matched with no increase in BAG3 protein levels indicates that this protein is being turned over effectively. This indicates that KY is neither fundamentally necessary for BAG3 turnover, nor necessary for CASA activation. This data would be consistent with KY having a role in preventing or limiting the irreversible unfolding of FLNC, thus leading to enhanced CASA activation due to increased FLNC unfolding in its absence. However, since the pathological increase of mislocalised FLNC is not reported in the EDL, it would appear that the mechanisms of FLNC turnover - or some other compensatory mechanism - are still sufficient to deal with any such increase in protein susceptibility to damage. This could be explained by the fact that fast-twitch muscle does not experience the same consistent levels of high tension. Given that the EDL is relatively spared from the *ky/ky* pathology, this indicates that upregulation of the CASA mechanism presents a primary effect of KY deficiency and is not a secondary effect of atrophy and structural disruption.

The soleus shows an increase in the cytoskeletal proportion of BAG3 protein. The lack of concurrent increase in soluble BAG3 protein or *Bag3* mRNA transcript indicates that this cannot be accounted for entirely by upregulation of protein expression, indicating some issue with BAG3 turnover. Co-localisation with FLNC in immunofluorescence analysis suggests that cytoskeletal BAG3 could be being sequestered with unfolded FLNC, suggesting KY is not required for the assembly of the CASA complex in response to FLNC unfolding, but failing to solubilise and be degraded effectively. This may indicate that in the soleus, which consistently experiences high tension, the inefficient CASA mechanism becomes insufficient to deal with the resultant protein unfolding. However, a fuller profile of the state of autophagy and other protein turnover mechanisms is needed to assess whether any limitation in CASA arises at the solubilisation or the degradation stage.

The major limitation on this data is the lack of protein level analysis of FLNC. In the literature, no difference in FLNC protein levels was observed between mutant and WT soleus muscle (Beatham et al. 2004), though this was not performed on fractionated samples, only on soluble FLNC. If FLNC displays the same higher turnover in the EDL and elevated cytoskeletal proportion of protein in the *ky/ky* soleus as is observed with BAG3, this would support these hypotheses. If FLNC turnover appears unaffected, this indicates that the structural disruption observed in the *ky/ky* mouse must occur by some other mechanism.

8.3 Insights from ky-deficient C2C12 models

The ability of ky-deficient myoblasts to differentiate normally indicates that this process is independent of KY, and thus indicates a distinct functional role from its interaction partner, IGFN1, which is required for efficient myoblast fusion (Li et al 2017). The smaller size of myoblasts appears to indicate altered regulation of cell size in the absence of KY, but the relevance of this phenotype is unclear given the lack of developmental phenotype in any of the other models that were examined. CASA could not effectively be assessed in the ky-deficient myoblasts due to a high level of noise. This may be resolved in repeat experiments, but given that myotubes best represent the physiology of skeletal muscle, focus was given to characterising CASA in differentiated myotubes. In this model, *Bag3*, *Fln*, *Chip* and *Hspb8* also showed trends towards upregulation in mutant clones, reaching significance in some clones but not others. The fact that these differences arise when myotubes are unchallenged and thus only experiencing normal endogenous tension is further evidence that the effect of KY deficiency on this pathway is not dependent on high levels of tension, and thus may represent a primary hallmark of the pathology rather than an effect of high levels of structural damage.

8.4 Insights from Ky-deficient zebrafish

The absence of an organism-level muscle phenotype in the ky^{y01}/ky^{y01} zebrafish indicates that ky does not play as critical a role in fish as it does in mice and humans. This may in part be because the impact of *ky/ky* pathology primarily affects postural muscles under constant mechanical strain from the force of gravity, suggesting ky is important for maintaining muscles under tension. Though zebrafish also have slow muscle tissue, utilised in constant swimming, they do not experience the same gravitational strains in water and thus may not require Ky as acutely.

However, molecular profiling does indicate elevated levels of *bag3* mRNA in ky_{y01}/ky_{y01} zebrafish muscle. Given BAG3 is upregulated in response to cellular stress, this indicates that Ky may still be important in maintaining muscle tissue. Given this upregulation occurs without any organismal- or tissue-level hallmarks of pathology, this is likely to be a primary effect of the absence of Ky. If the mechanism governing Ky function is conserved between mammals and fish, this could be a hallmark of the early events of the *ky/ky* pathology.

Intriguingly, in contrast to the C2C12 myoblasts which show expression of Ky, no early developmental expression was detected until 3dpf. By this stage, zebrafish

embryos are motile, suggesting that Ky expression correlates to the onset of muscle activity, but not development. It has been noted that ky expression in C2C12 models is particularly high, and thus the expression of KY in C2C12 myoblasts may be an artefact of their selection.

Attempts to induce damage in embryos by swimming them in methylcellulose-enriched media showed that WT zebrafish upregulate the CASA markers *bag3* and *flnc* isoforms in response to the increased mechanical strain of swimming in viscous media. *ky^{yo1} / ky^{yo1}* show constitutive upregulation of these markers, and do not increase transcriptional activation further in response to the methylcellulose treatment. This suggests an increased level of cell stress even under control conditions, and an inability to elevate this further under challenge. This may suggest that CASA in *ky^{yo1} / ky^{yo1}* is constitutively maximised and thus cannot increase further, or that the existing cause of cell stress undermines the embryos capacity to sense or respond to the increased physical strain. If Ky plays a structural role in muscle, this could reflect an increased susceptibility to muscle damage, even in conditions of low mechanical strain, which subsequently leads to the activation of cell stress pathways. However, since no signs of increased structural damage is observed in the adult or embryonic mutant fish, it seems less likely that this cell stress activation is a secondary effect of tissue damage. Additionally, this effect is observed in mutant embryos at 5 dpf, where normal Ky expression has been absent for only 48 hours. This suggests that the dysregulation of CASA may be an early effect of Ky-deficiency rather than a consequence of structural stability. Experiments examining the stress response and structural integrity of adult zebrafish muscle in response to acute exercise (for example, swimming against a current) may provide further evidence that an enhanced stress response occurs independently of increased levels of overt structural damage.

8.5 Insights from overexpression experiments

Overexpression of Ky via *in vivo* electroporation in mice indicates that KY is not sufficient to drive a hypertrophic response in WT muscle tissue. However, there is at least some suggestion that KY overexpression can induce a hypertrophic effect in *ky/ky* mouse muscle tissue, indicating some degree of phenotypic rescue. It also seems that the catalytic region of the transglutaminase domain, but not the specific catalytic residues, are important for efficient z-disc localisation.

Expression of murine, TdTomato-tagged KY in the zebrafish showed that the protein was capable of localising to striations in skeletal muscle fibre. This suggests that the localisation niche of ky is conserved between mice and zebrafish, though staining against a known z-disc protein such as alpha actinin is needed to determine this specifically, though it is known that this construct localises to the z-disc in cardiomyocytes and myotubes (Baker et. al, 2010).

8.6 Overall conclusions

The physiology of humans, mice, zebrafish and cultured myotubes will obviously have a number of differences and the results obtained in each require interpretation within that context. The lack of overt zebrafish pathology is a prime example of this, given the different mechanical stresses experienced in an aquatic environment compared to one where gravitational forces are felt more acutely. The disproportionate effect of KY-deficiency on postural muscles in mice and humans suggests that overt pathology only emerges in response to consistent high tension, which has lent itself to an interpretation of decreased structural integrity underlying the pathology. The blunted hypertrophic response in EDL muscle demonstrated in Blanco *et al* 2001 was the first suggestion that even non-pathological muscle exhibited an impaired capacity to respond normally to tension. Combined with the data in mice suggesting *Ky* expression is in fact lower in postural muscles than in fast-twitch muscles and the fact that the protein structure is atypical of a structural protein, this reduces the likelihood of KY being directly responsible for structural integrity in a purely physical sense.

All the models examined in this thesis show some evidence of CASA upregulation in the absence of KY; the mouse EDL, embryonic zebrafish and differentiated myotubes. The data presented is insufficient to specifically tie KY to a molecular function in this pathway, but there is at least some indication of impaired protein turnover with an increased proportion of cytoskeletal BAG3 in postural muscles lacking KY. Thus, CASA appears to be more highly activated in the absence of KY, but the “flow” of protein turnover may be limited by some inefficiency. This alone would account for the phenotypes in the models examined as per the diagram below:

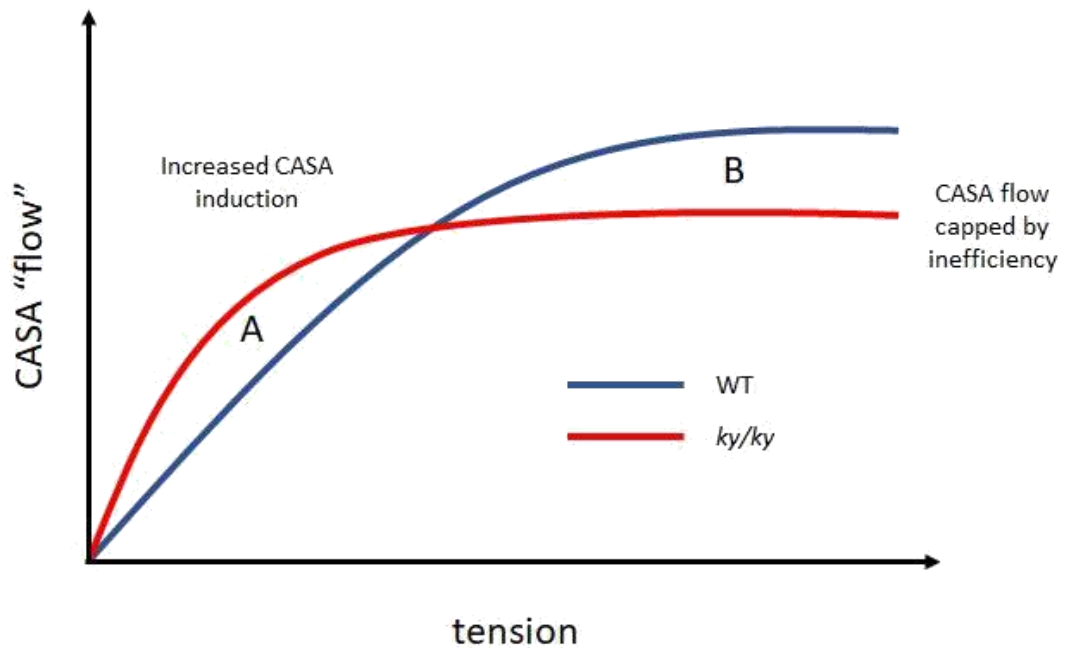


Figure 8.1 - Altered CASA activation explains the major phenotypes in KY-deficient models

KY- deficient models show increased CASA activation at low tension, but a lower upper limit of CASA flow due to an inefficiency in protein turnover. The differences to WT in area A and B explain the major phenotypes. A represents a “hypertrophy cost” as increased CASA may negatively shift the balance of protein synthesis, blunting hypertrophic responses to mechanical tension. B represents increased damage susceptibility, as the inefficient “flow” of CASA is no longer sufficient to meet the normal maintenance needs of the tissue.

Another possibility is that the apparent failure of CASA in postural *ky/ky* muscles is simply a hallmark of the pathology and not a causal mechanism. For example, if the function of KY is to translate tension into hypertrophy, failure to undergo hypertrophy could equally account for the structural damage observed as the muscle weight to body weight ratio falls critically low, which would in turn lead to increased activation of the CASA pathway. However, the presence of CASA marker upregulation in KY-deficient mouse EDL, myotubes and zebrafish embryos indicate that this is a primary event and not brought about by pathological effects of consistent high tension. For example, upregulation of CASA markers in 5dpf embryonic zebrafish, where ordinary onset of *ky* expression is only at 3dpf, suggests that CASA upregulation is a near-immediate consequence of *ky*-deficiency. This makes it less likely that impaired hypertrophic responses are the primary mechanism of the pathology.

A “BAG3 switch” has been proposed as a cellular mechanism by which autophagy becomes favoured during aging and cell stress (Gamerding, Hajjeva, and Behl 2009). The upregulation of CASA markers may therefore represent activation of this

mechanism. It may be possible to consider KY-deficiency as a model of premature muscle ageing. Though no evidence of enhanced autophagy activation was obtained in this thesis, the increased levels of autophagic vacuoles in pathological muscle in the *ky/ky* mouse indicates some phenotype at the level of macroautophagy which may be further unpicked in future experiments.

8.7 Future experiments

8.7.1 Cellular model

The KY-deficient C2C12s provide a highly tractable experimental model to explore the function of KY and the impact of its absence. This project was limited to profiling myoblasts and myotubes in an untreated state, and as such the full potential of this model has yet to be realised.

Stretching experiments, such as those performed on WT myoblasts, would reveal whether the direct relationship between mechanical tension and protein turnover mechanisms is preserved in the absence of KY. For example, changes in upregulation of *Bag3* or *Flnc* mRNA in *ky*-deficient C2C12s under tension relative to WT controls may represent increases or disruption to the induction of CASA. An increased proportion of cytoskeleton-associated BAG3 and FLNC may indicate a failure to solubilise unfolded FLNC, mirroring the phenotype observed in the *ky/ky* mouse. The relative activation of factors involved in hypertrophic signalling and protein synthesis (e.g., the relative phosphorylation of P70S6K) may also demonstrate whether the absence of KY blunts the activation or transmission of this signalling cascade. The presence or absence of these phenotypes will help to narrow down any functional role of *ky* in these mechanisms.

In addition, the cell model is more highly manipulatable pharmacologically. Given that activation and inhibition of protein degradation pathways have been shown to have therapeutic value in several myopathies, (Assereto et al. 2006; Gazzero et al. 2010; Bonuccelli et al. 2007; De Palma et al. 2012; Pauly et al. 2012) examining whether such treatments can reverse the apparent cell stress phenotype may provide insights as to whether the same might be true of myopathy associated with KY deficiency. Given that the phenotypes observed in mutant myotubes at rest appear to be fairly subtle, it is unclear whether any genuine therapeutic effects may be masked by the cell stresses induced by these treatments. However, this

approach may be more suitable if more overt phenotypes are observed in future analyses.

The cellular model can also be used to address whether KY is fundamentally important in macroautophagy. Our results and those of previous experiments are currently inconclusive with regards to the levels and functionality of autophagy in the *ky/ky* mouse. On the one hand, turnover of proteins in the mutant EDL appears to proceed unimpeded, e.g. elevated *Bag3* transcription and no resultant accumulation of protein. On the other hand, the soleus shows an apparent failure to break down unfolded FLNC whilst showing an accumulation of autophagic vesicles in electron microscopy. This suggests either that FLNC is not being delivered to the increased numbers of autophagosomes or that the flow of autophagy is impeded in the context of high mechanical stress and atrophy in the absence of *ky*, or some combination of the two.

This question can at least partly be clarified by simple experiments assessing the induction and flow of autophagy, for example measuring the induction of autophagosome formation in response to starvation or stretching. Flow can be determined by introducing an inhibitor, such as colchicine, to create a roadblock and the resultant buildup of LC3 protein can be measured. The greater the buildup of LC3, the greater the autophagic flow. If flow in the absence of *ky* is greater than or equal to flow in controls, this suggests that the failure to clear unfolded FLNC is likely to be an issue with solubilisation rather than an issue with the autophagy machinery. However, whether this can be directly translated to the animal model and human pathology is unclear.

8.7.2 Zebrafish model

The examination of the adult *ky^{yo1}/ky^{yo1}* zebrafish was entirely passive, searching for spontaneous emergence of organismal, tissue and molecular level phenotypes. However, since the absence of *Ky* appears to only produce pathology under high tension, it is likely that the zebrafish would have to be challenged before an overt phenotype emerges. Fish can be made to swim against a constant current, which would be likely to induce muscle damage and hypertrophic adaptations. The magnitude of these effects can be compared between *ky^{yo1}/ky^{yo1}* and control fish. If there is consistency between mouse and zebrafish models, we may expect elevated cellular stress and damage in mutant muscle tissue and a failure to increase muscle fibre cross-sectional area.

Overexpression of murine KY appeared to have a toxic effect when the doses of DNA and RNA were increased in an attempt to boost the efficiency of expression. Cloning the zebrafish Ky and overexpressing this via embryonic injection may be a more successful method of determining the effect of increased Ky expression. An inducible system or one under a promoter that would allow expression after about 3-4 dpf, when endogenous Ky expression is activated, may also prevent any potential deleterious effect during the early development of muscle.

8.7.3 Mouse model

The examination of mouse mutant muscle tissue was also largely passive. Subjecting mutant mice to exercise challenges may provide new insights into the effects of KY deficiency on muscle performance and protein turnover. For example, evidence of an increased proportion of cytoskeletal BAG3/FLNC in fast-twitch muscles of mutants post-exercise would support the hypothesis that inefficiencies in CASA are one of the immediate consequences of ky-deficiency as opposed to a secondary effect of other structural damage in the atrophic soleus. An increased activation of *Bag3* and *Flnc* transcription in mutant tissue post-exercise relative to WT would also indicate that muscles lacking KY are more prone to elevated cell stress. It could also be determined whether the absence of hypertrophic responses remains in post-exercise adaptations.

Similarly, recapitulating the experiments demonstrating the absence of compensatory hypertrophy in response to surgical ablation would provide a critical insight into whether the absence of hypertrophy drives sensitivity to damage or vice versa. If increased hallmarks of structural damage are observed early on in the compensating muscle in the mutant, this is consistent with the hypothesis that the pathology is driven by sensitivity to damage which leads to activation of cell stress pathways and inhibition of mTOR. If there are no differences in hallmarks of structural damage, this supports the hypothesis that the structural damage and muscle pathology are a product of a progressive increase in body-weight to muscle mass ratios.

8.8 Relevance to human KY-deficient myopathies and potential therapies

As described in the introduction, the reports of human myopathies driven by KY-deficiency underscore the importance of the KY protein in skeletal muscle

physiology. The value of model organisms to the understanding of the human pathology is limited by the extent to which the models reflect human physiology. Humans, mice and zebrafish place different demands on their skeletal muscle, due to differences in organism weight, posture and anatomical organisation. This makes it particularly remarkable that the human pathology shares common phenotypic elements with data historically derived using the *ky/ky* mouse model, including atrophy in postural muscles and aberrant localisation of the crosslinkers FLNC and XIRP1. Combined with the high level of protein conservation in mammals, and to a lesser degree in vertebrates, this indicates that data derived from models of KY-deficiency may provide valuable insights into the human pathology.

However, the accounts of human pathology have some differences, potentially accounted for by the accumulation of confounding mutations in consanguineous populations. This includes a supposed potential neurological element of the disorder, with impaired mental development observed in at least one individual (Straussberg et al. 2016) and the observation of *KY* expression in CNS tissue (Yogev et al. 2017), though the latter observation is contradicted by (Hedberg-Oldfors et al. 2016) and is also inconsistent with the mouse model (Blanco et al. 2001). Additionally, since none of these studies reported nonsense mediated decay of transcript, there is the potential for deleterious gain of function phenotypes contributing to the pathology. This may at least suggest that the severity of pathology arising from KY-deficiency in humans is variable and therapeutic interventions would need to be designed and implemented accordingly.

The model derived from the data in this thesis (Figure 8.1) suggests that the pathology might arise from constitutive upregulation of cell stress pathways, even in the absence of external physical stimuli. This in turn leads to inhibition of post-developmental muscle growth in the mouse, ordinarily stimulated by the onset of gravitational forces after birth. The resultant decrease in muscle to body weight ratios then generates an increased susceptibility to muscle damage which is particularly acute in postural muscles. At this stage the limited efficiency of the CASA pathway, due to inefficient CASA complex solubilisation, inhibits the ability of muscle to maintain and repair itself under tension, leading to pathology.

Though much more work needs to be done to establish the veracity of this model, on the assumption that it were true, it would suggest that the inhibition of CASA and cell stress pathways prior to the development of muscle pathology may help to rescue normal muscle growth. This could be tested by immediate intervention in

juvenile *ky/ky* mice post weaning. Given HSF1 is upstream of BAG3 upregulation, inhibition of HSF1 may be a candidate strategy. HSF1 inhibition is already an active area of drug development in the context of cancer therapeutics, thus treatments developed in cancer research might be repurposed for this context (Whitesell and Lindquist 2009). However, once pathology has emerged, enhancing CASA efficiency in pathological tissue, or some other compensatory mechanism, may be needed to eliminate aberrantly localised FLNC and restore the health of the tissue. Upregulation of autophagy via mTOR inhibition helps to clear BAG3 aggregates in a zebrafish model of myofibrillar myopathy (Ruparelia et al., 2014), and has been shown to enhance autophagy and alleviate myopathy associated with mutations in COL6 (Grumati et al. 2010), though the targeting of mTOR may further exacerbate inhibition of growth pathways. Thus, therapies may need to be tailored according to the progression of the disease and balanced carefully to avoid exacerbation of the pathology.



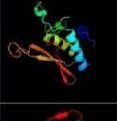

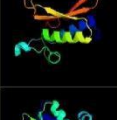
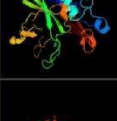
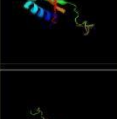
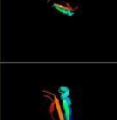
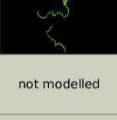
Glossary of abbreviations




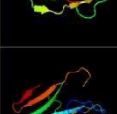
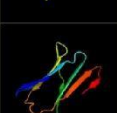


Abbreviation	Name
ACTA1	actin alpha 1
AKT	Protein kinase B
ATCN1	alpha actin
ATG7/5/12	Autophagy related 7/5/12
BAG1/3	Bcl2 Associated Athanogene 1/3
BCL2	B-Cell lymphoma 2
CAPZ	Capping actin protein of muscle z-line
CASA	Chaperone Assisted Selective Autophagy
CMA	chaperone mediated autophagy
DMD	Duchenne's Muscular Dystrophy
ECM	Extracellular matrix
EDL	Extensor digitorum longus
EF1a	Elongation Initiation Factor 1 alpha
EPG5	Ectopic P-granules autophagy protein homolog
ERK	extracellular signal related kinase
FLNC	Filamin C
FOXO	Forkhead box transcription factor
GH	Growth hormone
HDAC1	Histone deacetylase 1
HPRT	hypoxanthine-guanine phosphoribosyltransferase
HSC70	heat shock cognate 70
HSF1	heat shock factor 1
HSPB8	heat shock protein family b member 8
IGF-1	Insulin like growth factor 1
IGF-1R	Insulin like growth factor 1 receptor
IGFN1	Immunoglobulin-like and fibronectin type III domain containing 1
IRS-1	Insulin receptor substrate 1
JNK	c-Jun NH2-terminal Kinase
JUNB	JunB Proto-oncogene, Ap-1 transcription factor subunit
KY	Kyphoscoliosis peptidase
LAMP2A	Lysosomal associated membrane protein 2A
LC3	microtubule associated protein 1 light chain 3
LKB1	Liver Kinase B1
LMNA	Lamin A/C
MAPK	Mitogen Activated Protein Kinase
MLTK	mitogen-activated protein triple kinase 20
MSTN	myostatin


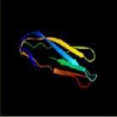
MTM1	myotubularin 1
MTMR14	myotubularin related protein 14
mTOR(C1)	Molecular target of rapamycin (complex 1)
MURF1	muscle specific ring finger protein 1
MYBC	Myosin binding protein C
MYF5	Myogenic factor 5
MYHC	Myosin heavy chain
MYL	Myosin regulatory light chain
MYOD1	Myoblast determination protein 1
NEB	Nebulin
p70s6k	ribosomal protein s6 kinase beta 1
PI3K	phosphatidylinositol 3 kinase
SMAD2/3	SMAD family member 2/3
TA	tibialis anterior
TCS2	tuberous sclerosis complex 2
TPM1-4	Tropomyosin (isoforms 1-4)
TPNI/C	Troponin
ULK1	Unc-51 like autophagy activating kinase 1
UPS	ubiquitin proteasome system
VCP	valosin containing protein
VMA21	Vacuolar ATPase assembly factor
VPS34	Vacuolar protein sorting-associated protein 34
XIRP1 (previously Xin)	Xin Actin binding repeat containing 1

Appendix 1 – Full murine KY Phyre2 output

#	Template	Alignment Coverage	3D Model	Confidence	% i.d.	Template Information
1	c4xz7A_	 Alignment		100.0	20	PDB header: transferase Chain: A; PDB Molecule: putative uncharacterized protein; PDBTitle: crystal structure of a tgase
2	c3lsrB_	 Alignment		99.9	16	PDB header: hydrolase Chain: B; PDB Molecule: transglutaminase-like enzymes, putative cysteine protease; PDBTitle: the crystal structure of a putative cysteine protease from cytophaga2 hutchinsonii to 1.9a
3	c3kd4A_	 Alignment		99.5	12	PDB header: hydrolase Chain: A; PDB Molecule: putative protease; PDBTitle: crystal structure of a putative protease (bdi_1141) from2 parabacteroides distasonis atcc 8503 at 2.00 a resolution
4	d2f4ma1	 Alignment		98.9	33	Fold: Cysteine proteinases Superfamily: Cysteine proteinases Family: Transglutaminase core
5	d2q3za4	 Alignment		98.9	16	Fold: Cysteine proteinases Superfamily: Cysteine proteinases Family: Transglutaminase core
6	d1g0da4	 Alignment		98.8	22	Fold: Cysteine proteinases Superfamily: Cysteine proteinases Family: Transglutaminase core
7	d1ex0a4	 Alignment		98.7	33	Fold: Cysteine proteinases Superfamily: Cysteine proteinases Family: Transglutaminase core
8	d1vjia4	 Alignment		98.6	22	Fold: Cysteine proteinases Superfamily: Cysteine proteinases Family: Transglutaminase core
9	d1x3za1	 Alignment		98.3	28	Fold: Cysteine proteinases Superfamily: Cysteine proteinases Family: Transglutaminase core
10	c4u65F_	 Alignment		98.0	14	PDB header: transferase/hydrolase Chain: F; PDB Molecule: putative cystine protease; PDBTitle: structure of the periplasmic output domain of the legionella2 pneumophila lapd ortholog cdgs9 in complex with pseudomonas3 fluorescens lapg
11	d1e2ta_	 Alignment		97.9	18	Fold: Cysteine proteinases Superfamily: Cysteine proteinases Family: Arylamine N-acetyltransferase

12	d2bsza1	Alignment		97.9	13	Fold: Cysteine proteinases Superfamily: Cysteine proteinases Family: Arylamine N-acetyltransferase
13	c3eswA	Alignment		97.9	27	PDB header: hydrolase Chain: A; PDB Molecule: peptide-n(4)-(n-acetyl-beta-glucosaminy)l)asparagine PDBTitle: complex of yeast pngase with glnac2-lac.
14	c2pfrB	Alignment		97.8	19	PDB header: transferase Chain: B; PDB Molecule: arylamine n-acetyltransferase 2; PDBTitle: human n-acetyltransferase 2
15	c3lnbA	Alignment		97.7	12	PDB header: transferase Chain: A; PDB Molecule: n-acetyltransferase family protein; PDBTitle: crystal structure analysis of arylamine n-acetyltransferase c from2 bacillus anthracis
16	c4quzA	Alignment		97.7	19	PDB header: transferase Chain: A; PDB Molecule: probable arylamine n-acetyl transferase; PDBTitle: structure of the arylamine n-acetyltransferase from mycobacterium2 abscessus
17	d1w4ta1	Alignment		97.6	13	Fold: Cysteine proteinases Superfamily: Cysteine proteinases Family: Arylamine N-acetyltransferase
18	c1l9mB	Alignment		97.6	23	PDB header: transferase Chain: B; PDB Molecule: protein-glutamine glutamyltransferase e3; PDBTitle: three-dimensional structure of the human transglutaminase 32 enzyme: binding of calcium ions change structure for3 activation
19	c1q0dA	Alignment		97.6	19	PDB header: transferase Chain: A; PDB Molecule: protein-glutamine gamma-glutamyltransferase; PDBTitle: crystal structure of red sea bream transglutaminase
20	c1kv3F	Alignment		97.5	19	PDB header: transferase Chain: F; PDB Molecule: protein-glutamine gamma-glutamyltransferase; PDBTitle: human tissue transglutaminase in gdp bound form
21	c3d9wA	Alignment	not modelled	97.4	18	PDB header: transferase Chain: A; PDB Molecule: putative acetyltransferase; PDBTitle: crystal structure analysis of nocardia farcinica arylamine n-2 acetyltransferase
22	c4dmoB	Alignment	not modelled	97.4	12	PDB header: transferase Chain: B; PDB Molecule: n-hydroxyarylamine o-acetyltransferase; PDBTitle: crystal structure of the (baccr)nat3 arylamine n-acetyltransferase2 from bacillus cereus reveals a unique cys-his-glu catalytic triad
23	c1f13A	Alignment	not modelled	97.3	32	PDB header: coagulation factor Chain: A; PDB Molecule: cellular coagulation factor xiii zymogen; PDBTitle: recombinant human cellular coagulation factor xiii
24	c2vfbA	Alignment	not modelled	97.2	16	PDB header: transferase Chain: A; PDB Molecule: arylamine n-acetyltransferase; PDBTitle: the structure of mycobacterium marinum arylamine n-2 acetyltransferase
25	d1w5ra1	Alignment	not modelled	97.1	15	Fold: Cysteine proteinases Superfamily: Cysteine proteinases Family: Arylamine N-acetyltransferase
26	c2qshA	Alignment	not modelled	95.9	18	PDB header: dna binding protein/dna Chain: A; PDB Molecule: dna repair protein rad4; PDBTitle: crystal structure of rad4-rad23 bound to a mismatch dna
27	c4fqpB	Alignment	not modelled	95.6	15	PDB header: hydrolase Chain: B; PDB Molecule: periplasmic protein; PDBTitle: legionella pneumophila lapp (egta-treated)

28	c3m07A	Alignment		92.5	18	PDB header: unknown function Chain: A; PDB Molecule: putative alpha amylase; PDBTitle: 1.4 angstrom resolution crystal structure of putative alpha2 amylase from salmonella typhimurium.
29	c5gquA	Alignment		91.4	18	PDB header: transferase Chain: A; PDB Molecule: 1,4-alpha-glucan branching enzyme glgb; PDBTitle: crystal structure of branching enzyme from cyanothecce sp. atcc 51142
30	c3k1dA	Alignment		90.1	22	PDB header: transferase Chain: A; PDB Molecule: 1,4-alpha-glucan-branching enzyme; PDBTitle: crystal structure of glycogen branching enzyme synonym: 1,4-alpha-d-2 glucan:1,4-alpha-d-glucan 6-glucosyl-transferase from mycobacterium3 tuberculosis h37rv
31	d2bhua1	Alignment		90.1	22	Fold: Immunoglobulin-like beta-sandwich Superfamily: E set domains Family: E-set domains of sugar-utilizing enzymes
32	c4bzyC	Alignment		90.1	16	PDB header: transferase Chain: C; PDB Molecule: 1,4-alpha-glucan-branching enzyme; PDBTitle: crystal structure of human glycogen branching enzyme (gbe1)
33	c2e8yA	Alignment		89.8	17	PDB header: hydrolase Chain: A; PDB Molecule: amyx protein; PDBTitle: crystal structure of pullulanase type i from bacillus subtilis str.2 168
34	c2vncB	Alignment	not modelled	89.7	12	PDB header: hydrolase Chain: B; PDB Molecule: glycogen operon protein glgx; PDBTitle: crystal structure of glycogen debranching enzyme trex from2 sulfolobus solfataricus
35	c2by0A	Alignment	not modelled	89.1	22	PDB header: hydrolase Chain: A; PDB Molecule: maltoigosyltrehalose trehalohydrolase; PDBTitle: is radiation damage dependent on the dose-rate used during2 macromolecular crystallography data collection
36	c2wskA	Alignment	not modelled	87.7	15	PDB header: hydrolase Chain: A; PDB Molecule: glycogen debranching enzyme; PDBTitle: crystal structure of glycogen debranching enzyme glgx from2 escherichia coli k-12
37	d1eh9a1	Alignment	not modelled	86.6	16	Fold: Immunoglobulin-like beta-sandwich Superfamily: E set domains Family: E-set domains of sugar-utilizing enzymes
38	c3v8aB	Alignment		85.4	8	PDB header: structural protein Chain: B; PDB Molecule: filamin-c; PDBTitle: human filamin c ig-like domains 4 and 5
39	c3wd1A	Alignment	not modelled	85.3	15	PDB header: hydrolase Chain: A; PDB Molecule: type i pullulanase; PDBTitle: crystal structure of pullulanase complexed with maltotetraose from2 anoxybacillus sp. Im18-11
40	c1bf2A	Alignment	not modelled	82.3	20	PDB header: hydrolase Chain: A; PDB Molecule: isoamylase; PDBTitle: structure of pseudomonas isoamylase
41	c1ehaA	Alignment	not modelled	81.2	15	PDB header: hydrolase Chain: A; PDB Molecule: glycosyltrehalose trehalohydrolase; PDBTitle: crystal structure of glycosyltrehalose trehalohydrolase2 from sulfolobus solfataricus
42	c3amkA	Alignment	not modelled	80.9	12	PDB header: transferase Chain: A; PDB Molecule: os06g0726400 protein; PDBTitle: structure of the starch branching enzyme i (bei) from oryza sativa l
43	c1m7xC	Alignment	not modelled	80.6	20	PDB header: transferase Chain: C; PDB Molecule: 1,4-alpha-glucan branching enzyme; PDBTitle: the x-ray crystallographic structure of branching enzyme
44	c3am1A	Alignment	not modelled	80.4	10	PDB header: transferase Chain: A; PDB Molecule: os06g0726400 protein; PDBTitle: structure of the starch branching enzyme i (bei) from oryza sativa l
45	d1m7xa1	Alignment	not modelled	78.9	19	Fold: Immunoglobulin-like beta-sandwich Superfamily: E set domains Family: E-set domains of sugar-utilizing enzymes

46	c2k7pA	Alignment		75.0	12	PDB header: structural protein Chain: A; PDB Molecule: filamin-a; PDBTitle: filamin a ig-like domains 16-17
47	c1ea9D	Alignment	not modelled	71.9	13	PDB header: hydrolase Chain: D; PDB Molecule: cyclomaltodextrinase; PDBTitle: cyclomaltodextrinase
48	c2ya0A	Alignment	not modelled	70.7	18	PDB header: hydrolase Chain: A; PDB Molecule: putative alkaline amylopullulanase; PDBTitle: catalytic module of the multi-modular glycogen-degrading pneumococcal2 virulence factor spua
49	d2dmba1	Alignment	not modelled	68.9	14	Fold: Immunoglobulin-like beta-sandwich Superfamily: E set domains Family: Filamin repeat (rod domain)
50	c1qfhB	Alignment	not modelled	66.1	14	PDB header: actin binding protein Chain: B; PDB Molecule: protein (gelation factor); PDBTitle: dimerization of gelation factor from dictyostelium2 discoideum: crystal structure of rod domains 5 and 6
51	c2k7qA	Alignment	not modelled	59.6	7	PDB header: structural protein Chain: A; PDB Molecule: filamin-a; PDBTitle: filamin a ig-like domains 18-19
52	d1nqib	Alignment		57.3	10	Fold: CUB-like Superfamily: Collagen-binding domain Family: Collagen-binding domain
53	d2d7pa1	Alignment	not modelled	54.1	14	Fold: Immunoglobulin-like beta-sandwich Superfamily: E set domains Family: Filamin repeat (rod domain)
54	c1up6F	Alignment	not modelled	50.6	21	PDB header: hydrolase Chain: F; PDB Molecule: 6-phospho-beta-glucosidase; PDBTitle: structure of the 6-phospho-beta glucosidase from thermotoga2 maritima at 2.55 angstrom resolution in the tetragonal form3 with manganese, nad+ and glucose-6-phosphate
55	c2xwxB	Alignment	not modelled	49.6	16	PDB header: chitin-binding protein Chain: B; PDB Molecule: glcnac-binding protein a; PDBTitle: vibrio cholerae colonization factor gbpa crystal structure
56	d2dmca1	Alignment	not modelled	49.6	15	Fold: Immunoglobulin-like beta-sandwich Superfamily: E set domains Family: Filamin repeat (rod domain)
57	c4dy5A	Alignment	not modelled	49.5	9	PDB header: hydrolase inhibitor Chain: A; PDB Molecule: gifsy-1 prophage protein; PDBTitle: crystal structure of salmonella typhimurium plig, a periplasmic2 lysozyme inhibitor of g-type lysozyme
58	c4r7fA	Alignment	not modelled	49.4	11	PDB header: structural genomics, unknown function Chain: A; PDB Molecule: uncharacterized protein; PDBTitle: crystal structure of a hypothetical protein (parmer_01801) from2 parabacteroides merdae atcc 43184 at 2.30 a resolution
59	c2wanA	Alignment	not modelled	49.0	16	PDB header: hydrolase Chain: A; PDB Molecule: pullulanase; PDBTitle: pullulanase from bacillus acidopullulyticus
60	c2i3sB	Alignment	not modelled	48.5	13	PDB header: structural protein Chain: B; PDB Molecule: filamin-a; PDBTitle: crystal structure of the human filamin a ig domains 19 to 22
61	d2fhfa1	Alignment	not modelled	47.8	9	Fold: Immunoglobulin-like beta-sandwich Superfamily: E set domains Family: E-set domains of sugar-utilizing enzymes
62	c2bqpa	Alignment	not modelled	47.2	14	PDB header: carbohydrate binding protein Chain: A; PDB Molecule: endo-b1,4-mannanase 5c; PDBTitle: mannan binding module from man5c in bound conformation
63	c4ruIA	Alignment	not modelled	45.8	27	PDB header: isomerase/dna Chain: A; PDB Molecule: dna topoisomerase 1; PDBTitle: crystal structure of full-length e.coli topoisomerase i in complex2 with ssdna
64	c5t3bB	Alignment	not modelled	43.8	26	PDB header: hydrolase Chain: B; PDB Molecule: glycoside hydrolase; PDBTitle: crystal structure of bpgH50
65	c1of0A	Alignment	not modelled	42.3	17	PDB header: oxidoreductase Chain: A; PDB Molecule: spore coat protein a; PDBTitle: crystal structure of bacillus subtilis cota after 1h2 soaking with ebs
66	c2mi6A	Alignment	not modelled	42.3	27	PDB header: structural genomics, unknown function Chain: A; PDB Molecule: uncharacterized protein; PDBTitle: nmr structure of protein zp_02069618.1 from bacteroides uniformis atcc2_8492
67	d2diba1	Alignment	not modelled	41.2	14	Fold: Immunoglobulin-like beta-sandwich Superfamily: E set domains Family: Filamin repeat (rod domain)
68	c4p3wE	Alignment	not modelled	41.0	16	PDB header: cell adhesion Chain: E; PDB Molecule: filamin-a; PDBTitle: crystal structure of the human filamin a ig-like domains 20-21 in2 complex with migfilin peptide
69	c4lwIA	Alignment	not modelled	40.5	34	PDB header: hydrolase activator Chain: A; PDB Molecule: effector protein b; PDBTitle: crystal structure of n-terminal 618-residue fragment of lepB from2 legionella pneumophila

70	c2w3jA	Alignment	not modelled	40.1	16	PDB header: sugar-binding protein Chain: A; PDB Molecule: carbohydrate binding module; PDBTitle: structure of a family 35 carbohydrate binding module from2 an environmental isolate
71	d2d7na1	Alignment	not modelled	39.4	17	Fold: Immunoglobulin-like beta-sandwich Superfamily: E set domains Family: Filamin repeat (rod domain)
72	d2diaa1	Alignment	not modelled	39.0	8	Fold: Immunoglobulin-like beta-sandwich Superfamily: E set domains Family: Filamin repeat (rod domain)
73	d2e9ja1	Alignment	not modelled	38.6	16	Fold: Immunoglobulin-like beta-sandwich Superfamily: E set domains Family: Filamin repeat (rod domain)
74	c3zm8A	Alignment	not modelled	37.6	18	PDB header: hydrolase Chain: A; PDB Molecule: gh26 endo-beta-1,4-mannanase; PDBTitle: crystal structure of podospora anserina gh26-cbm352 beta-(1,4)-mannanase
75	c4mqdB	Alignment	not modelled	37.2	14	PDB header: hydrolase inhibitor Chain: B; PDB Molecule: dna-entry nuclease inhibitor; PDBTitle: crystal structure of comj, inhibitor of the dna degrading activity of2 nuca, from bacillus subtilis
76	c4bq3A	Alignment	not modelled	35.3	24	PDB header: hydrolase Chain: A; PDB Molecule: b-agarase; PDBTitle: structural analysis of an exo-beta-agarase
77	c2lsyA	Alignment	not modelled	34.1	11	PDB header: protein binding Chain: A; PDB Molecule: dna repair protein rev1; PDBTitle: structure of the c-terminal domain from human rev1
78	c3qdcC	Alignment	not modelled	32.6	11	PDB header: oxidoreductase Chain: C; PDB Molecule: multicopper oxidase; PDBTitle: crystal structure of multicopper oxidase
79	c3cnkB	Alignment	not modelled	31.4	11	PDB header: structural protein Chain: B; PDB Molecule: filamin-a; PDBTitle: crystal structure of the dimerization domain of human2 filamin a
80	d2dj4a1	Alignment	not modelled	31.2	15	Fold: Immunoglobulin-like beta-sandwich Superfamily: E set domains Family: Filamin repeat (rod domain)
81	d1b77a2	Alignment	not modelled	30.4	19	Fold: DNA clamp Superfamily: DNA clamp Family: DNA polymerase processivity factor
82	c4umgA	Alignment	not modelled	30.4	20	PDB header: structural protein Chain: A; PDB Molecule: protein lin-41; PDBTitle: crystal structure of the lin-41 filamin domain
83	c2w1wB	Alignment	not modelled	29.7	20	PDB header: hydrolase Chain: B; PDB Molecule: lipolytic enzyme, g-d-s-l; PDBTitle: native structure of a family 35 carbohydrate binding module2 from clostridium thermocellum
84	c2ee6A	Alignment	not modelled	29.5	13	PDB header: structural protein Chain: A; PDB Molecule: filamin-b; PDBTitle: solution structure of the 21th filamin domain from human2 filamin-b
85	d1wlha1	Alignment	not modelled	29.1	9	Fold: Immunoglobulin-like beta-sandwich Superfamily: E set domains Family: Filamin repeat (rod domain)
86	d1bfua2	Alignment	not modelled	29.0	11	Fold: Cupredoxin-like Superfamily: Cupredoxins Family: Multidomain cupredoxins
87	c3rqhA	Alignment	not modelled	28.8	9	PDB header: cell adhesion Chain: A; PDB Molecule: filamin-a; PDBTitle: structure of filamin a immunoglobulin-like repeat 10 from homo sapiens
88	c3faxA	Alignment	not modelled	28.7	21	PDB header: hydrolase Chain: A; PDB Molecule: reticulocyte binding protein; PDBTitle: the crystal structure of gbs pullulanase sap in complex with2 maltotetraose
89	c4f7kA	Alignment	not modelled	28.4	15	PDB header: oxidoreductase Chain: A; PDB Molecule: laccase; PDBTitle: crystal structure of lac15 from a marine microbial metagenome
90	c1yuA	Alignment	not modelled	28.4	36	PDB header: dna binding protein Chain: A; PDB Molecule: topoisomerase i; PDBTitle: c-terminal domain of escherichia coli topoisomerase i
91	d1yuaa2	Alignment	not modelled	28.2	50	Fold: Rubredoxin-like Superfamily: Zinc beta-ribbon Family: Prokaryotic DNA topoisomerase I, a C-terminal fragment
92	d2p6ra2	Alignment	not modelled	28.2	18	Fold: Sec63 N-terminal domain-like Superfamily: Sec63 N-terminal domain-like Family: Achaael helicase C-terminal domain
93	c5msnA	Alignment	not modelled	27.6	6	PDB header: cell cycle Chain: A; PDB Molecule: dcc1 protein; PDBTitle: structure of the dcc1 protein
94	d2w0pa1	Alignment	not modelled	27.5	15	Fold: Immunoglobulin-like beta-sandwich Superfamily: E set domains Family: Filamin repeat (rod domain)
95	c1jibA	Alignment	not modelled	27.0	13	PDB header: hydrolase Chain: A; PDB Molecule: neopullulanase; PDBTitle: complex of alpha-amylase ii (tva ii) from thermoactinomyces2 vulgaris r-47 with maltotetraose based on a crystal soaked3 with maltohexaose.
96	c3re2A	Alignment	not modelled	27.0	19	PDB header: unknown function Chain: A; PDB Molecule: predicted protein; PDBTitle: crystal structure of menin reveals the binding site for

						mixed lineage2 leukemia (ml) protein
97	c4qa6A	Alignment	not modelled	26.6	17	PDB header: transcription/transcription inhibitor Chain: A; PDB Molecule: menin; PDBTitle: human menin in complex with ml1 peptide
98	c3u88B	Alignment	not modelled	26.1	17	PDB header: transcription Chain: B; PDB Molecule: menin; PDBTitle: crystal structure of human menin in complex with ml1 and ledgf
99	c4niqC	Alignment	not modelled	25.8	33	PDB header: protein transport Chain: C; PDB Molecule: vps4-associated protein 1; PDBTitle: crystal structure of vps4 mit-vfa1 mim2
100	d2bp3a1	Alignment	not modelled	25.8	17	Fold: Immunoglobulin-like beta-sandwich Superfamily: E set domains Family: Filamin repeat (rod domain)
101	c5by3A	Alignment	not modelled	25.3	18	PDB header: sugar binding protein Chain: A; PDB Molecule: btgh115a; PDBTitle: a novel family gh115 4-o-methyl-alpha-glucuronidase, btgh115a, with2 specificity for decorated arabinogalactans
102	c3iswA	Alignment	not modelled	23.3	15	PDB header: structural protein Chain: A; PDB Molecule: filamin-a; PDBTitle: crystal structure of filamin-a immunoglobulin-like repeat 21 bound to2 an n-terminal peptide of cfr
103	c2lsjA	Alignment	not modelled	23.3	11	PDB header: protein binding/protein binding Chain: A; PDB Molecule: dna repair protein rev1; PDBTitle: solution structure of the mouse rev1 ctd in complex with the rev1-2 interacting region (rir)of pol kappa
104	d1ngja	Alignment	not modelled	23.3	14	Fold: CUB-like Superfamily: Collagen-binding domain Family: Collagen-binding domain
105	d2d7ma1	Alignment	not modelled	23.2	10	Fold: Immunoglobulin-like beta-sandwich Superfamily: E set domains Family: Filamin repeat (rod domain)
106	c2lg5A	Alignment	not modelled	23.1	27	PDB header: structural genomics Chain: A; PDB Molecule: sec-c motif; PDBTitle: solution structure of rpa3114, a sec-c motif containing protein from 2 rhodospseudomonas palustris; northeast structural genomics consortium3 target rpt5 / ontario center for structural proteomics target rp3097
107	c2e9jA	Alignment	not modelled	22.9	13	PDB header: structural protein Chain: A; PDB Molecule: filamin-b; PDBTitle: solution structure of the 14th filamin domain from human2 filamin-b
108	c4m9pA	Alignment	not modelled	22.8	15	PDB header: cell adhesion Chain: A; PDB Molecule: filamin-a; PDBTitle: crystal structure of the human filamin a ig-like domains 3-5
109	c3pesA	Alignment	not modelled	22.8	33	PDB header: structural genomics, unknown function Chain: A; PDB Molecule: uncharacterized protein gp49; PDBTitle: crystal structure of uncharacterized protein from pseudomonas phage2 yua
110	c3k8uA	Alignment	not modelled	22.4	9	PDB header: hydrolase Chain: A; PDB Molecule: putative abc transporter, atp-binding protein coma; PDBTitle: crystal structure of the peptidase domain of streptococcus coma, a bi-2 functional abc transporter involved in quorum sensing pathway
111	c4mctD	Alignment	not modelled	21.9	9	PDB header: toxin Chain: D; PDB Molecule: killer protein; PDBTitle: p. vulgaris higba structure, crystal form 1
112	c5tkwA	Alignment	not modelled	21.8	18	PDB header: hydrolase Chain: A; PDB Molecule: type ii secretion system protein I; PDBTitle: 1.35 angstrom resolution crystal structure of a pullulanase-specific2 type ii secretion system integral cytoplasmic membrane protein gspI3 (n-terminal fragment; residues 1-237) from klebsiella pneumoniae.
113	d1ou9a	Alignment	not modelled	21.7	27	Fold: SspB-like Superfamily: SspB-like Family: Stringent starvation protein B, SspB
114	c5msmD	Alignment	not modelled	21.4	6	PDB header: cell cycle Chain: D; PDB Molecule: sister chromatid cohesion protein dcc1; PDBTitle: structure of the dcc1-ctf8-ctf18c trimer
115	d1ou8a	Alignment	not modelled	21.2	27	Fold: SspB-like Superfamily: SspB-like Family: Stringent starvation protein B, SspB
116	c4i7rA	Alignment	not modelled	21.1	18	PDB header: hydrolase Chain: A; PDB Molecule: isoamylase; PDBTitle: crystal structure of chlamydomonas reinhardtii isoamylase 1 (isa1)
117	c2x4bA	Alignment	not modelled	20.9	15	PDB header: hydrolase Chain: A; PDB Molecule: limit dextrinase; PDBTitle: barley limit dextrinase in complex with beta-cyclodextrin
118	d1zszc1	Alignment	not modelled	20.5	18	Fold: SspB-like Superfamily: SspB-like Family: Stringent starvation protein B, SspB
119	d1kv7a2	Alignment	not modelled	20.4	15	Fold: Cupredoxin-like Superfamily: Cupredoxins Family: Multidomain cupredoxins

Appendix 2 – Proteomics analysis and results

NB – This material was prepared by Adam Dowle (University of York Technology Facility)

Methods

In-gel Digestion

Samples were solubilised in NuPAGE LDS sample buffer (Life Technologies) with heating at 70°C for 10 mins before running into a 7 cm NuPAGE Novex 10% Bis-Tris Gel (Life Technologies) at 200 V for 6 mins. Gels were stained with SafeBLUE protein stain (NBS biologicals) for a minimum of 1 h before destaining with ultrapure water for a minimum of 1 h.

In-gel tryptic digestion was performed after reduction with DTE and S-carbamidomethylation with iodoacetamide. Gel pieces were washed two times with 50% (v/v) aqueous acetonitrile containing 25 mM ammonium bicarbonate, then once with acetonitrile and dried in a vacuum concentrator for 20 min. Sequencing-grade, modified porcine trypsin (Promega) was dissolved in 50 mM acetic acid, then diluted 5-fold with 25 mM ammonium bicarbonate to give a final trypsin concentration of 0.02 mg/mL. Gel pieces were rehydrated by adding 25 mL of trypsin solution, and after 10 min enough 25 mM ammonium bicarbonate solution was added to cover the gel pieces. Digests were incubated overnight at 37°C.

LC-MS/MS

Samples were loaded with five replicate injections onto a nanoAcquity UPLC system (Waters) equipped with a nanoAcquity Symmetry C₁₈, 5 µm trap (180 µm x 20 mm Waters) and a nanoAcquity HSS T3 1.8 µm C₁₈ capillary column (75 mm x 250 mm, Waters). The trap wash solvent was 0.1% (v/v) aqueous formic acid and the trapping flow rate was 10 µL/min. The trap was washed for 5 min before switching flow to the capillary column. Separation used a gradient elution of two solvents (solvent A: aqueous 0.1% (v/v) formic acid; solvent B: acetonitrile containing 0.1% (v/v) formic acid). The capillary column flow rate was 300 nL/min and the column temperature was 60°C. The gradient profile was linear 2-30% B over 125 mins then linear 30-50% B over 5 mins. All runs then proceeded to wash with 95% solvent B for 2.5 min. The column was returned to initial conditions and re-equilibrated for 25 min before subsequent injections.

The nanoLC system was interfaced with a maXis HD LC-MS/MS system (Bruker Daltonics) with CaptiveSpray ionisation source (Bruker Daltonics). Positive ESI-MS and MS/MS spectra were acquired using AutoMSMS mode. Instrument control, data acquisition and processing were performed using Compass 1.7 software (microTOF control, Hystar and DataAnalysis, Bruker Daltonics). Instrument settings were: ion spray voltage: 1,450 V, dry gas: 3 L/min, dry gas temperature 150°C, ion acquisition range: *m/z* 150-2,000, MS spectra rate: 5 Hz, MS/MS spectra rate: 5 Hz at 2,500 cts to 20 Hz at 250,000 cts, cycle time: 1 s, quadrupole low mass: 300 *m/z*, collision RF: 1,400 Vpp, transfer time 120 ms. The collision energy and isolation width settings were automatically calculated using the AutoMSMS fragmentation table, absolute threshold 200 counts, preferred charge states: 2 – 4, singly charged ions excluded. A single MS/MS spectrum was acquired for each precursor and former target ions were excluded for 0.8 min unless the precursor intensity increased fourfold.

Database Searching

Tandem mass spectral were searched against the mouse or rat subset of the UniProt database using a locally-running copy of the Mascot program (Matrix Science Ltd., version 2.5.1), through the Bruker ProteinScape interface (version 2.1). Search criteria specified: Enzyme, trypsin; Fixed modifications, Carbamidomethyl (C); Variable modifications, Oxidation (M); Peptide tolerance, 10 ppm; MS/MS tolerance, 0.05 Da; Instrument, ESI-QUAD-TOF. Results were processed with Mascot percolator and further filtered to accept only peptides with an expect score of 0.05 or lower.

MS: Peak Area Quantification

Bruker .d files were loaded into Progenesis QI (Waters) for label free quantification by comparison of MS_n precursor area. LC-MS chromatograms were calibrated against two internal calibrants (299.2945 *m/z* and 1221.9906 *m/z*) before aligning and peak picking using the default settings. Default normalisation was to the total identified protein content. An additional normalisation was performed for the skeletal sample against myosin-9, which was suggested to be unchanging from previous emPAI analysis.

Peptide identifications were imported from Mascot and only unique peptides were used for quantification. All p-values are taken from QI's unadjusted ANOVA scores.

Significantly altered proteins between stretched (S) and unstretched (U) replicates

UP IN S1	Protein	F.C. S/U	p-value S vs U
	Spermidine synthase OS=Mus musculus GN=Srm PE=2 SV=1 Q64674	6.00	1.70E-03
	NSFL1 cofactor p47 OS=Mus musculus GN=Nsf1c PE=1 SV=1 Q9CZ44	5.58	9.91E-03
	60S ribosomal protein L13a OS=Mus musculus GN=Rpl13a PE=1 SV=4 P19253	3.02	2.42E-03
	Protein Serpinb9b OS=Mus musculus GN=Serpinb9b PE=1 SV=1 Q9DAV6	2.54	6.19E-03
	Heterogeneous nuclear ribonucleoprotein A1 OS=Mus musculus GN=Hnrnpa1 PE=1 SV=2 P49312	2.49	1.45E-03
	40S ribosomal protein S17 OS=Mus musculus GN=Rps17 PE=1 SV=2 P63276	2.39	1.48E-02
	S-formylglutathione hydrolase OS=Mus musculus GN=Esd PE=1 SV=1 Q9R0P3	2.18	4.90E-03
	Voltage-dependent anion-selective channel protein 3 OS=Mus musculus GN=Vdac3 PE=1 SV=1 Q60931	2.13	1.97E-03
	Leucine-rich repeat-containing protein 59 OS=Mus musculus GN=Lrrc59 PE=1 SV=1 Q922Q8	2.11	1.58E-04
	40S ribosomal protein S25 OS=Mus musculus GN=Rps25 PE=1 SV=1 P62852	2.06	1.40E-02
	40S ribosomal protein S10 OS=Mus musculus GN=Rps10 PE=1 SV=1 P63325	2.05	4.73E-03
	40S ribosomal protein S14 OS=Mus musculus GN=Rps14 PE=2 SV=3 P62264	2.00	6.19E-03
	Aspartate--tRNA ligase, cytoplasmic OS=Mus musculus GN=Dars PE=2 SV=2 Q922B2	1.99	3.51E-02

40S ribosomal protein S15a OS=Mus musculus GN=Rps15a PE=1 SV=2 P62245	1.96	2.47E-02
Protein disulfide-isomerase A6 OS=Mus musculus GN=Pdia6 PE=1 SV=3 Q922R8	1.90	9.86E-03
26S proteasome non-ATPase regulatory subunit 11 OS=Mus musculus GN=Psm11 PE=1 SV=3 Q8BG32	1.88	7.23E-03
60S ribosomal protein L18 OS=Mus musculus GN=Rpl18 PE=2 SV=3 P35980	1.87	4.97E-02
Transmembrane protein 43 OS=Mus musculus GN=Tmem43 PE=1 SV=1 Q9DBS1	1.84	2.18E-02
60S ribosomal protein L35 OS=Mus musculus GN=Rpl35 PE=2 SV=1 Q6ZVV7	1.84	6.76E-03
Septin-7 OS=Mus musculus GN=Sept7 PE=1 SV=1 O55131	1.84	1.11E-02
Glycine--tRNA ligase OS=Mus musculus GN=Gars PE=1 SV=1 Q9CZD3	1.84	9.97E-05
Uncharacterized protein OS=Mus musculus GN=Gm10036 PE=3 SV=1 E9PYL9	1.83	3.60E-07
Aldehyde dehydrogenase, mitochondrial OS=Mus musculus GN=Aldh2 PE=1 SV=1 P47738	1.79	1.10E-03
Phosphoglycerate mutase 1 OS=Mus musculus GN=Pgam1 PE=1 SV=3 Q9DBJ1	1.73	5.20E-05
Prostaglandin G/H synthase 1 OS=Mus musculus GN=Ptgs1 PE=2 SV=1 P22437	1.71	3.44E-05
Heat shock protein 75 kDa, mitochondrial OS=Mus musculus GN=Trap1 PE=1 SV=1 Q9CQN1	1.70	8.46E-03
Heat shock protein beta-1 OS=Mus musculus GN=Hspb1 PE=1 SV=3 P14602	1.68	1.12E-05
Adenine phosphoribosyltransferase OS=Mus musculus GN=Aprt PE=1 SV=2 P08030	1.68	7.46E-03
Extended synaptotagmin-1 OS=Mus musculus GN=Esy1 PE=1 SV=2 Q3U7R1	1.68	4.06E-02
Annexin A2 OS=Mus musculus GN=Anxa2 PE=1 SV=2 P07356	1.67	1.34E-02
Septin-11 OS=Mus musculus GN=Sept11 PE=1 SV=4 Q8C1B7	1.66	2.80E-02
Staphylococcal nuclease domain-containing protein 1 OS=Mus musculus GN=Snd1 PE=1 SV=1 Q78PY7	1.65	2.14E-04
60S ribosomal protein L7 OS=Mus musculus GN=Rpl7 PE=1 SV=2 P14148	1.63	3.18E-02
Galectin-1 OS=Mus musculus GN=Lgals1 PE=1 SV=3 P16045	1.63	9.69E-04
Elongation factor 1-gamma OS=Mus musculus GN=Eef1g PE=1 SV=3 Q9D8N0	1.60	2.29E-02
Aldose reductase OS=Mus musculus GN=Akr1b1 PE=1 SV=3 P45376	1.60	3.81E-02
60S ribosomal protein L5 OS=Mus musculus GN=Rpl5 PE=1 SV=3 P47962	1.59	4.85E-02
Ras-related protein Rab-14 OS=Mus musculus GN=Rab14 PE=1 SV=3 Q91V41	1.59	7.10E-03
Importin subunit alpha-1 OS=Mus musculus GN=Kpna2 PE=1 SV=2 P52293	1.58	3.59E-02
60S ribosomal protein L14 OS=Mus musculus GN=Rpl14 PE=1 SV=3 Q9CR57	1.58	1.61E-02
Polyadenylate-binding protein 1 OS=Mus musculus GN=Pabpc1 PE=1 SV=2 P29341	1.56	4.49E-02

AP-1 complex subunit beta-1 OS=Mus musculus GN=Ap1b1 PE=1 SV=2 O35643	1.54	1.59E-03
40S ribosomal protein S13 OS=Mus musculus GN=Rps13 PE=1 SV=2 P62301	1.52	4.12E-03
Glutathione S-transferase P 1 OS=Mus musculus GN=Gstp1 PE=1 SV=2 P19157	1.50	3.09E-02
tRNA (cytosine(34)-C(5))-methyltransferase OS=Mus musculus GN=Nsun2 PE=1 SV=2 Q1HFZ0	1.50	1.68E-02
Protein Gm9493 OS=Mus musculus GN=Gm9493 PE=4 SV=1 F6SVV1	1.50	1.23E-02
Stress-70 protein, mitochondrial OS=Mus musculus GN=Hspa9 PE=1 SV=3 P38647	1.49	1.75E-03
Elongation factor Tu OS=Mus musculus GN=Gm9755 PE=3 SV=1 D3YVN7	1.47	4.23E-03
Histone H1.4 OS=Mus musculus GN=Hist1h1e PE=1 SV=2 P43274	1.47	4.94E-02
Heat shock protein HSP 90-beta OS=Mus musculus GN=Hsp90ab1 PE=1 SV=3 P11499	1.46	7.42E-04
ATP synthase subunit alpha, mitochondrial OS=Mus musculus GN=Atp5a1 PE=1 SV=1 Q03265	1.44	1.84E-04
Tubulin alpha-1A chain OS=Mus musculus GN=Tuba1a PE=1 SV=1 P68369	1.41	3.78E-04
L-lactate dehydrogenase A chain OS=Mus musculus GN=Ldha PE=1 SV=3 P06151	1.40	1.58E-02
60S ribosomal protein L7a OS=Mus musculus GN=Rpl7a PE=1 SV=2 P12970	1.38	4.18E-02
Ras-related protein Rab-1A OS=Mus musculus GN=Rab1A PE=1 SV=3 P62821	1.37	1.87E-02
Ras-related protein Rab-10 OS=Mus musculus GN=Rab10 PE=1 SV=1 P61027	1.37	1.47E-03
Serpin H1 OS=Mus musculus GN=Serpinh1 PE=1 SV=3 P19324	1.36	8.30E-03
Prohibitin-2 OS=Mus musculus GN=Phb2 PE=1 SV=1 O35129	1.35	1.26E-02
Alpha-enolase OS=Mus musculus GN=Eno1 PE=1 SV=3 P17182	1.28	2.48E-02
Cullin-associated NEDD8-dissociated protein 1 OS=Mus musculus GN=Cand1 PE=2 SV=2 Q6ZQ38	1.27	1.36E-02
Desmin OS=Mus musculus GN=Des PE=1 SV=3 P31001	1.27	3.76E-02
Triosephosphate isomerase OS=Mus musculus GN=Tpi1 PE=1 SV=4 P17751	1.25	2.13E-02
Probable ATP-dependent RNA helicase DDX17 OS=Mus musculus GN=Ddx17 PE=1 SV=1 Q501J6	1.23	3.75E-04
Elongation factor 1-alpha 1 OS=Mus musculus GN=Eef1a1 PE=1 SV=3 P10126	1.23	4.14E-02
Malate dehydrogenase, mitochondrial OS=Mus musculus GN=Mdh2 PE=1 SV=3 P08249	1.22	1.54E-02
Elongation factor 2 OS=Mus musculus GN=Eef2 PE=1 SV=2 P58252	1.20	1.90E-02
Alpha-centractin OS=Mus musculus GN=Actr1a PE=2 SV=1 P61164	1.11	9.61E-03

DOWN IN S1	26S protease regulatory subunit 7 OS=Mus musculus GN=Psmc2 PE=1 SV=5 P46471	- 3.50	3.24E-02
---------------	--	-----------	----------

Hypoxanthine-guanine phosphoribosyltransferase OS=Mus musculus GN=Hprt1 PE=1 SV=3 P00493	- 3.46	1.83E- 03
26S proteasome non-ATPase regulatory subunit 5 OS=Mus musculus GN=Psm5 PE=1 SV=4 Q8BJY1	- 3.36	1.15E- 02
Methionine--tRNA ligase, cytoplasmic OS=Mus musculus GN=Mars PE=2 SV=1 Q68FL6	- 3.07	4.75E- 02
Eukaryotic translation initiation factor 4 gamma 1 OS=Mus musculus GN=Eif4g1 PE=1 SV=1 Q6NZJ6	- 2.92	1.47E- 02
Cytosol aminopeptidase OS=Mus musculus GN=Lap3 PE=1 SV=3 Q9CPY7	- 2.67	1.67E- 02
Eukaryotic translation initiation factor 3 subunit D OS=Mus musculus GN=Eif3d PE=1 SV=2 O70194	- 2.66	1.93E- 02
Unconventional myosin-Ic OS=Mus musculus GN=Myo1c PE=1 SV=2 Q9WTI7	- 2.48	1.15E- 02
Leukotriene A-4 hydrolase OS=Mus musculus GN=Lta4h PE=1 SV=4 P24527	- 2.43	2.47E- 02
Leucine--tRNA ligase, cytoplasmic OS=Mus musculus GN=Lars PE=1 SV=2 Q8BMJ2	- 2.41	8.29E- 03
Cytoskeleton-associated protein 4 OS=Mus musculus GN=Ckap4 PE=1 SV=2 Q8BMK4	- 2.38	5.15E- 03
26S proteasome non-ATPase regulatory subunit 2 OS=Mus musculus GN=Psm2 PE=1 SV=1 Q8VDM4	- 2.33	4.24E- 02
26S protease regulatory subunit 6A OS=Mus musculus GN=Psmc3 PE=1 SV=2 O88685	- 2.32	1.06E- 03
Protein transport protein Sec31A OS=Mus musculus GN=Sec31a PE=1 SV=2 Q3UPL0	- 2.29	3.21E- 02
Transgelin-2 OS=Mus musculus GN=Tagln2 PE=1 SV=4 Q9WVA4	- 2.10	4.75E- 04
Protein Gcn1l1 OS=Mus musculus GN=Gcn1l1 PE=1 SV=1 E9PVA8	- 2.08	4.54E- 03
Programmed cell death 6-interacting protein OS=Mus musculus GN=Pdc6ip PE=1 SV=3 Q9WU78	- 2.04	1.68E- 02
Ran GTPase-activating protein 1 OS=Mus musculus GN=Rangap1 PE=1 SV=2 P46061	- 2.03	2.99E- 03
Myosin-10 OS=Mus musculus GN=Myh10 PE=1 SV=2 Q61879	- 2.02	1.53E- 02
Polymerase I and transcript release factor OS=Mus musculus GN=Ptrf PE=1 SV=1 O54724	- 1.78	8.42E- 03
Ubiquitin carboxyl-terminal hydrolase 5 OS=Mus musculus GN=Usp5 PE=1 SV=1 P56399	- 1.74	6.93E- 03
Prolyl endopeptidase OS=Mus musculus GN=Prep PE=2 SV=1 Q9QUR6	- 1.73	2.11E- 02
Multifunctional protein ADE2 OS=Mus musculus GN=Paics PE=1 SV=4 Q9DCL9	- 1.68	3.91E- 02
Talin-1 OS=Mus musculus GN=Tln1 PE=1 SV=2 P26039	- 1.68	1.93E- 03
Rho GDP-dissociation inhibitor 1 OS=Mus musculus GN=Arhgdia PE=1 SV=3 Q99PT1	- 1.67	2.77E- 02
Aspartate aminotransferase, mitochondrial OS=Mus musculus GN=Got2 PE=1 SV=1 P05202	- 1.63	4.95E- 02
Plastin-3 OS=Mus musculus GN=Pls3 PE=1 SV=3 Q99K51	- 1.61	9.32E- 03
T-complex protein 1 subunit gamma OS=Mus musculus GN=Cct3 PE=1 SV=1 P80318	- 1.60	1.51E- 02
Alpha-actinin-1 OS=Mus musculus GN=Actn1 PE=1 SV=1 Q7TPR4	- 1.60	2.58E- 03

Adenosylhomocysteinase OS=Mus musculus GN=Ahcy PE=1 SV=3 P50247	- 1.55	4.10E- 02
Delta-1-pyrroline-5-carboxylate synthase OS=Mus musculus GN=Aldh18a1 PE=1 SV=2 Q9Z110	- 1.55	4.00E- 03
Thioredoxin domain-containing protein 5 OS=Mus musculus GN=Txndc5 PE=1 SV=2 Q91W90	- 1.52	6.02E- 03
Kinesin-1 heavy chain OS=Mus musculus GN=Kif5b PE=1 SV=3 Q61768	- 1.45	3.53E- 02
Myosin light polypeptide 6 OS=Mus musculus GN=Myl6 PE=1 SV=3 Q60605	- 1.42	4.13E- 02
Adenylyl cyclase-associated protein 1 OS=Mus musculus GN=Cap1 PE=1 SV=4 P40124	- 1.39	2.11E- 02
T-complex protein 1 subunit beta OS=Mus musculus GN=Cct2 PE=1 SV=4 P80314	- 1.38	1.20E- 02
Tubulin alpha-4A chain OS=Mus musculus GN=Tuba4a PE=1 SV=1 P68368	- 1.37	1.02E- 02
Cytoplasmic dynein 1 heavy chain 1 OS=Mus musculus GN=Dync1h1 PE=1 SV=2 Q9JHU4	- 1.35	3.44E- 03
Heat shock 70 kDa protein 4 OS=Mus musculus GN=Hspa4 PE=1 SV=1 Q61316	- 1.35	4.81E- 02
Fatty acid synthase OS=Mus musculus GN=Fasn PE=1 SV=2 P19096	- 1.33	8.64E- 04
T-complex protein 1 subunit delta OS=Mus musculus GN=Cct4 PE=1 SV=3 P80315	- 1.32	4.52E- 02
60 kDa heat shock protein, mitochondrial OS=Mus musculus GN=Hspd1 PE=1 SV=1 P63038	- 1.22	3.95E- 02
Tubulin beta-4B chain OS=Mus musculus GN=Tubb4b PE=1 SV=1 P68372	- 1.21	1.58E- 02
Vinculin OS=Mus musculus GN=Vcl PE=1 SV=4 Q64727	- 1.20	1.03E- 02
Heat shock cognate 71 kDa protein OS=Mus musculus GN=Hspa8 PE=1 SV=1 P63017	- 1.15	3.21E- 02

UP IN
S2

Heterogeneous nuclear ribonucleoprotein A1 OS=Mus musculus GN=Hnrnpa1 PE=1 SV=2 P49312	2.57	6.55E- 04
NSFL1 cofactor p47 OS=Mus musculus GN=Nsf11c PE=1 SV=1 Q9CZ44	2.48	2.66E- 02
Calcium-binding mitochondrial carrier protein Aralar1 OS=Mus musculus GN=Slc25a12 PE=1 SV=1 Q8BH59	2.34	2.02E- 02
40S ribosomal protein S17 OS=Mus musculus GN=Rps17 PE=1 SV=2 P63276	2.25	3.15E- 02
Transferrin receptor protein 1 OS=Mus musculus GN=Tfrc PE=1 SV=1 Q62351	2.22	4.96E- 02
Splicing factor 3B subunit 3 OS=Mus musculus GN=Sf3b3 PE=2 SV=1 Q921M3	2.14	1.61E- 02
Inosine-5'-monophosphate dehydrogenase 2 OS=Mus musculus GN=Impdh2 PE=1 SV=2 P24547	2.08	2.18E- 02
Ras-related protein Rab-1B OS=Mus musculus GN=Rab1b PE=1 SV=1 Q9D1G1	2.07	4.06E- 02
Aspartate--tRNA ligase, cytoplasmic OS=Mus musculus GN=Dars PE=2 SV=2 Q922B2	1.84	7.91E- 03
Prohibitin OS=Mus musculus GN=Phb PE=1 SV=1 P67778	1.84	1.45E- 02
Far upstream element-binding protein 2 OS=Mus musculus GN=Khsrp PE=1 SV=2 Q3U0V1	1.80	4.21E- 03

Sarcoplasmic/endoplasmic reticulum calcium ATPase 2 OS=Mus musculus GN=Atp2a2 PE=1 SV=2 O55143	1.76	4.19E-02
Dolichyl-diphosphooligosaccharide--protein glycosyltransferase subunit 1 OS=Mus musculus GN=Rpn1 PE=1 SV=1 Q91YQ5	1.71	8.44E-04
40S ribosomal protein S14 OS=Mus musculus GN=Rps14 PE=2 SV=3 P62264	1.70	2.62E-04
RuvB-like 2 OS=Mus musculus GN=Ruvbl2 PE=2 SV=3 Q9WTM5	1.63	2.20E-02
Heat shock protein 105 kDa OS=Mus musculus GN=Hsph1 PE=1 SV=2 Q61699	1.60	3.83E-02
Serine/threonine-protein phosphatase PP1-alpha catalytic subunit OS=Mus musculus GN=Ppp1ca PE=1 SV=1 P62137	1.59	5.62E-03
Peroxiredoxin-2 OS=Mus musculus GN=Prdx2 PE=1 SV=3 Q61171	1.58	1.27E-02
40S ribosomal protein S25 OS=Mus musculus GN=Rps25 PE=1 SV=1 P62852	1.57	3.91E-02
Extended synaptotagmin-1 OS=Mus musculus GN=Esy1 PE=1 SV=2 Q3U7R1	1.51	1.62E-02
Heat shock protein 75 kDa, mitochondrial OS=Mus musculus GN=Trap1 PE=1 SV=1 Q9CQN1	1.47	4.38E-02
26S proteasome non-ATPase regulatory subunit 2 OS=Mus musculus GN=Psm2 PE=1 SV=1 Q8VDM4	1.46	3.76E-02
Glycine--tRNA ligase OS=Mus musculus GN=Gars PE=1 SV=1 Q9CZD3	1.45	1.11E-02
DNA damage-binding protein 1 OS=Mus musculus GN=Ddb1 PE=1 SV=2 Q3U1J4	1.44	2.05E-02
40S ribosomal protein S9 OS=Mus musculus GN=Rps9 PE=1 SV=3 Q6ZWN5	1.43	1.17E-02
Alpha-centractin OS=Mus musculus GN=Actr1a PE=2 SV=1 P61164	1.41	1.93E-02
Staphylococcal nuclease domain-containing protein 1 OS=Mus musculus GN=Snd1 PE=1 SV=1 Q78PY7	1.41	4.44E-04
Elongation factor 1-alpha 1 OS=Mus musculus GN=Eef1a1 PE=1 SV=3 P10126	1.40	3.25E-04
Aldehyde dehydrogenase, mitochondrial OS=Mus musculus GN=Aldh2 PE=1 SV=1 P47738	1.39	2.39E-02
Glutathione S-transferase P 1 OS=Mus musculus GN=Gstp1 PE=1 SV=2 P19157	1.37	4.51E-02
Calnexin OS=Mus musculus GN=Canx PE=1 SV=1 P35564	1.36	3.22E-02
Heat shock protein HSP 90-beta OS=Mus musculus GN=Hsp90ab1 PE=1 SV=3 P11499	1.30	5.29E-03
Heat shock protein HSP 90-alpha OS=Mus musculus GN=Hsp90aa1 PE=1 SV=4 P07901	1.28	6.82E-04
L-lactate dehydrogenase A chain OS=Mus musculus GN=Ldha PE=1 SV=3 P06151	1.26	1.19E-02
40S ribosomal protein S10 OS=Mus musculus GN=Rps10 PE=1 SV=1 P63325	1.26	5.82E-05
Annexin A1 OS=Mus musculus GN=Anxa1 PE=1 SV=2 P10107	1.26	4.92E-02
Tubulin alpha-1A chain OS=Mus musculus GN=Tuba1a PE=1 SV=1 P68369	1.26	5.33E-03
Elongation factor 2 OS=Mus musculus GN=Eef2 PE=1 SV=2 P58252	1.24	1.51E-02
ATP-dependent RNA helicase DDX3X OS=Mus musculus GN=Ddx3x PE=1 SV=3 Q62167	1.18	4.50E-02

	ATP-dependent 6-phosphofructokinase, liver type OS=Mus musculus GN=Pfkl PE=1 SV=4 P12382	1.14	4.69E-02
DOWN IN S2	Calpain small subunit 1 OS=Mus musculus GN=Capns1 PE=2 SV=1 O88456	- 3.83	3.53E-02
	Histone H2B type 1-C/E/G OS=Mus musculus GN=Hist1h2bc PE=1 SV=3 Q6ZWY9	- 3.30	4.51E-02
	Hypoxanthine-guanine phosphoribosyltransferase OS=Mus musculus GN=Hprt1 PE=1 SV=3 P00493	- 2.71	1.42E-03
	Ran GTPase-activating protein 1 OS=Mus musculus GN=Rangap1 PE=1 SV=2 P46061	- 2.46	8.57E-03
	Proteasome subunit beta type-5 OS=Mus musculus GN=Psmb5 PE=1 SV=3 O55234	- 2.44	2.07E-03
	26S protease regulatory subunit 6A OS=Mus musculus GN=Psmc3 PE=1 SV=2 O88685	- 2.15	5.59E-03
	Polymerase I and transcript release factor OS=Mus musculus GN=Ptrf PE=1 SV=1 O54724	- 2.12	2.65E-03
	UDP-N-acetylhexosamine pyrophosphorylase-like protein 1 OS=Mus musculus GN=Uap1l1 PE=2 SV=1 Q3TW96	- 2.11	4.00E-02
	Protein disulfide-isomerase A4 OS=Mus musculus GN=Pdia4 PE=1 SV=3 P08003	- 2.00	1.45E-02
	40S ribosomal protein S24 OS=Mus musculus GN=Rps24 PE=2 SV=1 P62849	- 1.87	2.28E-02
	Calponin-3 OS=Mus musculus GN=Cnn3 PE=1 SV=1 Q9DAW9	- 1.82	6.33E-03
	MCG23377, isoform CRA_b OS=Mus musculus GN=Gm8797 PE=4 SV=1 A0A0A6YW67	- 1.78	2.62E-02
	Myosin-10 OS=Mus musculus GN=Myh10 PE=1 SV=2 Q61879	- 1.73	2.00E-02
	Eukaryotic translation initiation factor 4 gamma 1 OS=Mus musculus GN=Eif4g1 PE=1 SV=1 Q6NZJ6	- 1.72	8.45E-03
	Unconventional myosin-Ic OS=Mus musculus GN=Myo1c PE=1 SV=2 Q9WTI7	- 1.72	1.87E-02
	Translationally-controlled tumor protein OS=Mus musculus GN=Tpt1 PE=1 SV=1 P63028	- 1.67	6.32E-03
	14-3-3 protein gamma OS=Mus musculus GN=Ywhag PE=1 SV=2 P61982	- 1.58	7.74E-05
	ADP-ribosylation factor 3 OS=Mus musculus GN=Arf3 PE=2 SV=2 P61205	- 1.50	4.39E-03
	Protein Gcn1l1 OS=Mus musculus GN=Gcn1l1 PE=1 SV=1 E9PVA8	- 1.42	3.26E-02
	Calreticulin OS=Mus musculus GN=Calr PE=1 SV=1 P14211	- 1.42	3.47E-02
	Nestin OS=Mus musculus GN=Nes PE=1 SV=1 Q6P5H2	- 1.42	1.12E-02
	Aconitate hydratase, mitochondrial OS=Mus musculus GN=Aco2 PE=1 SV=1 Q99KI0	- 1.36	3.51E-02
	Talin-1 OS=Mus musculus GN=Tln1 PE=1 SV=2 P26039	- 1.31	2.48E-02
	Cytoplasmic dynein 1 heavy chain 1 OS=Mus musculus GN=Dync1h1 PE=1 SV=2 Q9JHU4	- 1.25	5.67E-03
	Filamin-C OS=Mus musculus GN=Flnc PE=1 SV=3 Q8VHX6	- 1.18	6.58E-03
	Plectin OS=Mus musculus GN=Plec PE=1 SV=3 Q9QXS1	- 1.17	1.11E-02

Significantly altered pathways

	GO_id	Term	NumberOfGenes	p-value	p-value_fdr	p-value_bonferroni
UP IN S1	3010	Ribosome	9	1.07E-10	3.04E-08	3.04E-08
	1120	Microbial metabolism in diverse environments	7	6.75E-07	9.58E-05	1.92E-04
	10	Glycolysis / Gluconeogenesis	5	1.10E-06	1.04E-04	3.13E-04
	620	Pyruvate metabolism	4	7.17E-06	5.09E-04	2.04E-03
	1200	Carbon metabolism	5	1.63E-05	9.27E-04	4.64E-03
	270	Cysteine and methionine metabolism	3	1.64E-04	7.78E-03	4.67E-02
	5134	Legionellosis	3	6.44E-04	2.61E-02	1.83E-01
	1100	Metabolic pathways	11	8.11E-04	2.88E-02	2.30E-01
	3018	RNA degradation	3	1.38E-03	3.91E-02	3.91E-01
	1230	Biosynthesis of amino acids	3	1.38E-03	3.91E-02	3.91E-01
	410	beta-Alanine metabolism	2	3.79E-03	8.96E-02	1.00E+00
	640	Propanoate metabolism	2	3.79E-03	8.96E-02	1.00E+00
	51	Fructose and mannose metabolism	2	4.81E-03	9.75E-02	1.00E+00
	40	Pentose and glucuronate interconversions	2	4.81E-03	9.75E-02	1.00E+00
	4152	AMPK signalling pathway	3	6.20E-03	1.17E-01	1.00E+00
	480	Glutathione metabolism	2	1.12E-02	1.93E-01	1.00E+00
	561	Glycerolipid metabolism	2	1.16E-02	1.93E-01	1.00E+00
	330	Arginine and proline metabolism	2	1.24E-02	1.93E-01	1.00E+00
	4141	Protein processing in endoplasmic reticulum	3	1.29E-02	1.93E-01	1.00E+00
	5169	Epstein-Barr virus infection	3	2.09E-02	2.97E-01	1.00E+00
	5215	Prostate cancer	2	2.80E-02	3.78E-01	1.00E+00
	4066	HIF-1 signalling pathway	2	4.00E-02	5.16E-01	1.00E+00
	5146	Amoebiasis	2	4.77E-02	5.89E-01	1.00E+00
DOWN IN S1	3050	Proteasome	3	8.53E-05	2.42E-02	2.42E-02
	330	Arginine and proline metabolism	3	1.98E-04	2.82E-02	5.64E-02
	4141	Protein processing in endoplasmic reticulum	4	3.20E-04	3.03E-02	9.08E-02
	5169	Epstein-Barr virus infection	4	6.36E-04	4.51E-02	1.81E-01
	270	Cysteine and methionine	2	2.33E-02	1.15E-01	6.60E-01

metabolism		03		
110		2.44E-		
0	Metabolic pathways	8	03	1.15E-01 6.93E-01
970	Aminoacyl-tRNA biosynthesis	2	3.30E-03	1.23E-01 9.38E-01
496	Vasopressin-regulated water reabsorption	2	3.46E-03	1.23E-01 9.82E-01
301	RNA transport	3	3.94E-03	1.24E-01 1.00E+00
513	Legionellosis	2	5.74E-03	1.63E-01 1.00E+00
451	Focal adhesion	3	7.82E-03	1.80E-01 1.00E+00
481	Regulation of actin cytoskeleton	3	8.68E-03	1.80E-01 1.00E+00
461	Antigen processing and presentation	2	9.02E-03	1.80E-01 1.00E+00
452	Adherens junction	2	9.26E-03	1.80E-01 1.00E+00
123	Biosynthesis of amino acids	2	9.51E-03	1.80E-01 1.00E+00
514	Amoebiasis	2	2.30E-02	4.02E-01 1.00E+00
467	Leukocyte transendothelial migration	2	2.41E-02	4.02E-01 1.00E+00
453	Tight junction	2	2.91E-02	4.59E-01 1.00E+00
414	Phagosome	2	4.07E-02	6.08E-01 1.00E+00
230	Purine metabolism	2	4.58E-02	6.50E-01 1.00E+00

UP IN S2

414	Protein processing in endoplasmic reticulum	6	4.25E-07	1.21E-04 1.21E-04
301	Ribosome	4	6.69E-05	9.50E-03 1.90E-02
10	Glycolysis / Gluconeogenesis	3	1.79E-04	1.70E-02 5.09E-02
461	Antigen processing and presentation	3	2.79E-04	1.98E-02 7.92E-02
521	Prostate cancer	3	5.03E-04	2.86E-02 1.43E-01
406	HIF-1 signalling pathway	3	8.90E-04	4.21E-02 2.53E-01
640	Propanoate metabolism	2	1.37E-03	5.55E-02 3.88E-01
620	Pyruvate metabolism	2	2.50E-03	8.87E-02 7.10E-01
414	Phagosome	3	2.87E-03	9.04E-02 8.14E-01
112	Microbial metabolism in diverse environments	3	3.28E-03	9.33E-02 9.33E-01
462	NOD-like receptor signalling pathway	2	4.56E-03	1.08E-01 1.00E+00
513	Legionellosis	2	4.56E-03	1.08E-01 1.00E+00
520	Viral carcinogenesis	3	5.04E-03	1.10E-01 1.00E+00
491	Progesterone-mediated oocyte maturation	2	9.88E-03	2.00E-01 1.00E+00

491			1.20E-		
5	Estrogen signaling pathway	2	02	2.27E-01	1.00E+00
304			2.05E-		
0	Spliceosome	2	02	3.48E-01	1.00E+00
415			2.08E-		
2	AMPK signaling pathway	2	02	3.48E-01	1.00E+00
426	Adrenergic signaling in		2.57E-		
1	cardiomyocytes	2	02	3.94E-01	1.00E+00
516			2.64E-		
1	Hepatitis B	2	02	3.94E-01	1.00E+00
492			3.02E-		
1	Oxytocin signaling pathway	2	02	4.29E-01	1.00E+00
402			3.47E-		
2	cGMP-PKG signaling pathway	2	02	4.69E-01	1.00E+00
516			4.77E-		
9	Epstein-Barr virus infection	2	02	6.15E-01	1.00E+00

DOWN
IN S2

305			1.03E-		
0	Proteasome	2	03	2.91E-01	2.91E-01
513			3.33E-		
2	Salmonella infection	2	03	4.73E-01	9.46E-01

BIBLIOGRAPHY

- Al Madhoun, Ashraf Said, Virja Mehta, Grace Li, Daniel Figeys, Nadine Wiper-Bergeron, and Ilona S. Skerjanc. 2011. "Skeletal Myosin Light Chain Kinase Regulates Skeletal Myogenesis by Phosphorylation of MEF2C." *The EMBO Journal* 30 (12): 2477–89.
- Amthor, Helge, Raymond Macharia, Roberto Navarrete, Markus Schuelke, Susan C. Brown, Anthony Otto, Thomas Voit, et al. 2007. "Lack of Myostatin Results in Excessive Muscle Growth but Impaired Force Generation." *Proceedings of the National Academy of Sciences of the United States of America* 104 (6): 1835–40.
- Anantharaman, V., E. V. Koonin, and L. Aravind. 2001. "Peptide-N-Glycanases and DNA Repair Proteins, Xp-C/Rad4, Are, Respectively, Active and Inactivated Enzymes Sharing a Common Transglutaminase Fold." *Human Molecular Genetics* 10 (16): 1627–30.
- Anderson, Kimberley J., Aaron P. Russell, and Victoria C. Foletta. 2015. "NDRG2 Promotes Myoblast Proliferation and Caspase 3/7 Activities during Differentiation, and Attenuates Hydrogen Peroxide – But Not Palmitate-Induced Toxicity." *FEBS Open Bio* 5 (January): 668–81.
- Arndt, Verena, Nikolaus Dick, Riga Tawo, Michael Dreiseidler, Daniela Wenzel, Michael Hesse, Dieter O. Fürst, et al. 2010. "Chaperone-Assisted Selective Autophagy Is Essential for Muscle Maintenance." *Current Biology: CB* 20 (2): 143–48.
- Aronson, D., M. D. Boppart, S. D. Dufresne, R. A. Fielding, and L. J. Goodyear. 1998. "Exercise Stimulates c-Jun NH2 Kinase Activity and c-Jun Transcriptional Activity in Human Skeletal Muscle." *Biochemical and Biophysical Research Communications* 251 (1): 106–10.
- Aronson, D., S. D. Dufresne, and L. J. Goodyear. 1997. "Contractile Activity Stimulates the c-Jun NH2-Terminal Kinase Pathway in Rat Skeletal Muscle." *The Journal of Biological Chemistry* 272 (41): 25636–40.
- Aronson, D., M. A. Violan, S. D. Dufresne, D. Zangen, R. A. Fielding, and L. J. Goodyear. 1997. "Exercise Stimulates the Mitogen-Activated Protein Kinase Pathway in Human Skeletal Muscle." *The Journal of Clinical Investigation* 99 (6): 1251–57.
- Assereto, Stefania, Silvia Stringara, Federica Sotgia, Gloria Bonuccelli, Aldobrando Broccolini, Marina Pedemonte, Monica Traverso, et al. 2006. "Pharmacological Rescue of the Dystrophin-Glycoprotein Complex in Duchenne and Becker Skeletal Muscle Explants by Proteasome Inhibitor Treatment." *American Journal of Physiology. Cell Physiology* 290 (2). Am Physiological Soc: C577–82.
- Baker, Jane, Genna Riley, M. Rosario Romero, Andrew R. Haynes, Helen Hilton, Michelle Simon, John Hancock, Hilda Tateossian, Vera M. Ripoll, and Gonzalo Blanco. 2010. "Identification of a Z-Band Associated Protein Complex Involving KY, FLNC and IGFN1." *Experimental Cell Research* 316 (11): 1856–70.
- Barrangou, Rodolphe, Christophe Fremaux, H el ene Deveau, Melissa Richards, Patrick Boyaval, Sylvain Moineau, Dennis A. Romero, and Philippe Horvath. 2007. "CRISPR Provides Acquired Resistance against Viruses in Prokaryotes." *Science* 315 (5819): 1709–12.
- Beatham, Jane, Katja Gehmlich, Peter F. M. van der Ven, Jaakko Sarparanta, Debbie Williams, Peter Underhill, Christian Geier, Dieter O. F ur st, Bjarne Udd, and Gonzalo Blanco. 2006. "Constitutive Upregulations of Titin-Based Signalling Proteins in KY Deficient Muscles." *Neuromuscular Disorders: NMD* 16 (7): 437–45.
- Beatham, Jane, Rosario Romero, Stuart K. M. Townsend, Terry Hacker, Peter F. M. van der Ven, and Gonzalo Blanco. 2004. "Filamin C Interacts with the Muscular Dystrophy KY Protein and Is Abnormally Distributed in Mouse KY Deficient Muscle Fibres." *Human Molecular Genetics* 13 (22): 2863–74.

- Beehler, Blake C., Paul G. Sleph, Latifa Benmassaoud, and Gary J. Grover. 2006. "Reduction of Skeletal Muscle Atrophy by a Proteasome Inhibitor in a Rat Model of Denervation." *Experimental Biology and Medicine* 231 (3): 335–41.
- Beharry, Adam W., Pooja B. Sandesara, Brandon M. Roberts, Leonardo F. Ferreira, Sarah M. Senf, and Andrew R. Judge. 2014. "HDAC1 Activates FoxO and Is Both Sufficient and Required for Skeletal Muscle Atrophy." *Journal of Cell Science* 127 (Pt 7): 1441–53.
- Blanco, G., G. R. Coulton, A. Biggin, C. Grainge, J. Moss, M. Barrett, A. Berquin, et al. 2001. "The Kyphoscoliosis (ky) Mouse Is Deficient in Hypertrophic Responses and Is Caused by a Mutation in a Novel Muscle-Specific Protein." *Human Molecular Genetics* 10 (1): 9–16.
- Blanco, G., C. Pritchard, P. Underhill, S. Breeds, K. M. F. Townsend, A. Greenfield, and Steve D. M. Brown. 2004. "Molecular Phenotyping of the Mouse Ky Mutant Reveals UCP1 Upregulation at the Neuromuscular Junctions of Dystrophic Soleus Muscle." *Neuromuscular Disorders: NMD* 14 (3): 217–28.
- Bodine, S. C., E. Latres, S. Baumhueter, V. K. Lai, L. Nunez, B. A. Clarke, W. T. Poueymirou, et al. 2001. "Identification of Ubiquitin Ligases Required for Skeletal Muscle Atrophy." *Science* 294 (5547): 1704–8.
- Bodine, S. C., T. N. Stitt, M. Gonzalez, W. O. Kline, G. L. Stover, R. Bauerlein, E. Zlotchenko, et al. 2001. "Akt/mTOR Pathway Is a Crucial Regulator of Skeletal Muscle Hypertrophy and Can Prevent Muscle Atrophy in Vivo." *Nature Cell Biology* 3 (11): 1014–19.
- Bonaldo, Paolo, and Marco Sandri. 2013. "Cellular and Molecular Mechanisms of Muscle Atrophy." *Disease Models & Mechanisms* 6 (1): 25–39.
- Bonuccelli, Gloria, Federica Sotgia, Franco Capozza, Elisabetta Gazzo, Carlo Minetti, and Michael P. Lisanti. 2007. "Localized Treatment with a Novel FDA-Approved Proteasome Inhibitor Blocks the Degradation of Dystrophin and Dystrophin-Associated Proteins in Mdx Mice." *Cell Cycle* 6 (10). Taylor & Francis: 1242–48.
- Bridges, L. R., G. R. Coulton, G. Howard, J. Moss, and R. M. Mason. 1992. "The Neuromuscular Basis of Hereditary Kyphoscoliosis in the Mouse." *Muscle & Nerve* 15 (2): 172–79.
- Bührdel, John B., Sofia Hirth, Mirjam Keßler, Sören Westphal, Monika Forster, Linda Manta, Gerhard Wiche, et al. 2015. "In Vivo Characterization of Human Myofibrillar Myopathy Genes in Zebrafish." *Biochemical and Biophysical Research Communications* 461 (2): 217–23.
- Burattini, S., P. Ferri, M. Battistelli, R. Curci, F. Luchetti, and E. Falcieri. 2009. "C2C12 Murine Myoblasts as a Model of Skeletal Muscle Development: Morpho-Functional Characterization." *European Journal of Histochemistry: EJH* 48 (3): 223–34.
- Carmignac, Virginie, Martina Svensson, Zandra Körner, Linda Elowsson, Cintia Matsumura, Kinga I. Gawlik, Valerie Allamand, and Madeleine Durbeej. 2011. "Autophagy Is Increased in Laminin α 2 Chain-Deficient Muscle and Its Inhibition Improves Muscle Morphology in a Mouse Model of MDC1A." *Human Molecular Genetics* 20 (24): 4891–4902.
- Carnio, Silvia, Francesca LoVerso, Martin Andres Baraibar, Emanuela Longa, Muzamil Majid Khan, Manuela Maffei, Markus Reischl, et al. 2014. "Autophagy Impairment in Muscle Induces Neuromuscular Junction Degeneration and Precocious Aging." *Cell Reports* 8 (5): 1509–21.
- Caron, Annabelle Z., Sonia Haroun, Elisabeth Leblanc, Frédéric Trens, Chantal Guindi, Aziz Amrani, and Guillaume Grenier. 2011. "The Proteasome Inhibitor MG132 Reduces Immobilization-Induced Skeletal Muscle Atrophy in Mice." *BMC Musculoskeletal Disorders* 12 (August): 185.
- Cassel, Suzanne L., Stephanie C. Eisenbarth, Shankar S. Iyer, Jeffrey J. Sadler, Oscar R. Colegio, Linda A. Tephly, A. Brent Carter, Paul B. Rothman, Richard A. Flavell, and Fayyaz S. Sutterwala. 2008. "The Nalp3 Inflammasome Is Essential for the

- Development of Silicosis." *Proceedings of the National Academy of Sciences of the United States of America* 105 (26): 9035–40.
- Chen, Justin L., Kelly L. Walton, Catherine E. Winbanks, Kate T. Murphy, Rachel E. Thomson, Yogeshwar Mankanji, Hongwei Qian, Gordon S. Lynch, Craig A. Harrison, and Paul Gregorevic. 2014. "Elevated Expression of Activins Promotes Muscle Wasting and Cachexia." *FASEB Journal: Official Publication of the Federation of American Societies for Experimental Biology* 28 (4): 1711–23.
- Chevessier, Frédéric, Julia Schuld, Zacharias Orfanos, Anne-C Plank, Lucie Wolf, Alexandra Maerkens, Andreas Unger, et al. 2015. "Myofibrillar Instability Exacerbated by Acute Exercise in Filaminopathy." *Human Molecular Genetics* 24 (25): 7207–20.
- Choi, Jason C., Antoine Muchir, Wei Wu, Shinichi Iwata, Shunichi Homma, John P. Morrow, and Howard J. Worman. 2012. "Temsirolimus Activates Autophagy and Ameliorates Cardiomyopathy Caused by Lamin A/C Gene Mutation." *Science Translational Medicine* 4 (144): 144ra102.
- Cullup, Thomas, Ay Lin Kho, Carlo Dionisi-Vici, Birgit Brandmeier, Frances Smith, Zoe Urry, Michael A. Simpson, et al. 2013. "Recessive Mutations in EPG5 Cause Vici Syndrome, a Multisystem Disorder with Defective Autophagy." *Nature Genetics* 45 (1): 83–87.
- Custer, Sara K., Manuela Neumann, Hongbo Lu, Alexander C. Wright, and J. Paul Taylor. 2010. "Transgenic Mice Expressing Mutant Forms VCP/p97 Recapitulate the Full Spectrum of IBMPFD Including Degeneration in Muscle, Brain and Bone." *Human Molecular Genetics* 19 (9): 1741–55.
- De Palma, C., F. Morisi, S. Cheli, S. Pambianco, V. Cappello, M. Vezzoli, P. Rovere-Querini, et al. 2012. "Autophagy as a New Therapeutic Target in Duchenne Muscular Dystrophy." *Cell Death & Disease* 3 (November): e418.
- Dickinson, A. G., and V. M. Meikle. 1973. "Genetic Kyphoscoliosis in Mice." *The Lancet* 1 (7813): 1186.
- Ding, Yuduan, Hong Li, Ling-Ling Chen, and Kabin Xie. 2016. "Recent Advances in Genome Editing Using CRISPR/Cas9." *Frontiers in Plant Science* 7 (May): 703.
- Donner, Kati, Miina Ollikainen, Maaret Ridanpää, Hans-Jürgen Christen, Hans H. Goebel, Marianne de Visser, Katarina Pelin, and Carina Wallgren-Pettersson. 2002. "Mutations in the Beta-Tropomyosin (TPM2) Gene--a Rare Cause of Nemaline Myopathy." *Neuromuscular Disorders: NMD* 12 (2): 151–58.
- Doudna, Jennifer A., and Emmanuelle Charpentier. 2014. "Genome Editing. The New Frontier of Genome Engineering with CRISPR-Cas9." *Science* 346 (6213): 1258096.
- Drummond, Micah J., Christopher S. Fry, Erin L. Glynn, Hans C. Dreyer, Shaheen Dhanani, Kyle L. Timmerman, Elena Volpi, and Blake B. Rasmussen. 2009. "Rapamycin Administration in Humans Blocks the Contraction-Induced Increase in Skeletal Muscle Protein Synthesis." *The Journal of Physiology* 587 (Pt 7): 1535–46.
- Dumont, Nicolas A., Yu Xin Wang, Julia von Maltzahn, Alessandra Pasut, C. Florian Bentzinger, Caroline E. Brun, and Michael A. Rudnicki. 2015. "Dystrophin Expression in Muscle Stem Cells Regulates Their Polarity and Asymmetric Division." *Nature Medicine* 21 (12). Nature Research: 1455–63.
- Dyar, Kenneth A., Stefano Ciciliot, Guidantonio Malagoli Tagliacuzzi, Giorgia Pallafacchina, Jana Tothova, Carla Argentini, Lisa Agatea, et al. 2015. "The Calcineurin-NFAT Pathway Controls Activity-Dependent Circadian Gene Expression in Slow Skeletal Muscle." *Molecular Metabolism* 4 (11): 823–33.
- Eghtesad, Saman, Siddharth Jhunjhunwala, Steven R. Little, and Paula R. Clemens. 2011. "Rapamycin Ameliorates Dystrophic Phenotype in Mdx Mouse Skeletal Muscle." *Molecular Medicine* 17 (9-10): 917–24.
- Eskelinen, Eeva-Liisa, Anna Lena Illert, Yoshitaka Tanaka, Günter Schwarzmann, Judith Blanz, Kurt Von Figura, and Paul Saftig. 2002. "Role of LAMP-2 in Lysosome Biogenesis and Autophagy." *Molecular Biology of the Cell* 13 (9): 3355–68.

- Eskelinen, Eeva-Liisa, Christine Katrin Schmidt, Silja Neu, Marion Willenborg, Graciela Fuertes, Natalia Salvador, Yoshitaka Tanaka, et al. 2004. "Disturbed Cholesterol Traffic but Normal Proteolytic Function in LAMP-1/LAMP-2 Double-Deficient Fibroblasts." *Molecular Biology of the Cell* 15 (7): 3132–45.
- Fetalvero, Kristina M., Yenyen Yu, Margaret Goetschkes, Guiqing Liang, Reginald A. Valdez, Ty Gould, Ellen Triantafellow, et al. 2013. "Defective Autophagy and mTORC1 Signaling in Myotubularin Null Mice." *Molecular and Cellular Biology* 33 (1): 98–110.
- Flück, Martin. 2006. "Functional, Structural and Molecular Plasticity of Mammalian Skeletal Muscle in Response to Exercise Stimuli." *The Journal of Experimental Biology* 209 (Pt 12): 2239–48.
- Frank, Derk, Christian Kuhn, Hugo A. Katus, and Norbert Frey. 2006. "The Sarcomeric Z-Disc: A Nodal Point in Signalling and Disease." *Journal of Molecular Medicine* 84 (6): 446–68.
- Fürst, Dieter O., Lev G. Goldfarb, Rudolf A. Kley, Matthias Vorgerd, Montse Olivé, and Peter F. M. van der Ven. 2013. "Filamin C-Related Myopathies: Pathology and Mechanisms." *Acta Neuropathologica* 125 (1): 33–46.
- Gamerding, Martin, Parvana Hajjeva, and Christian Behl. 2009. "A Switch from BAG1 to BAG3 during Ageing Triggers the Enhanced Use of the Autophagic-Lysosomal System for the Degradation of Polyubiquitinated Proteins." *The FASEB Journal* 23 (1 Supplement): 668.1–668.1.
- Ganesan, Swamynathan, Seyyed Hani Moussavi Nik, Morgan Newman, and Michael Lardelli. 2014. "Identification and Expression Analysis of the Zebrafish Orthologues of the Mammalian MAP1LC3 Gene Family." *Experimental Cell Research* 328 (1): 228–37.
- Gazzerro, Elisabetta, Stefania Assereto, Andrea Bonetto, Federica Sotgia, Sonia Scarfi, Angela Pistorio, Gloria Bonuccelli, et al. 2010. "Therapeutic Potential of Proteasome Inhibition in Duchenne and Becker Muscular Dystrophies." *The American Journal of Pathology* 176 (4): 1863–77.
- Ghaoui, Roula, Johanna Palmio, Janice Brewer, Monkol Lek, Merrilee Needham, Anni Evilä, Peter Hackman, et al. 2016. "Mutations in HSPB8 Causing a New Phenotype of Distal Myopathy and Motor Neuropathy." *Neurology* 86 (4): 391–98.
- Gilbert, Matthew J. H., Tanja C. Zerulla, and Keith B. Tierney. 2014. "Zebrafish (*Danio Rerio*) as a Model for the Study of Aging and Exercise: Physical Ability and Trainability Decrease with Age." *Experimental Gerontology* 50 (February): 106–13.
- Glass, David J. 2005. "Skeletal Muscle Hypertrophy and Atrophy Signaling Pathways." *The International Journal of Biochemistry & Cell Biology* 37 (10): 1974–84.
- Grumati, Paolo, Luisa Coletto, Patrizia Sabatelli, Matilde Cescon, Alessia Angelin, Enrico Bertaglia, Bert Blaauw, et al. 2010. "Autophagy Is Defective in Collagen VI Muscular Dystrophies, and Its Reactivation Rescues Myofiber Degeneration." *Nature Medicine* 16 (11): 1313–20.
- Haehling, Stephan von, Markus S. Anker, and Stefan D. Anker. 2016. "Prevalence and Clinical Impact of Cachexia in Chronic Illness in Europe, USA, and Japan: Facts and Numbers Update 2016." *Journal of Cachexia, Sarcopenia and Muscle* 7 (5): 507–9.
- Haehling, Stephan von, John E. Morley, and Stefan D. Anker. 2010. "An Overview of Sarcopenia: Facts and Numbers on Prevalence and Clinical Impact." *Journal of Cachexia, Sarcopenia and Muscle* 1 (2): 129–33.
- He, Congcong, Michael C. Bassik, Viviana Moresi, Kai Sun, Yongjie Wei, Zhongju Zou, Zhenyi An, et al. 2012. "Exercise-Induced BCL2-Regulated Autophagy Is Required for Muscle Glucose Homeostasis." *Nature* 481 (7382): 511–15.
- Hedberg-Oldfors, Carola, Niklas Darin, Mia Olsson Engman, Zacharias Orfanos, Christer Thomsen, Peter F. M. van der Ven, and Anders Oldfors. 2016. "A New Early-Onset Neuromuscular Disorder Associated with Kyphoscoliosis Peptidase (KY)

- Deficiency." *European Journal of Human Genetics: EJHG* 24 (12). Nature Publishing Group: 1771–77.
- Heigwer, Florian, Grainne Kerr, and Michael Boutros. 2014. "E-CRISP: Fast CRISPR Target Site Identification." *Nature Methods* 11 (2): 122–23.
- Heikkinen, Outi K., Salla Ruskamo, Peter V. Konarev, Dmitri I. Svergun, Tatu Iivanainen, Sami M. Heikkinen, Perttu Permi, Harri Koskela, Ilkka Kilpeläinen, and Jari Yläanne. 2009. "Atomic Structures of Two Novel Immunoglobulin-like Domain Pairs in the Actin Cross-Linking Protein Filamin." *The Journal of Biological Chemistry* 284 (37): 25450–58.
- Hishiya, Akinori, Toshio Kitazawa, and Shinichi Takayama. 2010. "BAG3 and Hsc70 Interact with Actin Capping Protein CapZ to Maintain Myofibrillar Integrity under Mechanical Stress." *Circulation Research* 107 (10): 1220–31.
- Homma, Sachiko, Masahiro Iwasaki, G. Diane Shelton, Eva Engvall, John C. Reed, and Shinichi Takayama. 2006. "BAG3 Deficiency Results in Fulminant Myopathy and Early Lethality." *The American Journal of Pathology* 169 (3): 761–73.
- Hoppeler, Hans, and Martin Flück. 2002. "Normal Mammalian Skeletal Muscle and Its Phenotypic Plasticity." *The Journal of Experimental Biology* 205 (Pt 15): 2143–52.
- Hornberger, Troy A., Rudy Stuppard, Kevin E. Conley, Mark J. Fedele, Marta L. Fiorotto, Eva R. Chin, and Karyn A. Esser. 2004. "Mechanical Stimuli Regulate Rapamycin-Sensitive Signalling by a Phosphoinositide 3-Kinase-, Protein Kinase B- and Growth Factor-Independent Mechanism." *Biochemical Journal* 380 (Pt 3): 795–804.
- Horvath, Philippe, and Rodolphe Barrangou. 2010. "CRISPR/Cas, the Immune System of Bacteria and Archaea." *Science* 327 (5962): 167–70.
- Hsieh, You-Liang, Ying-Lan Tsai, Marthandam Asokan Shibu, Chia-Chi Su, Li-Chin Chung, Peiying Pai, Chia-Hua Kuo, Yu-Lan Yeh, Vijaya Padma Viswanadha, and Chih-Yang Huang. 2015. "ZAK Induces Cardiomyocyte Hypertrophy and Brain Natriuretic Peptide Expression via p38/JNK Signaling and GATA4/c-Jun Transcriptional Factor Activation." *Molecular and Cellular Biochemistry* 405 (1-2): 1–9.
- Huang, Chih-Yang, Pin Ju Chueh, Chien-Tang Tseng, Kuan-Yu Liu, Hsiao-Ya Tsai, Wei-Wen Kuo, Ming-Yung Chou, and Jaw-Ji Yang. 2004. "ZAK Re-Programs Atrial Natriuretic Factor Expression and Induces Hypertrophic Growth in H9c2 Cardiomyoblast Cells." *Biochemical and Biophysical Research Communications* 324 (3): 973–80.
- Huxley, A. F. 1957. "Muscle Structure and Theories of Contraction." *Progress in Biophysics and Biophysical Chemistry* 7: 255–318.
- Hwang, Peter M., and Brian D. Sykes. 2015. "Targeting the Sarcomere to Correct Muscle Function." *Nature Reviews. Drug Discovery* 14 (5): 313–28.
- Johnson, M. A., J. Polgar, D. Weightman, and D. Appleton. 1973. "Data on the Distribution of Fibre Types in Thirty-Six Human Muscles. An Autopsy Study." *Journal of the Neurological Sciences* 18 (1): 111–29.
- Jokl, Elliot J., and Gonzalo Blanco. 2016. "Disrupted Autophagy Undermines Skeletal Muscle Adaptation and Integrity." *Mammalian Genome: Official Journal of the International Mammalian Genome Society* 27 (11-12): 525–37.
- Kelley, Lawrence A., Stefans Mezulis, Christopher M. Yates, Mark N. Wass, and Michael J. E. Sternberg. 2015. "The Phyre2 Web Portal for Protein Modeling, Prediction and Analysis." *Nature Protocols* 10 (6): 845–58.
- Kihara, A., Y. Kabeya, Y. Ohsumi, and T. Yoshimori. 2001. "Beclin-Phosphatidylinositol 3-Kinase Complex Functions at the Trans-Golgi Network." *EMBO Reports* 2 (4): 330–35.
- Kim, Joungmok, Mondira Kundu, Benoit Viollet, and Kun-Liang Guan. 2011. "AMPK and mTOR Regulate Autophagy through Direct Phosphorylation of Ulk1." *Nature Cell Biology* 13 (2): 132–41.
- Kim, Kook Hwan, Yeon Taek Jeong, Hyunhee Oh, Seong Hun Kim, Jae Min Cho, Yo-Na Kim, Su Sung Kim, et al. 2013. "Autophagy Deficiency Leads to Protection from

- Obesity and Insulin Resistance by Inducing Fgf21 as a Mitokine." *Nature Medicine* 19 (1): 83–92.
- Kishta, Osama A., Yeting Guo, Mahroo Mofarrahi, Flavia Stana, Larry C. Lands, and Sabah N. A. Hussain. 2017. "Pulmonary *Pseudomonas Aeruginosa* Infection Induces Autophagy and Proteasome Proteolytic Pathways in Skeletal Muscles: Effects of a Pressurized Whey Protein-Based Diet in Mice." *Food & Nutrition Research* 61 (1). Taylor & Francis: 1325309.
- Klionsky, Daniel J. 2007. "Autophagy: From Phenomenology to Molecular Understanding in Less than a Decade." *Nature Reviews. Molecular Cell Biology* 8 (11): 931–37.
- Klionsky, Daniel J., Kotb Abdelmohsen, Akihisa Abe, Md Joynal Abedin, Hagai Abeliovich, Abraham Acevedo Arozena, Hiroaki Adachi, et al. 2016. "Guidelines for the Use and Interpretation of Assays for Monitoring Autophagy (3rd Edition)." *Autophagy* 12 (1): 1–222.
- Kokkonen, Kristen. 2013. "Engineering of a Cellular Model of Freeman-Sheldon Skeletal Muscle Myopathy." http://scholar.colorado.edu/cgi/viewcontent.cgi?article=1608&context=honr_theses.
- Kramer, Henning F., and Laurie J. Goodyear. 2007. "Exercise, MAPK, and NF-kappaB Signaling in Skeletal Muscle." *Journal of Applied Physiology* 103 (1): 388–95.
- Laing, Nigel G., Danielle E. Dye, Carina Wallgren-Pettersson, Gabriele Richard, Nicole Monnier, Suzanne Lillis, Thomas L. Winder, et al. 2009. "Mutations and Polymorphisms of the Skeletal Muscle Alpha-Actin Gene (ACTA1)." *Human Mutation* 30 (9): 1267–77.
- Langley, Brett, Mark Thomas, Amy Bishop, Mridula Sharma, Stewart Gilmour, and Ravi Kambadur. 2002. "Myostatin Inhibits Myoblast Differentiation by Down-Regulating MyoD Expression." *The Journal of Biological Chemistry* 277 (51): 49831–40.
- Laporte, J., C. Guiraud-Chaumeil, M. C. Vincent, J. L. Mandel, S. M. Tanner, S. Liechti-Gallati, C. Wallgren-Pettersson, et al. 1997. "Mutations in the MTM1 Gene Implicated in X-Linked Myotubular Myopathy. ENMC International Consortium on Myotubular Myopathy. European Neuro-Muscular Center." *Human Molecular Genetics* 6 (9): 1505–11.
- Lecker, Stewart H., Alfred L. Goldberg, and William E. Mitch. 2006. "Protein Degradation by the Ubiquitin-Proteasome Pathway in Normal and Disease States." *Journal of the American Society of Nephrology: JASN* 17 (7): 1807–19.
- Lehtokari, Vilma-Lotta, Katarina Pelin, Maria Sandbacka, Salla Ranta, Kati Donner, Francesco Muntoni, Caroline Sewry, et al. 2006. "Identification of 45 Novel Mutations in the Nebulin Gene Associated with Autosomal Recessive Nemaline Myopathy." *Human Mutation* 27 (9): 946–56.
- Li, J. B., and A. L. Goldberg. 1976. "Effects of Food Deprivation on Protein Synthesis and Degradation in Rat Skeletal Muscles." *The American Journal of Physiology* 231 (2): 441–48.
- Lim, Chee Chew, Christian Zuppinger, Xinxin Guo, Gabriela M. Kuster, Michiel Helmes, Hans M. Eppenberger, Thomas M. Suter, Ronglih Liao, and Douglas B. Sawyer. 2004. "Anthracyclines Induce Calpain-Dependent Titin Proteolysis and Necrosis in Cardiomyocytes." *The Journal of Biological Chemistry* 279 (9): 8290–99.
- Lira, Vitor A., Mitsuharu Okutsu, Mei Zhang, Nicholas P. Greene, Rhianna C. Laker, David S. Breen, Kyle L. Hoehn, and Zhen Yan. 2013. "Autophagy Is Required for Exercise Training-Induced Skeletal Muscle Adaptation and Improvement of Physical Performance." *FASEB Journal: Official Publication of the Federation of American Societies for Experimental Biology* 27 (10): 4184–93.
- Li, Xiang. 2017. "Exploring the Function of IGFN1 and MLTK in Skeletal Muscle." Edited by Gonzalo Blanco. Ph.D., University of York.
- Li, Xiang, Jane Baker, Tobias Cracknell, Andrew R. Haynes, and Gonzalo Blanco. 2017. "IGFN1_v1 Is Required for Myoblast Fusion and Differentiation." *PloS One* 12 (6): e0180217.

- Li, Xuefu, Bomeng Zhong, Weitian Han, Ning Zhao, Wei Liu, Yu Sui, Yawen Wang, et al. 2015. "Two Novel Mutations in Myosin Binding Protein C Slow Causing Distal Arthrogyrosis Type 2 in Two Large Han Chinese Families May Suggest Important Functional Role of Immunoglobulin Domain C2." *PloS One* 10 (2): e0117158.
- Llano-Diez, Monica, Ann-Marie Gustafson, Carl Olsson, Hanna Goransson, and Lars Larsson. 2011. "Muscle Wasting and the Temporal Gene Expression Pattern in a Novel Rat Intensive Care Unit Model." *BMC Genomics* 12 (December): 602.
- Lo Verso, Francesca, Silvia Carnio, Anna Vainshtein, and Marco Sandri. 2014. "Autophagy Is Not Required to Sustain Exercise and PRKAA1/AMPK Activity but Is Important to Prevent Mitochondrial Damage during Physical Activity." *Autophagy* 10 (11): 1883–94.
- Marcotte, George R., Daniel W. D. West, and Keith Baar. 2015. "The Molecular Basis for Load-Induced Skeletal Muscle Hypertrophy." *Calcified Tissue International* 96 (3): 196–210.
- Markus, Barak, Ginat Narkis, Daniella Landau, Ruth Z. Birk, Idan Cohen, and Ohad S. Birk. 2012. "Autosomal Recessive Lethal Congenital Contractural Syndrome Type 4 (LCCS4) Caused by a Mutation in MYBPC1." *Human Mutation* 33 (10): 1435–38.
- Martineau, L. C., and P. F. Gardiner. 2001. "Insight into Skeletal Muscle Mechanotransduction: MAPK Activation Is Quantitatively Related to Tension." *Journal of Applied Physiology* 91 (2): 693–702.
- Masiero, Eva, Lisa Agatea, Cristina Mammucari, Bert Blaauw, Emanuele Loro, Masaaki Komatsu, Daniel Metzger, Carlo Reggiani, Stefano Schiaffino, and Marco Sandri. 2009. "Autophagy Is Required to Maintain Muscle Mass." *Cell Metabolism* 10 (6): 507–15.
- Masiero, Eva, and Marco Sandri. 2010. "Autophagy Inhibition Induces Atrophy and Myopathy in Adult Skeletal Muscles." *Autophagy* 6 (2): 307–9.
- Mauras, Nelly. 1997. "Growth Hormone, IGF-I and Growth. New Views of Old Concepts. Modern Endocrinology and Diabetes Series, Volume 4." *Trends in Endocrinology and Metabolism: TEM* 8 (6). Elsevier: 256–57.
- McElhinny, Abigail S., Catherine Schwach, Melinda Valichnac, Sarah Mount-Patrick, and Carol C. Gregorio. 2005. "Nebulin Regulates the Assembly and Lengths of the Thin Filaments in Striated Muscle." *The Journal of Cell Biology* 170 (6): 947–57.
- McPherron, A. C., A. M. Lawler, and S. J. Lee. 1997. "Regulation of Skeletal Muscle Mass in Mice by a New TGF-Beta Superfamily Member." *Nature* 387 (6628): 83–90.
- Medina, R., S. S. Wing, A. Haas, and A. L. Goldberg. 1991. "Activation of the Ubiquitin-ATP-Dependent Proteolytic System in Skeletal Muscle during Fasting and Denervation Atrophy." *Biomedica Biochimica Acta* 50 (4-6): 347–56.
- Mendoza, Michelle C., E. Emrah Er, and John Blenis. 2011. "The Ras-ERK and PI3K-mTOR Pathways: Cross-Talk and Compensation." *Trends in Biochemical Sciences* 36 (6): 320–28.
- Miao, Yuanxin, Jinzeng Yang, Zhong Xu, Lu Jing, Shuhong Zhao, and Xinyun Li. 2015. "RNA Sequencing Identifies Upregulated Kyphoscoliosis Peptidase and Phosphatidic Acid Signaling Pathways in Muscle Hypertrophy Generated by Transgenic Expression of Myostatin Propeptide." *International Journal of Molecular Sciences* 16 (4): 7976–94.
- Minoia, Melania, Alessandra Boncoraglio, Jonathan Vinet, Federica F. Morelli, Jeanette F. Brunsting, Angelo Poletti, Sabine Krom, Eric Reits, Harm H. Kampinga, and Serena Carra. 2014. "BAG3 Induces the Sequestration of Proteasomal Clients into Cytoplasmic Puncta: Implications for a Proteasome-to-Autophagy Switch." *Autophagy* 10 (9): 1603–21.
- Miyazaki, Mitsunori, John J. McCarthy, Mark J. Fedele, and Karyn A. Esser. 2011. "Early Activation of mTORC1 Signalling in Response to Mechanical Overload Is Independent of Phosphoinositide 3-kinase/Akt Signalling." *The Journal of Physiology* 589 (Pt 7): 1831–46.

- Mizushima, Noboru, Akitsugu Yamamoto, Makoto Matsui, Tamotsu Yoshimori, and Yoshinori Ohsumi. 2004. "In Vivo Analysis of Autophagy in Response to Nutrient Starvation Using Transgenic Mice Expressing a Fluorescent Autophagosome Marker." *Molecular Biology of the Cell* 15 (3): 1101–11.
- Mofarrahi, Mahroo, Yeting Guo, Jeffrey A. Haspel, Augustine M. K. Choi, Elaine C. Davis, Gilles Gousspillou, Russell T. Hepple, Richard Godin, Yan Burelle, and Sabah N. A. Hussain. 2013. "Autophagic Flux and Oxidative Capacity of Skeletal Muscles during Acute Starvation." *Autophagy* 9 (10): 1604–20.
- Murthy, S. N. Prasanna, Siiri Iismaa, Gillian Begg, Douglas M. Freymann, Robert M. Graham, and Laszlo Lorand. 2002. "Conserved Tryptophan in the Core Domain of Transglutaminase Is Essential for Catalytic Activity." *Proceedings of the National Academy of Sciences of the United States of America* 99 (5): 2738–42.
- Nader, G. A., and K. A. Esser. 2001. "Intracellular Signaling Specificity in Skeletal Muscle in Response to Different Modes of Exercise." *Journal of Applied Physiology* 90 (5): 1936–42.
- Nakayama, Takuya, Margaret B. Fish, Marilyn Fisher, Jamina Oomen-Hajagos, Gerald H. Thomsen, and Robert M. Grainger. 2013. "Simple and Efficient CRISPR/Cas9-Mediated Targeted Mutagenesis in *Xenopus Tropicalis*." *Genesis* 51 (12): 835–43.
- Nascimbeni, A. C., M. Fanin, E. Masiero, C. Angelini, and M. Sandri. 2012. "The Role of Autophagy in the Pathogenesis of Glycogen Storage Disease Type II (GSDII)." *Cell Death and Differentiation* 19 (10): 1698–1708.
- Nishino, I., J. Fu, K. Tanji, T. Yamada, S. Shimojo, T. Koori, M. Mora, et al. 2000. "Primary LAMP-2 Deficiency Causes X-Linked Vacuolar Cardiomyopathy and Myopathy (Danon Disease)." *Nature* 406 (6798): 906–10.
- Nowak, Kristen J., and Kay E. Davies. 2004. "Duchenne Muscular Dystrophy and Dystrophin: Pathogenesis and Opportunities for Treatment." *EMBO Reports* 5 (9): 872–76.
- Parry, D. A., and J. M. Squire. 1973. "Structural Role of Tropomyosin in Muscle Regulation: Analysis of the X-Ray Diffraction Patterns from Relaxed and Contracting Muscles." *Journal of Molecular Biology* 75 (1): 33–55.
- Pattingre, Sophie, Amina Tassa, Xueping Qu, Rita Garuti, Xiao Huan Liang, Noboru Mizushima, Milton Packer, Michael D. Schneider, and Beth Levine. 2005. "Bcl-2 Antiapoptotic Proteins Inhibit Beclin 1-Dependent Autophagy." *Cell* 122 (6): 927–39.
- Pauly, Marion, Frederic Daussin, Yan Burelle, Tong Li, Richard Godin, Jeremy Fauconnier, Christelle Koechlin-Ramonatxo, et al. 2012. "AMPK Activation Stimulates Autophagy and Ameliorates Muscular Dystrophy in the Mdx Mouse Diaphragm." *The American Journal of Pathology* 181 (2): 583–92.
- Peter, Angela K., Hongqiang Cheng, Robert S. Ross, Kirk U. Knowlton, and Ju Chen. 2011. "The Costamere Bridges Sarcomeres to the Sarcolemma in Striated Muscle." *Progress in Pediatric Cardiology* 31 (2): 83–88.
- Peterson, Brenda A., David C. Haak, Marc T. Nishimura, Paulo J. P. L. Teixeira, Sean R. James, Jeffery L. Dangl, and Zachary L. Nimchuk. 2016. "Genome-Wide Assessment of Efficiency and Specificity in CRISPR/Cas9 Mediated Multiple Site Targeting in *Arabidopsis*." *PloS One* 11 (9): e0162169.
- Poetter, K., H. Jiang, S. Hassanzadeh, S. R. Master, A. Chang, M. C. Dalakas, I. Rayment, J. R. Sellers, L. Fananapazir, and N. D. Epstein. 1996. "Mutations in Either the Essential or Regulatory Light Chains of Myosin Are Associated with a Rare Myopathy in Human Heart and Skeletal Muscle." *Nature Genetics* 13 (1): 63–69.
- Raffaello, Anna, Giulia Milan, Eva Masiero, Silvia Carnio, Donghoon Lee, Gerolamo Lanfranchi, Alfred Lewis Goldberg, and Marco Sandri. 2010. "JunB Transcription Factor Maintains Skeletal Muscle Mass and Promotes Hypertrophy." *The Journal of Cell Biology* 191 (1): 101–13.
- Rahimov, Fedik, Oliver D. King, Leigh C. Warsing, Rachel E. Powell, Charles P. Emerson Jr, Louis M. Kunkel, and Kathryn R. Wagner. 2011. "Gene Expression

- Profiling of Skeletal Muscles Treated with a Soluble Activin Type IIB Receptor." *Physiological Genomics* 43 (8): 398–407.
- Ramachandran, Nivetha, Iulia Munteanu, Peixiang Wang, Pauline Aubourg, Jennifer J. Rilstone, Nyrie Israelian, Taline Naranian, et al. 2009. "VMA21 Deficiency Causes an Autophagic Myopathy by Compromising V-ATPase Activity and Lysosomal Acidification." *Cell* 137 (2): 235–46.
- Ramos, Fresnida J., Steven C. Chen, Michael G. Garelick, Dao-Fu Dai, Chen-Yu Liao, Katherine H. Schreiber, Vivian L. MacKay, et al. 2012. "Rapamycin Reverses Elevated mTORC1 Signaling in Lamin A/C-Deficient Mice, Rescues Cardiac and Skeletal Muscle Function, and Extends Survival." *Science Translational Medicine* 4 (144): 144ra103.
- Ran, F. Ann, Patrick D. Hsu, Jason Wright, Vineeta Agarwala, David A. Scott, and Feng Zhang. 2013. "Genome Engineering Using the CRISPR-Cas9 System." *Nature Protocols* 8 (11): 2281–2308.
- Rodríguez-Navarro, Jose A., Laura Rodríguez, María J. Casarejos, Rosa M. Solano, Ana Gómez, Juan Perucho, Ana María Cuervo, Justo García de Yébenes, and María A. Mena. 2010. "Trehalose Ameliorates Dopaminergic and Tau Pathology in Parkin Deleted/tau Overexpressing Mice through Autophagy Activation." *Neurobiology of Disease* 39 (3): 423–38.
- Rommel, C., S. C. Bodine, B. A. Clarke, R. Rossman, L. Nunez, T. N. Stitt, G. D. Yancopoulos, and D. J. Glass. 2001. "Mediation of IGF-1-Induced Skeletal Myotube Hypertrophy by PI(3)K/Akt/mTOR and PI(3)K/Akt/GSK3 Pathways." *Nature Cell Biology* 3 (11): 1009–13.
- Ruparelia, Avnika A., Viola Oorschot, Georg Ramm, and Robert J. Bryson-Richardson. 2016. "FLNC Myofibrillar Myopathy Results from Impaired Autophagy and Protein Insufficiency." *Human Molecular Genetics* 25 (11): 2131–42.
- Ruparelia, Avnika A., Viola Oorschot, Raquel Vaz, Georg Ramm, and Robert J. Bryson-Richardson. 2014. "Zebrafish Models of BAG3 Myofibrillar Myopathy Suggest a Toxic Gain of Function Leading to BAG3 Insufficiency." *Acta Neuropathologica* 128 (6): 821–33.
- Ruparelia, Avnika A., Mo Zhao, Peter D. Currie, and Robert J. Bryson-Richardson. 2012. "Characterization and Investigation of Zebrafish Models of Filamin-Related Myofibrillar Myopathy." *Human Molecular Genetics* 21 (18): 4073–83.
- Rusmini, Paola, Maria Josefa Polanco, Riccardo Cristofani, Maria Elena Cicardi, Marco Meroni, Mariarita Galbiati, Margherita Piccolella, et al. 2015. "Aberrant Autophagic Response in The Muscle of A Knock-in Mouse Model of Spinal and Bulbar Muscular Atrophy." *Scientific Reports* 5 (October): 15174.
- Sabatelli, Patrizia, Camilla Pellegrini, Cesare Faldini, and Luciano Merlini. 2012. "Cytoskeletal and Extracellular Matrix Alterations in Limb Girdle Muscular Dystrophy 2I Muscle Fibers." *Neurology India* 60 (5): 510–11.
- Sakuma, Kunihiro, Masakazu Kinoshita, Yoshinori Ito, Miki Aizawa, Wataru Aoi, and Akihiko Yamaguchi. 2016. "p62/SQSTM1 but Not LC3 Is Accumulated in Sarcopenic Muscle of Mice." *Journal of Cachexia, Sarcopenia and Muscle* 7 (2): 204–12.
- Sarparanta, Jaakko, Per Harald Jonson, Christelle Golzio, Satu Sandell, Helena Luque, Mark Screen, Kristin McDonald, et al. 2012. "Mutations Affecting the Cytoplasmic Functions of the Co-Chaperone DNAJB6 Cause Limb-Girdle Muscular Dystrophy." *Nature Genetics* 44 (4): 450–55, S1–2.
- Schaeffer, Véronique, Isabelle Lavenir, Sefika Ozcelik, Markus Tolnay, David T. Winkler, and Michel Goedert. 2012. "Stimulation of Autophagy Reduces Neurodegeneration in a Mouse Model of Human Tauopathy." *Brain: A Journal of Neurology* 135 (Pt 7): 2169–77.
- Sethi, Ritika, Jonne Seppälä, Helena Tossavainen, Mikko Ylilauri, Salla Ruskamo, Olli T. Pentikäinen, Ulla Pentikäinen, Perttu Permi, and Jari Yläanne. 2014. "A Novel

- Structural Unit in the N-Terminal Region of Filamins." *The Journal of Biological Chemistry* 289 (12): 8588–98.
- Sharples, Adam P., Nasser Al-Shanti, and Claire E. Stewart. 2010. "C2 and C2C12 Murine Skeletal Myoblast Models of Atrophic and Hypertrophic Potential: Relevance to Disease and Ageing?" *Journal of Cellular Physiology* 225 (1): 240–50.
- Smith, Laura L., Alan H. Beggs, and Vandana A. Gupta. 2013. "Analysis of Skeletal Muscle Defects in Larval Zebrafish by Birefringence and Touch-Evoke Escape Response Assays." *Journal of Visualized Experiments: JoVE*, no. 82 (December): e50925.
- Solchenberger, Barbara, Claire Russell, Elisabeth Kremmer, Christian Haass, and Bettina Schmid. 2015. "Granulin Knock Out Zebrafish Lack Frontotemporal Lobar Degeneration and Neuronal Ceroid Lipofuscinosis Pathology." *PLoS One* 10 (3). Public Library of Science: e0118956.
- Song, Young Joon, Jang Hyun Choi, and Hansol Lee. 2015. "Setdb1 Is Required for Myogenic Differentiation of C2C12 Myoblast Cells via Maintenance of MyoD Expression." *Molecules and Cells* 38 (4): 362–72.
- Spangenburg, Espen E., Derek Le Roith, Chris W. Ward, and Sue C. Bodine. 2008. "A Functional Insulin-like Growth Factor Receptor Is Not Necessary for Load-Induced Skeletal Muscle Hypertrophy." *The Journal of Physiology* 586 (1): 283–91.
- Steffen, Leta S., Jeffrey R. Guyon, Emily D. Vogel, Rosanna Beltre, Timothy J. Pusack, Yi Zhou, Leonard I. Zon, and Louis M. Kunkel. 2007. "Zebrafish Orthologs of Human Muscular Dystrophy Genes." *BMC Genomics* 8 (March): 79.
- Straussberg, Rachel, Gudrun Schottmann, Menachem Sadeh, Esther Gill, Franziska Seifert, Ayelet Halevy, Kaiyal Qassem, et al. 2016. "Kyphoscoliosis Peptidase (KY) Mutation Causes a Novel Congenital Myopathy with Core Targetoid Defects." *Acta Neuropathologica* 132 (3): 475–78.
- Sugie, K., A. Yamamoto, K. Murayama, S. J. Oh, M. Takahashi, M. Mora, J. E. Riggs, et al. 2002. "Clinicopathological Features of Genetically Confirmed Danon Disease." *Neurology* 58 (12): 1773–78.
- Tajsharghi, Homa, and Anders Oldfors. 2013. "Myosinopathies: Pathology and Mechanisms." *Acta Neuropathologica* 125 (1): 3–18.
- Tang, Rongying, Andrew Dodd, Daniel Lai, Warren C. McNabb, and Donald R. Love. 2007. "Validation of Zebrafish (*Danio Rerio*) Reference Genes for Quantitative Real-Time RT-PCR Normalization." *Acta Biochimica et Biophysica Sinica* 39 (5): 384–90.
- Tanida, I., E. Tanida-Miyake, T. Ueno, and E. Kominami. 2001. "The Human Homolog of *Saccharomyces Cerevisiae* Apg7p Is a Protein-Activating Enzyme for Multiple Substrates Including Human Apg12p, GATE-16, GABARAP, and MAP-LC3." *The Journal of Biological Chemistry* 276 (3): 1701–6.
- Theadom, Alice, Miriam Rodrigues, Richard Roxburgh, Shiavnthi Balalla, Chris Higgins, Rohit Bhattacharjee, Kelly Jones, Rita Krishnamurthi, and Valery Feigin. 2014. "Prevalence of Muscular Dystrophies: A Systematic Literature Review." *Neuroepidemiology* 43 (3-4): 259–68.
- Tian, Ye, Zhipeng Li, Wanqiu Hu, Haiyan Ren, E. Tian, Yu Zhao, Qun Lu, et al. 2010. "C. Elegans Screen Identifies Autophagy Genes Specific to Multicellular Organisms." *Cell* 141 (6): 1042–55.
- Tosch, Valérie, Holger M. Rohde, Hélène Tronchère, Edmar Zanoteli, Nancy Monroy, Christine Kretz, Nicolas Dondaine, Bernard Payrastre, Jean-Louis Mandel, and Jocelyn Laporte. 2006. "A Novel PtdIns3P and PtdIns(3,5)P2 Phosphatase with an Inactivating Variant in Centronuclear Myopathy." *Human Molecular Genetics* 15 (21): 3098–3106.
- Trendelenburg, Anne Ulrike, Angelika Meyer, Daisy Rohner, Joseph Boyle, Shinji Hatakeyama, and David J. Glass. 2009. "Myostatin Reduces Akt/TORC1/p70S6K Signaling, Inhibiting Myoblast Differentiation and Myotube Size." *American Journal of Physiology. Cell Physiology* 296 (6): C1258–70.

- Tresse, Emilie, Florian A. Salomons, Jouni Vesa, Laura C. Bott, Virginia Kimonis, Tso-Pang Yao, Nico P. Dantuma, and J. Paul Taylor. 2010. "VCP/p97 Is Essential for Maturation of Ubiquitin-Containing Autophagosomes and This Function Is Impaired by Mutations That Cause IBMPFD." *Autophagy* 6 (2): 217–27.
- Ulbricht, Anna, Felix J. Eppler, Victor E. Tapia, Peter F. M. van der Ven, Nico Hampe, Nils Hersch, Padmanabhan Vakeel, et al. 2013. "Cellular Mechanotransduction Relies on Tension-Induced and Chaperone-Assisted Autophagy." *Current Biology: CB* 23 (5): 430–35.
- Ulbricht, Anna, Sebastian Gehlert, Barbara Leciejewski, Thorsten Schiffer, Wilhelm Bloch, and Jörg Höfeld. 2015. "Induction and Adaptation of Chaperone-Assisted Selective Autophagy CASA in Response to Resistance Exercise in Human Skeletal Muscle." *Autophagy* 11 (3): 538–46.
- Velloso, C. P. 2008. "Regulation of Muscle Mass by Growth Hormone and IGF-I." *British Journal of Pharmacology* 154 (3): 557–68.
- Venn, G., and R. M. Mason. 1986. "Changes in Mouse Intervertebral-Disc Proteoglycan Synthesis with Age. Hereditary Kyphoscoliosis Is Associated with Elevated Synthesis." *Biochemical Journal* 234 (2): 475–79.
- Wang, Yun, Benoit Viollet, Robert Terkeltaub, and Ru Liu-Bryan. 2016. "AMP-Activated Protein Kinase Suppresses Urate Crystal-Induced Inflammation and Transduces Colchicine Effects in Macrophages." *Annals of the Rheumatic Diseases* 75 (1): 286–94.
- Wei, Yongjie, Sophie Pattingre, Sangita Sinha, Michael Bassik, and Beth Levine. 2008. "JNK1-Mediated Phosphorylation of Bcl-2 Regulates Starvation-Induced Autophagy." *Molecular Cell* 30 (6): 678–88.
- Whitesell, Luke, and Susan Lindquist. 2009. "Inhibiting the Transcription Factor HSF1 as an Anticancer Strategy." *Expert Opinion on Therapeutic Targets* 13 (4): 469–78.
- Whittemore, Lisa-Anne, Kening Song, Xiangping Li, Jane Aghajanian, Monique Davies, Stefan Girgenrath, Jennifer J. Hill, et al. 2003. "Inhibition of Myostatin in Adult Mice Increases Skeletal Muscle Mass and Strength." *Biochemical and Biophysical Research Communications* 300 (4): 965–71.
- Widegren, U., C. Wretman, A. Lionikas, G. Hedin, and J. Henriksson. 2000. "Influence of Exercise Intensity on ERK/MAP Kinase Signalling in Human Skeletal Muscle." *Pflügers Archiv: European Journal of Physiology* 441 (2-3): 317–22.
- Wong, T. S., and F. W. Booth. 1988. "Skeletal Muscle Enlargement with Weight-Lifting Exercise by Rats." *Journal of Applied Physiology* 65 (2): 950–54.
- Wright, Craig R., Erin L. Brown, Paul A. Della-Gatta, Alister C. Ward, Gordon S. Lynch, and Aaron P. Russell. 2014. "G-CSF Does Not Influence C2C12 Myogenesis despite Receptor Expression in Healthy and Dystrophic Skeletal Muscle." *Frontiers in Physiology* 5 (May): 170.
- Yaffe, D., and O. Saxel. 1977. "Serial Passaging and Differentiation of Myogenic Cells Isolated from Dystrophic Mouse Muscle." *Nature* 270 (5639): 725–27.
- Yogev, Yuval, Yonatan Perez, Iris Noyman, Anwar Abu Madegem, Hagit Flusser, Zamir Shorer, Eugene Cohen, et al. 2017. "Progressive Hereditary Spastic Paraplegia Caused by a Homozygous KY Mutation." *European Journal of Human Genetics: EJHG* 25 (8): 966–72.
- Zhao, Jinghui, Jeffrey J. Brault, Andreas Schild, Peirang Cao, Marco Sandri, Stefano Schiaffino, Stewart H. Lecker, and Alfred L. Goldberg. 2007. "FoxO3 Coordinately Activates Protein Degradation by the Autophagic/lysosomal and Proteasomal Pathways in Atrophying Muscle Cells." *Cell Metabolism* 6 (6): 472–83.
- Zhu, Xiaoxiao, Yajie Xu, Shanshan Yu, Lu Lu, Mingqin Ding, Jing Cheng, Guoxu Song, et al. 2014. "An Efficient Genotyping Method for Genome-Modified Animals and Human Cells Generated with CRISPR/Cas9 System." *Scientific Reports* 4 (September): 6420.